

Modification of Epoxy Systems for Mechanical Performance Improvement

Dem Fachbereich Maschinenbau und Verfahrenstechnik
der Technischen Universität Kaiserslautern
zur Erlangung des akademischen Grades

Doktor-Ingenieur (Dr.-Ing.)

vorgelegte

Dissertation

von

Herrn

M.Tech. Ankur Bajpai

aus Kanpur, Indien

2017

Tag der mündlichen Prüfung:	8. December 2017
Dekan:	Prof. Dr.-Ing. Jörg Seewig
Prüfungsvorsitzender:	Prof. Dr.-Ing. Jan C. Aurich
1. Berichterstatter:	Prof. Dr.-Ing. Ulf Breuer
2. Berichterstatter:	Prof. Dr.-Ing. Paul L. Geiss

D386

Acknowledgment

The present work was completed between July 2013 and December 2017 at the Institute for Composite materials (Institut für Verbundwerkstoff GmbH, IVW) of the University of Kaiserslautern, Germany. This work was carried out with the financial support of the SchäferRolls GmbH, as a part of the research project "Development of novel thermosetting resin systems for calender rolls".

First of all I would like express my gratitude to my supervisor, Prof. Dr.-Ing. Ulf Breuer, for giving me the opportunity to work in this institute and for all the fruitful scientific discussion during the course of this work. Dr.-Ing. Bernd Wetzels has been a fantastic mentor through the course of this PhD and has been genuine pleasure and privilege to work with. Many thanks to Prof. Dr.-Ing. Jan C. Aurich for accepting the presidency of the examination committee and to Prof. Dr.-Ing Paul L. Geiss for being co-referee of this PhD thesis.

I am thankful to Dr. Sergiy Grishchuk, for his wonderful suggestions and deep knowledge which helped me during the course of this work. Further I would like to thank the colleagues of the Institute , especially Heidi Plocharzik, Pia Eichert, Petra Volk, Hermann Giertzsch, Stefan Schmitt, and Ralf Schimmele for their kind help in the experiments. I am especially grateful to my dear good friends Andreas Klingler, Mark Kopietz, Benjamin Kelkel, Mohammad Muddassir, Kerstin Steidle and Liubov Soronchynska among many others for their constant encouragement and for the nice time spend together. I would also like to express my gratefulness to my HiWis and master students, Arun Alapati, Nitin Paruchuri, and Satyam Reddi without their help this work could not have been accomplished.

I wish to thank my entire family, especially my younger brother Anmol, my in-laws, my cousins for their love and care. Very special thanks to my wife Shivani for the courage, motivation and love that she has given me during the whole process.

Lastly, and most importantly I wish to thanks my parents, Sunita Bajpai and Shiv Kumar Bajpai. I have no words to acknowledge the sacrifices they made and the dreams they had to let go, just to give me a shot at achieving mine. With my deepest gratitude I dedicate them this thesis.

गायत्री मंत्र

ॐ भूर्भुवः स्वः
तत्सवितुर्वरेण्यं
भर्गो देवस्यः धीमहि
धियो यो नः प्रचोदयात्

Gayatri Mantra

We meditate on the glory of the radiant sun, may he illuminate our
intellect and lead us on to the righteous path.

Rig Veda (Mandala 3.62.10)

Table of Contents

Table of Contents	i
Abstract.....	vi
Kurzfassung.....	viii
List of abbreviations and symbols.....	ix
1. Introduction.....	1
1.1 Background	1
2. Motivation and objectives	3
3. State of the art	7
3.1 Epoxy resins	7
3.1.1 Structure of epoxy resin molecule	7
3.1.2 Synthesis of diglycidyl ether of bisphenol A	8
3.1.3 Curing of epoxy resins	9
3.1.4 Basic mechanism of ring opening of epoxy group.....	10
3.2 Time, temperature and cure	11
3.2.1 Gelation.....	11
3.2.2 Vitrification	11
3.3 Factors affecting the final cured properties of epoxy/hardener system....	12
3.3.1 Stoichiometry	12
3.3.2 Monomer functionality	13
3.3.3 Monomer's chemical structure	13
3.3.4 Influence of curing duration.....	14
3.3.5 Degree of cure	14
3.4 Glass Transition Temperature	15
3.5 Mechanical and fracture properties.....	16
3.6 Yield behavior of unmodified epoxies	18
3.6.1 Modified Von Mises yield criterion.....	19
3.7 Fracture behavior of unmodified epoxy.....	19
3.8 Toughening approaches for unmodified brittle epoxy matrices.....	22
3.8.1 Toughening via chemical modification	22

3.8.2	Addition of Rubber particles	23
3.8.3	Addition of Thermoplastics	25
3.8.4	Block copolymers (BCP)	25
3.8.5	Rigid Fillers	30
3.8.6	Hybrid toughening	31
3.9	Toughening mechanisms	32
3.9.1	Shear Yielding	32
3.9.2	Crack pinning and crack path deflection	33
3.9.3	Crack bridging or particle bridging	33
3.9.4	Crazing	34
3.9.5	Cavitation	35
3.10	Microstructural aspects	38
3.10.1	Volume fraction of rubber phase	38
3.10.2	Particle size of rubber phase	39
3.10.3	Interfacial Adhesion	39
3.10.4	Molecular weight of matrix phase	40
3.11	Analytical Modeling	40
3.11.1	Elastic Modulus	40
3.11.2	Tensile strength	43
3.11.3	Fracture Energy	44
4.	Materials and manufacturing	48
4.1	Introduction	48
4.2	Epoxy resins	48
4.2.1	Bisphenol-F based epoxy	48
4.2.2	Fluoren di epoxy.	49
4.2.3	Epoxy resin based on meta – amino phenol.	49
4.2.4	Epoxy resin based on 1, 6 – Naphthalene di-epoxy	49
4.3	Hardener systems	50
4.4	Toughening agents	51
4.4.1	Block copolymers	51
4.4.2	Core-shell rubber particles	51
4.4.3	Titanium dioxide (TiO ₂)	51
4.5	Manufacturing	52

4.5.1	Epoxy and block copolymers composites	52
4.5.2	Epoxy and core-shell rubber composites	54
4.5.3	Epoxy and TiO ₂ composites	55
5.	Experimental work.....	59
5.1	Rheometric measurement	59
5.2	Mechanical tests	60
5.2.1	Tensile tests.....	60
5.2.2	Plane strain compression tests	60
5.2.3	Fracture toughness tests.....	61
5.3	Viscoelastic properties	63
5.3.1	Dynamic mechanical thermal analysis (DMTA).....	63
5.3.2	Differential scanning calorimetry (DSC)	64
5.4	Microstructure	65
5.4.1	Scanning electron microscopy (SEM).....	65
5.4.2	Atomic force microscope (AFM).....	65
5.4.3	White light profilometry.....	66
6.	Results and discussion.....	67
6.1	Amine cured bis-F epoxy modified with multi-functional epoxies	67
6.1.1	Tensile properties	68
6.1.2	Thermal and viscoelastic properties.....	68
6.2	Anhydride cured bis-F epoxy modified with multi-functional epoxies	72
6.2.1	Tensile properties	73
6.2.2	Thermal and viscoelastic properties.....	74
6.3	Amine cured tailored epoxy system modified with D51N BCP's	78
6.3.1	Microstructure	78
6.3.2	Rheology.....	80
6.3.3	Glass transition temperature and viscoelastic properties	81
6.3.4	Tensile properties	83
6.3.5	Fracture properties.....	86
6.3.6	Fractography studies.....	88
6.3.7	Modeling of fracture energy	92
6.4	Anhydride cured tailored epoxy modified with D51N BCP's	96
6.4.1	Microstructure studies	96

6.4.2	Rheology.....	98
6.4.3	Glass transition temperature and viscoelastic properties.....	98
6.4.4	Tensile properties.....	100
6.4.5	Fracture properties.....	104
6.4.6	Fractography studies.....	105
6.4.7	Modeling of Fracture Energy.....	110
6.5	Amine cured tailored epoxy modified with CSR particles.....	113
6.5.1	Microstructure.....	113
6.5.2	Rheology.....	114
6.5.3	Glass transition temperature and viscoelastic properties.....	115
6.5.4	Tensile properties.....	117
6.5.5	Fracture properties.....	120
6.5.6	Fractography studies.....	122
6.5.7	Modeling of Fracture Energy.....	125
6.6	Anhydride cured tailored epoxy modified with CSR particles.....	128
6.6.1	Microstructure studies.....	128
6.6.2	Rheology.....	129
6.6.3	Glass transition temperature and viscoelastic properties.....	130
6.6.4	Tensile properties.....	132
6.6.5	Fracture properties.....	135
6.6.6	Fractography studies.....	136
6.6.7	Modeling of Fracture Energy.....	139
6.7	Amine cured epoxy hybrid composites modified with D51N BCP's and CSR particles.....	142
6.7.1	Rheology.....	142
6.7.2	Glass transition temperature and viscoelastic properties.....	143
6.7.3	Tensile properties.....	145
6.7.4	Fracture properties.....	147
6.7.5	Fractography studies.....	148
6.8	Anhydride cured epoxy hybrid composites modified with D51N BCP's and CSR particles.....	151
6.8.1	Rheology.....	151
6.8.2	Glass transition temperature and viscoelastic properties.....	152
6.8.3	Tensile properties.....	154

6.8.4	Fracture properties.....	155
6.8.5	Fractography studies.....	157
6.9	Amine cured epoxy hybrid composites modified with D51N BCP's and TiO ₂ nanoparticles	159
6.9.1	Rheology.....	159
6.9.2	Glass transition temperature and viscoelastic properties	160
6.9.3	Tensile properties	161
6.9.4	Fracture properties.....	163
6.9.5	Fractography studies.....	163
6.10	Effect of morphology on different mechanical properties	165
6.11	Toughening mechanisms for all the systems	167
6.12	Map of reinforcing effect	169
7.	Conclusion and outlook.....	172
8.	Literature	177
9.	Appendix	194
9.1	Surface roughness measurement of fractured surfaces	194
9.2	Compressive test results data.....	196
9.3	Viscosity values at different temperatures	197
9.4	Mixing ratios for different formulations	198
9.5	Boiling water test results	202
10.	List of publications.....	204
11.	List of student support works	205
12.	Curriculum Vitae.....	206

Abstract

Epoxy belongs to a category of high-performance thermosetting polymers which have been used extensively in industrial and consumer applications. Highly cross-linked epoxy polymers offer excellent mechanical properties, adhesion, and chemical resistance. However, unmodified epoxies are prone to brittle fracture and crack propagation due to their highly crosslinked structure. As a result, epoxies are normally toughened to ensure the usability of these materials in practical applications.

This research work focuses on the development of novel modified epoxy matrices, with enhanced mechanical, fracture mechanical and thermal properties, suitable to be processed by filament winding technology, to manufacture composite based calender roller covers with improved performance in comparison to commercially available products.

In the first stage, a neat epoxy resin (EP) was modified using three different high functionality epoxy resins with two type of hardeners i.e. amine-based (H1) and anhydride-based (H2). Series of hybrid epoxy resins were obtained by systematic variation of high functionality epoxy resin contents with reference epoxy system. The resulting matrices were characterized by their tensile properties and the best system was chosen from each hardener system i.e. amine and anhydride. For tailored amine based system (MEP_H1) 14 % improvement was measured for bulk samples similarly, for tailored anhydride system (MEP_H2) 11 % improvement was measured when tested at 23 °C.

Further, tailored epoxy systems (MEP_H1 and MEP_H2) were modified using specially designed block copolymer (BCP), and core-shell rubber nanoparticles (CSR). Series of nanocomposites were obtained by systematic variation of filler contents. The resulting matrices were extensively characterized qualitatively and quantitatively to reveal the effect of each filler on the polymer properties. It was shown that the BCP confer better fracture properties to the epoxy resin at low filler loading without losing the other mechanical properties. These characteristics were accompanied by ductility and temperature stability. All composites were tested at 23

°C and at 80 °C to understand the effect of temperature on the mechanical and fracture properties.

Examinations on fractured specimen surfaces provided information about the mechanisms responsible for reinforcement. Nanoparticles generate several energy dissipating mechanisms in the epoxy, e.g. plastic deformation of the matrix, cavitation, void growth, debonding and crack pinning. These were closely related to the microstructure of the materials. The characteristic of the microstructure was verified by microscopy methods (SEM and AFM). The microstructure of neat epoxy hardener system was strongly influenced by the nanoparticles and the resulting interfacial interactions. The interaction of nanoparticles with a different hardener system will result in different morphology which will ultimately influence the mechanical and fracture mechanical properties of the nanocomposites. Hybrid toughening using a combination of the block-copolymer / core-shell rubber nanoparticles and block copolymer / TiO₂ nanoparticles has been investigated in the epoxy systems. It was found out that addition of rigid phase with a soft phase recovers the loss of strength in the nanocomposites caused by a softer phase.

In order to clarify the relevant relationships, the microstructural and mechanical properties were correlated. The Counto's, Halpin-Tsai, and Lewis-Nielsen equations were used to calculate the modulus of the composites and predicted modulus fit well with the measured values. Modeling was done to predict the toughening contribution from block copolymers and core-shell rubber nanoparticles. There was good agreement between the predicted values and the experimental values for the fracture energy.

Kurzfassung

Epoxidharze sind eine Klasse hochleistender, duroplastischer Polymere, welche in unzähligen industriellen sowie Verbraucheranwendungen zum Einsatz kommen. Die hochvernetzten Epoxidpolymere bieten exzellente mechanische Eigenschaften, Adhäsion und Chemikalienresistenz. Allerdings sind nicht modifizierte Epoxidharze durch ihren hohen Vernetzungsgrad äußerst spröde und anfällig Brüche und deren Ausbreitung. Um praktische Anwendungen dieser Materialklasse zu realisieren werden Epoxidharze deswegen in der Regel zähmodifiziert.

Diese Forschungsarbeit fokussiert daher auf die Entwicklung neuartiger, modifizierter Epoxidharzmatrizes mit verbesserten mechanischen, bruchmechanischen und thermischen Eigenschaften. Gleichzeitig eignen sie sich für die Verarbeitung im Wickelverfahren, zur Herstellung von kompositbasierten Kalanderverfahren mit gesteigerter Leistung (gegenüber den kommerziell verfügbaren Systemen).

Im ersten Schritt wurde ein reines Epoxidharz (EP) mit drei verschiedenen, hochfunktionalisierten Epoxidharzen sowie mit zwei Härter typen – amin-basiert (H1) und anhydrid-basiert (H2) – modifiziert. Die systematische Variation unterschiedlicher Verhältnisse zwischen Referenzepoxidharz und hochfunktionalisierten Epoxidharzen resultierte in Hybridharz-systemen. Diese wurden mittels Zugversuchen charakterisiert und für beide Härter typen je das beste System ausgewählt. Das maßgeschneiderte amin-basierte System (MEP_H1) resultierte in 14 % und das anhydrid-basierte System (MEP_H2) 11 % verbesserten Materialeigenschaften (bei Prüfung bei 23 °C).

Weiterhin wurden die vorigen Systeme (MEP_H1 und MEP_H2) mit Block-Copolymeren (D51N) sowie Kern-Schale-Nanopartikeln (MX170) modifiziert. Durch systematische Variation des Füllstoffgehalts wurden Nanokomposit-Serien erzeugt. Die resultierenden Matrizes wurden ausgiebig, qualitativ wie auch quantitativ, geprüft um den Effekt der Füllstoffe auf die Polymereigenschaften zu charakterisieren. Es wurde gezeigt, dass die Block-Copolymere (BCP) vergleichsweise bessere bruchmechanische Eigenschaften bei niedrigen Füllstoffgehalten generieren, ohne dabei die weiteren mechanischen Eigenschaften negativ zu beeinflussen. Ebenso

werden Duktilität und Temperaturstabilität beibehalten. Alle Nanokomposite wurden bei 23 °C und 80 °C getestet, um aus thermischen Effekten auf mechanische sowie Brucheigenschaften zu ermitteln.

Die Erkenntnisse der Mikrostrukturanalyse konnte mittels mikroskopischer Methoden verifiziert werden (REM und AFM). Es wurde gezeigt, dass die Mikrostruktur des reinen Epoxy-Härter-Systems stark durch Nanopartikel und deren härter abhängige Grenzflächenbindung beeinflusst wird, und die mechanischen und bruchmechanischen Eigenschaften von der Morphologie des Nanokomposits abhängen. Die Untersuchung der Bruchflächen von Probekörpern gab Aufschluss über die Mechanismen, welche zur Verstärkung führen. Die Nanopartikel erzeugen verschiedene energiedissipative Mechanismen im Epoxidharz, bspw. plastische Deformation der Matrix, Kavitation, Hohlraumwachstum, Ablösung und Rissumlenkung. Diese wiederum haben einen direkten Einfluss auf die Mikroeigenschaften der Materialien. Durch die Kombination von Blockcopolymeren und Kern-Schale-Nanopartikeln sowie Blockcopolymeren und TiO₂-Nanopartikeln wurde in den Epoxidsystemen eine Hybridmodifizierung durchgeführt. Es zeigte sich, dass die Zugabe einer starren Phase (TiO₂-Nanopartikel) zu einer weichen Phase (Blockcopolymer) den Festigkeitsverlust in den Nanokompositen, der durch eine weiche Phase verursacht werden, wiederherstellt.

Um die relevanten Zusammenhänge zu klären, wurden die mikrostrukturellen und mechanischen Eigenschaften miteinander korreliert. Das Counto-Modell, sowie die Halpin-Tsai und Lewis-Nielsen-Gleichung wurden verwendet, um den E-Modul der verschiedenen Systeme zu modellieren. Weiterhin wurden die energetischen Beiträge der Zähigkeitssteigerung durch Blockcopolymer und Kern-Schale-Nanopartikel modelliert. Es zeigte sich eine sehr gute Übereinstimmung zwischen den vorhergesagten und den experimentell ermittelten Werten für die Bruchenergie.

List of abbreviations and symbols

Abbreviations

AEW	:	Anhydride equivalent weight
AFM	:	Atomic-force microscopy
ASTM	:	American Society for Testing and Materials
BCP	:	Block copolymer
CSR	:	Core shell rubber
CT	:	Compact Tension
CTBN	:	carboxyl-terminated butadiene-acrylonitrile
DGEBA	:	Di-glycidyl ether of bisphenol A
DGEBF	:	Di-glycidyl ether of bisphenol F
DMTA	:	Dynamic mechanical thermal analysis
DSC	:	Differential Scanning Calorimetry
EEW	:	Epoxy equivalent weight
EP	:	Epoxy
EP/H1	:	Epoxy system amine hardener based
EP/H2	:	Epoxy system anhydride hardener based
H1	:	Amine based hardener
H2	:	Anhydride based hardener
ISO	:	International Organization for Standardization
LEFM	:	Linear elastic fracture mechanics
MAM	:	Poly (methyl methacrylate)-b-poly (butyl acrylate)
MEP_H1	:	Modified epoxy system amine hardener based
MEP_H2	:	Modified epoxy system anhydride hardener based
PbuA	:	Poly (butyl acrylate)
PMMA	:	Poly (methyl methacrylate)
Phr	:	Parts per hundred
PVT	:	Pressure Volume Temperature
SEM	:	Scanning Electron Microscopy
SENB	:	Single edge notched three point bending
TBCP	:	Tri-Block Copolymer
TiO ₂	:	Titanium dioxide
TMA	:	Thermomechanical Analysis

TML	:	Torus bead Mill
UTS	:	Ultimate tensile strength
vol. %	:	Volume percentage
wt. %	:	Weight percentage

Symbols

a_o	[mm]	Distance from the applied load to the crack tip (CT sample)
B	[mm]	Thickness of compact tension samples
E	[MPa]	Young's Modulus
$f(\alpha)$	-	Geometry function
F_{max}	[N]	Maximum sustained force (tensile tests)
E'	[MPa]	Storage Modulus
E''	[MPa]	Loss Modulus
K_{IC}	[MPa.m ^{1/2}]	Critical stress intensity factor (mode I)
M_w	[g/mol]	Molecular weight
$\tan \delta$	-	Damping factor
T_g	[°C]	Glass transition temperature
T_α, T_β	-	Transition temperatures in DMTA curve
α	-	Normalized crack length (a_o/W)
ϵ_m	[%]	Tensile strain at maximum stress
η	[Pa.s]	Viscosity
ν	-	Poisson's ratio
ρ	[g/cm ³]	Density
σ_m	[MPa]	Tensile strength
ω	[S ⁻¹]	Frequency

1. Introduction

1.1 Background

Epoxies are commonly used as a matrix in a wide range of composite based calender rollers (Figure 1), electronics applications, aerospace applications and in many other applications. Due to their very good electrical and chemical properties, good strength, low shrinkage and low absorption of moisture make them the most used matrix system [1]. A wide range of epoxy resin and hardener combinations makes them versatile, each combination conferring different molecular structure and properties for the specific application. Hydroxyl group present in the resin [2] and high polar nature [3] are responsible for the strong adhesion of dissimilar material, independent of epoxy group, molecular weight, and hydrocarbon content.

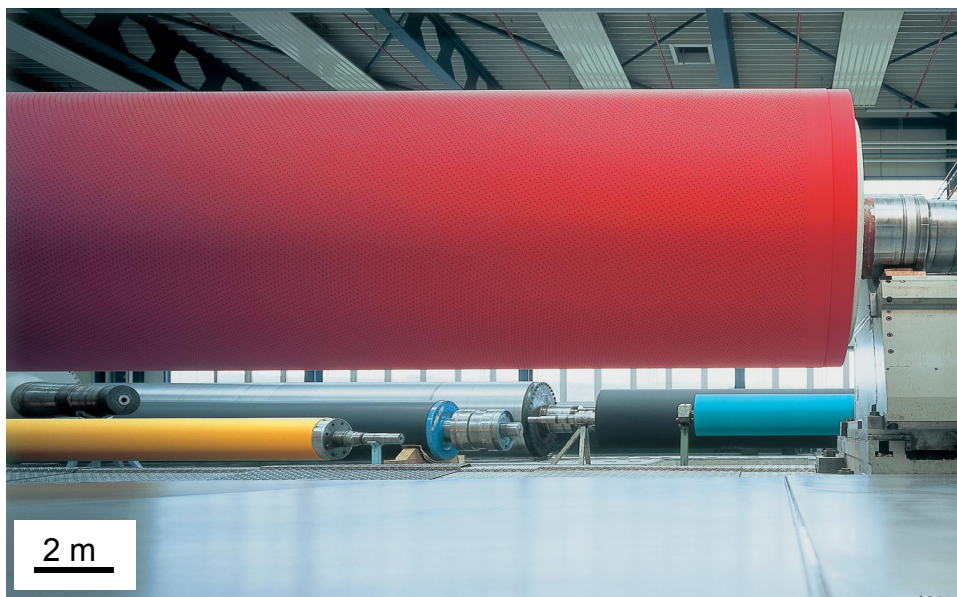


Figure 1: Different types of calender roller covers with varying sizes [4].

Apart from good mechanical and thermal properties, high crosslink microstructure makes unmodified epoxy systems brittle and suffers from poor resistance to crack initiation and propagation. As a consequence of action, epoxies are toughened with the addition of the second phase to combat crack initiation and propagation. Previous studies have shown that the incorporation of ductile organic and hard inorganic micro- and Nano-particulate fillers are a well-known pathway to improve mechanical properties, and in particular toughness, of brittle thermosetting polymers such as epoxy resins. To overcome brittleness, reactive rubber modifiers, e.g. carboxyl-terminated butadiene acrylonitrile (CTBN) can react into the epoxy which increases

its toughness but with the sacrifice of worse strength, modulus and thermal properties [5]. Rigid fillers such as alumina, titanium dioxide [6], clay [7] and CNT's [8] have been added in low concentrations to the epoxies to increase their stiffness, strength and thermal properties; but they have also demonstrated a favorable toughening effect. From the past decade, a new generation of alternative toughening agents such as pre-formed elastomeric particles [9] [10], block copolymers [11] [12] [13] and silica nanoparticles [5] have been developed to toughen epoxies.

The epoxy, curing agent, filler material, particle size, morphology, surface treatment, amount and the used dispersion method as well as the homogeneity within the matrix strongly influence the nanocomposite performance. However, the improvement of the fracture toughness and other mechanical properties by the addition of organic and rigid fillers can only be achieved when an adequate interaction between the nanoparticles and the matrix polymer takes place, which can only be effective if the nanoparticles are well dispersed in the polymer matrix.

Filament winding is one of the fabrication techniques mainly used for manufacturing hollow pipes and closed structures i.e. pressure vessels for missile casings, aircraft fuselages, calender rolls etc. The filament winding process consists of winding continuous roving's of fiber onto to a rotating mandrel which is permanent in case of pressure vessels. In the wet winding method the roving's pass through a resin bath before they are winded over a rotating mandrel.

2. Motivation and objectives

Properties like high tensile strength and high fracture toughness are required for epoxy-based thermoset systems to be used as covering agents of calender rollers in industrial environments with a long service life (Figure 2). Epoxy based composite roller covers are used in the paper machine industry typically operate at high speed (1800 m/min) with line loads of up to 80 - 150 N/mm for a running time of 500 hours in the temperature range of 23 °C – 60 °C, depending upon the type of finish and gloss properties required for the paper. During operation, the calender encounters severe impacts due to breakage of the paper web and the presence of unwanted impurities in the paper pulp. The calender roller covers operate in hot and humid conditions, hence temperature and moisture adversely affect the mechanical properties of the roller cover material, and therefore high damage tolerance is required for an epoxy system which is used as a matrix material in composite roller covers. System properties are dominated by the epoxy matrix which accounts (up to 70 vol. %), fillers (up to 30 vol. %) and fiber (up to 12 vol. %).

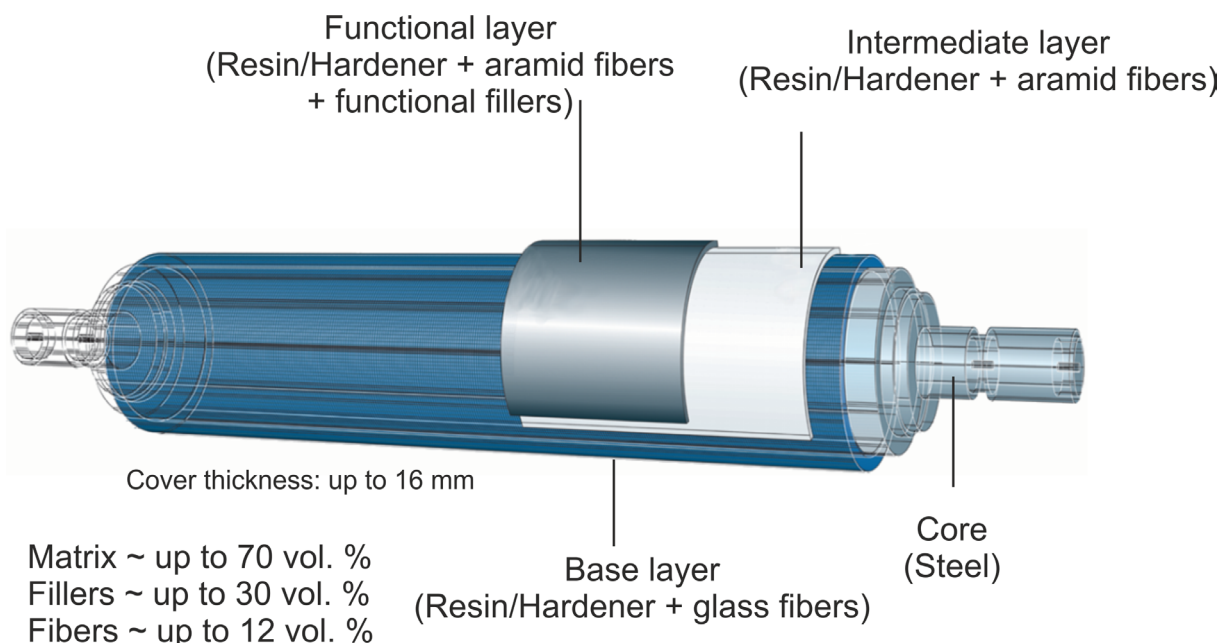


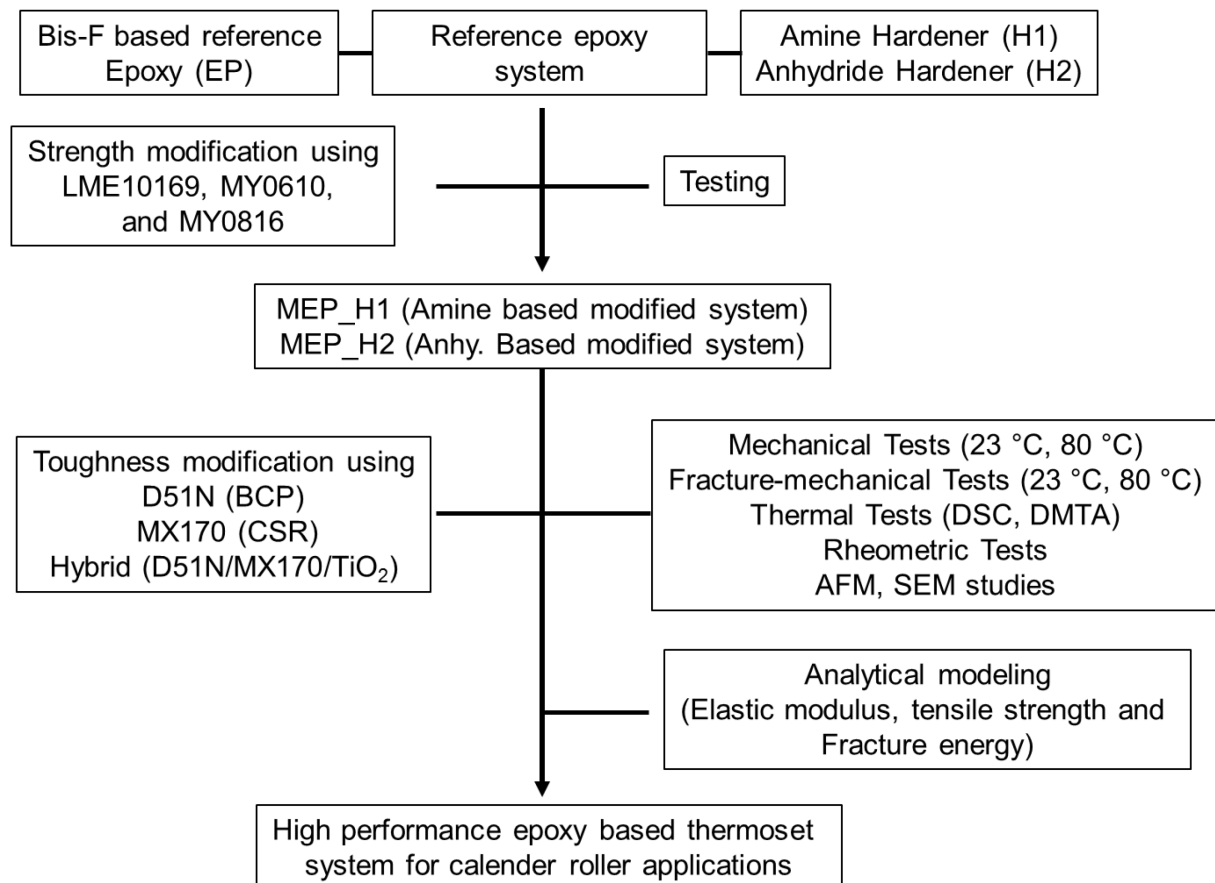
Figure 2: Structure of epoxy-based composite calender roller cover [4].

It can be inferred that a lot of literature was reported to reduce the brittleness of the epoxy polymer via chemical modification and by the addition of secondary phase. Properties like strength, modulus and glass transition temperature have an adverse effect when soft (rubber) like modifier is added to the epoxy, but the strength and modulus can be increased to a certain extent when the ceramic-based nanoparticles

are used. Since very few literature sources were reported for strength modification via chemical modification of epoxy matrix, this creates a gap of knowledge and forms the basis for this research work.

The main motivation behind taking up this project was to impart high tensile strength into the epoxy/hardener system so that it can easily counter the adverse effects caused by moisture, high temperature, and the addition of soft modifiers. Further modifying the tailored epoxy systems with specially designed toughening agents i.e. block copolymers and core-shell rubber particles, and investigating their influence on mechanical properties, fracture properties, and thermal properties.

A brief outline of the strategy followed to achieve the desired results:



Key research questions address the following topics:

(1) To which extent can the reference Bis-F based epoxy/hardener system (amine hardener based and anhydride hardener based) be strengthened by adding commercially available high functionality epoxy system by chemical modification?

(2) To which extent can the tailored epoxy system be toughened by block copolymer and core-shell rubber particles?

(3) To which extent and in which way do block copolymer and core-shell rubber particles affect or alter other mechanical properties e.g. stiffness, strength, thermal and viscoelastic properties of the tailored epoxy system at 23 °C and at 80 °C?

(4) To which extent will hybridization of different toughening agents affect or alter the important mechanical properties e.g. stiffness, strength, thermal and viscoelastic properties of epoxy systems at 23 °C and at 80 °C?

(5) Which tangible relationships between matrix toughness, other mechanical properties and the materials' structural features (morphology) can be derived for nanocomposites? The complexity of this task affords to concentrate on selected aspects which depend upon results gained during this work.

In order to find answers to the questions raised above, the following key research steps will be undertaken:

(1) Detailed examination of mechanical and thermal properties of systems obtained from the systematic variation of high functionality epoxy resins with standard bisphenol-F based epoxy resin will be performed for gaining insight into the mechanical and thermal performance of the tailored epoxy systems.

(2) Detailed examination of mechanical, fracture mechanical, thermal and viscoelastic properties of the tailored epoxy thermosetting matrix modified with BCP's and CSR particles. Systematic variation of BCP's and CSR particles volume concentration will be performed for gaining insight into mechanical and fracture performance.

(3) Detailed and thorough characterization of material properties and morphologies. Structural characteristics will be examined, e.g. the dimension and homogeneity of nanophase distribution in the nanocomposites.

(4) Development and understanding of related toughening mechanisms. Derivation and understanding the relationship between mechanical and fracture mechanical properties of the composites. Resulting knowledge is a key to tailor modified nanocomposites formulations for calender roller applications.

(5) Development of a material model to better understand and describe selected behaviors at the nano- and micro-scale.

3. State of the art

3.1 Epoxy resins

Epoxy resins are one of the most important thermosetting polymers which exhibit outstanding mechanical and thermal properties. Epoxy resins are polyether resins containing more than one epoxy groups in a molecule. Epoxy groups react with curing agents with or without the application of heat to form insoluble and infusible 3-D networks. Epoxy resins were first offered commercially in 1946. The first commercial possibilities for epoxy resins were realized in Switzerland by Pierre Castan of De Trey Freres and in the United States by Sylvan Greenlee of DeVoe and Raynolds. In 1936, Castan produced a bisphenol-A based epoxy resin via reaction with epichlorohydrin and subsequently prepared a thermoset composition after curing the resin with phthalic anhydride [14].

3.1.1 Structure of epoxy resin molecule

The term epoxy resins refer to a family of monomers that contain an oxirane/epoxy ring, which is a three-membered ring consisting an oxygen atom and two carbon atoms linked with one and two hydrogen atoms respectively, shown in Figure 3 [15]. The epoxy resin can be any molecule containing more than one of these epoxy groups. The number of epoxy groups per molecule is the functionality of the resin. The groups can be situated internally, terminally, on cyclic structures [1].

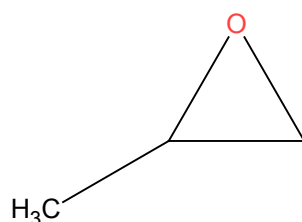


Figure 3: Chemical structure of epoxy (oxirane) ring [15].

If this ring is reacted with the suitable hardener, then a three-dimensional structure will be developed. The arrangement of the ring is in such a manner that a reaction involves either nucleophilic attack on one of the carbon atom or electrophilic attack on the oxygen atom as shown in Figure 4.

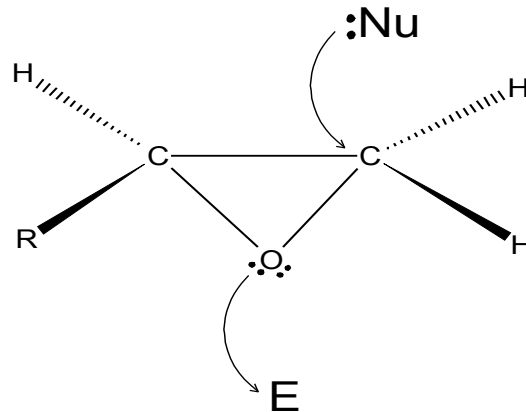


Figure 4: Mechanisms for the opening of the oxirane ring by either an electrophile (E) or a nucleophile (Nu) [16]

3.1.2 Synthesis of diglycidyl ether of bisphenol A

Epoxy resins are prepared from either epichlorohydrin or by direct epoxidation of olefins with peracids. The most important intermediate for epoxy resins is the diglycidyl ether of bisphenol A (DGEBA), which is synthesized from bisphenol A and epichlorohydrin. Figure 5 shows the synthesizing process of bisphenol A. Semi-solid or solid resins are synthesized by increasing molecular weight of the formulation by adding the more bisphenol A to liquid DGEBA. These solid resins are used as a cut in a solvent as maintenance primers for steel or as corrosion-resistant films. The higher the molecular weight is, the higher the viscosity and functionality of the resin are.

The curing (polymerization) process is a chemical reaction in which the epoxy groups react with a curing agent (hardener) and/or catalyst to form a highly crosslinked, three-dimensional network, which results in a hard, infusible, and rigid material [1]. The resulting physical and performance properties of the composites are determined by a combination of the selected epoxy resins, hardeners and/or catalysts, the curing temperature and curing schedule. Furthermore, the variation of cross-link density, and therefore the intrinsic ductility of the resulting unmodified epoxies determines the toughenability and the effectiveness of the various toughening mechanisms in the epoxies. Hence, a thorough understanding of the chemical and physical properties of unmodified epoxies is essential in order to the study of the toughening mechanisms of modified epoxies.

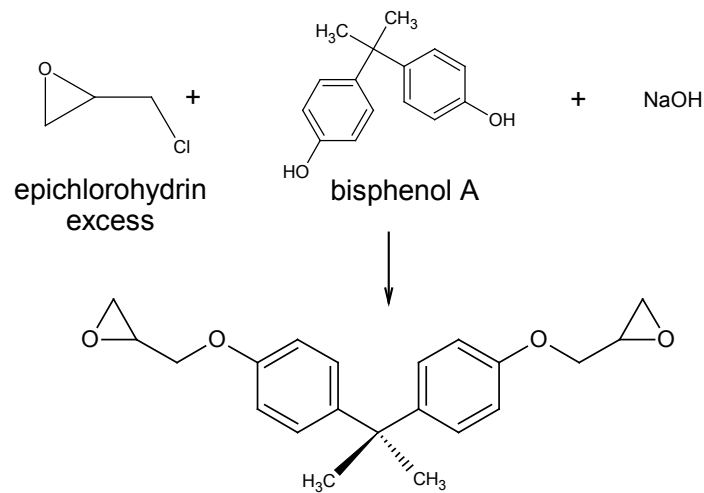


Figure 5: The Synthesizing process of Bisphenol A.

3.1.3 Curing of epoxy resins

The curing reactions of epoxy resins are stepped growth polymerization and chain homopolymerization, which is initiated by one or several curing agents and catalysts either separately or in combination [1, 17]. Both curing reactions are exothermic, proceeding without formation of by-products and with a low shrinkage rate because the curing reaction essentially proceeds by a ring-opening mechanism.

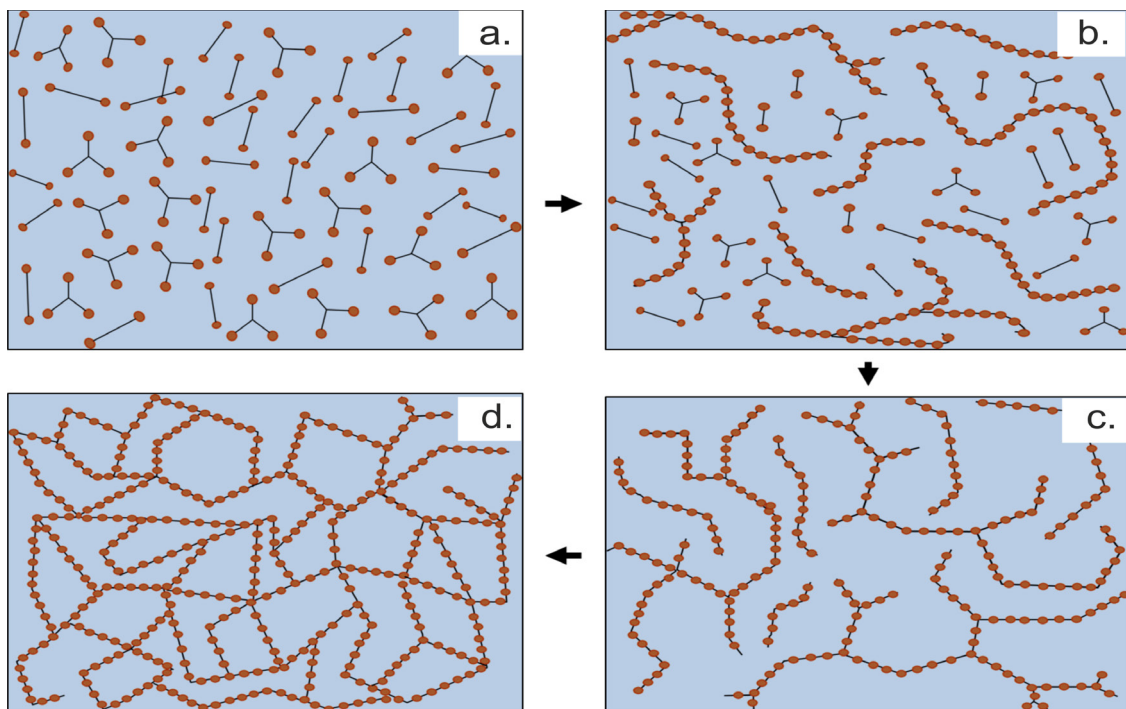


Figure 6: Schematic 2-D presentation of thermoset formation a) partially polyfunctional monomer b) linear and branched materials below gel point c) gelation started but incomplete cross linked network d) fully cured thermoset, cross-linked three-dimensional networks [18].

Though the selection of curing agents (also known as hardeners) or catalysts (accelerators) mostly depends on the manufacturing requirements and the final product requirements, the curing reactions of epoxy-hardener have a great influence on the degree of crosslinking and the type of bond formation within the structure [1]. The main reactive crosslinking agents (hardeners) are polyfunctional primary and secondary amines and dibasic or acid anhydrides. Tertiary amines are usually used as accelerators. Once the curing of hardener is completed with epoxy resin, a three dimensional crossed linked structure is obtained which is shown in Figure 6

3.1.4 Basic mechanism of ring opening of epoxy group

The epoxy resin may react in either of two ways i.e. anionically or cationically.

1. Anionic Reaction

In the anionic reaction, the epoxy group is opened to produce an anion as shown in Figure 7. The anion produced is an active group and is, therefore, capable of further reaction.

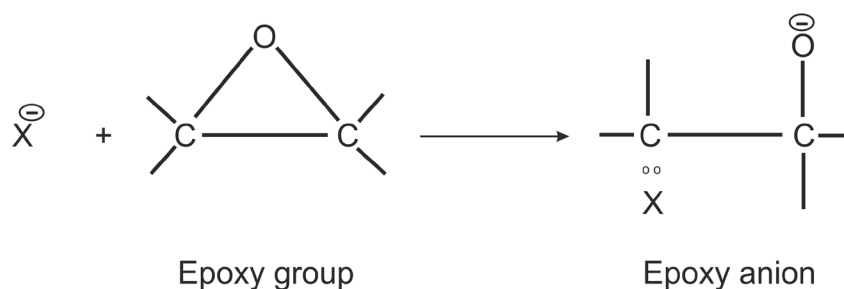


Figure 7: Anion formation of the epoxy group [19]

2. Cationic Reaction

During the cationic reaction, the epoxy group is opened by active hydrogen to give a new chemical bond and a hydroxyl group. This means there are a number of ways in which the cationic mechanism may proceed, and three possible routes are shown in Figure 8. The two reaction mechanisms allow the epoxy group to react with many chemical groupings. The cationic route means that epoxy resins may be cured by basic curing agents. Basic curing agents commonly used are - Lewis bases, inorganic bases, amides and secondary and primary amines.

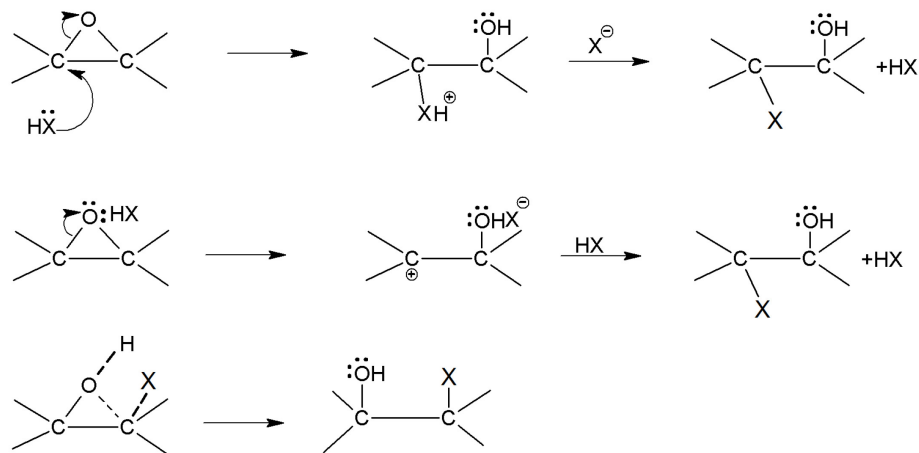


Figure 8: Cationic formation in epoxy group, reproduce from [21]

3.2 Time, temperature and cure

Time and temperature are most important parameters for selecting a cure cycle. For producing an epoxy based composite with desired mechanical properties one requires precise control of the curing cycle. Temperature not only controls cure rates but also reaction pathways. High-temperature cure favor cross-linking thus producing rigid composites and low-temperature cure favor chain extension producing flexible composites.

3.2.1 Gelation

Gelation is defined as the point at which covalent bonds connect across the network and an infinite molecular network is formed. A thermoset loses its ability to flow freely and is no longer processable above gel point, therefore setting the upper limit of the working life. According to Flory's theory of gelation [20], it occurs at a specific point of chemical conversion for a given system and depends on the curing system and the environment in which the reaction takes place. Practically, the gelation occurs when the bulk polymer transforms from the liquid state to a rubbery state. This is observed by the deflection of the viscosity towards infinity.

3.2.2 Vitrification

It is the process in which a polymer enters in to a glassy state. Vitrification slows down the chemical conversion process. The Vitrification point of a reacting system is the point at which further reaction is stopped. Wisanrakkit et al [21] showed slow diffusion controlled reactions may occur in the vitrified state. Basically, Vitrification is

not considered as a point rather it's a gradual process that extends over a large part of the curing process [22].

The most commonly perceived cure diagram is the isothermal time temperature transformation (TTT) cure diagram, which was developed by Gillham [23], to relate the properties of thermosetting systems to process conditions. TTT diagram was developed by using Torsional Braid Analysis to see when the onset of gelation and vitrification takes place in polymer and later he adopted the same for epoxy resin curing as well. Figure 9 shows gelation and vitrification process.

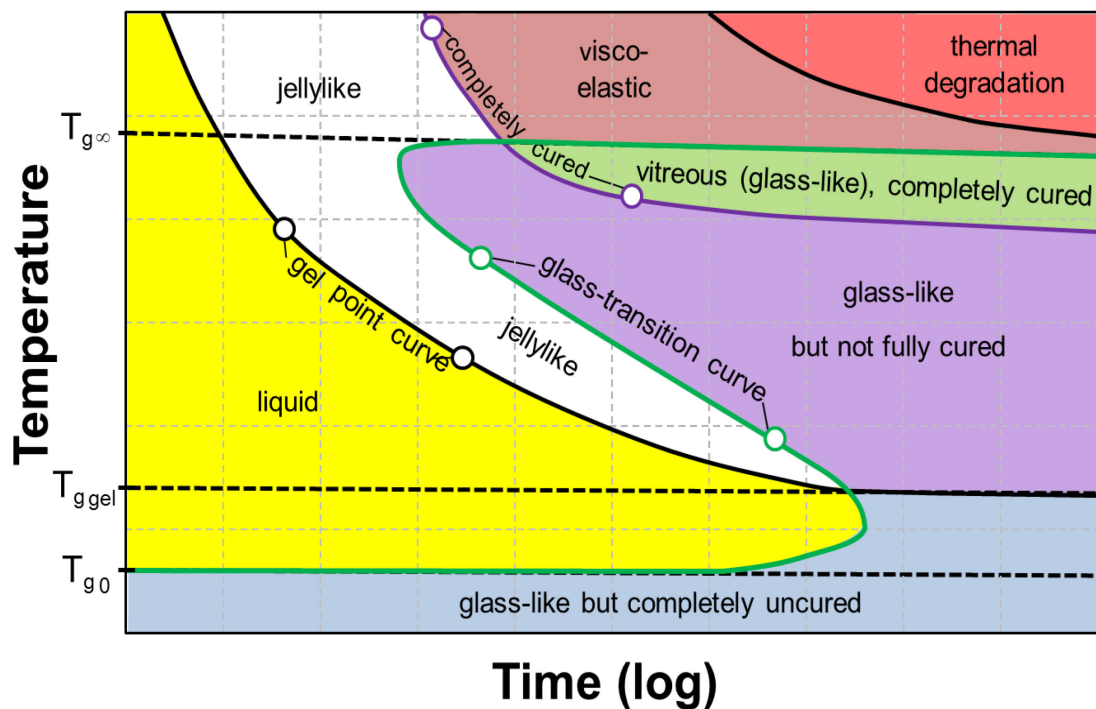


Figure 9: Isothermal cure time-temperature-transformation (TTT) for a thermosetting system [24]

3.3 Factors affecting the final cured properties of epoxy/hardener system

3.3.1 Stoichiometry

Stoichiometry is the exact amount of hardener (curing agent) to be added to the resin such that the number of the reacting groups of resin and hardener are equal. The stoichiometric ratio is considered important variable in controlling the final structure and it significantly affects properties such as glass transition temperature, modulus, crosslink density, and strength. The effect of the stoichiometric ratio of epoxy resins and curing agents in order to govern the degree of crosslinking were reported by several researchers. Mostovoy et al. [25] show that the ultimate tensile strength

reaches its maximum value at stoichiometry while others [26] [27] shows that the ultimate strength was insensitive to the stoichiometric ratio. It can be inferred that varying the stoichiometric ratio would definitely alter the chemical composition of the materials. Properties such as resin/hardener ratio, hardener chemistry, and resin/hardener molecular ratio are known to affect the visco elastic properties of the thermosetting epoxy resin systems [28]. Some researchers reported [29] [30] [31] that the antiplasticization phenomenon occurs when the non-stoichiometric variation of hardener is done with epoxy, which leads to an increase in quasi-static modulus with a decrease in glass transition temperature.

3.3.2 Monomer functionality

The thermosetting polymers form a cross linked three-dimensional network from the monomers which have a functionality greater than two. This causes the fundamental property difference between thermosets and thermoplastics. In the case of thermoplastics, the polymer chain grows in the linear direction where all the monomers have the functionality of two. Monomer functionality has a significant effect on the cross link density of a thermosetting polymer. A monomer with the functionality of three can form half as many crosslinks in its final structure than a monomer with the functionality of four. A higher crosslink density means more dimensional stability, high glass transition temperature, and higher mechanical strength.

3.3.3 Monomer's chemical structure

Monomer size plays an important role in crosslink density of the thermosetting polymer. The chemical structure affects the glass transition temperature by affecting the mobility.

- Increasing main chain polarity increases the T_g .
- Bulky side groups increase the T_g of the final cured system.
- Increasing the length of flexible side groups lowers the T_g of the system.
- Flexible main chain components lower the T_g

3.3.4 Influence of curing duration

In the case of snap cure some of the unreacted polymer chains do not have sufficient time to connect the reacting sites within the network to which they can cross link. Sometimes the snap cure causes the higher shrinkages as compared to longer cure cycles [32]. In the case of longer cure, the rate of reaction is much slower and the unreacted polymer chains have sufficient time to orient themselves to the correct position for cross linking reactions to occur. Depending upon the final product and the kind of properties needed, one should carefully select the type of cure i.e. longer cure or faster cure.

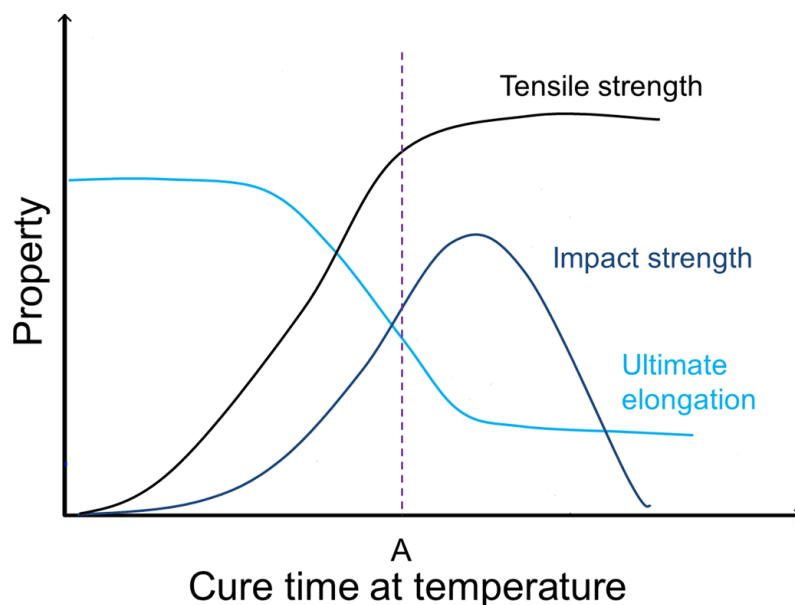


Figure 10: Optimization of cure schedule for thermosetting plastics. Optimum properties occur at point A, reproduce from [33].

3.3.5 Degree of cure

Theoretically, the state when all the reactive sites are reacted during cure until the conversion has been stopped may be defined as the maximum 'Degree of cure'. In more practical terms, a properly cured system is one in which the degree of crosslinking is sufficient enough to provide optimum properties for a particular application. During the curing mainly two conditions of the reactions involved, the first are crosslinking (formation of three-dimensional networks of molecules through reactive constituents) and second is conversion (the desertion of reactive elements). In highly cross-linked networks, sometimes the reactive groups are sterically hindered from reacting and this ultimately leads to the incomplete reaction between

hardener (ex. amine or anhydride) and the epoxy group as a consequence of caging effect [34].

3.4 Glass Transition Temperature

The glass transition temperature (T_g) is defined as the temperature at which the forces holding the different constituents of a polymeric material together are overcome so that these constituents are able to undergo large-scale viscous flow, limited mainly by the inherent resistance of each component to such flow [35].

Mechanical properties show significant changes in the region of the glass transition. For example, the Young's modulus may decrease by a factor of 1000 times as the temperature raises to the glass transition region in the cured epoxy system. Many other physical properties like tensile strength, ultimate elongation coefficient of thermal expansion, heat capacity, and refractive index in the thermoset systems change drastically with the temperature in glass transition zone.

When a polymer is heated to its glass transition temperature, it gains sufficient thermal energy to be able to surpass two type of hindrance to the large-scale motion of its components:

- a. Internal friction between individual components is somehow responsible for resisting the viscous flow. This resistance to the viscous flow is further related to the geometrical and topological arrangements of their atoms. It is expressed by the concept of chain stiffness. The glass transition occurs when there is enough freedom of motion for chain segments up to several statical (Kuhn) segments in length to be able to execute cooperative motions [36]. As a general rule, the length of Kuhn segments increases with increasing chain stiffness.
- b. The cohesive forces responsible for holding different components together consist of Van der Waals forces between different molecules and molecular segments which are somehow applicable to everything. The main components for the T_g in amorphous polymers are chain segments. The cohesive forces can be measured in terms of properties such as cohesive energy density. The increase in polarity increases the cohesive forces which ultimately lead to the increase in glass transition temperature [37].

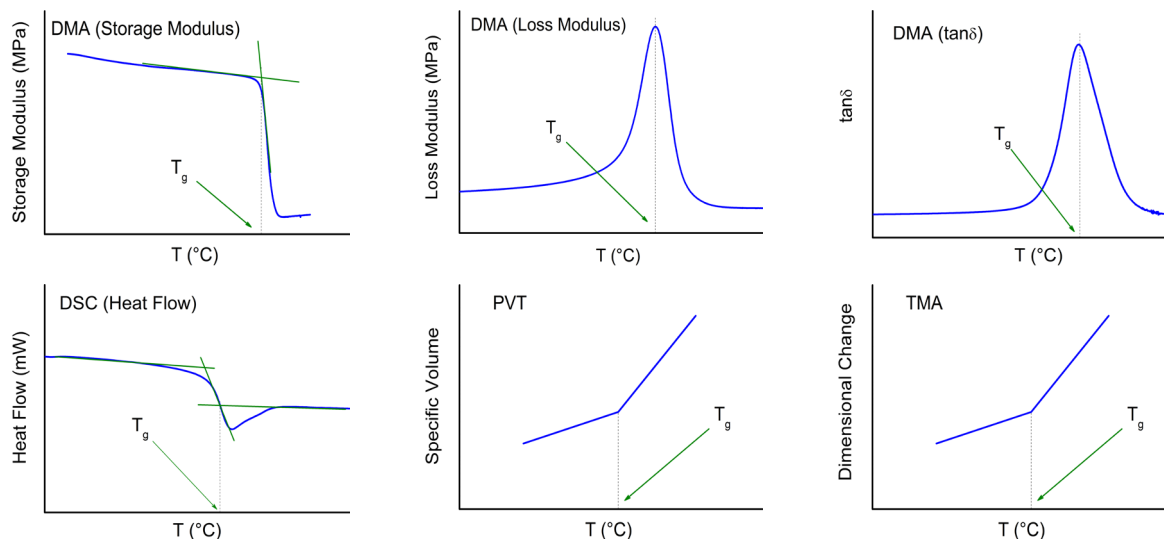


Figure 11: T_g determination using experimental techniques (a) At the drop in storage modulus at 1Hz frequency (b) Max. peak of loss modulus curve at 1Hz frequency (c) Max. peak of the $\tan \delta$ curve at 1Hz frequency (d) Mid-point of the drop in the heat flow (e,f) point of intersection of linear regions.

3.5 Mechanical and fracture properties

a. Strength: The strength of material is the maximum tensile stress that it can take before failure. There are three type of strengths (i) Yield strength (stress sustained by material without permanent deformation) (ii) Ultimate strength (maximum strength a material can with stand) and (iii) Breaking strength (stress at which rupture takes place) as shown in Figure 12.

The polymers follow the following order of increasing strength: linear < branched < cross-linked < network structures [38].

Strength of polymers depends upon the following factors [38]:

1. **Crystallinity:** The crystallinity of the polymer increases strength, because in the crystalline phase, the intermolecular bonding is more significant. Hence, the polymer deformation can result in the higher strength leading to oriented chains.

2. **Molecular Weight:** The tensile strength of the polymer rises with increase in molecular weight and reaches the saturation level at some value of the molecular weight. Relation between tensile strength and molecular weight is given by following equation.

$$\sigma = \sigma_{\infty} - \frac{X}{M_w} \quad (3.1)$$

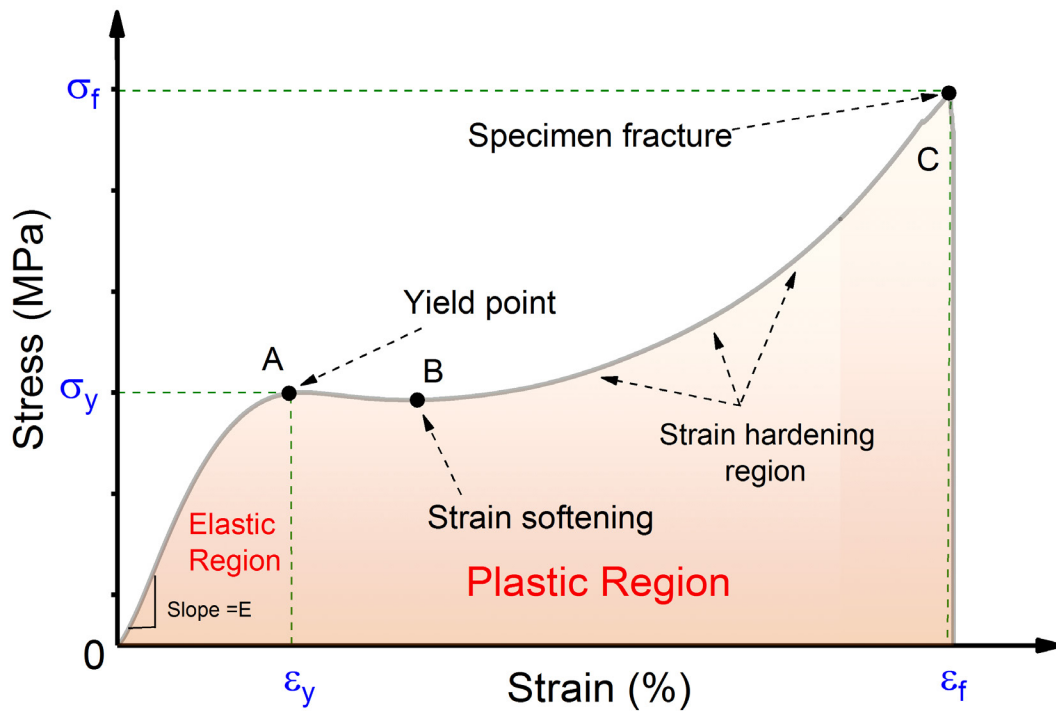


Figure 12: Representative stress-strain curve for epoxy amine system from compressive test measurement, showing different regions.

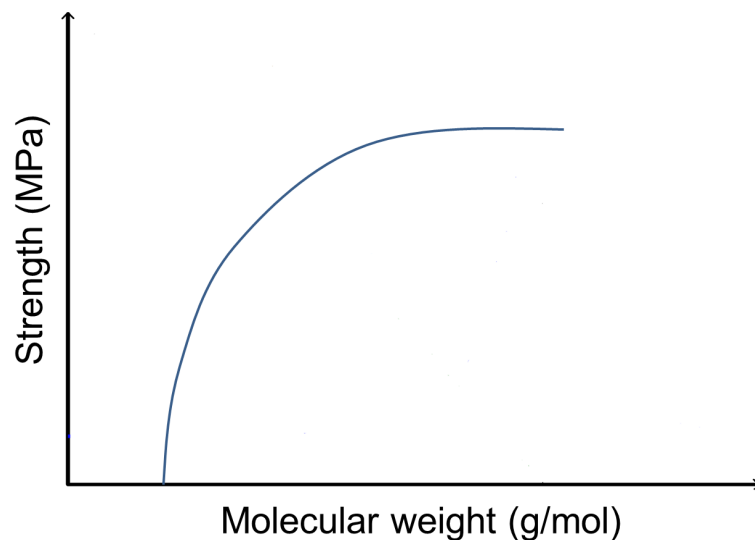


Figure 13: Tensile strength variation with molecular weight of the polymer, reproduced from [38].

where σ_{∞} is the tensile strength of the polymer with molecular weight of infinity. X is some constant, and M_w is the molecular weight. At lower molecular weight, the polymer chains are loosely bonded by weak van der Waals forces and the chains can

move easily, led to low strength. In case of large molecular weight polymer, the chains become large and hence are entangled, giving strength to the polymer.

3. Cross-linking: The cross-linking forms a three dimensional network and restricts the chain motions which led to increase in tensile strength.

b. Percentage elongation to break: It is the strain in the material on its breakage. It measures the percentage change in the length of the material before fracture. It is a measure of ductility. Thermosets (< 5 %) value of elongation to break in tensile mode.

c. Young's Modulus (Tensile Modulus): Young's Modulus is the ratio of stress to the strain in the linearly elastic region. Elastic modulus is a measure of the stiffness of the material.

d. Toughness: The toughness of a material is given by the area under a stress–strain curve as shown in Figure 12. The toughness measures the energy absorbed by the material before it breaks.

e. Brittleness: Material which is liable to break or fragile in nature is called brittle material. In this thesis brittleness is used to describe fractures in which sharp cracks propagate through bodies with small amounts of deformation around the tip [39].

f. Ductile: Opposite to brittle or ability to be drawn into wire is called ductile. In this thesis ductile failure refers when there is large-scale deformation around the crack, often leading to observable crack tip blunting [39].

3.6 Yield behavior of unmodified epoxies

Compression tests are performed to study the yield behavior of unmodified epoxies [40]. Epoxies are the brittle materials due to high cross linked structure, and they usually fracture before yielding in tensile tests at a temperature lower than their glass transition temperature [41]. On contrary, unmodified epoxy shows yielding and plasticity under compression, even at lower temperature [42] [43]. The different regions in the typical compressive strain-strain curve are further discussed in upcoming chapters. The yielding phenomenon in epoxies is dependent on factors such as strain rate, temperature, and hydrostatic pressure. The yielding behavior of amine cured DGEBA epoxies with different crosslink densities increased as testing strain rate increased or the temperature is decreased [42]. The same trend was

reported by other researchers confirming the strain rate and temperature dependence of the yielding behavior of unmodified epoxies [43] [44]. Several models are described to explain the pressure, temperature and strain rate dependence of the yield behavior of the epoxies. Initially, these models are developed for describing the yield behavior of thermoplastic polymers. If these models are applied to unmodified epoxies then excellent predictions can be made up to yield point. Here we briefly discuss only one such model.

3.6.1 Modified Von Mises yield criterion

The Von Mises criterion describes the pressure dependence of the yield behavior of the unmodified epoxies [45] [46] [47] as shown in equation

$$(\sigma_1 - \sigma_2)^2 + (\sigma_2 - \sigma_3)^2 + (\sigma_3 - \sigma_1)^2 = 6(\tau_y^0 + \mu p_{hs})^2 \quad (3.2)$$

where σ_1 , σ_2 , and σ_3 are the principle stresses, τ_y^0 is the shear stress in pure shear and under zero pressure, $p_{hs} = -\frac{(\sigma_1 + \sigma_2 + \sigma_3)}{3}$ is the hydrostatic pressure, and μ is the internal friction coefficient. The standard Von Mises yield criterion is modified by letting the shear stress τ_y^0 vary linearly with the fraction of the hydrostatic pressure.

3.7 Fracture behavior of unmodified epoxy

The unmodified epoxies are prone to brittle failure, in which fracture is dominated by a tensile stress field, where the problems of stress concentrations at defects (cracks) become significant. The fracture behavior of these epoxies has mainly been studied through the application of linear elastic fracture mechanics (LEFM) [48], since they are very brittle materials with only localized plastic deformation during fracture. Hence, the quantitative measurement of the resistance to fracture for epoxies is normally in terms of a critical strain-energy release rate or fracture energy, G_{IC} (energy per unit area necessary to generate a new crack surface) or a critical stress intensity factor, K_{IC} (value needed to produce catastrophic failure under simple uniaxial loading in presence of natural crack) under plane strain conditions. Most of the time, only Mode I (opening mode) crack propagation is considered because it is technically more important than other crack propagation modes (mode II: In- plane shear and mode III: Out of plane shear) and gives the lowest value of toughness

which is quite important in design consideration as shown in Figure 14. The Mode I fracture energy, G_{IC} , of unmodified epoxies is typically in the order of 100-300 J/m² at room temperature [49]. However, energy dissipation processes in the form of plastic deformation must still take place during fracture, because of the values of G_{IC} , are far higher than the energy theoretically estimated for purely brittle fracture [48]. This finding was evidenced by fractography observations of riverline patterns, caused by matrix tearing, randomly emanating from the initial crack front [50], as shown in Figure 15.

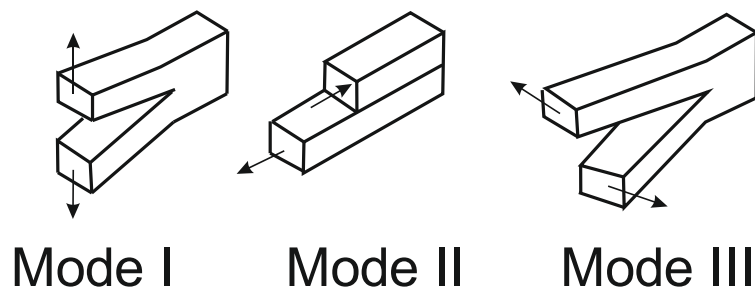


Figure 14: Different crack modes. Mode I (Opening), Mode II (In plane shear) and Mode III (Out of plane shear).

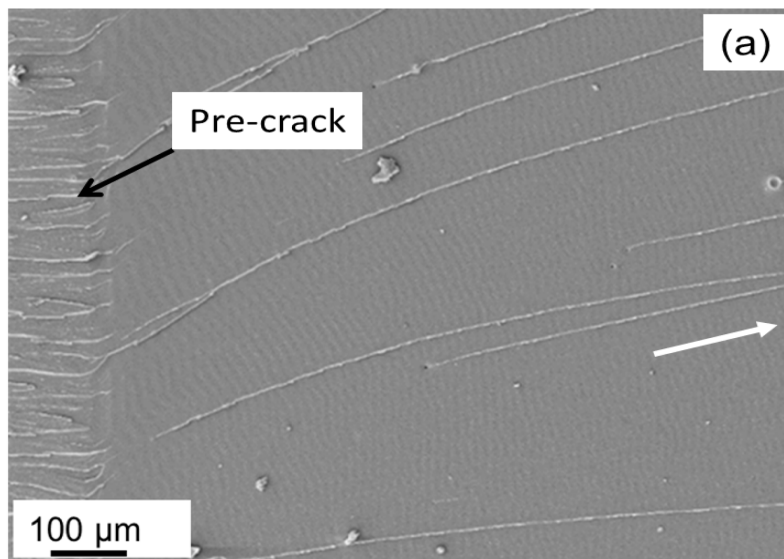


Figure 15: SEM image of river lines starting from the crack front of an unmodified anhydride cured DGEBF epoxy. White arrow represents crack propagation direction.

Three main types of crack propagation are observed in the fracture of unmodified epoxies (also in toughened epoxies) depends on the test temperature and test loading rate [51]. These are stable brittle propagation, unstable semi-brittle propagation and stable ductile propagation as shown in Figure 16.

The influence of strain rate and temperature on the fracture behaviour of an unmodified epoxy depends on strain rate and temperature dependence of the yield

stress, since according to LEFM the yield stress governs the size of the plastic deformation zone and crack tip blunting process [47]. According to the equation (3.3) the radius of curvature of blunting tip and plastic deformation zone during the crack propagation is inversely proportional to yield stress. For unmodified epoxy the decrease in yield strength value will increase the G_{IC} .

$$r_{pzu} = \left(\frac{1}{6\pi}\right) \left(\frac{1}{\sigma_{yt}}\right)^2 \frac{G_{IC}E}{(1-\nu^2)} \quad (3.3)$$

For constant strain rate, a decrease in temperature results an increase of yield strength and further decrease of G_{IC} . Therefore, the stable brittle crack propagation occurs at low temperature, and unstable brittle crack propagation seen at higher temperature. Secondly, at a constant temperature, a lower strain rate causes a reduction in yield strength and an increase in G_{IC} , which led to stable brittle crack propagation at higher strain rate, but unstable semi-brittle crack propagation at low strain rate.

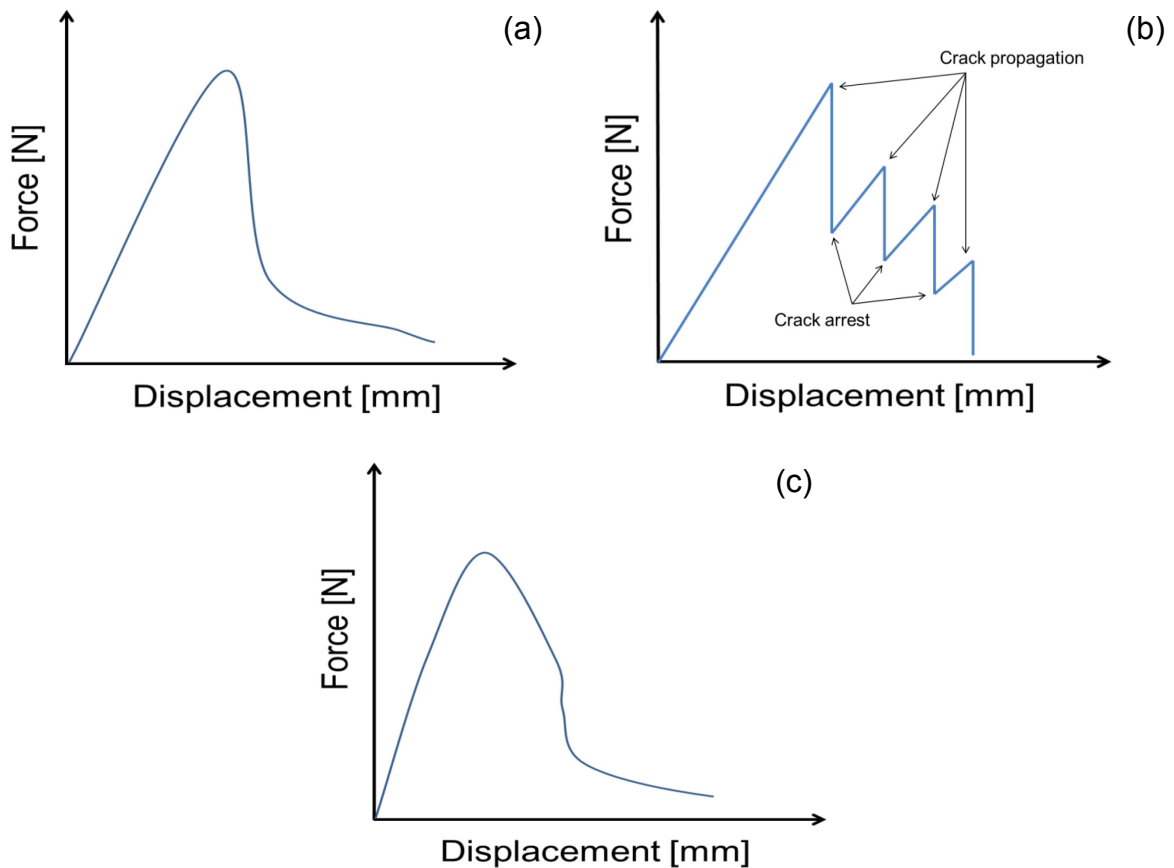


Figure 16: Force displacement diagram for (a) stable brittle crack propagation, (b) unstable brittle crack propagation, and (c) stable ductile crack propagation of unmodified epoxy in SENB test [51]

3.8 Toughening approaches for unmodified brittle epoxy matrices

Appropriate literature survey suggests that there are many ways to enhance the toughness of unmodified epoxy resins. They are as follows:

- a. Chemical modification of the epoxy resin to make it more flexible
- b. Addition of thermoplastics dispersed elastomeric phase
- c. Incorporation of hard inorganic particles like silica, alumina, titanium

3.8.1 Toughening via chemical modification

As discussed in the above paragraph briefly about the chemical modification, this can be done by the addition of plasticizers to promote the ductile fracture mechanisms such as shear yielding or tearing. These plasticizers are also called chain extenders because they increase the chain length and make the whole network more flexible. Reactive diluents [52], aniline [53], poly (ethylene glycol) [54] are more adaptively used as plasticizers and chain extenders for reducing the crosslink density.

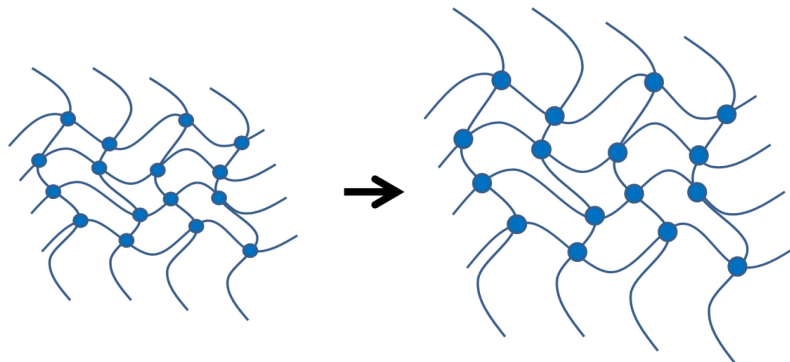


Figure 17: Toughening of epoxy polymers by chemical modification.

Interpenetrating polymer network (IPN), Figure 18, is an alternate method to toughen the brittle epoxy polymers. An interpenetrating polymer network is a type of network in which two polymers combine together to form a network [55]. The second polymer needs to be mixed with epoxy in order to create IPNs. These IPNs can be formed simultaneously or sequentially by independent reactions but the proper bonding between them will enhance the mechanical properties. This is because of the increase in the bond formation caused by permanent entanglement of chains. Many of the researchers have reported the use of thermosets such as unsaturated polyesters [56] [57], cyanate esters [58] and elastomers such as polyurethane [59] to create IPNs.

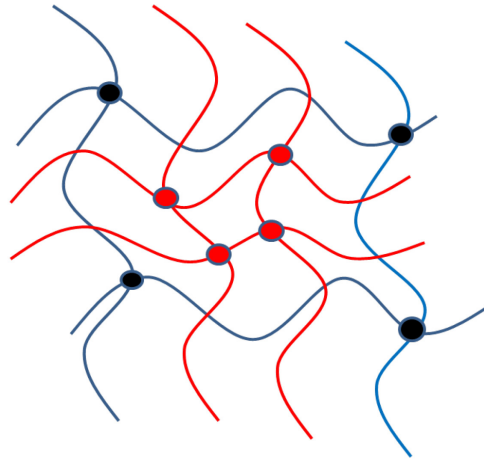


Figure 18: Interpenetrating Polymer Network (IPN)

The chemical modification show some improvement in fracture toughness values. However, it further causes the reduction in glass transition temperature and other mechanical properties like tensile modulus and tensile strength, therefore these methods are not widely used.

3.8.2 Addition of Rubber particles

As epoxies are brittle in nature and prone to develop micro-cracks due to the lack of good energy dissipation mechanisms under the application of stress, several researchers have focussed on increasing the ductile nature of them by introducing the ductile materials as the second phase. The results pointed out to the use of rubber particles which are effective in increasing the ductility during the fracture by plastic deformation and rubber cavitation. It was first attempted by Aylsworth [60] when he was trying to create a tough, crosslinked material for Thomas Edison's phonograph records by using polymer composition of phenols and rubber crosslinked with sulfur. He found that the rubber adheres with great tenacity to a hard phenolic condensate when vulcanized therewith, making an improved polymer-rubber composition very super to the neat polymer.

Generally, the rubber particles are blended with the epoxy thermoset resin before curing them with the hardener. An elastomeric modifier is incorporated into the epoxy matrix as a second phase and there is an improvement in toughness without a significant reduction of the T_g and mechanical properties. The different types of rubber modifiers that have been in practice so far are a carboxyl-terminated copolymer of butadiene and acrylonitrile (CTBN), an amine-terminated copolymer of

butadiene and acrylonitrile (ATBN) [52], a multi-functional liquid rubber (nitrile-diene-acrylamide terpolymer) developed by the Wolverine Gasket division of Eagle-Picher Industries [61], rubbers having end groups like amine [62], mercaptan [63], and hydroxyl [64]. The work which was done by Cunliffe et al. [65] is a proof that rubbers increased the shear strength of the epoxy-based adhesive system. They have generated rubber-modified epoxy prepared by anionic polymerization of monomers such as isoprene, butadiene, and acrylonitrile. But the main problem with their method was that the instability of the rubber particles which tended to agglomerate upon curing. Rezaiford and co-workers [66] have used poly (methyl methacrylate) (PMMA) grafted natural rubber instead of CTBN for toughening of epoxy and have achieved adhesive joint failure strengths by controlling the resin solubility parameter. The pre-formed elastomeric particles also come under the category of rubber modification of epoxy polymers. These are the particles formed by a rubber core surrounded by a thin glassy shell which does not allow the rubber particles to agglomerate. They are also called core-shell rubber particles (CSR). Butadiene, butyl (acrylate), styrene butadiene or siloxane are used for the core material and PMMA as the commonly used shell material. Giannakopoulos and co-workers [9] have modified epoxy resin by the addition of pre-formed core-shell rubber particles of size 100 to 300 nm in diameter and confirmed that the glass transition temperature T_g of the used epoxy polymer was unchanged even after curing though there is a significant decrease in Young's modulus and tensile strength. The fracture energy was also increased from 77 J/m² to 840 J/m² for the epoxy with 15 wt. % of 100 nm diameter CSR particles.

Table 1: Properties of an epoxy resin modified with different toughening phases, [5 wt. %] [67]

Polymer	Flexural Modulus [GPa]	Flexural Strength [MPa]	K_{IC} [MPa.m^{1/2}]	G_{IC} [kJ/m²]	T_g [°C]
EP (Epoxy)	3.12	149.1	0.55	0.142	140.1
EP / Acrylic Rubber	2.74	127.8	0.87	0.299	143.4
EP / Core Shell Rubber	2.94	108.4	0.93	0.358	142.5
EP / CTBN	3.08	122.9	0.74	0.259	134.2
EP / ABS	2.92	122	0.79	0.323	143.8
EP / PDMS	2.57	122.7	0.72	0.259	137

This was in contrary to the epoxy system modified with CTBN rubber where there was a decrease in glass transition temperature but larger toughening effect than that of CSR particles modified epoxy.

By employing emulsion polymerization techniques, the size, morphology, shell thickness, and crosslink density of the rubber cores can be controlled [68]. However, the toughening effect of rubber particles is largely dependent on the molecular weight M_w and the functionality of the rubber particles. So, when selecting the rubber, care should be taken that it is a low molecular weight liquid to ensure easy miscibility with the epoxy resin, have functional groups capable of reacting with the base epoxy resin, and have borderline miscibility with the epoxy resin [52]. Table 1 summarizes the properties of an epoxy resin modified with different elastomeric secondary toughened phases.

3.8.3 Addition of Thermoplastics

The addition of thermoplastics to epoxy has been reported by several researchers and this approach is recognized as an alternative to rubber toughening in order to improve the toughness of brittle epoxy networks. Thermoplastics such as poly (phenylene oxide) (PPO) [69], poly (ether imide) (PEI) [70], poly (ether ether ketone) (PEEK) [71] and poly (ether sulphone) (PES) [72] [73] added to epoxy in order to tailor the fracture properties of the whole system without reducing the glass transition temperature. Thermoplastics are dispersed in epoxy by reaction-induced phase separation [74] or either by the suspension of pre-formed particles. Studies show that morphologies of these systems have a direct influence on the properties of modified systems [73] [75]. In some cases, the satisfactory results have been achieved using thermoplastics as toughening agents in epoxy matrices but they could not bring significant improvement in fracture toughness and in some cases even fracture toughness value decreases due to poor filler-matrix adhesion [76]. Further epoxy-thermoplastic systems also have processing issues, which is due to poor compatibility between the uncured epoxy resin and toughening phase [77].

3.8.4 Block copolymers (BCP)

When two or more chemically distinct monomers joined together by covalent bonds to form blocks of repeating units, they are called block copolymers (BCP) [78]. They

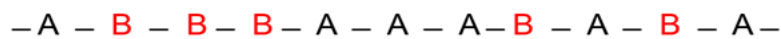
have gained importance as the latest type of rubbery modifiers which are used for toughening epoxy polymers. There are different types of copolymers such as an alternating copolymer, random copolymer, block copolymer, and graft copolymer [79]. According to the International Union for Pure and Applied Chemistry (IUPAC) recommendations, Jenkins et al. [79] summarize the definitions of above copolymer types. Homopolymer is a polymer derived from one species of monomer, copolymer is a polymer derived from more than one species of monomer, random copolymer is a copolymer consisting of macromolecules comprising two species of monomeric units in alternating sequence, and graft copolymer is the one in which adjacent blocks comprise constitutional units derived from different species of monomer or from the same species of monomer but with a different composition or sequence distribution of constitutional units.



(a) Homopolymer



(b) Alternating copolymer



(c) Random polymer



(d) Block copolymer



(e) Graft polymer

Figure 19: Different types of copolymers, reproduced from [79].

Liu et al. [80] from their work reported that, with an incorporation of 5 wt. % of the BCP material into bisphenol A-based epoxy resin, there was an improvement in the fracture toughness of 100% over the neat epoxy resin. This is because in general, at low concentrations in epoxy resins, a BCP may self-assemble into well-defined micro/nanostructures in the form of three distinct morphologies; spherical micelles, wormlike micelles, and vesicles. The type of structure formed depends on the molecular weight, block length, composition, and block-block and block-matrix

interaction parameters. These morphologies mimic those of the BCP when dispersed in selective solvents or homopolymers. Symmetric BCPs tend to form spherical micelles in the dilute limit when the solvent or homopolymer is highly selective for one block, whereas asymmetric BCPs form either wormlike micelles or vesicles. Such kinds of BCPs are called as amphiphilic block copolymers [81].

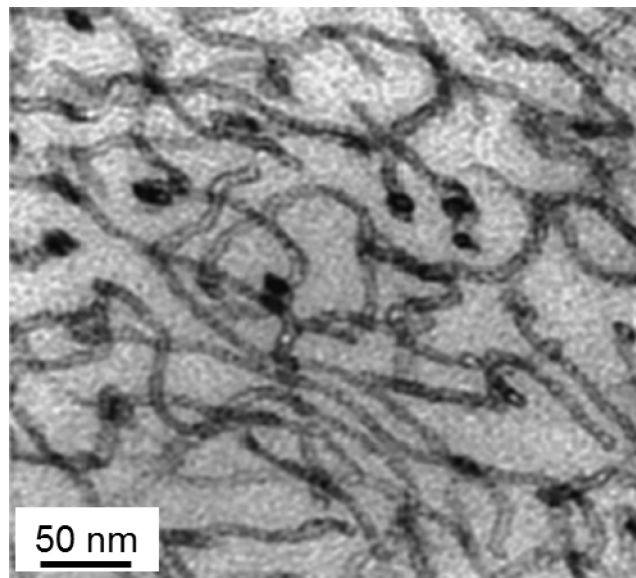


Figure 20: TEM image showing wormlike micelles [82]

Several combinations of regular BCPs and amphiphilic BCPs are possible depending on the required toughening of the epoxy resin. These BCPs may have an epoxy miscible block (hydrophilic core) and an epoxy immiscible block (hydrophobic core) which is cause for the formation of the micelle structures and microphase separation at the scale of approximately 10s of a nanometer. This is mainly because of the thermodynamic immiscibility of the blocks present in the block copolymers.

The number of polymer chains that assemble to form a micelle is the aggregation number [83] [84]. In the simplest form, the aggregation number (N_{ag}) is given by the equation as $N_{ag} = M/M_o$ where M is the molecular weight of one micelle and M_o is the molecular weight of the polymer backbone [84]. The critical micelle concentration is defined as the concentration at which micelles will start to form to reduce the system free energy. The hydrophilic blocks will aggregate to form the outside of the micelle in contact with the epoxy, almost like a shell, to shield the hydrophobic block in the center as the core. But, there is a possibility for the self-assembled structures to be destroyed at the higher temperatures.

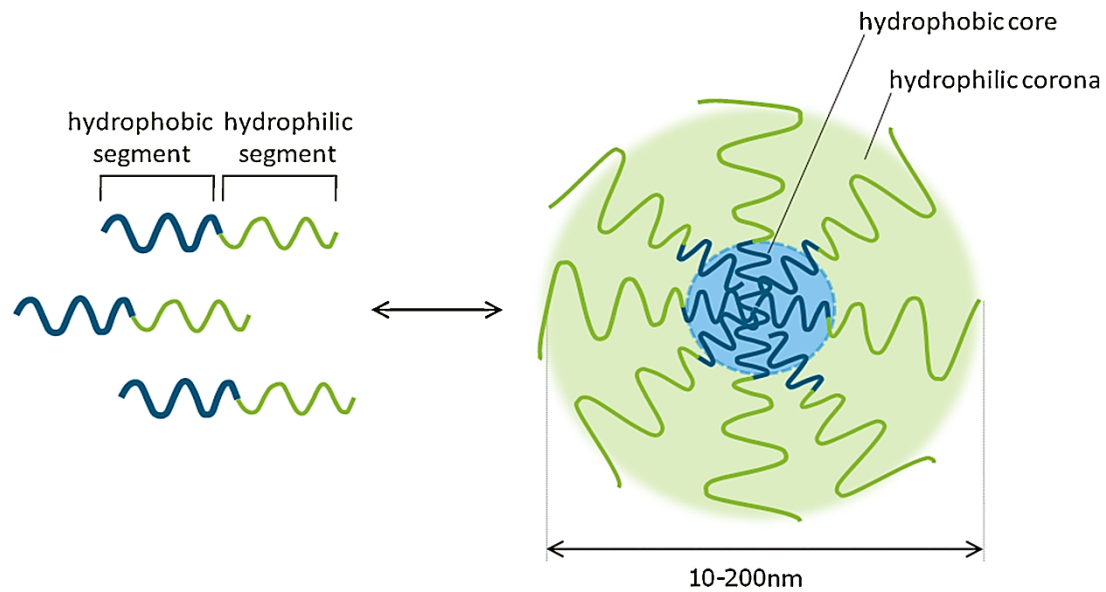


Figure 21: An illustration of spherical polymer micelle formation in an aqueous environment by self-assembling of hydrophobic and hydrophilic cores [83]

These micelles also found to change their structures and transform from one structure to another based on the modifier content. The same was reported by Ritzenthaler et al. [85] when they characterized the change in morphology of the polystyrene-polybutadiene-poly (methyl methacrylate) (SBM) phase with modifier content. The particles change from a core-shell structure (Figure 22 (a)) to spheres on spheres or raspberry-like structure (Figure 22 (b) and Figure 22 (c)) to cylindrical PB blocks around a sphere (Figure 22(d)). An increase in particle size with modifier content was also observed which was in contrast to an SBM BCP with higher PB block ratios, where a core-shell onion-like structure was observed (compare Figure 22(d) and Figure 22 (e)). The morphologies tend to be close to that of the neat BCPs at very high weight percentages up to 80 wt. % as shown in Figure 22 (f).

Barsotti et al. [86] reported a higher value of fracture toughness for epoxy system modified with block copolymer poly (methyl methacrylate)-b-poly (butyl acrylate)-b-poly (methyl methacrylate) (MAM) than that of the epoxy system modified with CTBN at the same wt. % of loading. Different researchers from their research have summarized that the BCPs are capable of toughening the epoxy system to a higher toughness when compared to traditional homopolymers and random copolymer toughening agents but they also tagged the same BCPs as a reason for the reduction of Elastic modulus, tensile strength and also the glass transition temperature T_g .

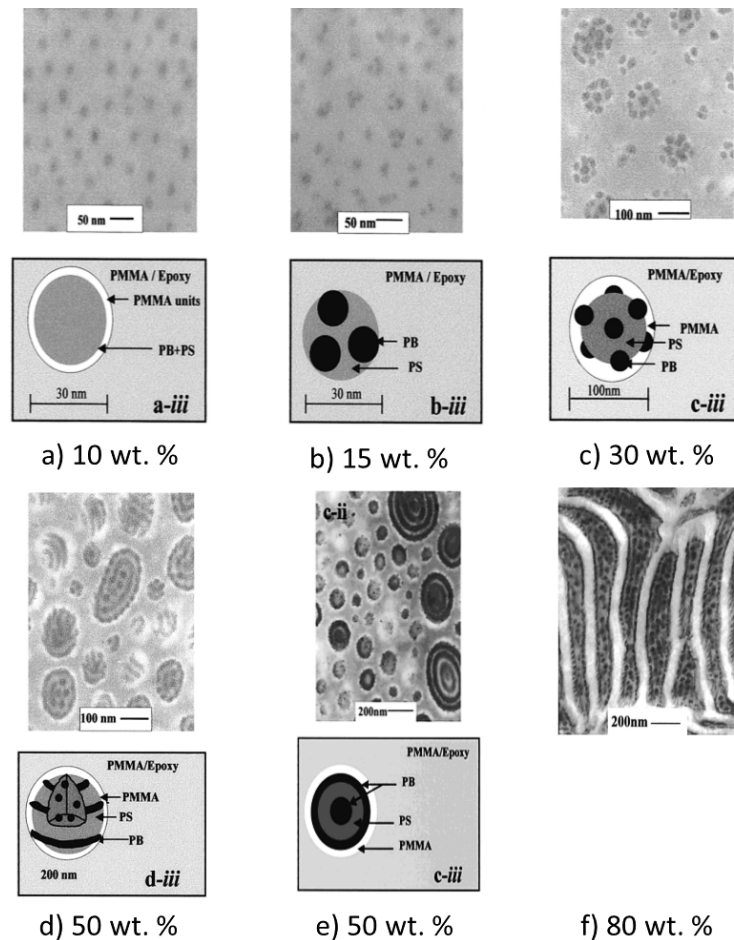


Figure 22: Variation of the morphology of SBM BCP with varying content [85].

Barsotti et al. [12] compared the fracture toughness improvement ability of block copolymer and CTBN in the same epoxy system but using another block copolymer poly (methyl methacrylate)-*b*-poly (butyl acrylate)-*b*-poly(methyl methacrylate) (MAM). These researchers reported that MAM modified epoxies have a significantly higher fracture toughness than the CTBN modified epoxies by adding the same wt. % loading. They reported that, for example, in a dicyandiamide (DICY) cured DGEBA epoxy, 5 wt. % MAM modified epoxy gave a value of $K_{IC} = 1.64 \text{ MPa}\cdot\text{m}^{1/2}$ while a value of $K_{IC} = 1.32 \text{ MPa}\cdot\text{m}^{1/2}$ was measured for a 5 wt. % CTBN modified epoxy. Pearson et al. [87] compared the fracture toughness improvement ability of SBM block copolymer, core-shell rubber particles and CTBN rubber on a lightly cross-linked piperidine cured epoxy. These researchers found that the SBM block copolymers could continuously toughen the epoxies up to 25 wt. % of the SBM were added, while a plateau or a peak of fracture toughness was observed at about 10 wt. % for the core-shell rubber particle or CTBN modified epoxies see Figure 23. More importantly, the maximum value of K_{IC} for the SBM modified epoxies was reported to

nearly approach $5 \text{ MPa}\cdot\text{m}^{1/2}$, while the core-shell rubber particle or CTBN modified epoxies reached a plateau or maximum at about $3 \text{ MPa}\cdot\text{m}^{1/2}$.

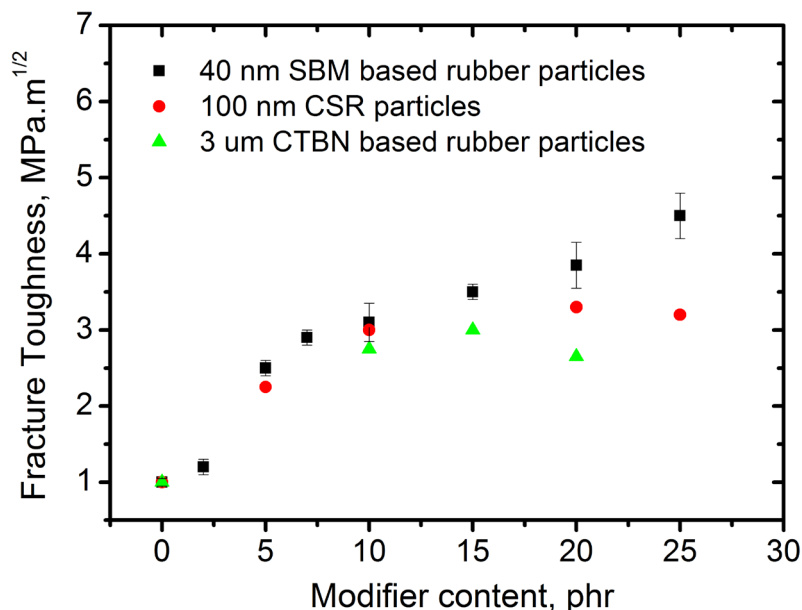


Figure 23: Graph showing fracture toughness versus modifier content for various types of rubber modified epoxies, reproduced from [87].

Wu et al. [88] studied the structure and properties of epoxies modified with PBO-PEO diblock copolymers by varying the composition of the diblock copolymers. These researchers found that the fracture energy of the block copolymer modified epoxies was dependent on the morphologies of the modified epoxies. They reported that, for the same block copolymer loading, epoxies with dispersed branched worm-like micelles have the highest fracture toughness. The results from the past research have demonstrated that block copolymer toughening has the potential to provide a higher toughness improvement compared to traditional homopolymers and random copolymer toughening agents. And the main problem involved in the addition of BCP is they can reduce all other properties like Elastic modulus, tensile strength, and T_g .

3.8.5 Rigid Fillers

Blending rigid particles can improve the strength and modulus of epoxy nanocomposites while also increasing the fracture toughness [89] without decreasing the glass transition temperature of the nanocomposites. Many authors have studied the use of rigid particles such titanium dioxide (TiO_2) [89] [90], alumina (Al_2O_3) [89] [91], silicates [92], silica (SiO_2) [93] and glass [94] [95] [96].

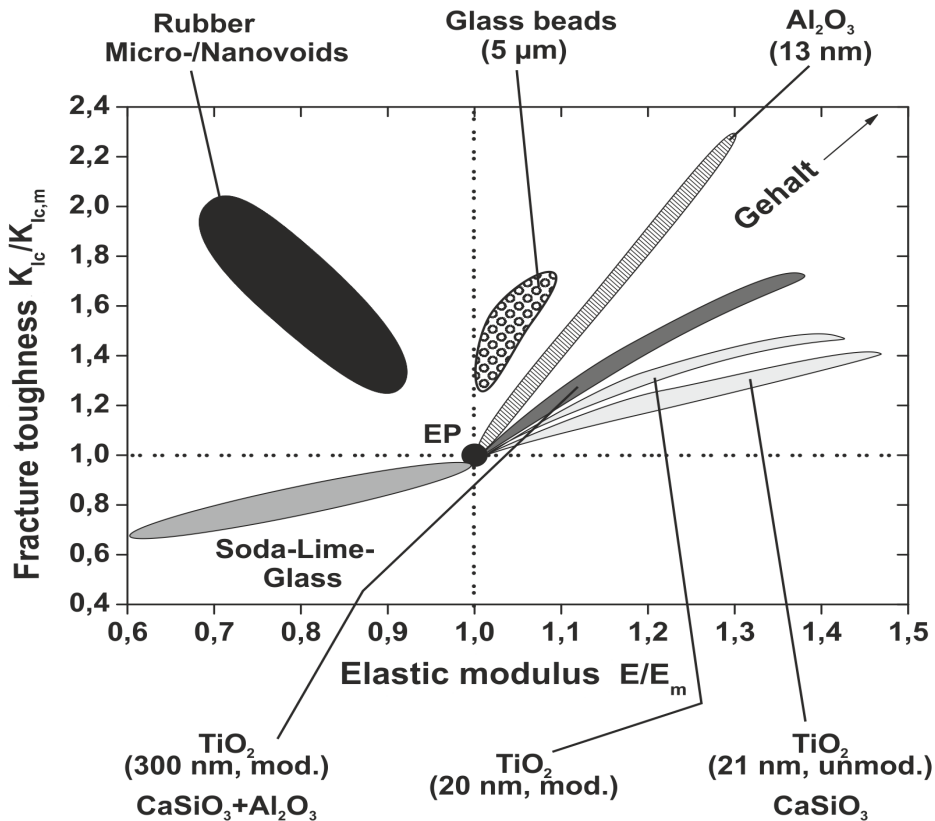


Figure 24: Effect of micro-nano rigid particles on the properties of the epoxy system [89].

The ample availability of nanoparticles shows that use of nanoparticles is kept on increasing nowadays [97]. These nanoparticles may be used in resin infusion process since the dimension of these particles lies in the range of nano range and they are not blocked by the inter-fiber spacing which is not possible in the case of microparticles, moreover, nanoparticles have lower viscosity for the same volume percentage when compared to micro counterparts.

3.8.6 Hybrid toughening

Though the rubber toughened epoxy system gained prominence for the improvement of the impact properties of cured epoxy, there is a significant decrease in the modulus and thermal stability of the materials and increase the tendency to absorb water with an adjacent loss of properties at elevated temperatures. So, the search for alternative toughening method led to discover the new method with the use of two different types of fillers simultaneously while one will increase the fracture toughness and the other at the same time may increase the modulus and glass transition temperature or at least hinder them from decreasing. Such type of approach is called as hybrid toughening and this was first adapted by Kinloch et al [98] while trying to

restore the lost stiffness caused by the application of rubber modification. Since then, several researchers have started examining many combinations of different sized particles for hybrid toughening.

3.9 Toughening mechanisms

Several toughening mechanisms will be involved when an epoxy system is toughened by the addition of the second phase. These mechanisms depend on the type of the materials used for toughening. Nevertheless, many theories based on the fractographic features and fracture properties of toughened thermoset networks have been proposed to explain the toughening mechanisms. A research work which was done by Carmelo [99] suggests that the main toughening mechanism in the block copolymer modified epoxies is the plastic deformation of the matrix initiated by cavitation of ductile domains. Several toughening mechanisms have been proposed from the research conducted for rubber modified epoxy systems [100].

3.9.1 Shear Yielding

Shear yielding is nothing but the material response to an applied shear stress by plastic deformation through the translation of chain molecules past each other with keeping the volume of specimen essentially constant and leads to a permanent change in shape. The terms yield or plastic zone, localized shear, and diffuse-shear are used interchangeably to describe the failure events of ductile polymers [101]. According to the research done by Newman and Strella [102], the principal function of the rubber particles is to produce sufficient triaxial tension in the matrix to increase the local free volume and hence enable shear yielding and drawing of the matrix to initiate. They identified that spherical voids that have a higher stress concentration at the equator (where the maximum tensile stress concentration occurs) could also initiate shear yielding of the matrix. Also, plastic shear bands are initiated as a result of the stress concentration caused in the matrix by the presence of rubber particles, considerably more plastic energy dissipation exists. The theory of Newman and Strella was backed by Petrich [103] by suggesting that a change in the refractive index of the oriented rubber particles by birefringence is the major cause of stress whitening.

3.9.2 Crack pinning and crack path deflection

Crack pinning theory was first suggested by Lange [104] and further enhanced by Evans [105] and Green [106]. It is a mechanism in which assumes that the propagation of a crack can be delayed or hindered when it tries to propagate through the hard particles. This is because, when a crack meets such an array of hard particles, it is pinned and tries to bow out between the particles by formation of secondary cracks. Crack path deflection is nothing but diverting the direction of the crack front by altering the local stresses around the crack tip. This can be possible by the introduction of various sizes of filler particles into the matrix system. When the crack approaches a big particle, it can deflect the crack more effectively than a smaller particle. Even though, a cluster of small particles integrated at one place in the matrix can also be served as one big particle and can deflect the crack. This deflection causes the continuous change in the local stress state from Mode I (crack opening) to mixed-mode conditions which help in absorbing more energy [107]. The crack requires more and more energy each time it is deflected into a new plane of propagation thereby resulting in the increase of fracture toughness of the material. With this, it can be indicated that the crack path deflection is dependent on the particle size [108]. Faber and Evans [109] [110] proposed that this mechanism does not depend on the particle size but it is believed that uneven spacing provides better results than uniform spacing or particle size.

3.9.3 Crack bridging or particle bridging

Crack or particle bridging occurs when the particles do not completely cavitate or break from the matrix material and form a bridge-like structure in between the crack planes. This type of mechanism is most commonly seen in rubber modified systems. It is that when a crack advances through the rubber particles which are perfectly bonded to the matrix system, and then they get stretched and undergo plastic deformation and forms like a connecting bridge in between the two crack planes [52]. During this deformation process, the particles absorb energy before they are completely torn out and this causes the increase of toughness. Pearson and Yee [111] attributed the enhancement in toughness to the rubber bridging mechanism by studying a highly cross-linked rubber-modified epoxy system. This model assumes that the taken matrix system is truly brittle and does not plastically deform so that the

applied energy is purely absorbed by the rubber particles. However, it is known that even some highly cross-linked matrix systems undergo minimal plastic deformation. So, this theory has drawbacks that it can only explain the modest increase in toughness but not the dramatic increase in fracture energy. The reason for stress whitening observed in the fracture surfaces due to the plastic deformation of particles also could not be explained by this theory. Therefore, it may not be considered as a major energy-dissipating mechanism for highly cross-linked systems.

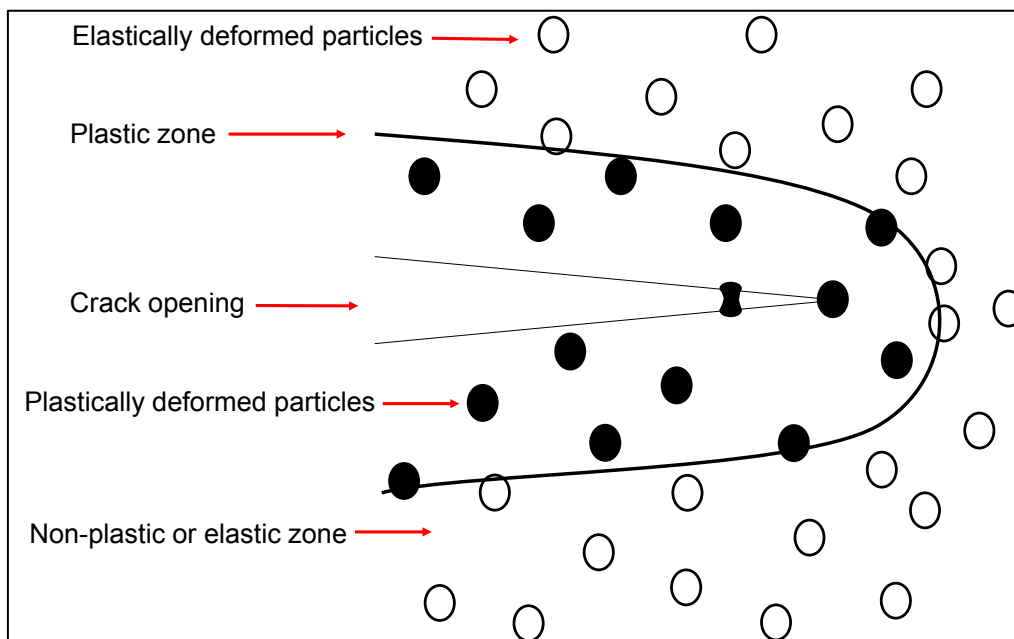


Figure 25: An illustration of the crack bridging mechanism, reproduced from [69].

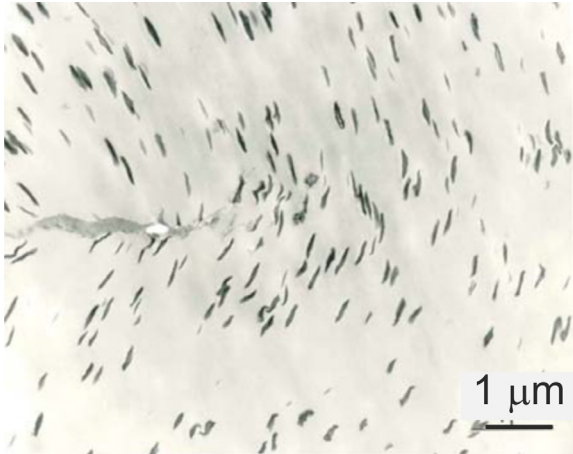
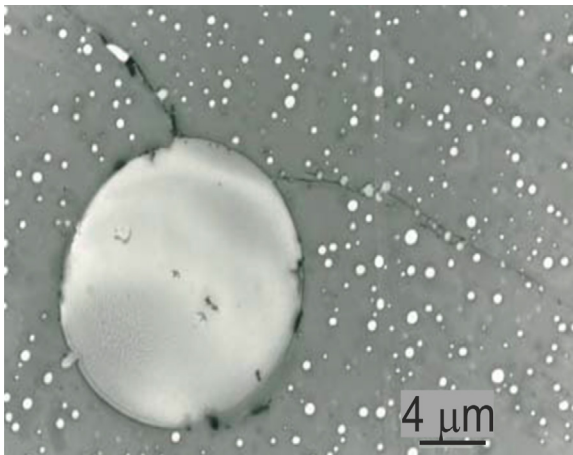
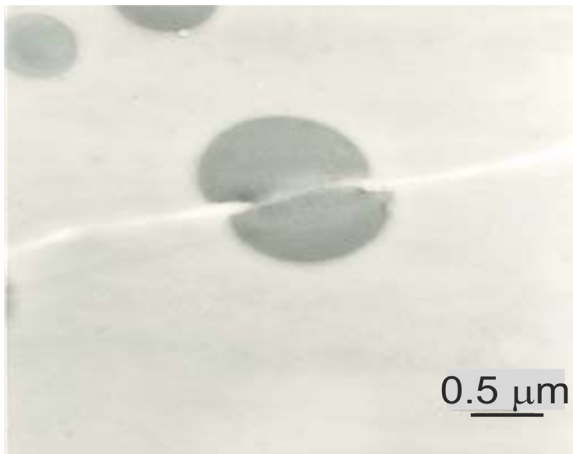
3.9.4 Crazeing

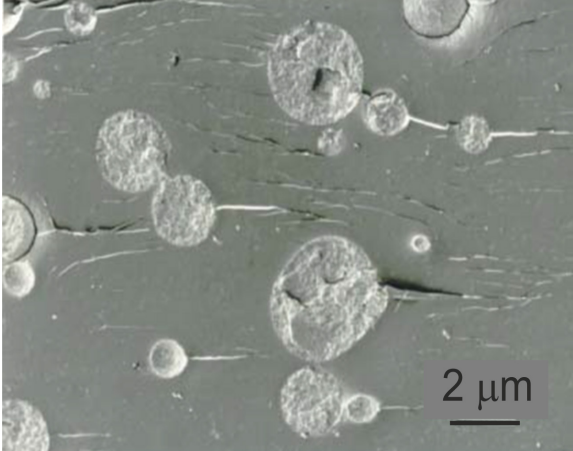
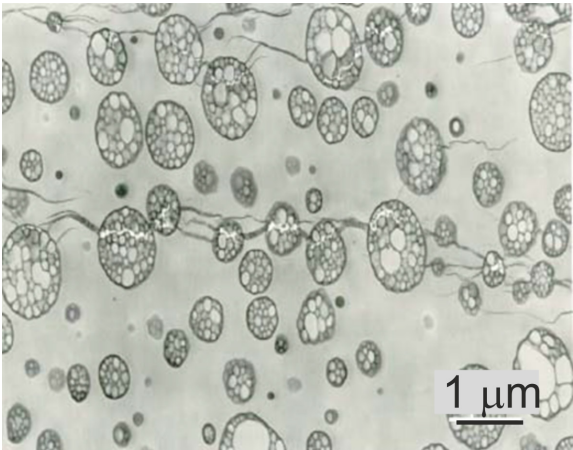
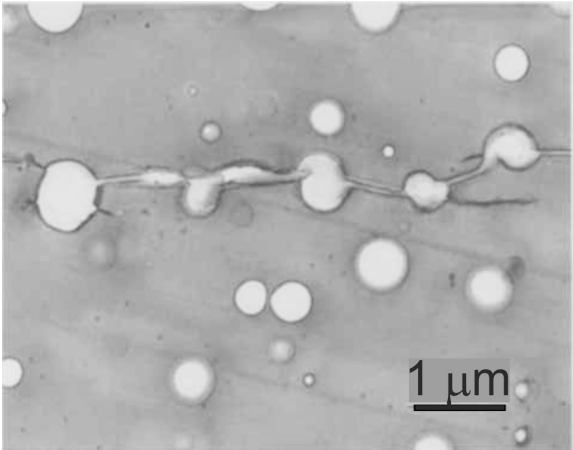
Crazeing is also one of the toughening mechanisms seen mostly in brittle thermoplastics and thermosets. It is also responsible for the increment of fracture toughness of the material by formation of networks which are made up of voids and polymer fibrils. Crazeing occurs when the applied triaxial stress overcomes the Van der Waals forces of the material by initiation of an interpenetrating network of microvoids connected by fine filaments of stretched polymer backbone chain called stress [112]. Unlike the crack, a craze always tends to grow in different indefinite lengths by spreading in different directions [52] and is always normal to the applied stress [112]. It can also transmit the applied load across different faces and the process of this energy dissipation is often termed as crazeing [52].

3.9.5 Cavitation

When a load is applied, under triaxial tensile stresses, voids are initiated within the rubber particles. Once the void growth has taken place, the rubber particle debonds from the matrix by causing the surrounding matrix to deform plastically and cavities are left in the material. Due to this, the hydrostatic tension in the material is relieved and uniaxial tensile stress state is created.

Table 2: Various toughening mechanisms in rubber-modified epoxy systems [113]

Example	Toughening Effect	Toughening Mechanism
 <p>A micrograph showing a crack in a rubber-modified epoxy system. The crack is a thin, dark line running horizontally across the center. The surrounding matrix is light gray with numerous small, dark, elongated particles. A scale bar in the bottom right corner indicates 1 μm.</p>	<p>Up to an order of magnitude improvement in fracture toughness</p>	<p>Shear yielding</p>
 <p>A micrograph showing a large, circular, light-colored rubber particle in a dark matrix. A crack is visible, passing through the particle and extending into the matrix. A scale bar in the bottom right corner indicates 4 μm.</p>	<p>Up to double improvement in fracture toughness</p>	<p>Crack deflection</p>
 <p>A micrograph showing a crack bridged by a large, dark, circular rubber particle. The crack is a thin, light-colored line that passes through the particle. A scale bar in the bottom right corner indicates 0.5 μm.</p>	<p>Incremental improvement in toughness</p>	<p>Crack bridging</p>

Example	Toughening Effect	Toughening Mechanism
 <p>A micrograph showing a crack path through a material. The crack is significantly deflected and arrested by several large, spherical particles. A scale bar in the bottom right corner indicates 2 μm.</p>	Fractional improvement in fracture toughness	Crack pinning
 <p>A micrograph showing a network of fine, interconnected craze structures. The crazes are small, circular or oval in cross-section, and form a dense web. A scale bar in the bottom right corner indicates 1 μm.</p>	Up to several folds improvement in toughness	Crazing
 <p>A micrograph showing a crack that has bifurcated into multiple smaller cracks. The main crack path is interrupted by several smaller, branching cracks. A scale bar in the bottom right corner indicates 1 μm.</p>	Fractional improvement in fracture toughness	Crack bifurcation

3.10 Microstructural aspects

The microstructure of rubber toughened epoxy-based thermosetting polymers may affect the properties of toughened systems.

Factors affecting the rubber toughened systems are as follows [114]

Dispersed Rubber phase	Epoxy matrix phase
1. Microstructure	1. Cross-link density
2. Volume fraction	2. Glass transition temperature of matrix
3. Particle size	3. Molecular weight
4. Nature and type	
5. Morphology of dispersed phase	
6. Intrinsic adhesion across particle matrix interface.	

3.10.1 Volume fraction of rubber phase

By increasing the concentration of elastomer the fracture energy of the toughened epoxy system is increased, up to a limit where it becomes difficult to obtain the desired particle matrix morphology. Bucknall et al [115] have calculated the fracture energy of rubber-modified epoxy resins, all containing 8.7 wt. % of CTBN rubber but with various rubbery phase volume fractions, with varying cure conditions. They found a linear relation between fracture energy and volume fraction of rubber up to a value of volume fraction of about 0.2 for different epoxy resin hardener system using a CTBN rubber. However, Kunz et. al. [116] reported that a volume fraction of about 0.1 had been achieved in the polymer, further increases in volume fraction resulted only minor increase in the value of fracture energy for both CTBN and ATBN modified epoxy systems. Kinloch et al [117] has assisted in explaining these apparently conflicting observations and has also shown that the linear relation shown by Bucknall et al. [115] is somewhat unexpected. It has been reported by authors that fracture energy in rubber toughened epoxy is dependent on the test temperature and the test rate [118, 119, 120]. In most of the studies [121, 122] phase inversion is reported for more than 20 vol. %, in some studies phase inversion, is reported [123] at a very low volume percentage (2%).

3.10.2 Particle size of rubber phase

The particle size of toughening phase is one of the main factors that affect the measured toughness of the composites. Sultan and McGary [124] [125] proposed that small particles with size 0.1 μm in diameter initiate shear yielding, and the large particles of size 0.1-1 μm in diameter causes crazing which is responsible for a fivefold increment of toughening effect. This was backed by Kunz et al [126] when they stated that large particles are not as efficient as small particles by comparing particle of size 40 μm in diameter and 1 μm in diameter. Also, when Pearson and Yee [127] studied the influence of particle size (ranging 0.2-200 μm) and particle size distribution on the toughening mechanism in rubber modified epoxies, they reported that the small particles of size 0.1 μm have increased the toughness in tenfold when compared to the larger ones of size 100 μm . However, there are quite contradictions to these above statements when some other researchers [128] [129] [130] reported the independency of the fracture energy on the particle size even though the average particle size is between 0.5-5 μm .

Nevertheless, the role played by these particles depends on the process zone. The larger particles outside this process zone do not initiate any cavitation but act as bridging particles whereas small particles in this process zone get cavitated and help in increase of the fracture toughness. This is in good agreement with the concept of inter-particle distance proposed by Wu [131] for rubber toughened nylon who argued that critical inter-particle distance is the main fundamental parameter which is responsible for brittleness or ductility of the material and it is independent of the particle size and volume fraction.

3.10.3 Interfacial Adhesion

The proper bonding between the filler material and matrix also plays an important role in increasing or decreasing of toughness of a material. The stronger the adhesion between the particle and matrix, the higher the toughening effect. If the bonding between the particle and matrix is weak, easy debonding of rubber particles takes place resulting in a more sudden failure.

In earlier studies, the poor bonding problem was tackled by using non-reactive rubber particles [125]. Levita et al [132] reported that the non-reactive rubbers with poor interfacial adhesion had actually toughened the matrix. In contrary, Huang et al [133]

reported that interfacial adhesion has only modest effect on the fracture properties if the non-reactive rubbers are of micron-sized particles. Further, researchers [134] [135] have reported that by using reactive rubber resulted in good interfacial chemical bonding because of the chemical reactivity with epoxy matrix.

3.10.4 Molecular weight of matrix phase

Molecular weight plays an important role in the increment of fracture toughness of the materials. Many researchers found that the fracture toughness was increased with respect to the increase in the M_w between cross-links. A research was done by Kinloch et al. [136] varying the molecular weight by using different epoxy resins having different epoxy equivalent weights and 4,4 - diamino-diphenyl sulphone as curing agent had proved that the former statement proves to be true. An increase in molecular weight between the crosslinks further increases a small amount of fracture energy for unmodified epoxy systems which were coupled with increased ductility of the system. However in case of rubber modified systems substantial increased was observed due to the creation of large numbers of energy dissipating shear zones.

3.11 Analytical Modeling

The prediction of the mechanical properties, such as tensile modulus, tensile strength and fracture energy of heterogeneous composites is important for understanding the mechanical response of such materials. In the following section most widely used analytical approaches are reviewed:

3.11.1 Elastic Modulus

The elastic modulus of a particulate – polymer composite is usually determined by the elastic properties of its constituents (filler and matrix), particle loading and aspect ratio of each phase [137]. These models are developed from inherent relationships or by semi-empirical methods. The simplest models are the upper and the lower bounds of the composite modulus.

The upper limit of the composite modulus is given by Voigt model. This is also known as “rule of mixtures” or parallel model

$$E_c^{upper} = E_p V_p + E_m (1 - V_p) \quad (3.4)$$

The lower limit E_L is proposed by Reuss model which is also known by series model:

$$E_c^{lower} = E_p E_m / [E_p (1 - V_p) + E_m V_p] \quad (3.5)$$

where V_f is the volume fraction of modifier, E_p is the modifier modulus and E_m is the matrix modulus. The Voigt model assumes constant strain and the Reuss model assumes constant stress across both phases.

A. Counto Model

This model was proposed for a two-phase particulate composite by assuming perfect bonding between filler and matrix [138]. This was originally developed for predicting the elastic behavior of concrete. However, considering the brittle nature of concrete, the structure development through a chemical hardening reaction and the internal structure with near spherical fillers (sand, gravel) in a matrix, there are important similarities between concrete and a system of particle reinforced epoxy resin. Counto's model consists of a combination of the linear (parallel, Voigt) and inverse (series, Reuss) rules of mixtures. This model predicts moduli in good agreement with a wide range of test data [89].

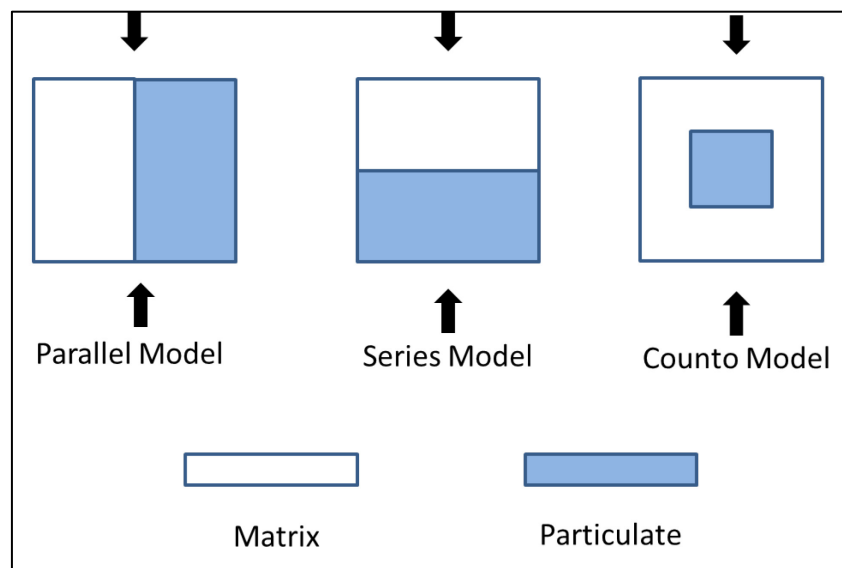


Figure 26: Two-phase model for epoxy composites [138]

The elastic modulus of the composite according to Counto can be estimated with the following expression:

$$\frac{1}{E_c} = \frac{1 - V_p^{1/2}}{E_m} + \frac{V_p^{1/2} E_m + E_p}{\left(1 - V_p^{1/2}\right)} \quad (3.6)$$

where V_p is the volume fraction of the particulates, E_p is the elastic modulus of particulate, E_m is the modulus of matrix and E_c is the modulus of composite.

B. Halpin Tsai Model:

Halpin and Tsai found that the modulus of particulate polymers can be predicted by the semi-empirical relationship [139] [140]

$$\frac{E_c}{E_m} = \frac{1 + A_1 B_1 V_p}{1 - B_1 V_p} \quad (3.7)$$

$$B_1 = \frac{\frac{E_p}{E_m} - 1}{\frac{E_p}{E_m} + A_1} \quad (3.8)$$

where A_1 and B_1 are constants for a given composite. A_1 is a function of the particle shape and matrix Poisson ratio, and B_1 is related to the modulus of the particle (E_p) and matrix (E_m). The shape factor of the Halpin-Tsai model is a function of the aspect ratio (w/t) of the particles, where w and t are the length and thickness of the particles respectively. Halpin and Kardos [141] recommended that a shape factor of $A_1 = 2 w/t$ should be used for calculating the modulus for filler particles aligned with the loading direction, and $A_1 = 2$ for fillers perpendicular to the loading direction. In the later chapters for all the modifiers a shape factor of 2 is considered.

C. Lewis and Nielsen Model

Lewis and Nielsen proposed a modification to the Halpin-Tsai model and accounted for particle matrix adhesion and a limit in maximum packing and using the work of McGee and McCullough [142] proposed a model to evaluate the value of E_c

$$\frac{E_c}{E_m} = \frac{1 + A_1 B_1 V_p}{1 - \Psi B_1 V_p} \quad (3.9)$$

where Ψ depends on the particle packing fraction and constants A_1 and B_1 are defined below. Thus, we have

$$A_1 = k_E - 1, \quad B_1 = \frac{\frac{E_p}{E_m} - 1}{\frac{E_p}{E_m} + A_1} \quad (3.10)$$

$$\Psi = 1 + \left(\frac{1 - V_p}{V_{max}} \right) [V_{max}V_f + (1 - V_{max})(1 - V_f)] \quad (3.11)$$

where k_E is the generalized Einstein coefficient, $V_{p\ max}$ is the maximum volume fraction. The theoretical value of $V_{p\ max}$ has been calculated by Nielsen and Landel [143] for various types of packing and arrangement. For randomly distributed close packing particles which are agglomerated $V_{p\ max} = 0.37$ and for particles which are not agglomerated $V_{p\ max} = 0.632$. The value of generalized Einstein coefficient k_E , varies with the Poisson's ratio of the polymer matrix and the degree of the adhesion of the polymer matrix to the particles. The $k_E = 2.5$ for no-slip condition and $k_E = 1$ for slip condition has been proposed [143].

3.11.2 Tensile strength

Prediction of tensile strength in composites is difficult since the ultimate strength of a composite depends on the weakest fracture path through the material. The problem arises because the strength of composites is determined by the fracture behavior which is linked with parameters as interfacial adhesion, spatial distribution, and stress concentration. Thus the strength of a composite depends on the strength of the weakest path throughout the microstructure [144]. Although numerous theories of composite strength have been published before, there is no universally accepted theory to date. Here, a semi-empirical equation is given which was used by different authors [145] [146].

$$\sigma_c = \sigma_m(1 - V_p) \quad (3.12)$$

where σ_c is the strength of composite, σ_m is the strength of matrix and V_p is the volume fraction of filler material.

3.11.3 Fracture Energy

Rubber particle toughening

The toughening effects due to the mechanisms discussed in § 3.9 may be estimated by using an analytical model developed by Hsieh et al. [147] based on the previous Huang and Kinloch model [148] [149]. This model was used by several researchers [5] [13] [150] [151] [152] [9] and results revealed that this analytical model can accurately predict the fracture energy of particle modified epoxies with toughening mechanisms of void growth and shear band yielding.

Huang et al. proposed that the toughening increment of fracture energy can be written as

$$G_{cm} = G_{cu} + \Psi \quad (3.13)$$

where G_{cu} is the fracture energy of the unmodified epoxy polymer and Ψ represents the overall toughening contribution provided by the presence of the particulate phase. The model directly addresses the toughening mechanisms observed from the experimental observations and assumes that the mechanisms are mutually exclusive to each other. The overall toughening contribution, divided into the relative toughening contributions;

$$\Psi_{EP} = \Delta G_s + \Delta G_v + \Delta G_r \quad (3.14)$$

(i) Localized shear band yielding, ΔG_s , (ii) plastic void growth of the epoxy polymer, ΔG_v , and (iii) rubber bridging, ΔG_r

The fracture energy contribution from **plastic shear band yielding**, ΔG_s initiated by the particles is referred to the size of the plastic zone from [147] as:

$$\Delta G_s = 0.5V_{fp}\sigma_{ycu}\gamma_{fu}F'(r_y) \quad (3.15)$$

where V_{fp} is the particle volume fraction, σ_{ycu} is the plane strain compressive true yield stress, γ_{fu} is the fracture strain for the unmodified epoxy, and $F'(r_y)$ is given by:

$$F'(r_y) = r_y \left[\left(\frac{4\pi}{3V_{fp}} \right)^{\frac{1}{3}} \left(1 - \frac{r_p}{r_y} \right)^3 - \frac{40}{35} \left(\frac{r_p}{r_y} - 1 \right)^{\frac{3}{2}} - \left(\frac{r_p}{r_y} \right) \left(\frac{7}{5} - \frac{r_p}{r_y} \right) - 2 \left(1 - \frac{r_p}{r_y} \right)^2 + \frac{16}{35} \right] \quad (3.16)$$

where r_p is the particle radius, r_y is the increased plastic zone size due to the stress concentrations in the epoxy matrix and it is defined as

$$r_y = K_{vm}^2 \left(1 + \frac{\mu_m}{3^{1/2}} \right)^2 r_{pzu} \quad (3.17)$$

where K_{vm} is the maximum stress concentration for the von Mises stresses around the particle and μ_m is a material constant which allows for the pressure-dependency of the yield stress. The value of μ_m is a material constant relating to the hydrostatic dependence of yielding, and was measured to be between 0.175 and 0.225 for rubber modified epoxy polymers [153]. The value of K_{vm} is dependent on the volume fraction of particles, and was calculated numerically by Huang and Kinloch [148]. The value of K_{vm} varies with volume fraction and simple linear relationship can be obtained for soft modifiers

$$K_{vm} = 3.9337V_{fp} + 2.1126 \quad (3.18)$$

Similarly for hard (rigid) modifiers the value of K_{vm} is given by

$$K_{vm} = 0.918V_{fp} + 2.1126 \quad (3.19)$$

The Irwin prediction of plain strain plastic zone radius for the unmodified epoxy at fracture was calculated by [154]

$$r_{pzu} = \left(\frac{1}{6\pi} \right) \left(\frac{K_{IC}}{\sigma_{yt}} \right)^2 \quad (3.20)$$

where K_{IC} is the fracture toughness and σ_{yt} is the tensile true yield strength for the unmodified epoxy polymer.

The contribution of ΔG_v through **plastic void growth mechanism** can be calculated using [149]

$$\Delta G_v = \left(1 + \frac{\mu_m}{3^{1/2}} \right)^2 (V_{fv} - V_{fp}) \sigma_{yt} r_{pzu} K_{vm}^2 \quad (3.21)$$

where μ_m is material constant as discussed above, V_{fp} is the particle volume fraction and V_{fv} is the volume fraction of voids. The term $V_{fv} - V_{fp}$ can either determine experimentally from SEM pics, or predicted from the following relationship:

$$r_{fv} = (1 + \gamma_{fu})r_p \quad (3.22)$$

$$V_{fv} - V_{fp} = V_{fp} \frac{r_{fv}^3 - r_p^3}{r_p^3} \quad (3.23)$$

where r_{fv} is the void radius and γ_{fu} is the failure strain. The measured values of V_{fv} were found in good agreement with the value measured from the fracture surfaces with in experimental error by several authors [152] [155] [156].

Kunz-Douglass et al. [126] proposed the contribution of rubber bridging ΔG_r .

$$\Delta G_r = 4 \varphi_t V_{fp} \quad (3.24)$$

where φ_t is the tearing energy of the rubber particles, which was reported approximately to be 460 J/m² [157].

It is worth noting that the contribution from shear band yielding and void growth dominates the total energy contribution at various volume fractions, as well as at different test temperatures [149]. The contribution from void growth and shear band yielding is of the same order of magnitude up to 10 volume % and above 10 vol. % plastic void growth becomes the dominant toughening mechanism, and rubber bridging does not appear to be a significant toughening mechanism based on the model as it only contributing up to 12% of the total contribution at 10 vol. %. Hence the total predicted fracture energy equation is given by

$$G_{cm} = G_{cu} + \Psi_{EP} \quad (3.25)$$

Where Ψ_{EP} is the summation of energy contribution by shear yielding, void growth and rubber bridging.

putting the values of ΔG_s , ΔG_v and ΔG_r from equations (3.15), (3.21) and (3.24) respectively. The equation (2.22) will becomes

$$G_{cm} = G_{cu} + 0.5V_{fp}\sigma_{ycu}\gamma_{fu}F'(r_y) + \left(1 + \frac{\mu_m}{3^{1/2}}\right)^2 (V_{fv} - V_{fp})\sigma_{yt}r_{pzu}K_{vm}^2 + 4 \varphi_t V_{fp} \quad (3.26)$$

where the G_{cu} is the fracture energy of the unmodified epoxy system and G_{cm} is the predicted energy of the modified system based on the contribution from shear yielding, void growth, and rubber bridging.

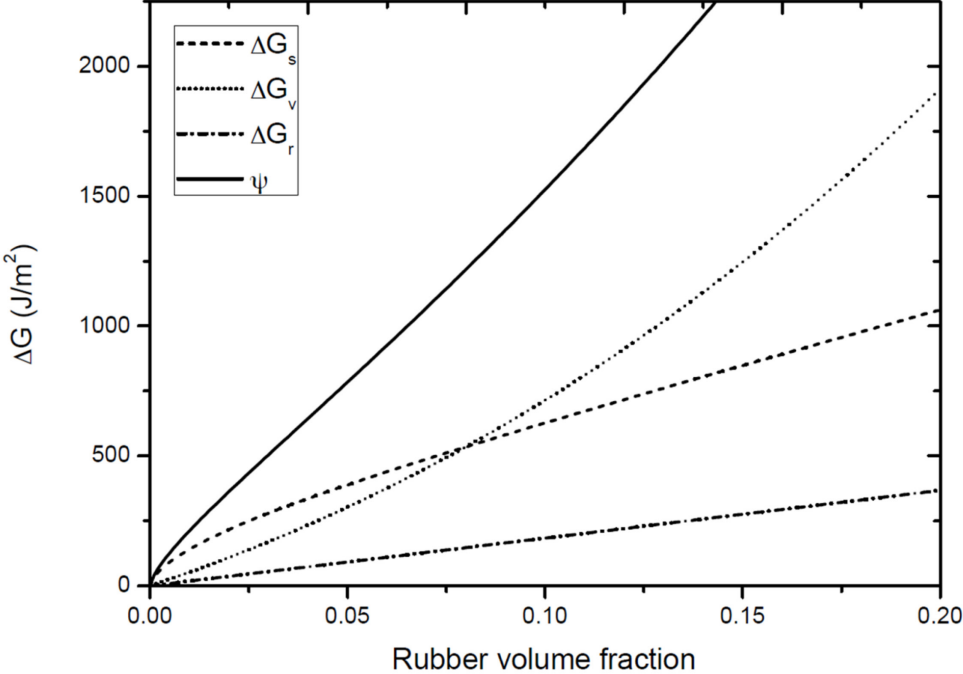


Figure 27: Energy contributions comparison for shear banding, void growth and rubber bridging based on Huang-Kinloch fracture energy model [152].

4. Materials and manufacturing

4.1 Introduction

The aim of this chapter was to give information about the materials used and their preparation methods that were followed to prepare the bulk samples used for different testing. The first section gives details of the different types of epoxy systems and hardeners used. In the second section different types of toughening agents are discussed and lastly, the manufacturing of unmodified and modified bulk epoxies was discussed.

4.2 Epoxy resins

4.2.1 Bisphenol-F based epoxy

In the present work, EPON™ Resin 862 (Diglycidyl Ether of Bisphenol F) liquid epoxy resin produced by Hexion Inc, low viscosity, liquid epoxy resin manufactured from epichlorohydrin and Bisphenol-F is used as a base matrix [158]. Bisphenol F is similar to bisphenol A except phenol is reacted with formaldehyde rather than acetone. Bisphenol F is reacted with epichlorohydrin to form Diglycidyl ether of bisphenol F (DGEBF) resins. The resultant phenolic chemical does not have the two methyl groups that are present between the ring structures in bisphenol A resins (Figure 28).

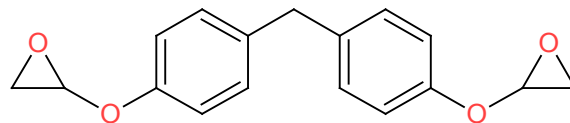


Figure 28: Molecular structure of diglycidyl ether of bisphenol - F

Due to the absence of the methyl group, the viscosity of the bisphenol F resins is lower than that of bisphenol A based epoxy resins [159].

4.2.2 Fluoren di epoxy.

The developmental resin LME10169 is manufactured by Huntsman and supplied in the form of white powder. It's a di-functional epoxy resin, with large/bulky backbone showing structural rigidity with high aromatic content. It was recommended to use for structural composite matrices [160].

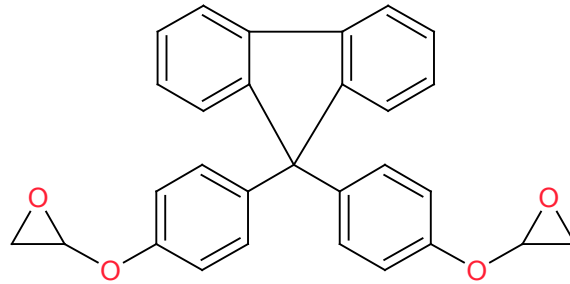


Figure 29: Molecular structure of fluoren di epoxy resin (LME10169).

4.2.3 Epoxy resin based on meta – amino phenol.

Araldite MY0610 is a particularly effective resin in a wide variety of formulating applications including composites, adhesives, laminating systems requiring high modulus, high hot-wet performance, and toughness. It's a high purity, low viscosity trifunctional epoxy resin based on meta-amino phenol [161].

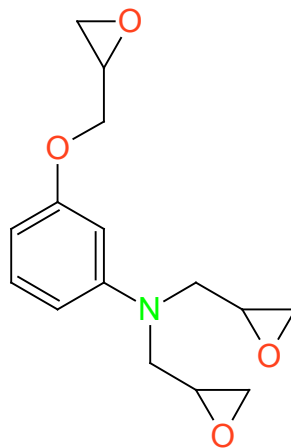


Figure 30: Epoxy resin based on meta-amino phenol (Araldite MY0610)

4.2.4 Epoxy resin based on 1, 6 – Naphthalene di-epoxy.

Araldite MY0816 is a di functional, low viscosity resin which provides flat rigid core facilitating multi molecular association leading to the high compact network. It is having strong aromatic character and low polarity backbone [162].

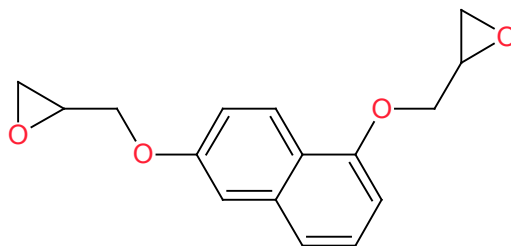


Figure 31: Epoxy based resin based on 1, 6 - Naphthalene di epoxy (Araldite MY0816)

Table 3: Properties of different epoxy systems used [158] [163] [161]

Property	EP862	MY0610	MY0816	LME10169
Manufacturer	Hexion	Huntsman	Huntsman	Huntsman
Viscosity @ 25 °C (Pa.s)	2.5 - 4.5	1.5 - 4.8	25 - 80	--
Epoxy equivalent weight (gm / eq.)	165 - 173	94 - 102	133 - 154	245 - 255
Functionality	2.1	3	2	2

4.3 Hardener systems

In the current work, two types of curing agents are used as hardeners, one is aromatic amine-based hardener system (**H1**) and another one is anhydride based (carboxylic acid anhydride) hardener system (**H2**) and (1-methylimidazole) as an accelerator.

Selected properties of the hardener and the accelerator are listed in Table 4.

Table 4: Properties of amine hardener, anhydride hardener, and accelerator used in the present work

Properties	Amine Hardener (H1)	Anhydride Hardener (H2)	Accelerator
Manufacturer	-	-	Huntsman
Equivalent weight (gm / eq.)	45.2	168	-
Density (g/cm^3)	1	1.20	0.95-1.05
Viscosity at 25 °C (Pa.s)	~ 0.175	< 0.01	<0.05

4.4 Toughening agents

4.4.1 Block copolymers

A poly[(Methyl)methacrylate-co-polar comonomer] -b- poly(Butyl Acrylate) functional block copolymer (diblock D51N) supplied as powders by Arkema, France, were used as the toughening agent. They are a family of self-assembling block copolymers, which are constituted of two blocks of linear chains covalently bonded to one other [164]. Functional (D51N) consists of one side block of poly(Methyl methacrylate) and one block of poly(butyl acrylate). The suffix N indicates that the MAM incorporates dimethyl acrylamide (DMA) functional groups into the poly (methyl methacrylate) (PMMA) blocks to increase the compatibility of the miscible block with more polar curing agents [165].

Table 5: Different blocks in D51N block copolymers [164].

Grade	Soft block	Rigid block	Number of blocks
D51N	Poly(butyl acrylate)	Poly(methyl methacrylate-co-dimethylacrylamide)	Two

4.4.2 Core-shell rubber particles

The CSR nanoparticles used in this thesis work was Kane Ace MX170 supplied by Kaneka Belgium NV. The material supplied was in the form of a masterbatch which was a 25 % concentrate of core-shell rubber toughening agent in unmodified liquid epoxy resin based on Bisphenol-A. Specific gravity was 1.1 and nominal viscosity @ 50 °C was 12,000 cps (mPa.s) [166].

4.4.3 Titanium dioxide (TiO₂)

Today TiO₂ was widely used in many commercial and consumer applications. Generally, TiO₂ was sourced from ilmenite, rutile, and anatase. TiO₂ nanoparticles (AEROXIDE[®] TiO₂ P25) used in this research were provided by Evonik Resource Efficiency GmbH as a dry powder. TiO₂ was produced by utilizing high-purity liquid titanium chlorides as raw material, vaporized and mixed with air and hydrogen. The gases are reacted at temperatures between 1000 °C and 2400 °C in a burner leading to the formation of pure and nanostructured TiO₂ [167]. TiO₂ P25 was a spherical

shaped fine white powder with hydrophilic character caused by hydroxyl groups on the surface [168]. The primary particles have a mean diameter of approx. 21 nm. Particle size and density of 4 g/cm³ lead to a specific surface of ca. 50 m²/g. They form agglomerates in the range of micrometers (Figure 32, left) mainly due to electrostatic van der Waals' forces [169].

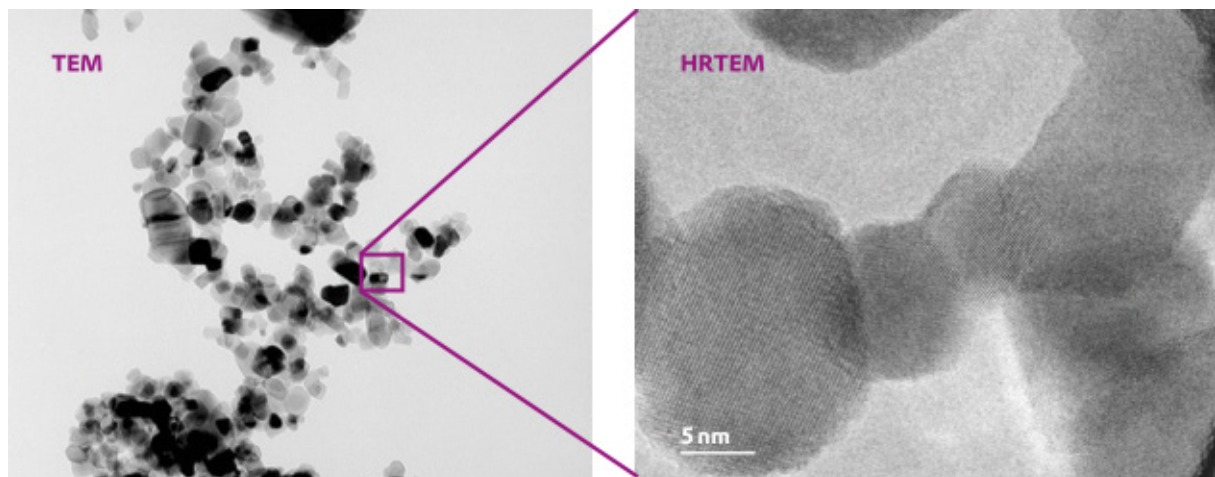


Figure 32: TEM images of AEROXIDE[®] TiO₂ P25 depicting the primary crystals (right graph) and their aggregates and agglomerates (left graph) [167].

Table 6: Properties of P25 TiO₂ [167]

Properties	Units	TiO ₂
Manufacturer	-	Evonik
Designation	-	P25
Form	-	Powder
Density	(g/cm ³)	4
Primary particles mean diameter	(nm)	21, spherical
Surface area	(m ² /g)	35-65

4.5 Manufacturing

4.5.1 Epoxy and block copolymers composites

The manufacturing of block copolymer modified bulk epoxies was difficult because the block copolymer (D51N) was supplied as a powder. At first 25 wt. % block copolymers powder was mixed with the epoxy resin and heated overnight in an oven at 100 °C. And then, next day the mixture was dispersed in a dissolver for homogenous epoxy- block copolymers masterbatch mixture. Later, the master-batch was thinned down to the required wt. % according to formulations. In the manual

mixing, the resin mixture was stirred using a dissolver (Dispermat, Getzmann GmbH) with a propeller blade at 90 °C and 120 rpm for at least 30 minutes to ensure all the block copolymers-epoxy masterbatch was completely dissolved in the epoxy resin. The mixture was cooled down to 50 °C before mixing the hardener. A stoichiometric amount of the amine or the anhydride curing agent was then added. The mixture was stirred thoroughly for 5-10 minutes at 350 rpm. Immediately, the mixture was transferred into glass moulds (Figure 33(left)) which were surface coated with releasing agent (Würtz PAT-607/FB) and left for 30 min to dry and assembled with clips and pre-heated at 80 °C in an oven before pouring the dispersed mixture to produce tensile and DMTA samples and steel moulds (Figure 33(right)) coated with releasing agent (Indrosil 2000) and pre-heated at 80 °C in an oven before pouring the dispersed mixture for compact tension (CT) samples respectively. These glass and aluminum molds allow the air bubbles to escape through the top of the molds as the temperature was raised in the curing oven. The samples were cured in a temperature programmed oven and the curing schedule was dependent on the curing agents employed. The long curing cycles shown in Figure 34 were adopted in order to minimize the internal stresses.

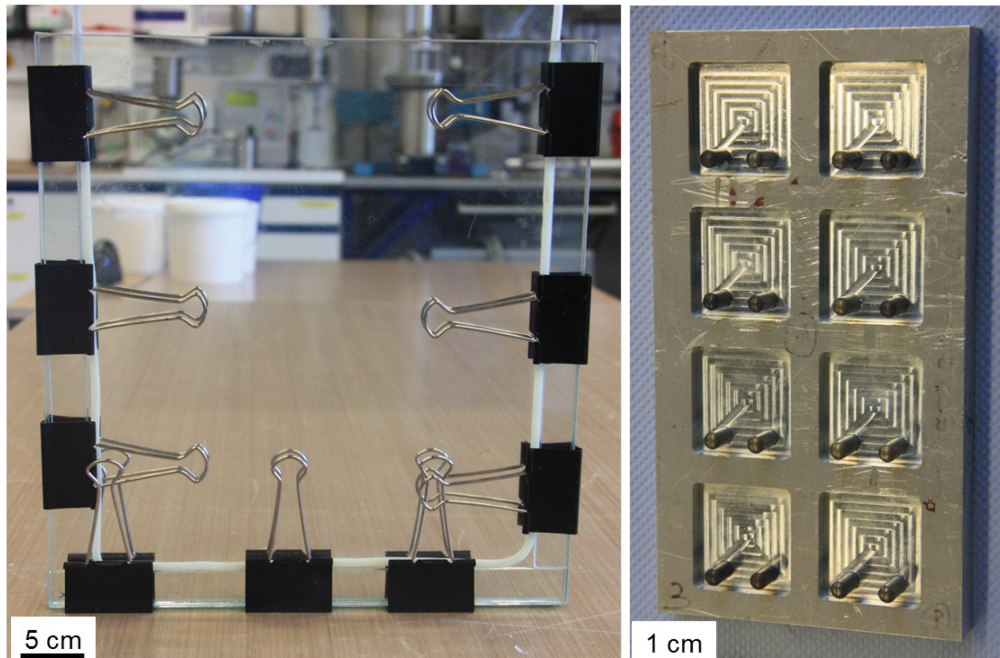


Figure 33: Glass molds for plates preparation (left) and steel molds for CT specimen curing.

After curing, composites were left in the oven and allowed to cool until they reached room temperature. Dog bone shaped samples for tensile tests were machined from

the cured composite plates with a precision milling cutter. Compact tension (CT) specimens ($37 \times 37 \times 6 \text{ mm}^3$) were used for fracture toughness tests

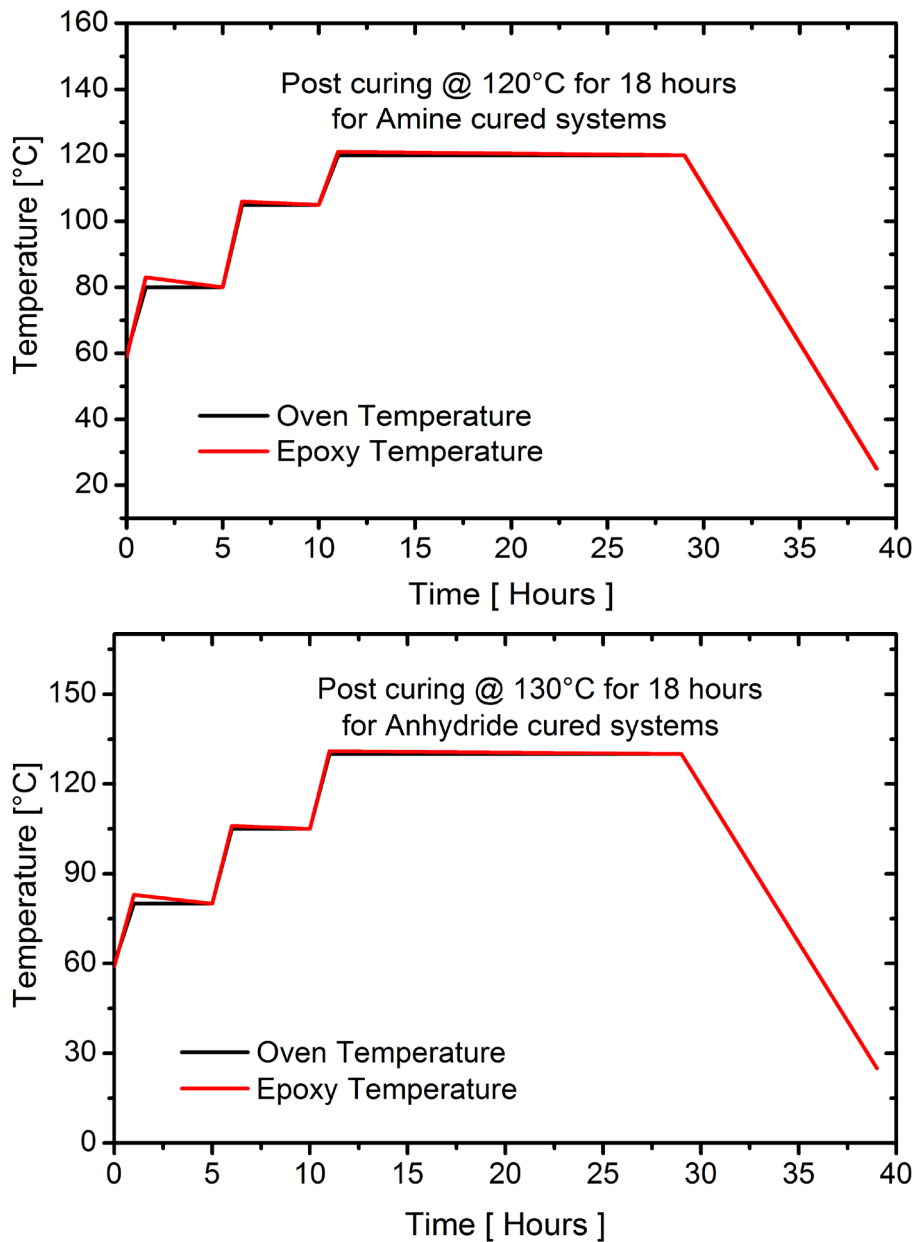


Figure 34: Curing cycle adopted for amine hardener (above) and anhydride hardener (below) based epoxy systems.

4.5.2 Epoxy and core-shell rubber composites

The epoxy and core-shell rubber composites were manufactured using the masterbatch technique. The masterbatch was a 25 wt. % core-shell rubber particles dispersed in the bisphenol-A based epoxy resin supplied by Kaneka Belgium NV. At first, the masterbatch and bisphenol-F epoxy were kept in the oven at 80 °C for 60 mins for preheating. According to the concentration of filler material that has to be

added, calculated amount of masterbatch was taken and thinned by adding it to the epoxy. After that, the mixture was stirred using a dissolver, by Dispermat, Getzmann GmbH, with three blade propeller at 200 rpm and 80 °C for 15 - 20 mins to obtain a homogenous mixture. It was cooled down to 50 °C before adding the stoichiometric quantity of amine or anhydride hardener to prevent quick gelation. In the meanwhile, glass molds of 4 mm thickness coated with a releasing agent (Würtz PAT-607/FB) and steel CT molds of 6 mm thickness coated with a releasing agent (Indrosil 2000) were prepared and kept in the oven at 80 °C for some period to attain heat. This prevents the formation of air bubbles or encourages them to escape easily while pouring the final mixture into them. The required amount of mixture was taken in small cups for rheology testing before addition of the hardener.

Later, the hardener was added to the mixture and stirred at 200 rpm and 50 °C for 5-10 mins and then the final mixture was transferred to the glass and steel molds. They were kept in a temperature programmed oven for curing according to the adopted curing schedule (Figure 34) which depend on the type of hardener used.

After curing, they were allowed to reach room temperature and then the plates were machined on a CNC milling machine to prepare tensile specimens (dog-bone shape) according to the prescribed DIN standards. The cured CT specimens with the dimensions of 37 x 37 x 6 mm³ were removed from steel molds and used for fracture toughness tests.

4.5.3 Epoxy and TiO₂ composites

The TiO₂ nanoparticles materials were conditioned in the oven before processing for 12 hours at 80 °C. The conditioning of the particles was done in order to remove the excess moisture content in the TiO₂ powder before adding to the resin. Nanoparticles were then directly added into the liquid epoxy resin which was also heated to 70 °C and then dispersed coarsely on a vacuum dissolver mixer (Dispermat®, VMA-Getzmann GmbH, Germany). The solution was then dispersed for 120 min at 65 °C with a torus-mill laboratory mixing device (TML 5, VMA-Getzmann GmbH, Germany), (see section 2.3.3). The mill was operated at 3000 rpm, 65 °C, under vacuum, during 120 min; a 60 vol. % of the milling chamber was filled up with ZrO₂ pearls with 1.2 - 1.7 mm of diameter. A masterbatch was produced containing a high weight fraction of nano-fillers (25 wt. %). After dispersing, the masterbatch was thinned down by the neat epoxy resin in order to systematically gain nanocomposites with varying

nanoparticle content ranging from 3 wt. % to 7 wt. %. Again the thinned down masterbatch was added to the resin and dispersed under vacuum for 1 hr. at a temperature of 85 °C at 350 rpm until the remaining trapped air was removed. The mixture was cooled down to 50 °C and a stoichiometric amount of amine curing agent was added and stirred thoroughly for 5-10 min at 650 rpm. Immediately after the mixture was properly dispersed, the mixture was transferred into glass moulds (Figure 33(left)) which are surface coated with releasing agent (Würtz PAT-607/FB) and left for 30 min to dry and assembled with clips and pre-heated at 80 °C in an oven before pouring the dispersed mixture to produce tensile and DMTA samples and steel moulds (Figure 33(right)) coated with releasing agent (Indrosil 2000) and pre-heated at 80 °C in an oven before pouring the dispersed mixture for compact tension (CT) samples respectively. These glass and aluminum molds allow the air bubbles to escape through the top of the molds as the temperature was raised and viscosity decreases. The glass and aluminum molds used were of 4 mm and 6 mm thickness. The samples were cured in a temperature programmed oven and the curing schedule was dependent on the curing agents employed.

Table 7: For different formulations corresponding wt. % to vol. % conversion.

Series	D51N (wt. %)						(vol. %)					
	2	4	6	8	10	12	2.15	4.26	6.39	8.50	10.61	12.72
MEP_D51N_H1	2	4	6	8	10	12	2.15	4.26	6.39	8.50	10.61	12.72
MEP_MX170_H1	2	4	6	8	10	12	2.42	4.83	7.18	9.52	11.86	14.18
MEP_D51N_H2	2	4	6	8	10	12	2.23	4.45	6.66	8.87	11.05	13.24
MEP_MX170_H2	2	4	6	8	10	12	2.53	5.01	7.48	9.91	12.33	14.72

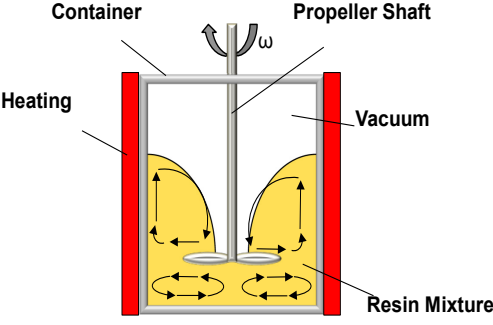
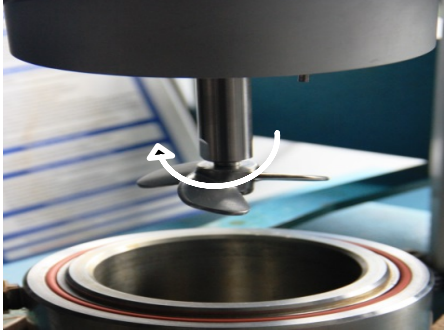
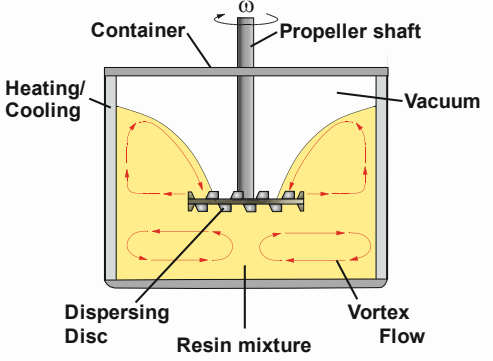
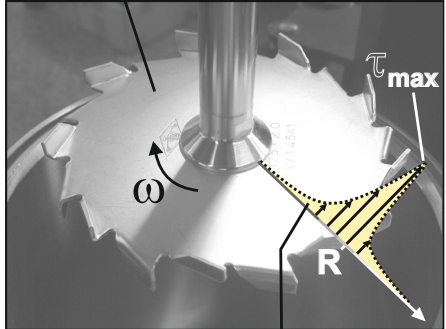
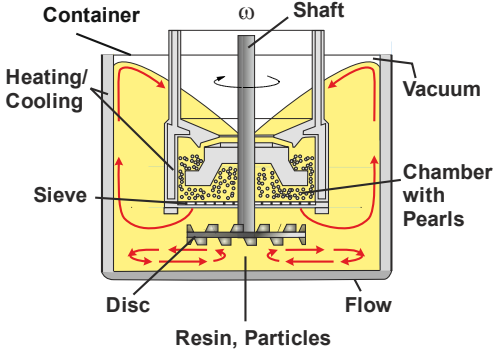
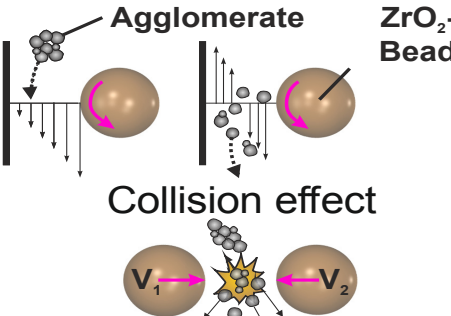
Table 8: Dispersion process used for different composites manufacturing

Series	Particles	Dissolver	Bead Mill
MEP / D51N	Di - block copolymer	▪	
MEP / MX170	Core-shell rubber	▪	
MEP / MX170 / D51N	Block copolymer / core shell	▪	
EP / TiO₂	TiO ₂ nanoparticles	▪	▪
EP / TiO₂ / D51N	TiO ₂ / di-block copolymer	▪	▪

Table 9: A complete overview of the different formulations prepared and testing methods used in the present work.

Series (H1- Amine) (H2- Anhydride)	D51N (wt. %)						MX170 (wt. %)						Tensile (23 °C, 80 °C)	Compressive (23 °C)	Fracture (23°C, 80°C)	DSC, DMTA	SEM, AFM	Analytical Modeling
	2	4	6	8	10	12	2	4	6	8	10	12	X	X	X	X	X	
MEP_H1	0						0						X	X	X	X	X	
MEP_H2	0						0						X	X	X	X	X	
MEP_D51N_H1	2	4	6	8	10	12	0						X	X	X	X	X	X
MEP_D51N_H2	2	4	6	8	10	12	0						X	X	X	X	X	X
MEP_MX170_H1	0						2	4	6	8	10	12	X	X	X	X	X	X
MEP_MX170_H2	0						2	4	6	8	10	12	X	X	X	X	X	X
MEP_D51N_MX170_H1	2	4	6				2	4	6				X	X	X	X	X	
MEP_D51N_MX170_H2	2	4	6				2	4	6				X	X	X	X	X	
Series (H1- Amine)	TiO ₂ (wt. %)			D51N (wt. %)						Tensile (23 °C)	Compressive (23 °C)	Fracture (23°C, 80°C)	DSC, DMTA	SEM, AFM	Analytical Modeling			
	3	5	7	0						X		X	X	X				
EP_H1_TiO ₂	3	5	7	0						X		X	X	X				
EP_H1_TiO ₂ _D51N	3			4	6	8			X		X	X	X					

Table 10: Different devices used in composite manufacturing [89]

Device	Structure	Working Principle
(a) PROPELLER	 <p>Container, Propeller Shaft, Heating, Vacuum, Resin Mixture</p>	
(b) DISSOLVER	 <p>Container, Propeller shaft, Heating/Cooling, Vacuum, Dispersing Disc, Resin mixture, Vortex Flow</p>	<p>Dispersion disc</p>  <p>Shear stress</p>
(c) TORUS MILL	 <p>Container, Shaft, Heating/Cooling, Vacuum, Sieve, Chamber with Pearls, Disc, Resin, Particles, Flow</p>	<p>Shear effect</p>  <p>Agglomerate, ZrO₂-Bead, Collision effect, V₁, V₂</p>

5. Experimental work

This chapter summarizes the various test methods and procedures that were employed to characterize the material properties and microstructure.

5.1 Rheometric measurement

An important parameter to consider while manufacturing thermoset based nanocomposites and especially in filament winding is the viscosity of the pre-cured mixture of matrix and fillers. Rheology is the study of flow and deformation of materials. Deformation and flow are referred to as strain or strain rate, respectively, and indicate the distance over which a body moves under the influence of an external force, or stress. For this reason, rheology is also considered to be the study of stress-strain relationships in materials. The viscosity of the epoxy resin–nanofillers mixture plays an important role in the production of nanocomposites and the industrial processing of materials to fabricate mechanical components. A low viscosity of the stabilized nanofillers suspension and a low yield point are beneficial for the degassing, mixing and casting of the components. On the other hand, to achieve a good dispersion of nanofillers in the resin, high shear forces need to be applied, a higher viscosity of the mixture is desirable for this purpose.

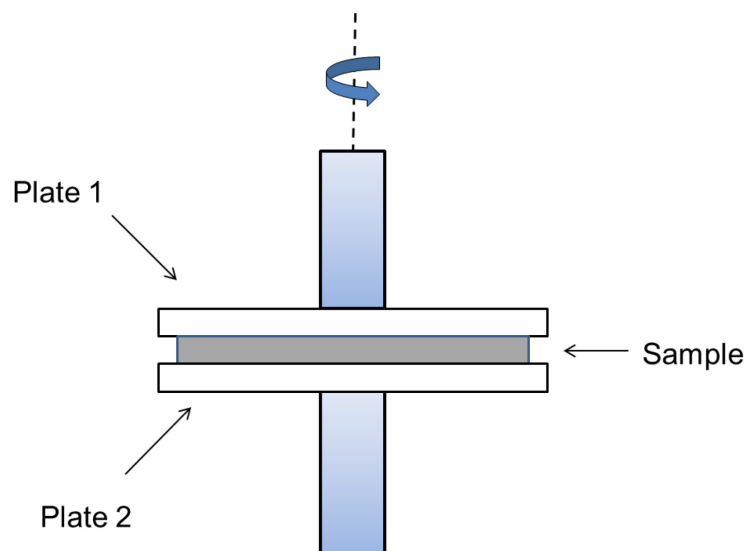


Figure 35: Basic working principle of rheometer [170]

Rheological measurements were performed for the temperature range 40 °C - 80 °C on a Rheometric Scientific ARES parallel plate rheometer under dynamic temperature ramp test at a ramp rate of 5 °C/min, the frequency of 62.8 rad/s using

45 mm diameter parallel plates separated at a distance of 0.6 mm. The sample is “soaked” or equilibrated for 1 min of time at 80 °C to ensure temperature uniformity in the material.

5.2 Mechanical tests

5.2.1 Tensile tests

Tensile tests were conducted at 23 °C and 80 °C on a universal testing machine (Zwick 1474, Zwick Roell AG, Ulm, Germany) in a tensile configuration according to standard DIN EN ISO 527-2. Dog-bone shape (ISO 527-2 type 1B (Figure 36)) samples were used for the testing. Samples have a gauge length of 50 mm, 10 mm width, and thickness of 4 mm. The distance between the sample clamping’s was 115 mm and the testing speed was chosen to be 2 mm/min with a 10 kN load cell, a precision sensor-arm extensometer was used to determine the specimen strain.

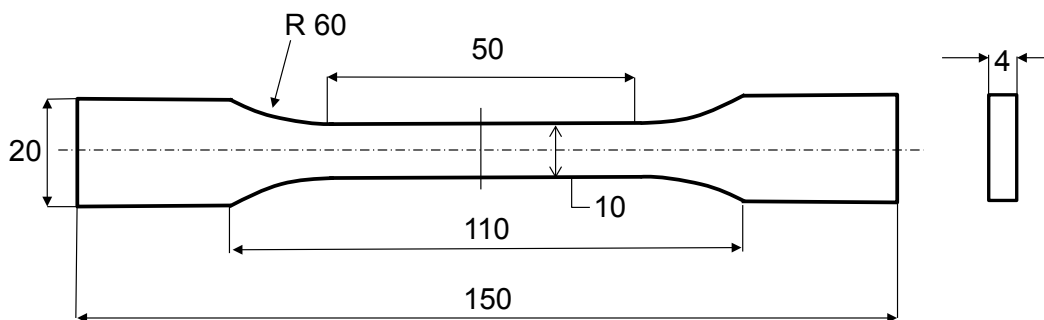


Figure 36: EN ISO 527-2 type 1B geometry for the tensile test specimen [171]

From the resulting stress-strain diagrams, the tensile modulus was determined from the slope of the curve between 0.05 % and 0.25 % of the total strain. The tensile strength was determined from the material maximum sustained stress. For tests at a higher temperature, a temperature cabinet was attached which maintain the environment near the clamps and specimens at the prescribed temperature and all the specimens for testing are kept in this chamber for a minimum of 2 hours so that final temperature was attained in samples. A minimum of five samples were tested for each formulation as required [172]

5.2.2 Plane strain compression tests

Plane strain compression (PSC) tests were conducted to determine the yield stress and failure strain according to standard DIN EN ISO 604. Since yield stress and

failure strain could not be obtained from tensile tests due to the inherent brittle nature of epoxies.

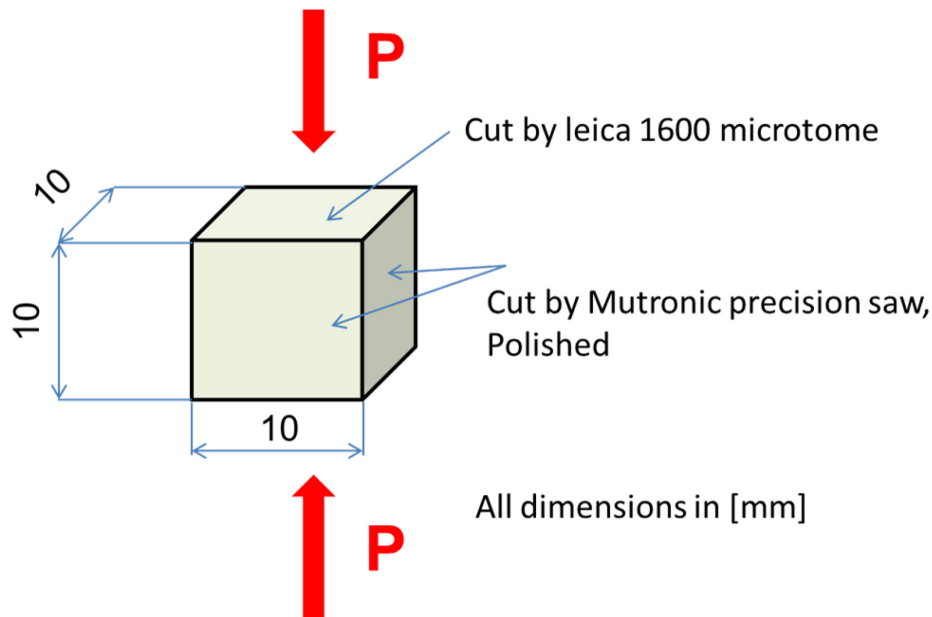


Figure 37: Plane strain compression test sample

PSC tests performed on the universal testing machine (Zwick 1474, Zwick Roell AG, Ulm, Germany) in compression configuration with a constant strain rate of 2 mm/min, to match the strain rate of tensile tests. All the tests were performed at 23 °C. Samples are cut in microtome so as to ensure the parallel and smooth surfaces.

5.2.3 Fracture toughness tests

Linear elastic fracture mechanics (LEFM) allows measuring the intrinsic fracture toughness of brittle solids [173]. Independent of the specimen geometry the LEFM provides information about the initiation of cracks in epoxy nanocomposites. The plane strain fracture toughness (K_{Ic}) of the composites was determined experimentally at 23 °C and at 80 °C by using compact tension (CT) samples under tensile loading conditions according to the Norm ISO 13586 and at strain rate of 0.2 mm/min. The thickness B and the width W of specimens were chosen to be 6 mm and 36 mm, respectively. The samples were tested in a universal testing machine (Zwick 1474, Zwick Roell AG, Ulm, Germany). To generate the required critical stress state in the material, a sharp crack of length a_0 ($0.45*W \leq a_0 \leq 0.55*W$), W is the distance between the applied load and the end of the sample) was created by the controlled impact of a fresh razor blade. Figure 38, shows the shape and dimensions of the compact tension sample used for fracture testing.

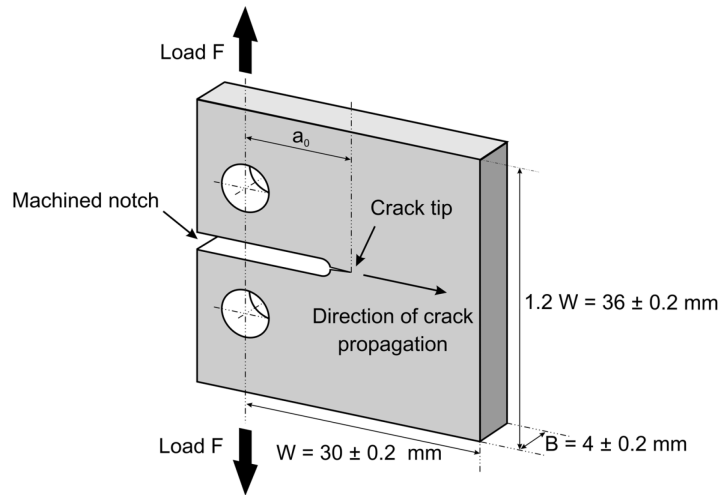


Figure 38: Geometry of Compact Tension samples used for fracture testing in mode-I condition.

Previous research [174] demonstrated that this razor blade tapping was an adequate method of introducing an initial crack in rubber toughened and pure epoxy resin specimens. The linear elastic fracture mechanics approach assumes that the plastically deformed area in front of the crack tip is small compared with the overall crack length, if done carefully, the tapping produces a straight crack front with the smallest pre-crack tip radius and low residual stresses around the crack tip. Therefore, the requirement to use the linear elastic approach is fulfilled and the experimental results give us reasonable values for the materials' fracture toughness. The fracture toughness K_{IC} was then calculated by Eq. (5.1)

$$K_{IC} = \frac{F}{B\sqrt{W}} \cdot f(a/W) \quad (5.1)$$

where F is the maximum force observed in the load-displacement curve, B is the sample width, W the distance from the point where the force is applied to the end of the sample and a_0 is the initial crack length for calculating $\alpha = a_0/W$ and $f(a_0/W)$ is a function of the dimensions of the sample, in present work compact tension (C.T.) specimens are used, has the following form (Eq. 5.2) [175].

$$f(\alpha) = \frac{(2 + \alpha)}{(1 - \alpha)^{3/2}} \cdot (0.866 + 4.64\alpha - 13.32\alpha^2 + 14.72\alpha^3 - 5.60\alpha^4) \quad (5.2)$$

The knowledge of the critical stress intensity factor K_{IC} , the elastic modulus E_t and Poisson's ratio ν (~ 0.35) allows calculating the critical energy release rate G_{IC} :

$$G_{IC} = \frac{K_{Ic}^2(1 - \nu^2)}{E_t} \quad (5.3)$$

5.3 Viscoelastic properties

5.3.1 Dynamic mechanical thermal analysis (DMTA)

DMTA can be simply described as simple technique applying an oscillating force to a sample and analyzing the material's response to that force [176]. One advantage of DMTA is that one can obtain a modulus each time a sine wave is applied, allowing us to sweep across a temperature or frequency range. By measuring both the amplitude of the deformation at the peak of the sine wave and the lag between the stress and strain sine waves, quantities like the modulus, the viscosity, and the damping can be calculated. The storage modulus, E' is the measure of the sample's elastic behavior. The ratio of the loss modulus (E'') to the storage modulus (E') is the $\tan \delta$ and is often called damping. It is a measure of the energy dissipation of a material.

$$\tan \delta = \frac{E''}{E'} \quad (5.4)$$

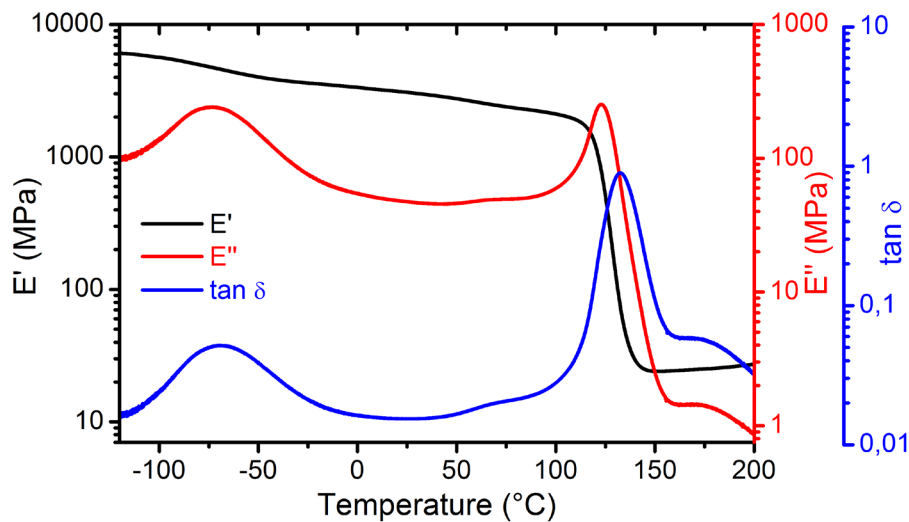


Figure 39: Typical DMTA graph showing storage modulus, loss modulus and $\tan \delta$ for the EP_H1 system.

In the present study, the storage modulus, the loss modulus, and $\tan \delta$ of all the bulk samples were measured by dynamic mechanical thermal analysis using a Q800 V7.5 Build 127 DMTA machine from TA Instruments in 3 point bending mode operating at 1 Hz, on specimens of 60 mm x 10 mm x 4 mm. The glass transition temperature, T_g

of the bulk epoxy samples was determined by the peak value of $\tan \delta$. The temperature range was set from $-120\text{ }^{\circ}\text{C}$ to $200\text{ }^{\circ}\text{C}$ with a heating rate of $2\text{ }^{\circ}\text{C}/\text{min}$. Figure 39 shows typical DMTA graph showing storage modulus, loss modulus, and $\tan \delta$.

5.3.2 Differential scanning calorimetry (DSC)

Differences in heat flow arise when a sample absorbs or releases heat due to thermal effects such as melting, crystallization, chemical reactions, polymorphic transitions, vaporization and many other processes.

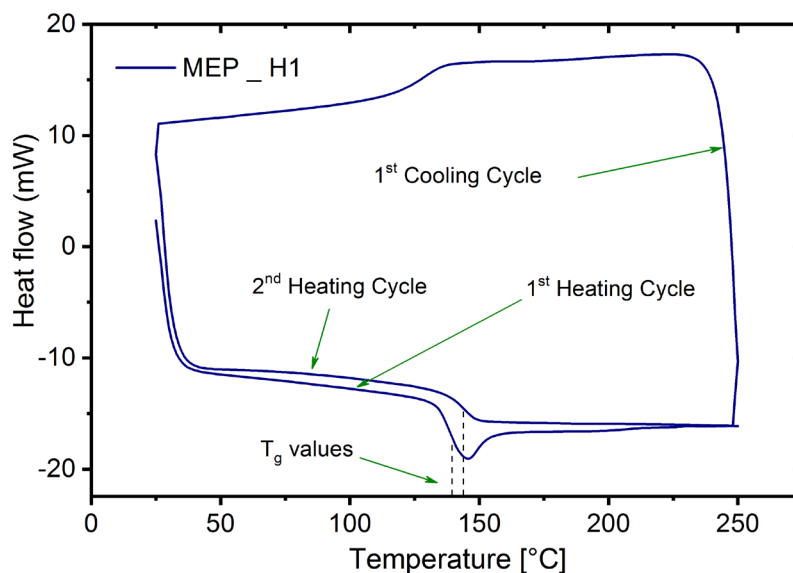


Figure 40: Different cycles during glass transition temperature measurement for amine based tailored epoxy system.

Specific heat capacities and changes in heat capacity, for example during a glass transition, can also be determined from the difference in heat flow. DSC measures the difference between the heat flows from the sample and reference sides of a sensor as a function of temperature or time. DSC was performed on a Mettler-Toledo DSC1 STAR[®] system to determine thermal quantities and to characterize the material. Firstly, the cured sample material was weighed ($\sim 7\text{--}13\text{ mg}$) and placed in a crucible, sealed with lids with the help of crucible sealing press. In the first cycle, the sample was heated from room temperature up to $250\text{ }^{\circ}\text{C}$ and cooled down to room temperature and again heated to $250\text{ }^{\circ}\text{C}$. In chapter 6, T_g (dry) was measured for all the formulations.

5.4 Microstructure

5.4.1 Scanning electron microscopy (SEM)

The fractured surfaces of the CT tested nanocomposites were studied with the help of a field emission scanning electron microscope (SEM SUPRA™ 40 VP, Carl Zeiss NTS GmbH, Germany). A SEM is a type of microscope capable of producing high-resolution pictures of a sample surface using electrons instead of light photons to form an image. A beam of electrons is produced at the top of the microscope by an electron gun. The electron beam follows a vertical path through the microscope, which is held in a vacuum. The electrons travel through electromagnetic fields which act as lenses focusing the beam down toward the sample. Once the beam hits the sample, electrons and X-rays are ejected from the sample. Detectors collect these X-rays, backscattered electrons, and secondary electrons and convert them into a signal that can interpret as an image of the scattering surface. SEM images have a characteristic three-dimensional appearance and are extremely useful to assess the surface structure of the samples.

Before inspecting the fracture surface under a microscope, the surfaces of the samples were sputtered with an Au/Pd alloy for 70 s using a sputtering device (SCD-050, Balzers, Liechtenstein. This sputtering process creates an ultra-thin electrically conductive metal coating over the polymer surface which is a non-conducting or poorly conducting. Sputter coating even prevents charging of the specimen, which would otherwise occur because of the accumulation of static electric fields. It also increases the number of secondary electrons that can be detected from the surface of the specimen in the SEM and therefore increases the signal to noise ratio. The use of the SEM technology delivered high-resolution surface information which was effective to investigate different mechanisms (i.e., adhesion between filler and matrix, crack deflecting mechanisms at the nanofillers, location of failures) involved in the mechanical properties of the nanocomposites developed in this research.

5.4.2 Atomic force microscope (AFM)

The atomic force microscope (AFM) is a very high-resolution (in nanometer range) type of scanning probe microscope. In AFM, a probe consisting of a sharp tip located near the end of a cantilever beam is raster scanned across the sample surface using

piezoelectric scanners. Changes in the tip-sample interaction are often monitored using an optical lever detection system, in which a laser beam is reflected from the cantilever onto a position-sensitive photodiode. During scanning, a particular operating parameter is maintained at a constant level, and images are generated through a feedback loop between the optical detection system and the piezoelectric scanners. Three imaging modes, contact mode, non-contact mode, and intermittent contact or tapping mode, can be used to produce topography, roughness and friction forces in the samples [177] [178]. In the present work Multimode AFM (MMAFM-2)/ Serial nos. 7410 with Nanoscope 3a controller and Nanoscope ® 3a software version 5.31R1 from Digital instruments/ Hysitron is used which has a lateral resolution: 2 nm, vertical resolution: 2 nm, x/y scan range: 0.3 μm to 120 μm and z scan range: 0 to 5 μm .

In the present work, AFM was performed in tapping mode to obtain the morphology of epoxy nanocomposites. A smooth surface of the samples is obtained using Power microtome. The phase and height images were captured at 512 x 512 - pixel resolution and scan speed of 1Hz is selected.

5.4.3 White light profilometry

A white light profilometer (FRT MicroProf, FRT GmbH) is employed to measure the surface roughness of fractured compact tension samples in non-contact mode. It has a lateral resolution of 1 μm , the vertical resolution of 3 nm, x/y scan range: 100 mm x 100 mm and z- scan range: 3 mm. The two chromatic sensors for different vertical measuring ranges (300 μm and 3 mm) permit the entry, illustration, and evaluation of almost all the surfaces.

6. Results and discussion

The present chapter investigates the modification of the epoxy polymers using different commercially available multi-functional epoxy resins such as LME10169, Araldite MY0816 and Araldite MY0610. Tensile and thermal properties were investigated for different formulations with varying concentrations.

6.1 Amine cured bis-F epoxy modified with multi-functional epoxies

This section discusses details of systems involving bis-F based EP862 and various multifunctional epoxies such as fluoren di-epoxy (LME10169), 1,6 – naphthalene di-epoxy (Araldite MY0816) and trifunctional epoxy resin based on meta amino phenol (Araldite MY0610). Each of the multifunctional epoxy resin was mixed with reference EP862 epoxy resin in small wt. % such as 5 wt. %, 7 wt. % and 10 wt. % and the stoichiometric amount of hardener were added to the system.

Table 11: Mechanical and thermal properties of the amine-based reference system and amine-based modified systems at 23 °C.

LME10169 [wt%]	E_t [MPa]	σ_m [MPa]	ϵ_m [%]	T_g [°C]	K_{IC} [MPa.m ^{1/2}]
0	2979 (±8)	85 (±0.4)	6.3 (±0.2)	136	0.57 (±0.05)
5	2990 (±29)	89 (±0.5)	6.9 (±0.2)	135	0.62 (±0.04)
7	3230 (±19)	95 (±0.4)	7.0 (±0.1)	134	0.73 (±0.08)
10	3020 (±41)	90 (±0.6)	6.9 (±0.2)	136	0.69 (±0.05)
MY0816 [wt. %]	E_t [MPa]	σ_m [MPa]	ϵ_m [%]	T_g [°C]	K_{IC} [MPa.m ^{1/2}]
0	2979 (±8)	85 (±0.4)	6.3 (±0.2)	136	0.57 (±0.05)
5	2985 (±14)	87 (±0.4)	6.8 (±0.4)	137	0.59 (±0.05)
7	3160 (±24)	92 (±1.5)	6.9 (±0.3)	138	0.63 (±0.05)
10	2950 (±17)	88 (±0.6)	6.8 (±0.6)	138	0.55 (±0.05)
MY0610 [wt. %]	E_t [MPa]	σ_m [MPa]	ϵ_m [%]	T_g [°C]	K_{IC} [MPa.m ^{1/2}]
0	2979 (±8)	85 (±0.45)	6.3 (±0.2)	136	0.57 (±0.05)
5	2940 (±14)	87 (±0.42)	6.5 (±0.4)	137	0.60 (±0.08)
7	3140 (±24)	92 (±0.32)	6.8 (±0.4)	138	0.65 (±0.03)
10	2990 (±17)	89 (±0.41)	6.6 (±0.5)	139	0.59 (±0.07)

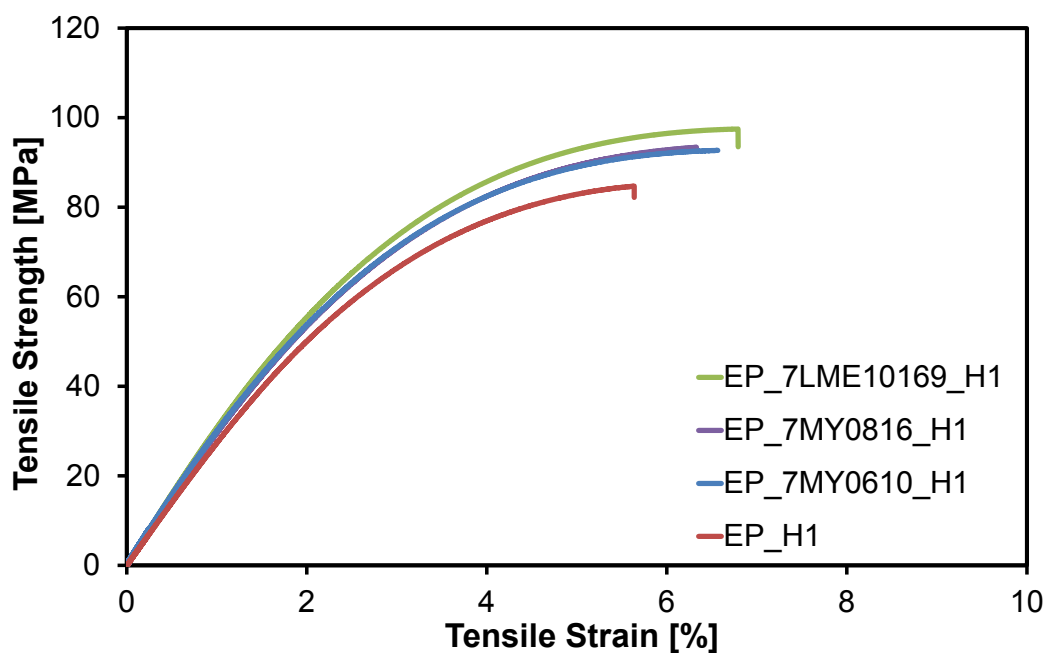


Figure 41: Representative stress-strain curves show the comparison of 7 wt. % of different modifiers for the amine-based system at 23 °C.

6.1.1 Tensile properties

The tensile modulus and tensile strength increase with the increasing wt. % of the multifunctional epoxies (LME10169, MY0816 and MY0610) and the maximum value of strength was obtained at 7 wt. % for all the three systems. The tensile strength of 95 MPa was measured for the EP_7LME10169_H1 system. The improvement in tensile strength over that of base resin for all wt. % of the multifunctional epoxies was due to a high degree of compatibility, enhanced cross-linking as well as chain extension. This can also be attributed to some amount of entangling among polymer chains due to hybrid network formation. At 7 wt. % the degree of cross-linking becomes optimum beyond which further addition of modifiers does not show any strengthening effect.

EP_7LME10169_H1 was selected as the best system if overall properties were considered from Table 11. For the sake of simplicity, the amine-modified system is termed as **MEP_H1** and amine-based reference system is **EP_H1**.

6.1.2 Thermal and viscoelastic properties

The T_g values were listed in Table 11 for all the modified systems. It was clearly evident that all the systems have glass transition temperature in the same range with

a difference of ± 3 °C as compared to the reference system. The selected modified system has T_g of 134 °C (from DSC) however, for the same system, it is measured 139 °C as shown in Figure 42 (right) by $\tan \delta$ vs. temperature (DMTA) graph. In Figure 42 the storage modulus vs. temperature curve shifts towards the right in glass transition zone showing that storage modulus is higher for the same temperature in glass transition zone. Similarly, the $\tan \delta$ curve shows the same tendency of right shift for modified system showing higher T_g and lower damping factor as compared to the reference amine system.

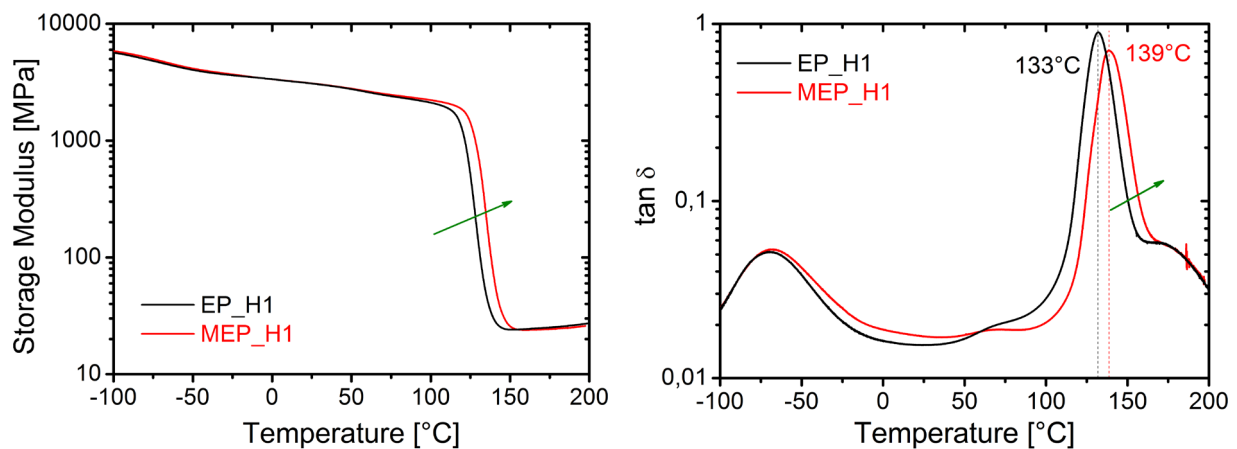


Figure 42: DMTA curve comparison between anhydride based reference epoxy (**EP_H1**) and modified epoxy system (**MEP_H1**). Storage modulus vs. temperature (left) and $\tan \delta$ vs. temperature (right).

Following effects were investigated on both the systems i.e. the reference bis-F based epoxy system (EP_H1) and 7 wt. % LME10169 modified bis-F based epoxy system which is denoted by MEP_H1. In both cases, H1 is denoting the amine-based hardener.

a) Effect of strain rate:

As we saw in Figure 43, with the increasing strain rate the tensile strength was also increasing and the strain at break was found to be maximum at 2 mm/min for both the systems. All these tests were performed at 23 °C. It can be inferred that at the temperature below T_g the strain rate has a pronounced effect on maximum tensile stress, but modulus remains almost same at all strain rate. For tensile strain, no such behavior was observed as only yield strength was affected by the variation of pressure, temperature and strain rate [42] [43].

b) Effect of temperature:

In Figure 44 it was observed that with the increase in temperature, the ductile response of the epoxy system increases. Tensile modulus and maximum tensile strength were decreasing with the increase in temperature.

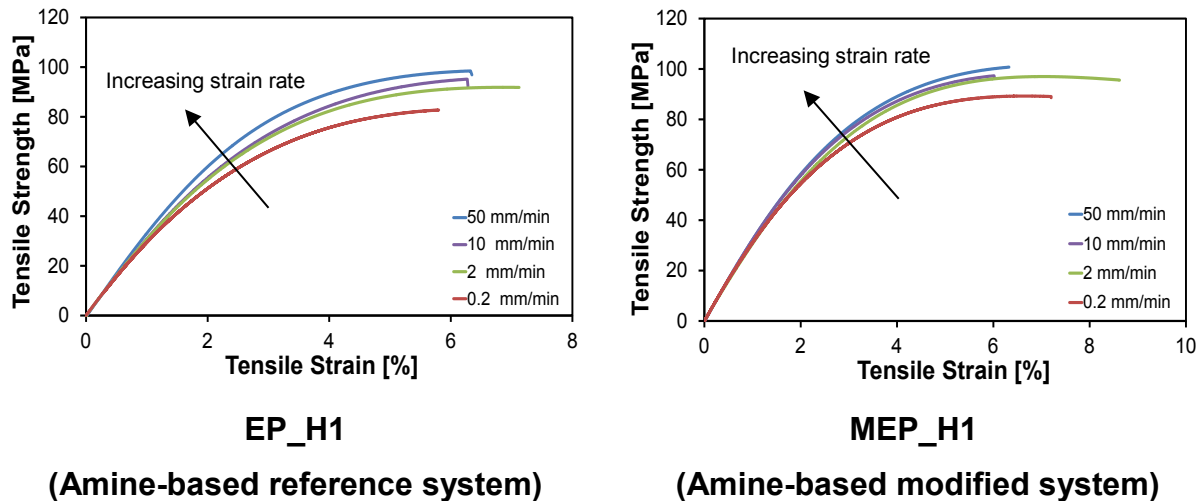


Figure 43: Effect of different strain rate on the representative stress-strain curve for amine based reference system and amine-based modified system at 23 °C.

At 80 °C, the decrease in ultimate tensile strength (UTS) was more pronounced as the temperature is moving towards T_g and the epoxy is going to be in transition from glassy to the rubbery region via glass transition stage. It can also be concluded that as the temperature increases, the epoxy becomes more ductile, resulting in higher strain to failure. The tendency of higher strain to failure is due to increased mobility of the polymer chains in the epoxy hardener system as the temperature is rising. It's worth mentioning that the modified system MEP_H1 exhibits better tensile properties when compared to the reference system EP_H1 at all the temperatures.

c) Effect of moisture:

The dog-bone samples of anhydride based reference (EP_H1) and modified epoxy (MEP_H1) system were dipped in water for 1 week time, later they were taken out and dried in an oven at 40 °C for an hour and further tensile tests were performed. An increase of 0.13 % and 0.12 % in weight was measured for EP_H1 and MEP_H1 systems respectively. Many researchers showed that moisture can adversely affect the mechanical properties of epoxy adhesives by decreasing the elastic modulus [179], yield stress [180] and ultimate stress [180]. They have all attributed the decrease in modulus due to the plasticizing action of the water on the adhesive. By

acting as an external plasticizer to the polymer adhesive, water spreads the polymer molecules apart and reduces the polymer-polymer chain secondary bonding. This gives more space for the polymer molecules to untangle and move around, which results in a softer, easily deformable mass [181].

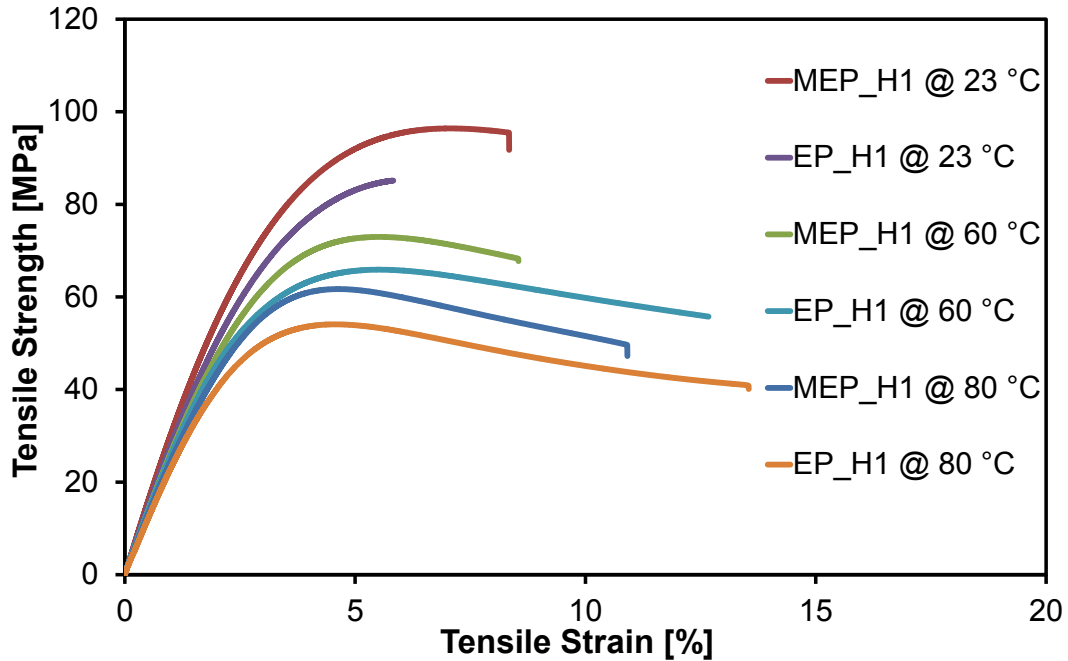


Figure 44: Effect of temperature on the representative stress-strain curves at temperature 23 °C, 60 °C and 80 °C for reference and modified amine-based epoxy system.

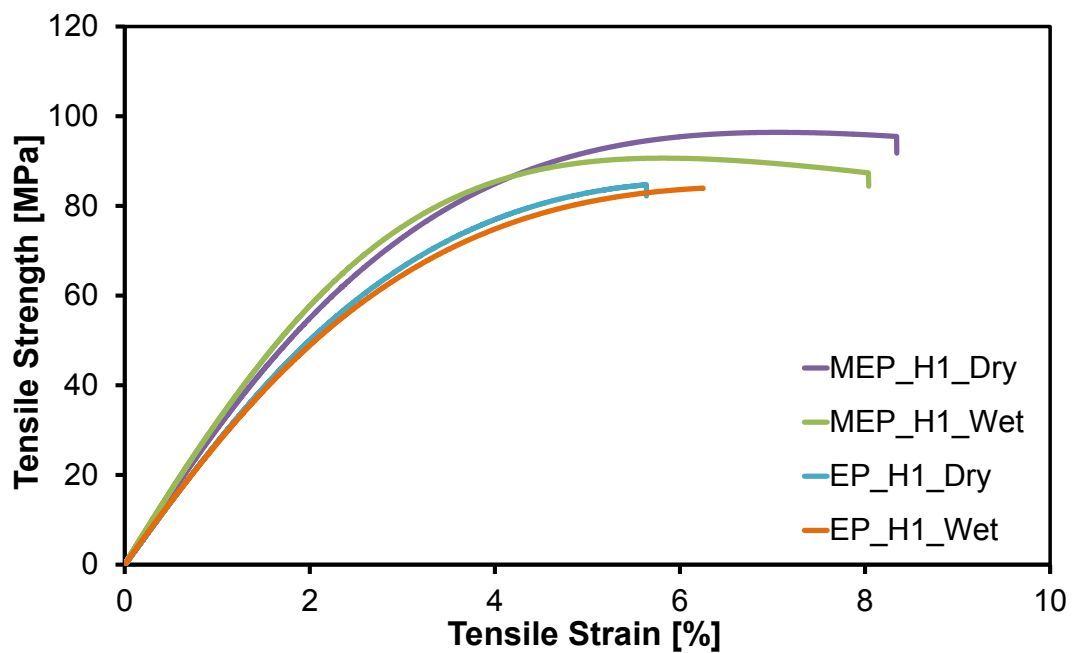


Figure 45: Representative stress-strain curves for amine based reference and amine-based modified system in dry and wet conditions at 23 °C.

6.2 Anhydride cured bis-F epoxy modified with multi-functional epoxies

This section discusses systems involving reference bis-F based epoxy and various multifunctional epoxies such as fluoren di-epoxy (LME10169), 1,6 – naphthalene di-epoxy (Araldite MY0816) and trifunctional epoxy resin based on meta amino phenol (Araldite MY0610). Each of the modifiers is mixed with reference EP862 epoxy resin in small wt. % such as 5 wt. %, 7 wt. % and 10 wt. % stoichiometrically and non-stoichiometrically (± 10 % hardener). Here only those systems discussed which were having superior properties as compared to reference system properties.

Table 12: The mechanical and thermal properties of the anhydride based reference system and modified systems.

LME10169	E_t [MPa]	σ_m [MPa]	ε_m [%]	T_g [°C]	K_{IC} [MPa.m^{1/2}]
EP_H2	3450 (± 40)	92 (± 0.66)	5.7 (± 0.01)	141	0.59 (± 0.10)
EP_A	3470 (± 34)	91 (± 0.95)	5.7 (± 0.04)	144	0.62 (± 0.05)
EP_B	3440 (± 10)	92 (± 0.28)	5.7 (± 0.08)	141	0.58 (± 0.12)
EP_C	3520 (± 30)	100 (± 1.0)	5.8 (± 0.03)	141	0.66 (± 0.06)
MY0816	E_t [MPa]	σ_m [MPa]	ε_m [%]	T_g [°C]	K_{IC} [MPa.m^{1/2}]
EP_H2	3450 (± 40)	92 (± 0.66)	5.7 (± 0.01)	141	0.59 (± 0.10)
EP_D	3500 (± 65)	98 (± 0.58)	5.8 (± 0.06)	143	0.60 (± 0.07)
EP_E	3330 (± 18)	95 (± 0.50)	5.8 (± 0.02)	141	0.55 (± 0.05)
EP_F	3510 (± 36)	100 (± 0.65)	5.8 (± 0.02)	144	0.65 (± 0.08)
MY0610	E_t [MPa]	σ_m [MPa]	ε_m [%]	T_g [°C]	K_{IC} [MPa.m^{1/2}]
EP_H2	3450 (± 40)	92 (± 0.66)	5.7 (± 0.01)	141	0.59 (± 0.14)
EP_I	3460 (± 77)	94 (± 0.66)	5.7 (± 0.04)	143	0.56 (± 0.09)
EP_J	3440 (± 45)	97 (± 0.66)	5.8 (± 0.06)	141	0.60 (± 0.16)
EP_K	3580 (± 78)	102 (± 0.66)	5.8 (± 0.01)	148	0.64 (± 0.11)

Systems (EP_A, EP_D and EP_I) have 7 wt. % of LME10169, MY0816 and MY0610 modifiers respectively, systems (EP_B, EP_E and EP_J) have 7 wt. % of LME10169, MY0816 and MY0610 with 10 % less hardener in the whole systems and finally systems (EP_C, EP_F, and EP_K) have 7 wt. % of LME10169, MY0816 and MY0610 with 10 % extra hardener in the whole systems.

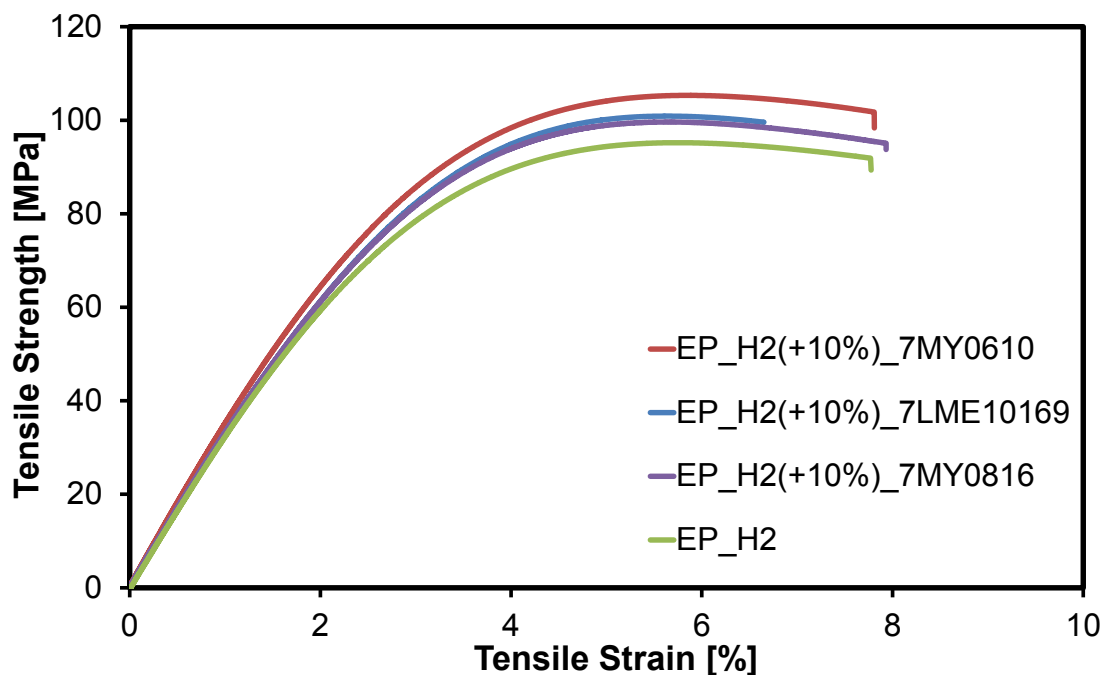


Figure 46: Representative stress-strain diagram for anhydride-based reference and anhydride based modified systems at 23 °C.

6.2.1 Tensile properties

From Table 12, it was concluded that for all the modified epoxy systems the maximum tensile strength and tensile modulus was obtained for 7wt. % modifier concentration plus 10% extra hardener.

From the Table 12, we can see that EP_I (EP_H2 (+10%) _7 MY0610) was having the superior properties in terms of tensile strength, tensile modulus, and glass transition temperature. The possible reason behind this trend would be epoxy curing by anhydride occurs via both esterification with hydroxyl present in epoxy and ether formation after epoxy reacts with the generated hydroxyl group. Thus the ratio was used around 0.5 to 1. If anhydride was increased the more and more hydroxyl will react to form ester and hydroxyl. The generated hydroxyl, in turn, will react with epoxy. Thus although complicated, more cross-linking will occur with increased hardener. From anhydride based system the (EP_H2 (+10%) _7 MY0610) was selected and further testing was performed in the following section and denoted further as **MEP_H2**, and reference anhydride system was denoted by **EP_H2**.

6.2.2 Thermal and viscoelastic properties

For all the modified systems T_g values obtained from DSC measurements were listed in Table 12. It was clearly evident that all the systems have either same or higher glass transition temperature as compared to the reference system obtained from DSC measurements. For the selected modified system the T_g was 148 °C (from DSC), and for the same system, it was also confirmed by $\tan \delta$ vs temperature (DMTA) graph shown in Figure 47 (right). In Figure 47 storage modulus vs. temperature curve shifts towards right in glass transition zone showing that storage modulus was higher for the same temperature in glass transition and indicates the higher T_g of the modified system as compared to reference anhydride system. Similarly, the $\tan \delta$ curve shows the same tendency of right shift for modified system showing higher T_g and lower damping factor as compared to the reference anhydride system.

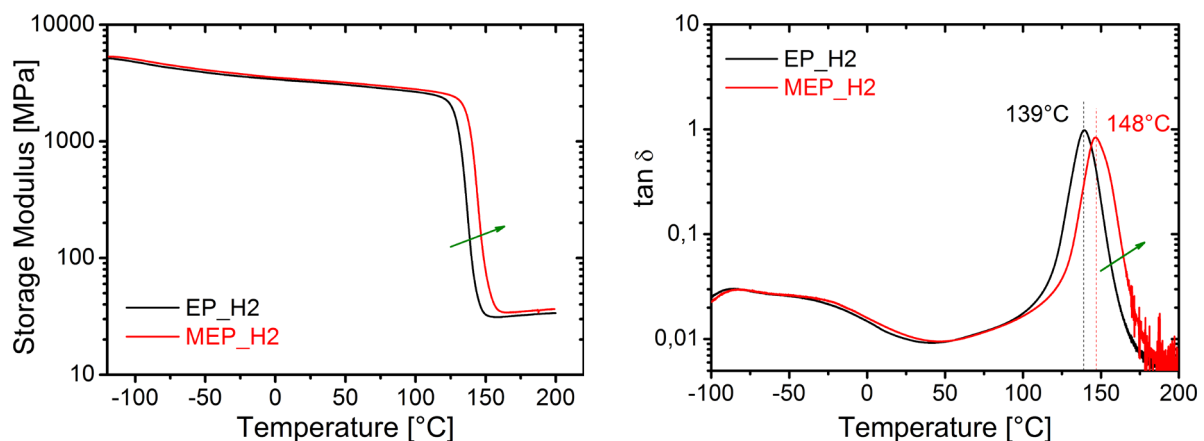


Figure 47: DMTA curve comparison between anhydride-based reference epoxy (EP_H2) and modified epoxy system (MEP_H2). Storage modulus vs. temperature (left) and $\tan \delta$ vs. temperature (right).

Figure 48 shows the variation of frequency on the $\tan \delta$ vs. temperature and elastic modulus vs. temperature curve, from both the graphs it can be concluded that with the increase in frequency the glass transition temperature of the system also increases, however in the present work standard 1 Hz frequency was used for all the systems.

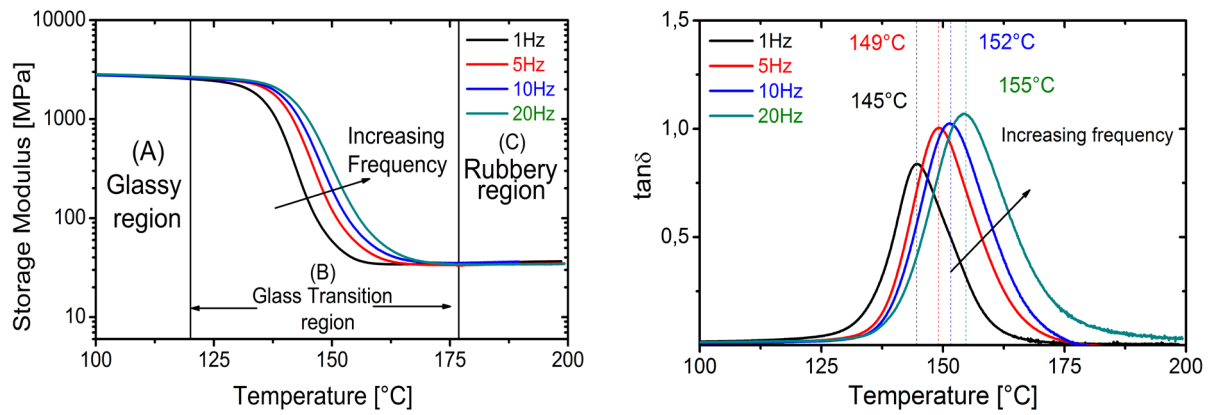


Figure 48: Effect of varying frequencies on the MEP_H2 system. Storage modulus vs. temperature curve (left) and $\tan \delta$ vs. temperature (right).

a) Effect of strain rate:

From Figure 49 it was clear that with the increasing strain rate the tensile strength was also increasing. All the tests were performed at 23 °C. It can be inferred that at the temperature below T_g the strain rate has a pronounced effect on maximum tensile stress, and Young's modulus remains almost same for all strain rates. For tensile strain, no such behavior was observed which was due to the fact that, only yield strength depends on the pressure, temperature and strain rate [42] [43].

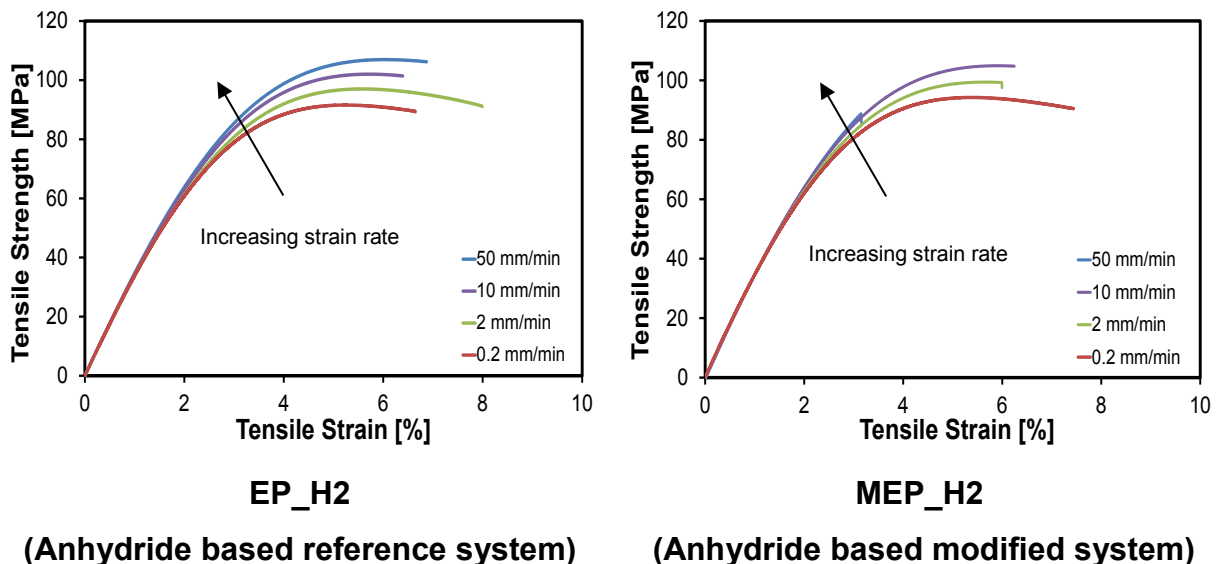


Figure 49: Effect of different strain rate on the representative stress-strain curve for amine based reference system and amine-based modified system at 23 °C.

b) Effect of Temperature:

It was observed in Figure 50 that with the increase in temperature, ductile response of the epoxy system increases, tensile modulus and maximum tensile strength was decreasing with the increase in temperature. At 80 °C, the decrease in ultimate tensile strength (UTS) was more pronounced as the temperature was moving towards T_g and the epoxy/hardener system was going to be in transition from glassy to the rubbery region via glass transition stage. It can also be concluded that as the temperature increases, the epoxy becomes more ductile, resulting in higher strain to failure. The tendency of higher strain to failure was due to increased mobility of the polymer chains in the epoxy hardener system with the rise in temperature. Figure 50 shows that (MEP_H2) system exhibit superior property if compared with (EP_H2) system for all the temperatures.

c) Effect of moisture:

The dog-bone samples of anhydride based reference (EP_H2) and modified epoxy (MEP_H2) system were dipped in water for 1 week time, later they were taken out and dried in an oven at 40 °C for an hour and further tensile tests were performed. An increase of 0.15 % and 0.13 % in weight was measured for EP_H2 and MEP_H2 systems respectively. Water acts as a plasticizing agent and reduces the mechanical properties such as strength and moduli [179] [180] see Figure 51. But it was clearly evident that the modified system has superior properties as compared to the reference system both in dry and wet conditions.

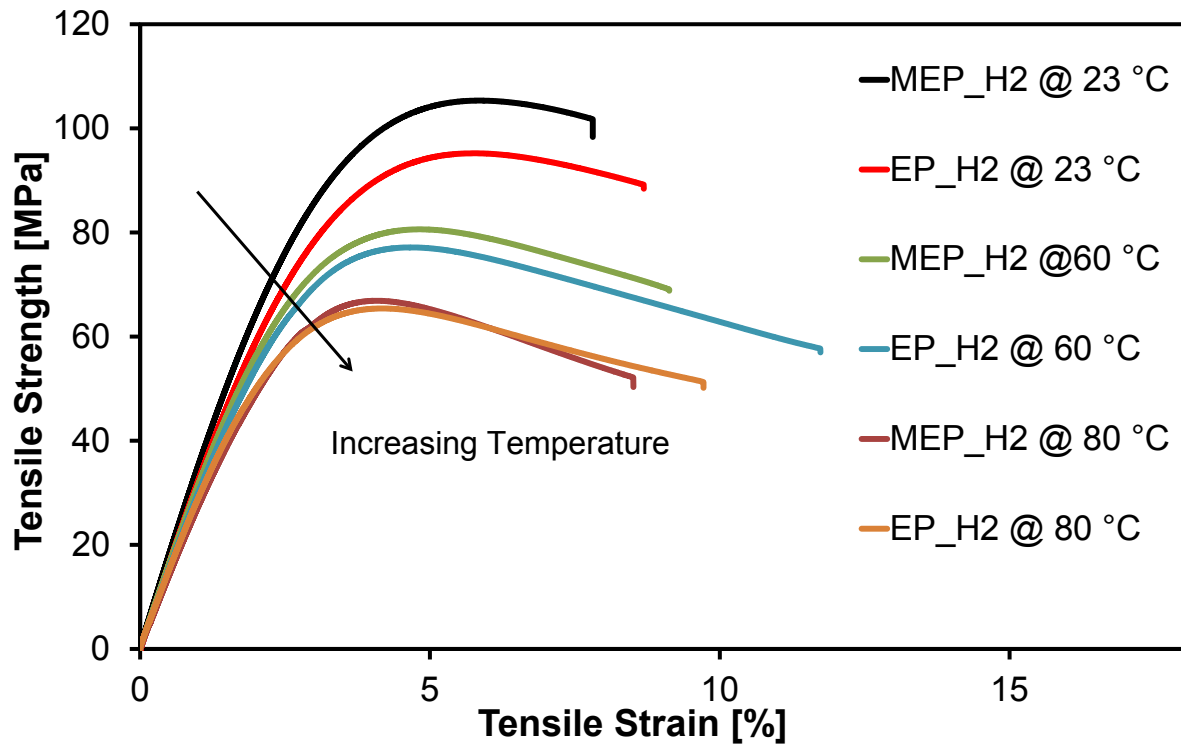


Figure 50: Effect of temperature on the stress-strain curve for anhydride based reference (EP_H2) and modified epoxy (MEP_H2) systems at 23 °C, 60 °C and 80 °C.

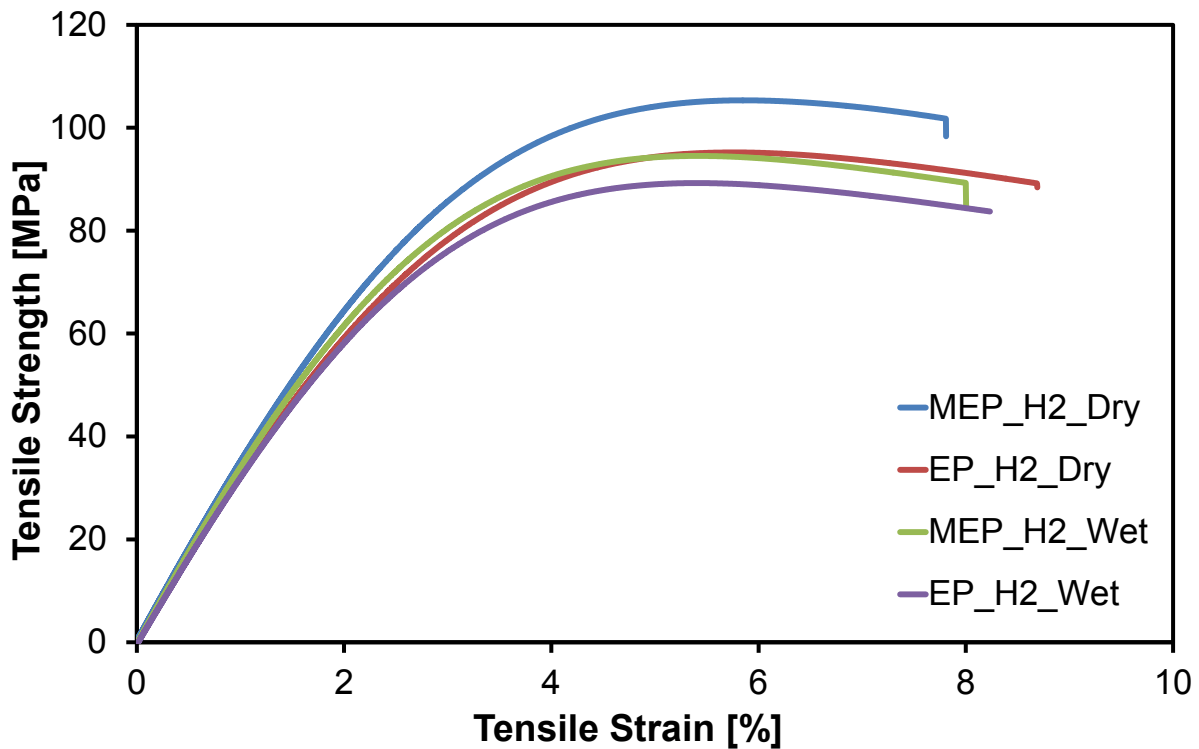


Figure 51: Representative stress-strain curves for anhydride based reference and modified epoxy system in dry and wet conditions at 23 °C.

6.3 Amine cured tailored epoxy system modified with D51N BCP's

The epoxy was modified with a diblock copolymer which was commercially available called as 'Nanostrength D51N' supplied by Arkema, France. It contains two blocks out of which one was a softer poly(butyl acrylate) also called as PbuA and the other was harder poly(Methyl methacrylate) also called as PMMA. Amine-based modified epoxy system i.e. MEP_H1 was used as the epoxy hardener system and it was systematically modified with D51N block copolymer for 2 wt. %, 4 wt. %, 6 wt. %, 8 wt. %, 10 wt. % and 12 wt. % respectively and the appropriate curing cycle was used for all the formulations.

6.3.1 Microstructure

The unmodified epoxy was found to be a homogeneous single phase material as expected, see Figure 52. All the epoxy amine hardener system modified with D51N were transparent before and after the curing process.

This suggests that, after the curing process, no macrophase separation occurred and nanostructure was formed in all D51N modified epoxies since particle exceeding $1/15$ of the wavelength of visible light scatter light and reduces the transparency of the materials [182]. This also suggests that D51N BCP was more compatible with amine-based hardener systems.

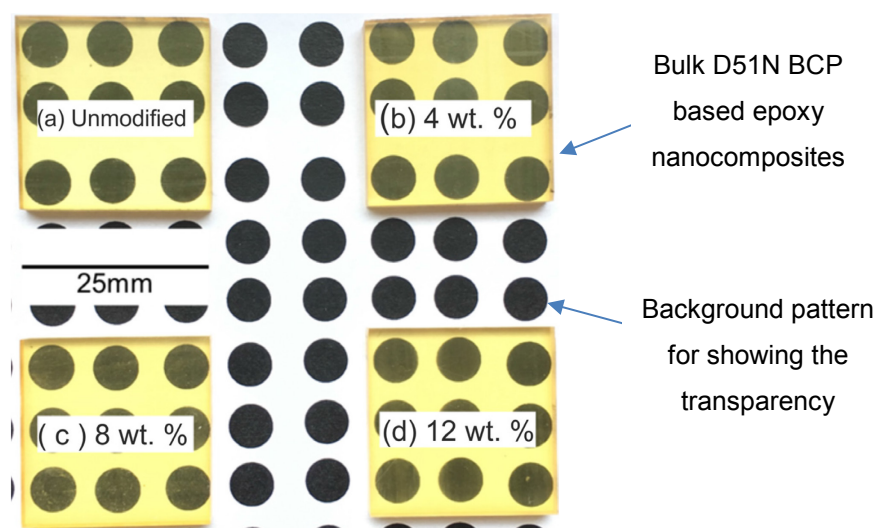


Figure 52: Bulk samples of the unmodified and D51N modified amine cured epoxy samples. (a) Unmodified epoxy; (b) 4 wt. % D51N modified epoxy; (c) 8 wt. % D51N modified epoxy; (d) 12 wt. % D51N modified epoxy.

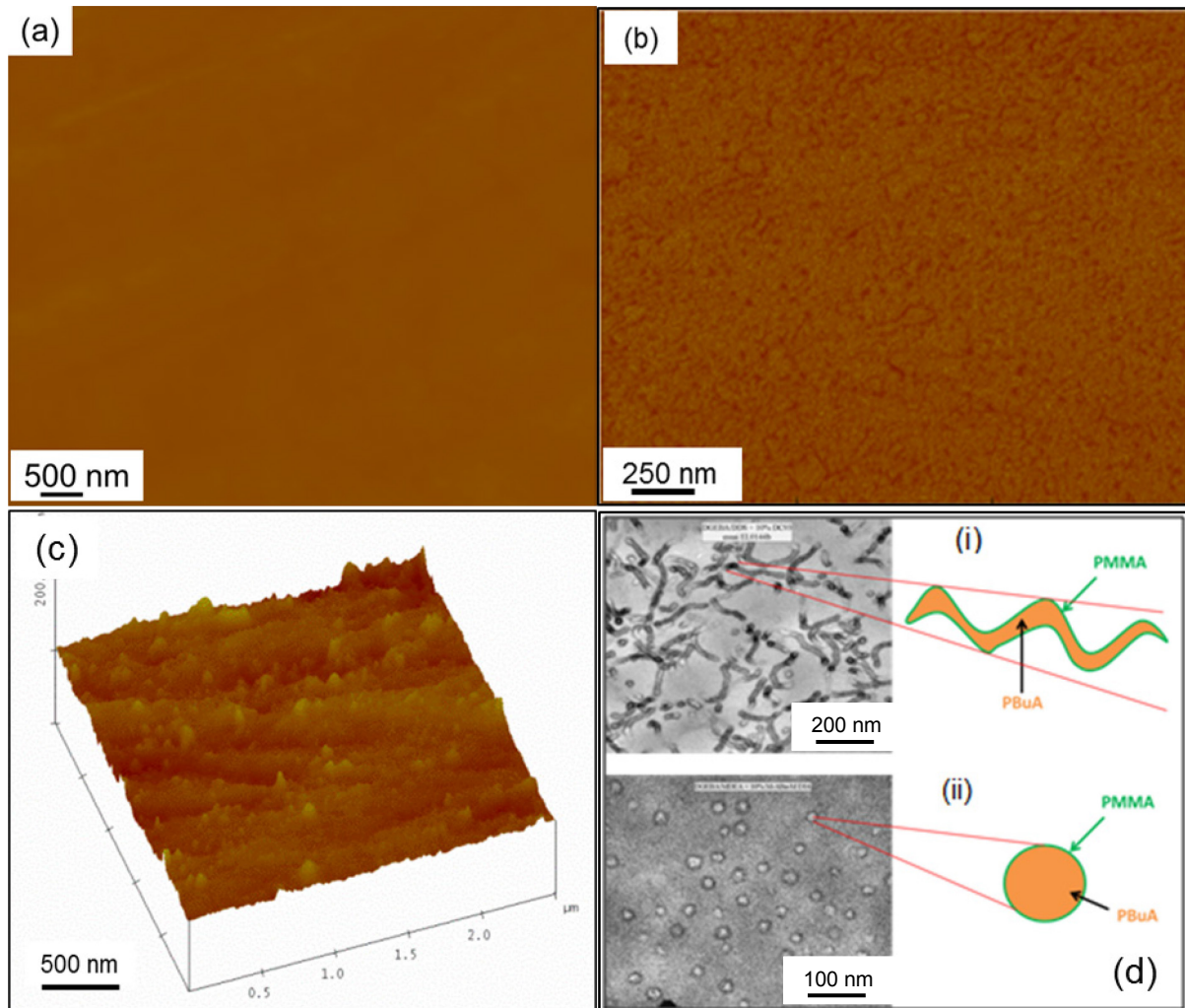


Figure 53: (a) AFM height image of the polished surface of bulk unmodified epoxy. (b) AFM height image of the polished surface of bulk 6 wt. % D51N modified epoxy system. (c) The surface profile polished surface of the bulk of 6 wt. % D51N modified epoxy system. (d) TEM images of self-assembled structures in epoxy (i) worm-like micelles (ii) core-shell particles [12].

The morphologies of the unmodified and EP-D51N particles modified epoxies were observed using AFM. The morphology of the unmodified epoxy was homogeneous and featureless Figure 53 (a) and the AFM height images show the same kind of morphologies for D51N modified nanocomposites up to 12 wt. % D51N particle content. Chen [13] postulated that the worm-like micelles might have a 3D bicontinuous gyroid structure, or be co-continuous. However, this would be difficult to show with 2D microscopy techniques such as AFM or TEM. Laboratory grade X-ray micro-tomography techniques do not have sufficient resolution to resolve the relatively small dimensions of the worm-like micelles. The particles were too small to determine if these particles were spherical micelles, had a core-shell structure or phase separated as homogeneous MAM. Indeed, the transparency of the D51N MAM modified epoxies was due to the nanostructures.

Several other authors have also reported such morphologies for MAM modified epoxies [13] [86] [152]. The microstructure of the worm-like micelles and core-shell particles can be determined by considering the amphiphilic nature of the block copolymers. The PMMA block was miscible in the epoxy and “epoxy-philic”, whereas the PBuA block was immiscible and “epoxy-phobic”. Hence the PBuA block would naturally self-assemble as the core, with the PMMA block as the shell, as shown in Figure 53 (d).

6.3.2 Rheology

The viscosity of a resin employed in the filament winding process was of supreme importance. As a prerequisite, the resin viscosity has to range between 0.35 - 3 Pa.s throughout the whole winding process in the temperature range of 50 °C - 70 °C, to ensure easy processability and complete wetting of the fibers. If the viscosity was much lower than the 0.35 Pa.s, the resin will flow excessively when on the mandrel, which could result in it dripping off the part and possibly leaving some fibers insufficiently wetted.

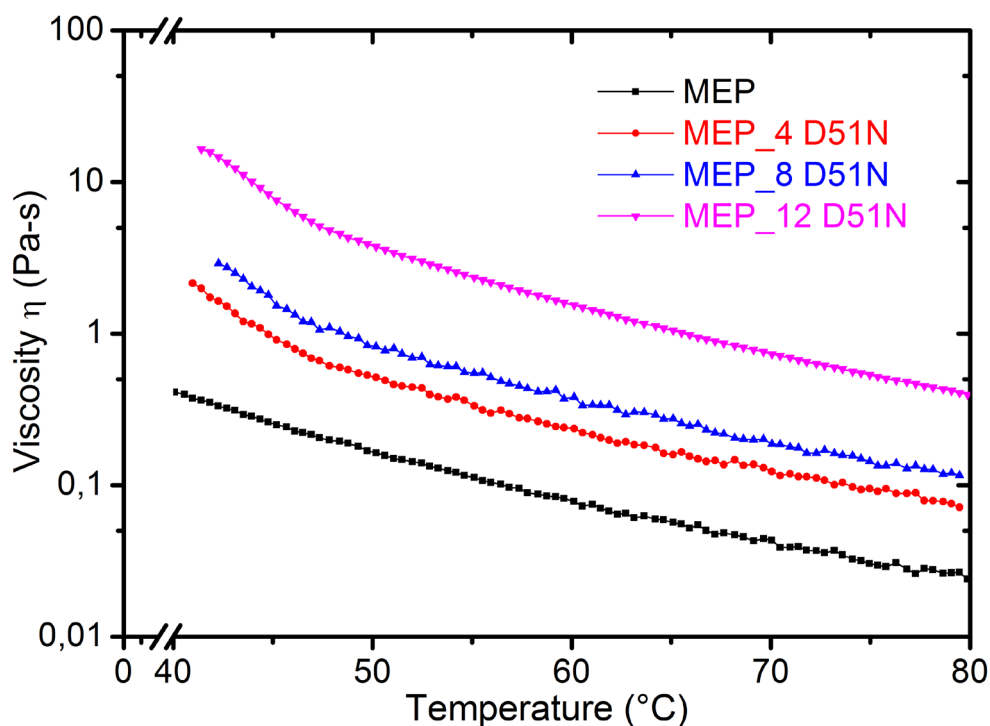


Figure 54: Graph showing variation in viscosity with respect to temperature for different tailored epoxy systems modified with D51N BCP's.

In general when a second phase was introduced to the epoxy resin, there will be an increase in the viscosity. The viscosity change of the different epoxy systems as a function of temperature was shown in Figure 54. This was because the particles present in the system tends to offer a resistance to the resin flow owing to increase in the viscosity. The viscosity of pure epoxy is 0.423 Pa.s at 40 °C and the addition of 12 wt. % of D51N block copolymers raised the viscosity to 10.071 Pa.s at the same temperature of 40 °C. The results obtained from the rheological tests were used to produce the graphs for showing the change in the viscosity with respect to temperature.

6.3.3 Glass transition temperature and viscoelastic properties

The glass transition temperatures of amine-cured unmodified and D51N modified epoxy systems were measured with the help of DSC and DMTA techniques. The results were tabulated as shown in Table 13. It's observed that for the unmodified epoxy system, the glass transition temperature was 134 °C and with the addition of block copolymer, the T_g either increase or remains same. The T_g values measured for unmodified, 4 wt. %, 8 wt. % and 12 wt. % formulations from $\tan \delta$ curve also reported in Table 13 which have a difference in the T_g values as compared to the ones measured by DSC technique, it was due to different measurement principle employed in both techniques.

Table 13: Glass transition temperature, T_g of the amine-cured unmodified epoxy system and amine cured epoxy system modified with the D51N block copolymer.

D51N [wt %]	T_g [°C]	T_g [°C]
	DSC	DMTA [$\tan \delta$]
0	134	137
2	135	n/a
4	135	140
6	137	n/a
8	137	138
10	137	n/a
12	134	138

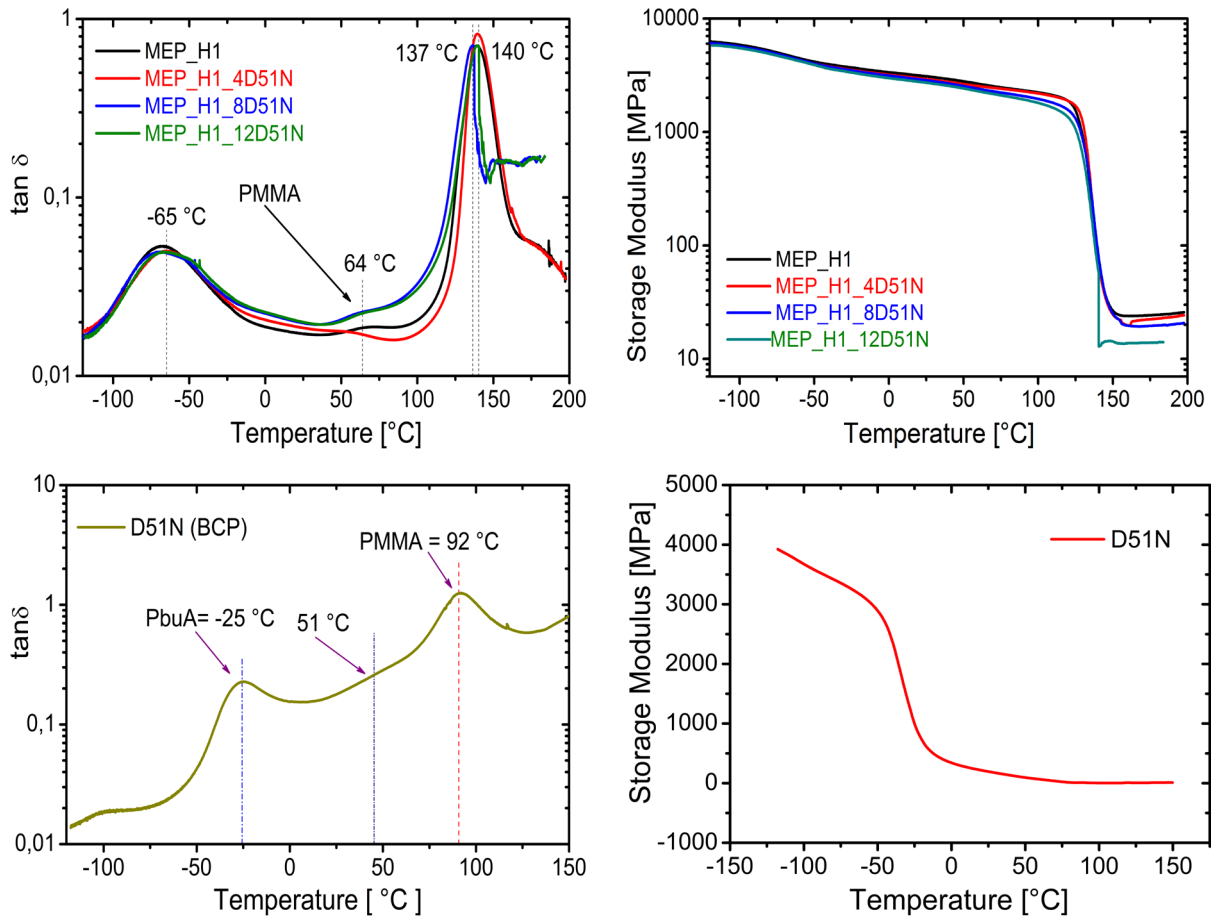


Figure 55: Graphs showing damping $\tan \delta$ vs. temperature (top-left) and storage modulus vs. temperature (top-right), for the unmodified amine cured epoxy and amine cured epoxies modified with D51N. $\tan \delta$ vs. temperature (bottom-left) for D51N BCP and storage modulus vs. temperature (bottom right) for D51N BCP.

The graph of the $\tan \delta$ vs. temperature (top-left) and storage modulus vs. temperature (top-right) was shown in Figure 55. It was observed that the storage modulus (E') for unmodified epoxy at the temperature 180 °C was approximately 25 MPa and for the D51N modified epoxy with 12 wt. % of the particle content in the same temperature range was 14 MPa. This was about 43 % decrement when compared to the neat epoxy system which implies that the crosslink density was decreased. Phase separation of the epoxy miscible PMMA block was found in the results of the DMTA, as shown in Figure 55, Small shoulders were observed next to the main α relaxation of the epoxies on the $\tan \delta$ curves of the D51N modified epoxies, and a similar shoulder was not observed in the $\tan \delta$ curve of the unmodified epoxy. These shoulders represent the micro-phase separation of the PMMA block occurred in the D51N modified epoxy during the polymerization process because the α relaxation of PMMA has been reported to be in the same temperature range (about 100 °C) as the small shoulders [13] [183] [184]. The main α relaxation was found

around 137 °C, which was associated with the glass transition temperature of the epoxy-rich phase, where larger segments of the polymer become mobile. A beta transition peak, T_{β} , was observed at -65 °C. The β relaxation of epoxy results from molecular motions of the epoxy network. The addition of BCP was found to have no effect on the β relaxation of the epoxy, however for all the modified systems a dip is observed in β -transition peak the because of the plasticization effect caused by the PbuA blocks incorporation in the epoxy and temperature of β relaxation was considered as -65 °C which is the mean temperature of the broad peak.

6.3.4 Tensile properties

The tensile properties such as tensile strength σ_m , strain ϵ_m , and elastic modulus E_t were measured at room temperature and were tabulated as shown in Table 14. For the unmodified epoxy system, the modulus was 3230 MPa and tensile strength was 95.0 MPa. Later, with the addition of block copolymers to the epoxy, the modulus and tensile strength were decreased with the increase in particle content. This was because of the presence of soft blocks present in the block copolymer ($E_{D51N} = 245$ MPa, $\sigma_m = 7$ MPa). Due to this, BCP's plasticize the whole network leading to decrease in modulus and strength at relative higher wt. %.

Similarly at 80 °C, for the unmodified system the modulus and strength were measured as 2510 MPa and 62 MPa respectively and with the increase in D51N BCP content the values decreases linearly and for 12 wt. % the modulus of 2100 MPa and strength of 50 MPa was obtained.

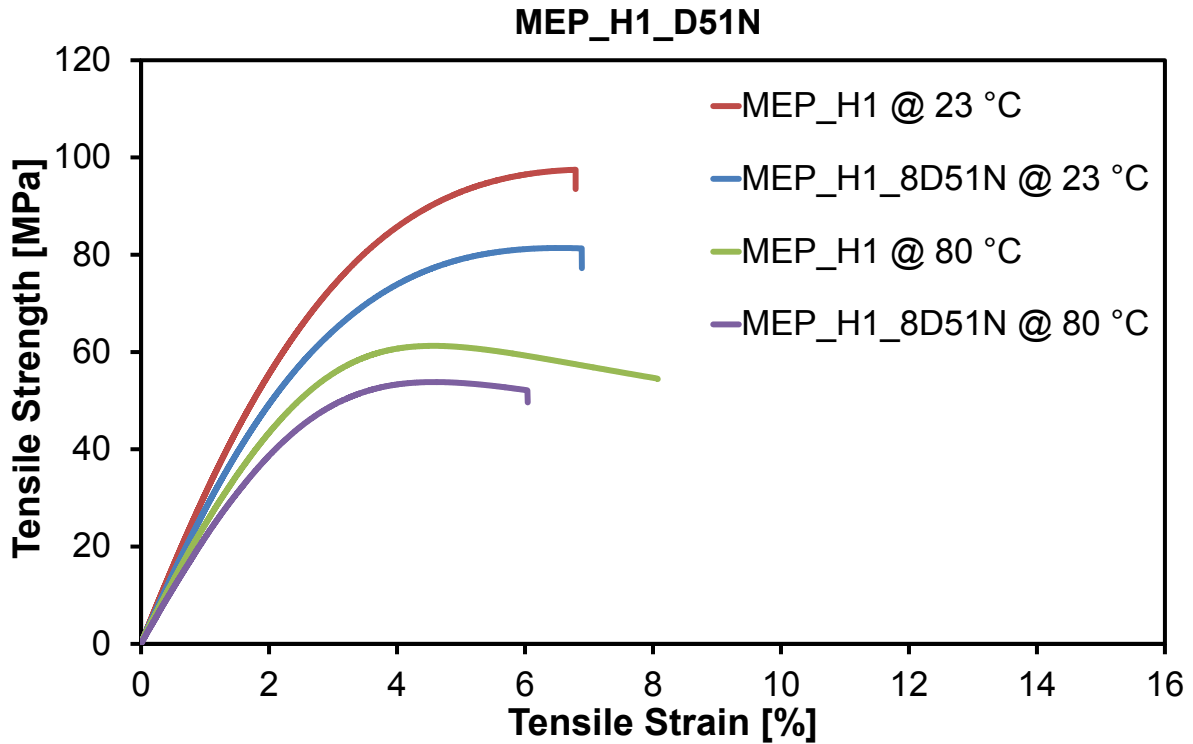


Figure 56: Graph showing representative tensile stress versus strain curves of amine-cured unmodified epoxy and amine cured epoxy system modified with 8 wt. % D51N block copolymer measured at 23 °C and at 80 °C.

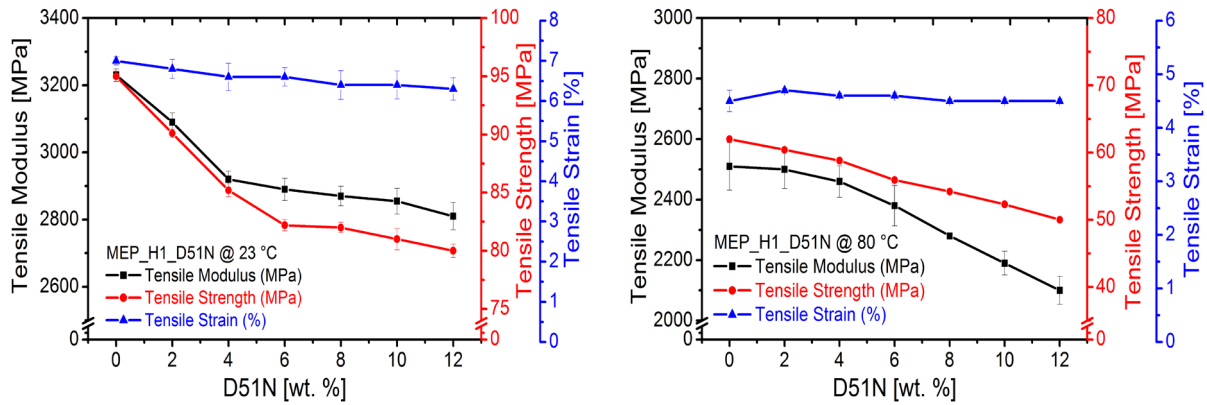


Figure 57: Graph showing tensile properties of the amine-cured unmodified epoxy system and amine cured epoxy system modified with the D51N block copolymer at 23 °C and 80 °C.

Table 14: Tensile properties E_t , σ_m and ϵ_m of the amine-cured unmodified epoxy system and amine cured epoxy system modified with D51N block copolymer measured at 23 °C and at 80 °C.

D51N [wt. %]	E_t [MPa] @ 23 °C	σ_m [MPa] @ 23 °C	ϵ_m [%] @ 23 °C
0	3230 (± 18.7)	95.0 (± 0.4)	7.0 (± 0.1)
2	3090 (± 28.1)	90.1 (± 0.3)	6.8 (± 0.2)
4	2920 (± 24.1)	85.2 (± 0.6)	6.6 (± 0.3)
6	2890 (± 33.0)	82.2 (± 0.5)	6.6 (± 0.2)
8	2870 (± 29.4)	82.0 (± 0.4)	6.4 (± 0.4)
10	2855 (± 38.2)	81.0 (± 0.9)	6.4 (± 0.3)
12	2810 (± 40.5)	80.0 (± 0.6)	6.3 (± 0.3)
D51N [wt. %]	E_t [MPa] @ 80 °C	σ_m [MPa] @ 80 °C	ϵ_m [%] @ 80 °C
0	2510 (± 54.4)	62 (± 0.28)	4.5 (± 0.02)
2	2500 (± 63.4)	60 (± 0.10)	4.7 (± 0.03)
4	2460 (± 52.0)	59 (± 0.08)	4.6 (± 0.04)
6	2380 (± 67.1)	56 (± 0.37)	4.6 (± 0.05)
8	2280 (± 39.6)	54 (± 0.30)	4.5 (± 0.04)
10	2190 (± 39.1)	52 (± 0.29)	4.5 (± 0.05)
12	2100 (± 46.2)	50 (± 0.28)	4.5 (± 0.04)

The details of all the models used to evaluate the elastic modulus were discussed in section §3.11.1. The parameters incorporated into the model were $E_m=3230$ MPa, $E_{D51N}= 245$ MPa and BCP's were considered to be in spherical shape so shape factor was taken as 2 for Halpin Tsai model and $V_{max}= 0.632$ and the no-slip condition was considered for Lewis-Nielsen model. The predictions of the Counto, Halpin Tsai, and Lewis Nielsen models were compared with the experimental data in Table 15 and the agreement was fairly good. Up to 4 wt. % all the models overestimate the modulus of the composite except Lewis-Nielsen model, however the difference between theoretical and experimental values in no case higher than 5.5 %. For 6 wt. % and 8 wt. % the experimental data lie between Halpin – Tsai, and Lewis – Nielsen predictions, where Halpin – Tsai gives the upper bound and Lewis – Nielsen gives the lower bound. For 10 wt. % and 12 wt. % all the models underestimate the modulus of the composite. For all except 4 wt. % the data was above the Lewis –

Nielsen predictions which confirm that slip or debonding does not occur. Similarly, for tensile strength model which was discussed in §3.11.2 gives a fair prediction for tensile strength values with a deviation less than 9 %.

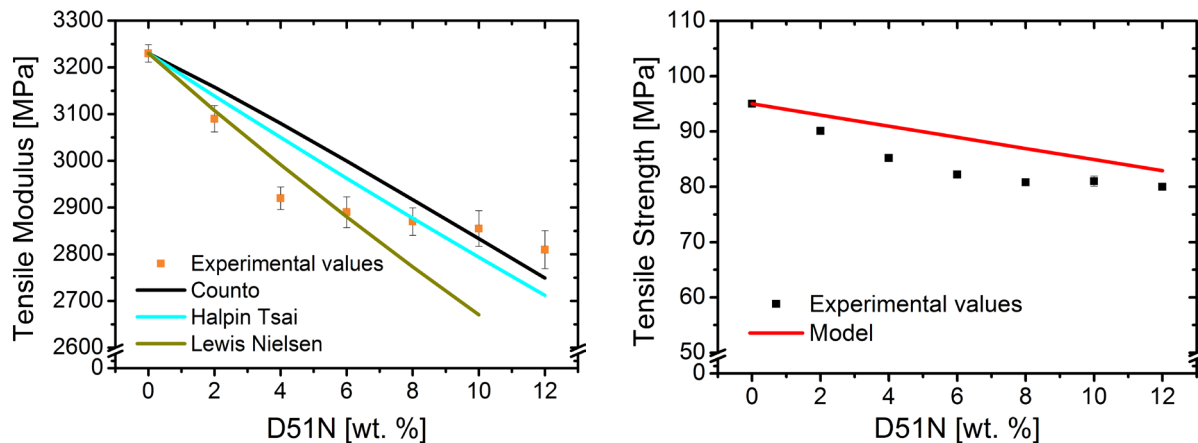


Figure 58: Tensile modulus vs D51N [wt. %] (Left) and tensile strength vs D51N [wt. %] (Right) for MEP_H1_D51N systems at 23 °C. Points were experimental data, lines were theoretical predictions.

Table 15: Tensile modulus and tensile strength of D51N modified composites as a function of D51N volume content. Comparison between experimental results and different theoretical predictions for MEP_H1_D51N systems at 23 °C.

D51N		Tensile Modulus [MPa]				Tensile Strength [MPa]	
wt. %	vol. %	Exp. [MPa]	Counto [MPa]	Halpin Tsai	Lewis Nielsen	Exp.	Model
0	0	3230	3230	3230	3230	95	95
2	2.15	3090	3158	3139	3108	90	93
4	4.26	2920	3080	3050	2992	85	91
6	6.39	2890	3000	2963	2880	82	89
8	8.50	2870	2917	2877	2773	81	87
10	10.61	2855	2833	2794	2671	81	85
12	12.72	2810	2749	2712	2572	80	83

6.3.5 Fracture properties

The fracture toughness, K_{IC} , and fracture energy, G_{IC} , values of the amine cured unmodified epoxy system and D51N modified epoxy systems were tabulated below in Table 16. The fracture toughness and fracture energy of the unmodified epoxy were observed to be $0.73 \text{ MPa}\cdot\text{m}^{1/2}$ and 0.14 kJ/m^2 . By the addition of block copolymers,

these properties were increased gradually to $1.43 \text{ MPa}\cdot\text{m}^{1/2}$ and 0.64 kJ/m^2 for 12 wt. % of the D51N BCP content. These were 195 % and 457 % increase compared to the reference values measured for the unmodified epoxy respectively for fracture toughness values and fracture energy values. These values were in line with the fracture toughness reported in the product technical data sheet [164]. The gains in the values of G_{IC} and K_{IC} by the addition of the D51N were found to be almost linear, as shown in Figure 59.

Similarly, at $80 \text{ }^\circ\text{C}$, The fracture toughness and fracture energy of the unmodified epoxy were observed to be $1.03 \text{ MPa}\cdot\text{m}^{1/2}$ and 0.37 kJ/m^2 . By the addition of D51N BCP's maximum values obtained at 4 wt. % and later the value decrease linearly to $1.23 \text{ MPa}\cdot\text{m}^{1/2}$ and 0.63 kJ/m^2 for 12 wt. % of D51N. Here two factors were primarily responsible for the increase in fracture toughness values, firstly the softening caused by PbuA and PMMA blocks present in the epoxy and secondly the ductility of epoxy system at elevated temperature which can be clearly seen as a difference in the K_{IC} values for the reference system at $23 \text{ }^\circ\text{C}$ and at $80 \text{ }^\circ\text{C}$. Particle to particle interaction may be an important parameter in the sudden rise in fracture toughness values at relatively lower particles loading at a higher temperature.

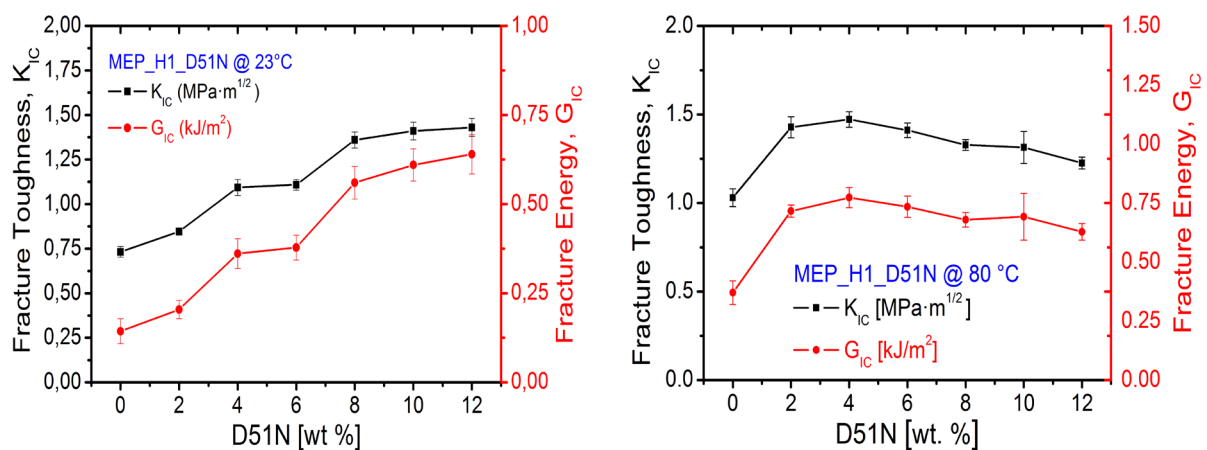


Figure 59: Graph showing fracture toughness, K_{IC} and fracture energy, G_{IC} , values of the amine cured unmodified epoxy system and D51N modified epoxy systems at $23 \text{ }^\circ\text{C}$ and at $80 \text{ }^\circ\text{C}$.

Table 16: Fracture toughness, K_{IC} and fracture energy, G_{IC} , values of the amine cured unmodified epoxy system and D51N modified epoxy systems at 23 °C and at 80 °C.

D51N [wt. %]	K_{IC} [MPa.m^{1/2}] @23 °C	G_{IC} [kJ/m²] @23 °C
0	0.73 (±0.08)	0.14 (±0.03)
2	0.85 (±0.05)	0.20 (±0.02)
4	1.09 (±0.06)	0.36 (±0.04)
6	1.11 (±0.12)	0.38 (±0.09)
8	1.36 (±0.05)	0.56 (±0.04)
10	1.41 (±0.12)	0.61 (±0.09)
12	1.43 (±0.07)	0.64 (±0.08)
D51N [wt. %]	K_{IC} [MPa.m^{1/2}] @80 °C	G_{IC} [kJ/m²] @80 °C
0	1.03 (±0.10)	0.37 (±0.09)
2	1.43 (±0.06)	0.72 (±0.06)
4	1.47 (±0.04)	0.77 (±0.05)
6	1.41 (±0.04)	0.74 (±0.04)
8	1.33 (±0.03)	0.68 (±0.03)
10	1.31 (±0.12)	0.70 (±0.13)
12	1.23 (±0.03)	0.63 (±0.03)

6.3.6 Fractography studies

A comprehensive fractography studies were performed on the fractured surfaces by using scanning electron microscope (SEM) to find reasons for the improvement of fracture toughness and bonding between the epoxy matrix and filler material. Several mechanisms were identified that were responsible for the increase in fracture toughness and they will be discussed in the following sections accordingly

The fractured surface of the amine cured unmodified epoxy seems to be smooth without any traces of plastic deformation. This was usually seen in all types of unmodified brittle epoxies due to the absence of any filler materials that promote plastic deformation and toughness. The addition of D51N has changed the roughness of the surface and witnessed the presence of riverlines and matrix tearing

that indicates enhanced plastic deformation. With the addition of 2 wt. %, 6 wt. % and 12 wt. % of D51N, riverlines and matrix tearing were observed as shown in Figure 61.

Examination of Figure 61 shows that the fracture surface of D51N modified systems was rough at the nanometer scale with many small nodule-like protrusions. It should be noted that the cavities and nodule like protrusions were not artifacts of the sputtering process used prior to the SEM imaging because they were not observed on the coated unmodified epoxy, and the presence of the cavities and protrusions was independent of the coating material used. Furthermore, small-scale matrix tearing was observed on the fracture surfaces of the D51N modified epoxies with all morphologies were also observed. These features indicate the enhanced plastic deformation of the epoxies. The obtained morphologies are in a good agreement with the work of Chen et.al [13].

Based on the SEM images of the fracture surfaces described above, the toughening mechanisms involved in the D51N modified amine cured epoxies with different morphologies can be proposed. The filler particles can induce shear yielding in the matrix by building up a change in stress state. This may result in the formation of voids, cavities and debonding effects in the process zone at the crack tip vicinity [185]. For the D51N modified epoxy with spherical micelles, the toughening mechanism was the cavitation of the spherical micelles and the plastic deformation of the epoxy matrix due to the localized plasticization effect of the epoxy/PMMA interface or mixing region. This theory was supported by the observation of the numerous nanoscale cavities, as well as considerably enhanced matrix tearing and multi-planar features on the fracture surfaces.

At higher temperature (80 °C) stress whitening was observed near the crack tip which was related to void formation. The generation of voids attributed to the cavitation of rubber particles which was most important energy dissipating mechanism and enhanced shear yielding was also observed on the fracture surface of specimens tested at 80 °C.

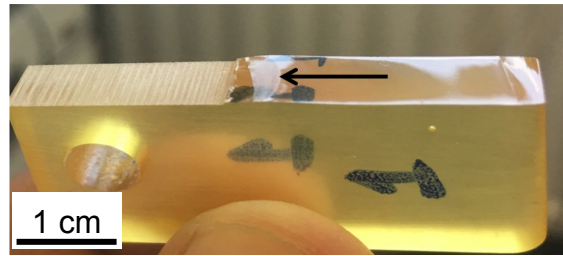


Figure 60: Fractured compact tension with stress whitening zone for amine-based epoxy system modified with 10 wt. % D51N at 80 °C.

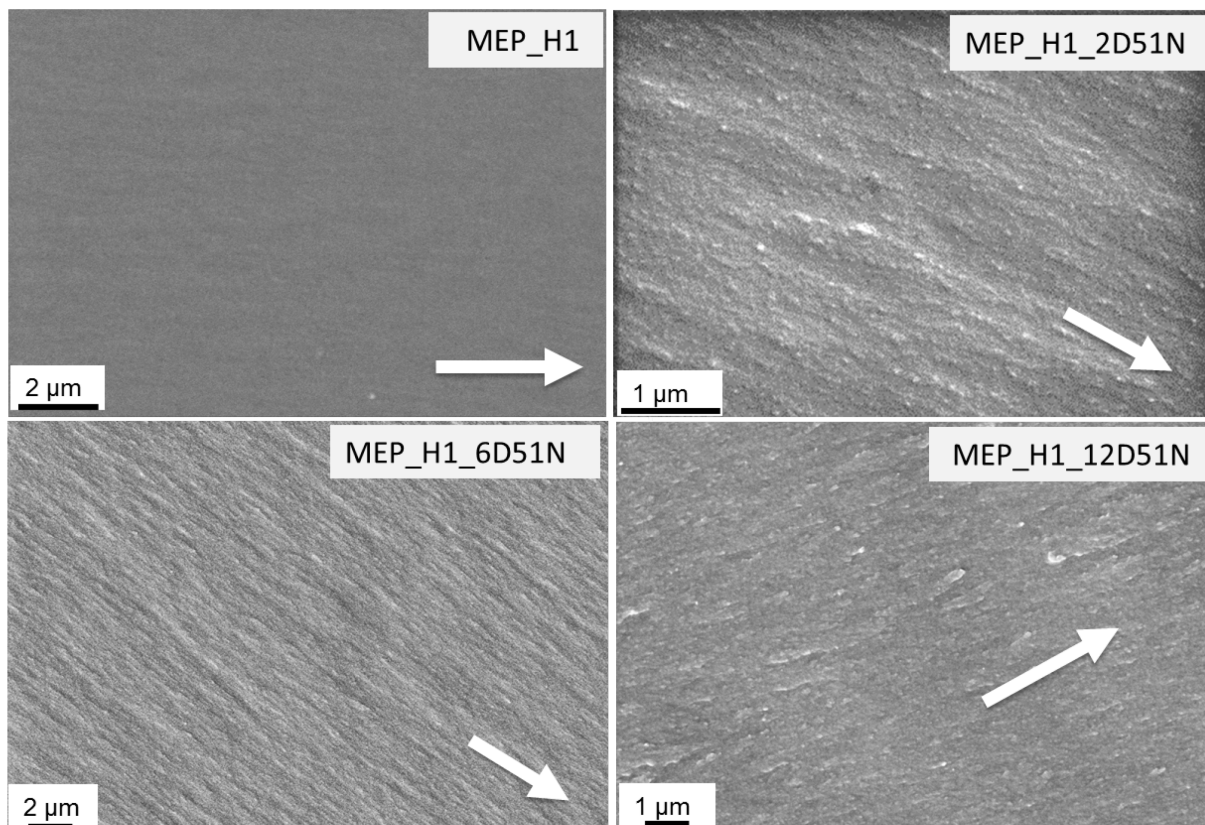


Figure 61: SEM micrographs showing the rough fracture surface of unmodified amine system and amine cured epoxy modified with 2 wt. %, 6 wt. % and 12 wt. % of D51N, taken in the vicinity of the tip of the pre-crack at 23 °C. White arrows were indicating the direction of crack propagation.

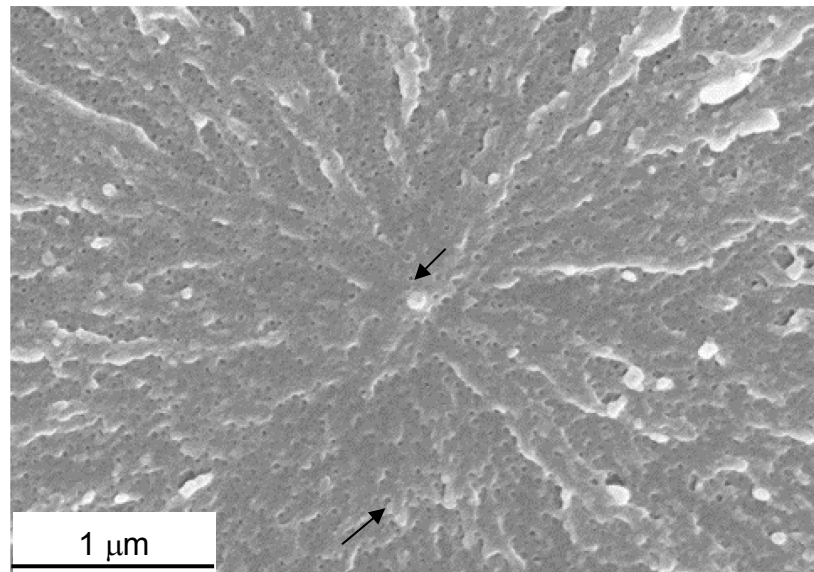


Figure 62: SEM micrograph of the cryo-fracture surface of the amine cured epoxy modified with 10 wt. % D51N at 23 °C. Cavities were indicated by black arrows.

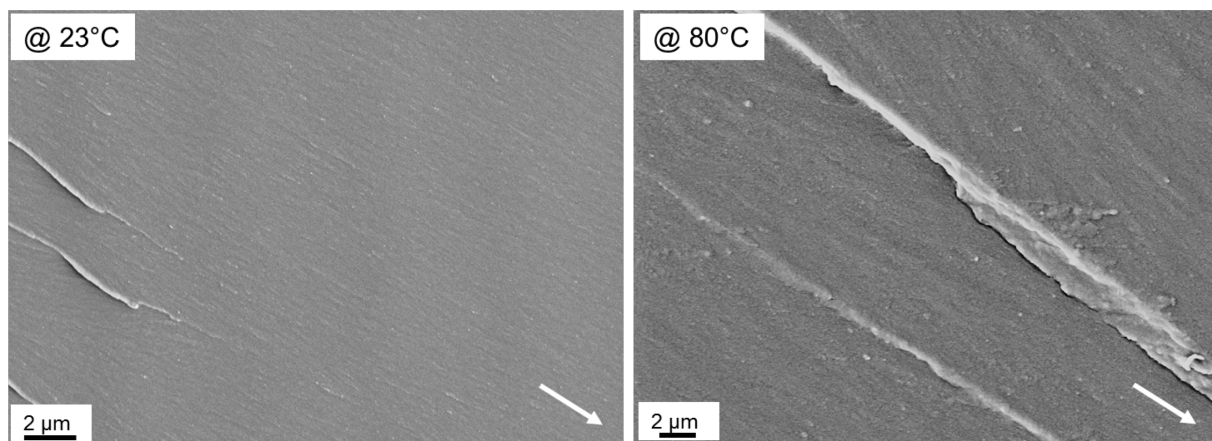


Figure 63: FEG-SEM micrograph of the amine cured 8 wt. % D51N modified epoxy system, taken in the vicinity of the tip of the pre-crack. White arrows were indicating the crack propagation.

The high temperature tested composites show a typical fracture surface divided into two regions; the stress whitened and the fast-crack growth region. In the stress whitened region (Figure 60) or plastic zone, ahead of the crack tip, the crack propagates slowly. It was characterized by a very rough fracture surface with numerous cavities and significant plastic deformation [186]. The cavities in this region were larger than those in the fast crack section and massive shear bands connecting the cavitated particles were also observed. The fast-crack growth region, located beyond the plastic zone, was characterized by rapid fracture propagation, smoother surface and some cavities of approximately same size as the undeformed rubber

particles. Similar behavior was reported in a CTBN rubber-modified epoxy resin and was explained due to the rubber particles induce more localized plastic deformations around the crack tip increasing the size of the plastic zone leading to a somewhat rougher fracture surface [187]. Yee also suggested that the triaxial tension at the crack tip must be relieved before the crack propagates, so the deviatoric stress can reach a critical value for yielding to occur [188]. The plastic zone absorbs the major fracture energy and once that the critical force was reached the total fracture takes place.

6.3.7 Modeling of fracture energy

The main toughening mechanisms for D51N BCP particles modified epoxy polymers were identified as localized shear yielding and plastic void growth initiated by the cavitation of spherical micelles and as discussed in section §6.3.6. The individual contributions for each toughening mechanism can be predicted and compared with the experimental results as detailed in § 3.11.3. The used parameter in the modeling as tabulated in Table 17. From cryo-fracture specimens of the bulk samples the radius of the block copolymer phase in epoxy was calculated as 10 nm.

Table 17: Parameters and values for the modeling studies to predict the fracture energy for the MEP_H1_D51N system.

Name	Variable	Value
Radius of the BCP particles	r_p (nm)	10
Void radius	r_{fv}	Table 18
$V_{fv} - V_{fp}$	V_{fv}, V_{fp}	Table 18
Poisson's ratio of the unmodified epoxy	ν	0.35
Plane-strain compressive yield true stress	σ_{yc} (MPa)	108
Plane-strain compressive fracture true strain	γ_f	0.98
Uniaxial tensile yield true stress	σ_{yt} (MPa)	95
Pressure-dependent yield stress parameter	μ_m	0.2
Fracture energy	G_{cu} (J/m ²)	143
Critical stress intensity factor	K_{cu}	0.73
von Mises stress concentration factor	K_{vm}	$K_{vm} = 3.9337V_f + 2.1126$

The contribution in fracture energy from shear yielding was calculated by equation (3.15) and plastic void growth by equation (3.21), here the contribution from rubber bridging was not considered since rubber bridging was not found in fractography investigation.

The calculated and measured values of fracture energy were tabulated in Table 19. It was difficult to accurately determine the volume fraction of particles that undergo cavitation experimentally. Finite element studies by Guild et al. [189] suggest that all rubbery particles should cavitate, and analysis of the fracture surfaces confirms this. Moreover, it was not assumed that all the cavities would undergo the maximum extent of plastic void growth, i.e. until void radius becomes equal to $(1 + \gamma_{fu})r_p$, due to a local reduction in stress near a void. An upper bound of 100 % and lower bound of 14.3 % [189] [190] of particles which cavitate and undergo full plastic void growth would be expected. However, in the current work, fractography examination reveals that D51N particles were not undergone full cavitation. Therefore for the current work, only 15 % of D51N particles were to be assumed to undergone cavitation. For D51N BCP particles amine-based epoxy system, a good agreement was found between experimentally measured and predicted values of fracture energy G_{IC} .

Table 18 Mean radius (D51N BCP particles), void radius and $(V_{fv} - V_{fp})$ for amine based D51N modified tailored epoxy systems.

D51N (wt. %)	D51N (vol. fraction)	Radius (nm)	Void radius (nm)	$V_{fv} - V_{fp}$
2	0,021	10	19.8	0.145
4	0,042	10	19.8	0.288
6	0,063	10	19.8	0.432
8	0,085	10	19.8	0.575
10	0,106	10	19.8	0.718
12	0,127	10	19.8	0.860

Table 19 Predicted and measured values of fracture energy for D51N BCP modified MEP_H1 system at 23 °C.

MEP_H1_D51N		(15 %) ΔG_v	ΔG_s	G_{IC} predicted	G_{IC} experimental
[D51N] wt. %	[D51N] v_f	[J/m ²]	[J/m ²]	[J/m ²]	[J/m ²]
0	0,000	0	0	143	143
2	0,021	34	87	264	200
4	0,042	72	134	349	360
6	0,063	116	176	434	380
8	0,085	165	214	522	560
10	0,106	221	250	614	610
12	0,127	282	285	710	640

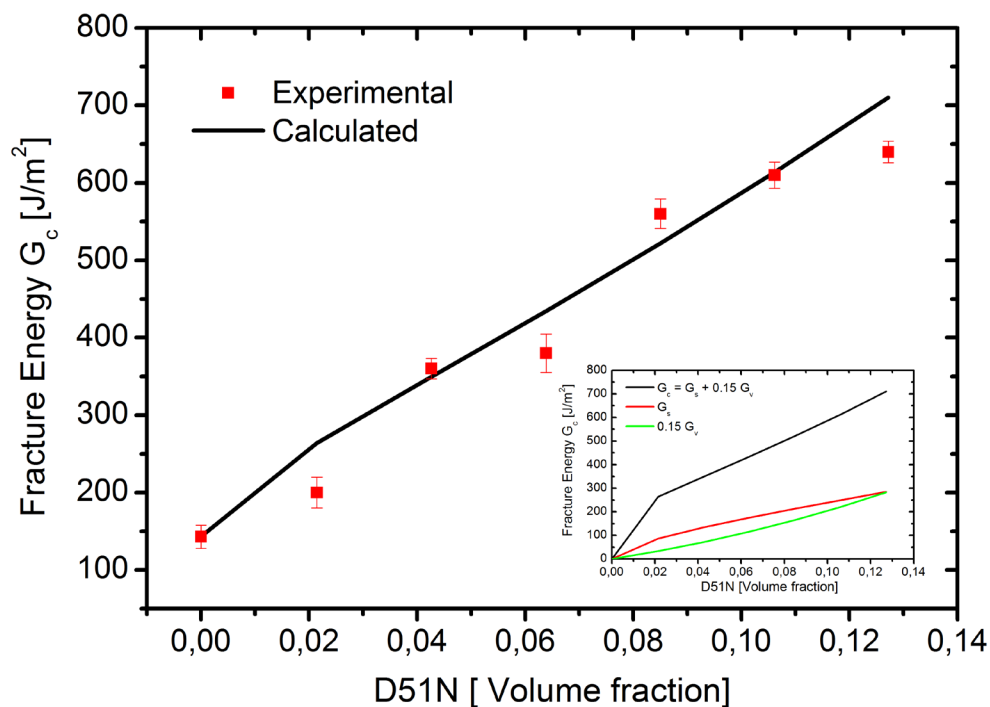


Figure 64: Fracture energy vs volume fraction for the D51N BCP modified MEP_H1 system at 23 °C. Data points were experimental data, the line represents theoretical prediction. The contributions of G_s and G_v were shown in the inset.

Note:

1. The surface roughness values (obtained from white light profilometry) of fractured compact tension samples were tabulated in the appendix (9.1).
2. Compressive strength, compressive modulus values were tabulated in appendix (9.2).
3. For each system, the value of viscosity was tabulated in the appendix (9.3).
4. All the mixing ratios with corresponding weights of constituents were tabulated in the appendix (9.4).
5. Boiling water tests for all the systems were tabulated in the appendix (9.5).

6.4 Anhydride cured tailored epoxy modified with D51N BCP's

The tailored epoxy was modified with a diblock copolymer which was commercially available called as 'Nanostrength D51N' supplied by Arkema, France. It contains two blocks out of which one was a softer poly(butyl acrylate) also called as PbuA and the other was harder poly(Methyl methacrylate) also called as PMMA. Anhydride based modified epoxy system i.e. MEP_H2 was used as the epoxy hardener system and it was systematically modified with D51N block copolymer for 2 wt. %, 4 wt. %, 6 wt. %, 8 wt. %, 10 wt. % and 12 wt. % respectively and the appropriate curing cycle was used for all the formulations.

6.4.1 Microstructure studies

The unmodified epoxy was found to be a homogeneous single phase material as expected, see Figure 65. All the epoxy-anhydride hardener systems modified with D51N were transparent before curing and opaque after the gelation process.

This suggests that macrophase separation occurred which gave rise to opacity in all D51N modified epoxies since particle exceeding $1/15$ of the wavelength of visible light scatter light and reduce the transparency of the materials [182].

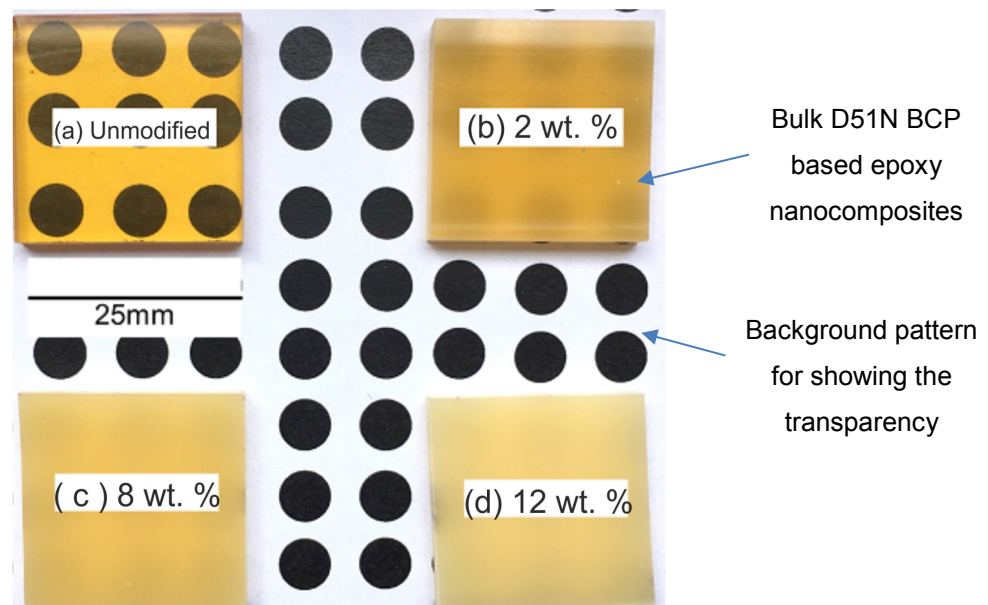


Figure 65: Pictures of the unmodified and D51N modified anhydride cured bulk epoxy samples. (a) Unmodified epoxy; (b) 2 wt. % D51N modified epoxy; (c) 8 wt. % D51N modified epoxy; (d) 12 wt. % D51N modified epoxy.

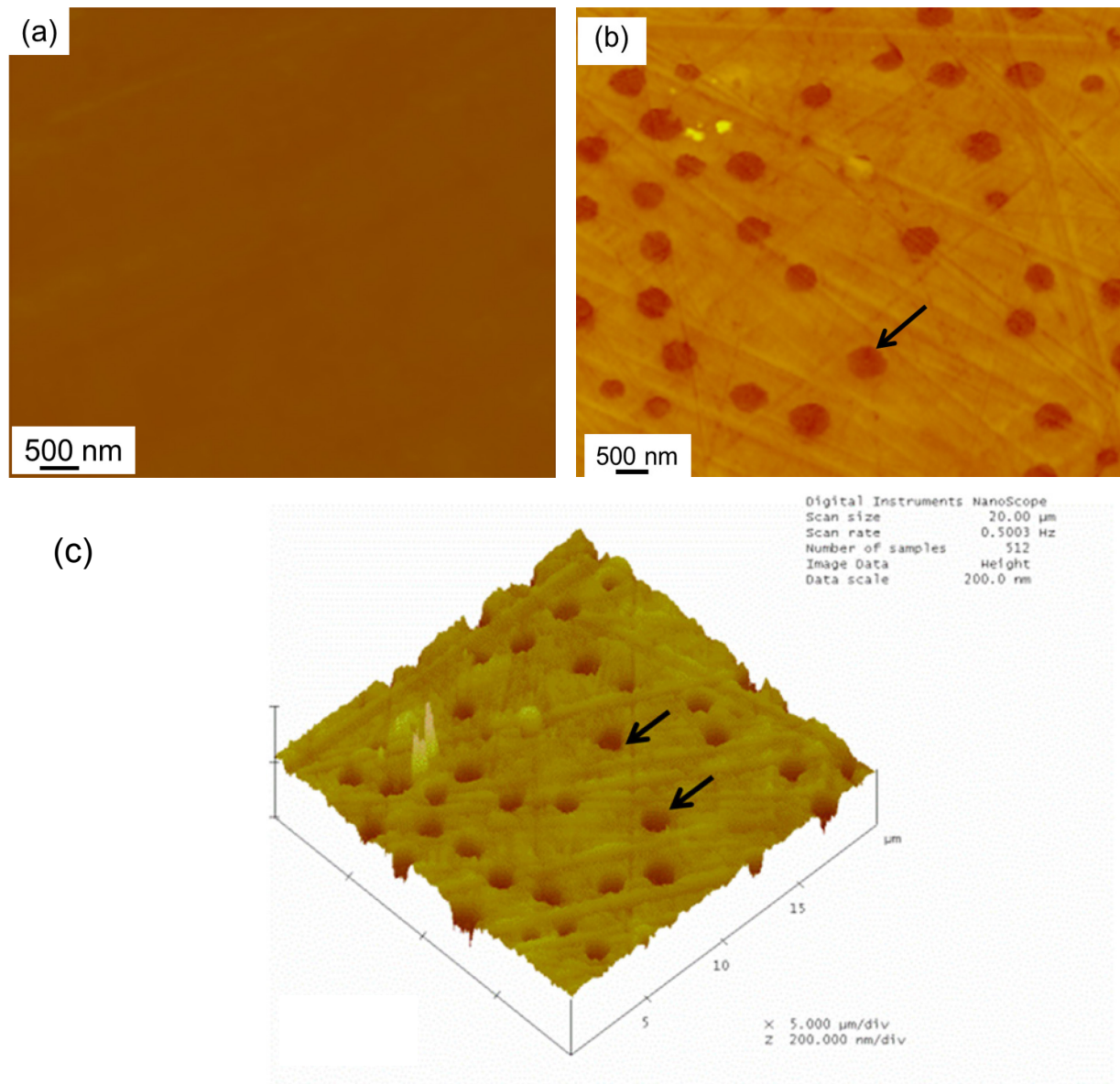


Figure 66: (a) AFM height image of polished bulk unmodified epoxy. (b) AFM height image of polished bulk 4 wt. % D51N modified bulk epoxy anhydride system. (c) The surface profile of polished bulk 4 wt. % D51N modified bulk epoxy system.

The morphologies of the anhydride based unmodified and EP-D51N particles modified epoxies were observed using AFM. The morphology of the unmodified epoxy was homogeneous and featureless. The D51N BCPs were initially dissolved in the epoxy resin. Later, this mixture phase separates during the curing process to form a network of small agglomerates at D51N BCP's concentrations up to 6 wt. %, as shown in Figure 66 (b). At concentrations of greater than 6 wt. % and above for the D51N modified epoxies, the small agglomerates become increasingly interconnected to form a co-continuous structure. This was where both the MAM and epoxy phases were continuous in structure.

6.4.2 Rheology

The viscosity change of the different epoxy systems as a function of temperature was shown in Figure 67. This was because the particles present in the system tends to offer a resistance to the resin flow owing to increase in the viscosity.

The viscosity of pure epoxy was 0.030 Pa.s at 40 °C and the addition of 12 wt. % of D51N block copolymers raised the viscosity to 0.951 Pa.s at the same temperature of 40 °C. The results obtained from the rheological tests were used to produce the graphs for showing the change in the viscosity with respect to temperature.

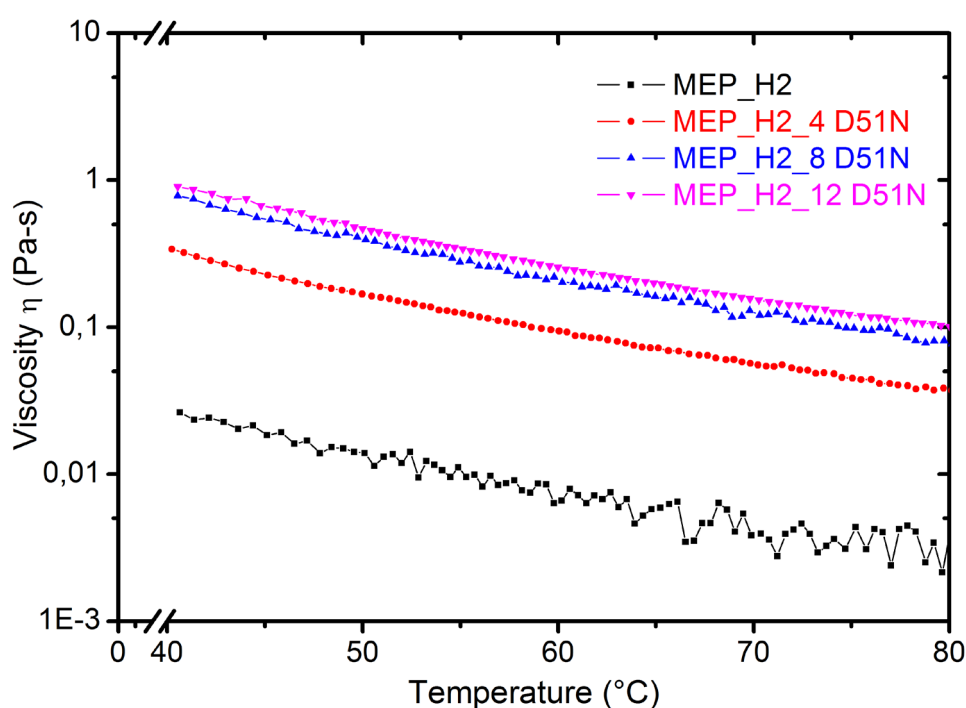


Figure 67: Graph showing variation in viscosity with respect to temperature for different anhydride based tailored epoxy systems modified with D51N BCP.

6.4.3 Glass transition temperature and viscoelastic properties

The glass transition temperatures of amine-cured unmodified and D51N modified epoxy systems were measured with the help DSC and DMTA techniques. The results were tabulated as shown in Table 20. It was observed that for the unmodified epoxy system, the glass transition temperature T_g was 144 °C. By the addition of block copolymers, the temperature has started decreasing and it was continued till 6 wt. % of the particle content with the temperature resulting 140 °C. This was about 2.1 % decrement when compared with the unmodified epoxy system. It can be concluded that addition of BCP's has no or very less effect on the T_g of anhydride based epoxy

systems, which was evident from the $\tan \delta$ peak of D51N modified anhydride based epoxy systems as well.

Table 20: Glass transition temperature, T_g of anhydride cured unmodified epoxy system and anhydride cured epoxy system modified with D51N block copolymer

D51N [wt %]	T_g [°C] DSC	T_g [°C] DMTA [$\tan \delta$]
0	144	147
2	143	n/a
4	143	146
6	140	n/a
8	144	146
10	144	n/a
12	143	146

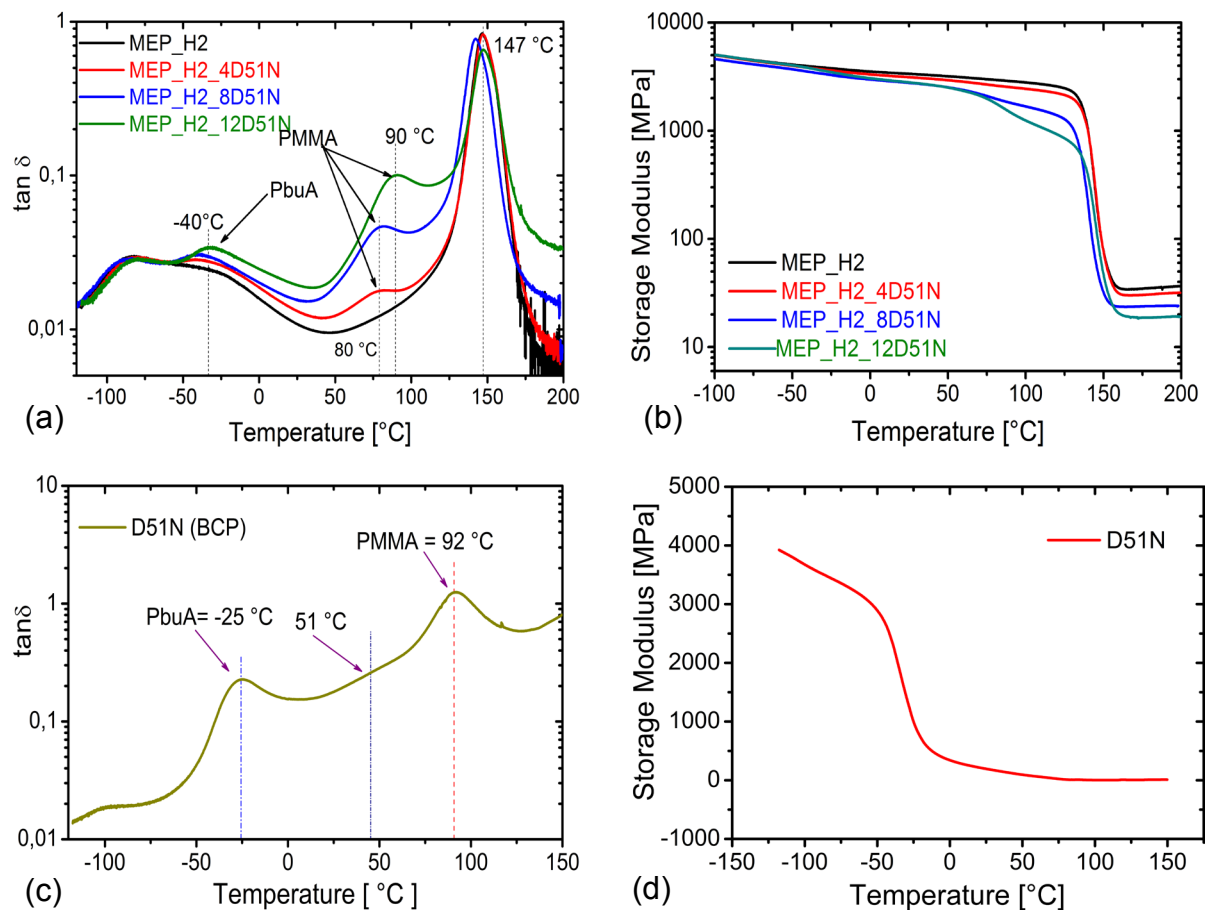


Figure 68: Graph showing (a) storage modulus and (b) damping $\tan \delta$, with respect to temperature, for the anhydride cured unmodified and D51N modified epoxy systems (c) storage modulus and (d) damping $\tan \delta$, with respect to temperature for pure D51N block copolymer.

With DMTA test, a variable sinusoidal stress was applied to the viscoelastic polymer material and the difference in phase shift was used to determine the viscoelastic material properties such as storage modulus E' , loss modulus E'' , and $\tan \delta$. The graph of the $\tan \delta$ versus temperature was shown in Figure 68 (a). It was observed that the storage modulus E' for unmodified epoxy at the temperature 180 °C is approximately 35.09 MPa and for the D51N modified epoxy with 12 wt. % of the particle content in the same temperature range was 18.69 MPa. This was about 54% decrement when compared to the neat epoxy system which implies that the crosslink density was decreased by an increase in fracture toughness. From the addition of 8 wt. % of the block copolymers, there was a significant phase separation of the epoxy matrix and filler material due to the poor bonding in between them. It was evident from the Figure 68 (a) where there was a significant progressive deviation of the $\tan \delta$ curve in the graph at 170 °C for 8 wt. % and 10 wt. % of the particle content and around 160 °C for 12 wt. % of the particle content. There were also noticeable peaks measured at the temperature around 90 °C. These peaks represent the T_g of the PMMA blocks present in the D51N which was reported to be around 85 °C – 100 °C according to the datasheet [164]. Another peak at -40 °C observed which was representing the T_g of PbuA blocks present in D51N BCP's.

6.4.4 Tensile properties

The tensile properties such as tensile strength σ_m , strain ϵ_m , and elastic modulus E_t were measured at 23 °C and 80 °C were tabulated as shown in Table 21. For the unmodified epoxy system, the modulus of 3580 MPa and tensile strength of 101 MPa measured at 23 °C. Later, with the addition of block copolymers to the epoxy, the modulus and tensile strength were decreased with the increase in particle content. For the addition of 12 wt. % of block copolymers, the tensile modulus and strength were decreased to 2890 MPa and 37.8 MPa. This high deviation in the tensile modulus and strength after 6 wt. % of D51N epoxy nanocomposites was due to the co-continuous phase generation (up to 10 wt. %) and phase inversion (12 wt. %) of the epoxy matrix and block copolymers which were caused by weak bonding between matrix and filler.

At 80 °C, for unmodified epoxy system, the modulus of 2880 MPa and tensile strength of 68 MPa was measured which can be explained by analyzing the viscoelastic curve of epoxy system, when the temperature was approaching towards the

glass transition zone then sudden drop in elastic modulus was observed which will be accompanied by sudden drop in strength value. Later, with the increase in D51N wt. % the values keep on decreasing and for 12 wt. % of D51N, the modulus and strength were measured to be 1650 MPa and 17 MPa respectively.

Table 21: Tensile properties E_t , σ_m and ϵ_m of anhydride cured unmodified epoxy system and anhydride cured epoxy system modified with D51N block copolymer measured at 23 °C and at 80 °C.

D51N [wt. %]	E_t [MPa] @ 23 °C	σ_m [MPa] @ 23 °C	ϵ_m [%] @ 23 °C
0	3580 (± 78.0)	101 (± 2.58)	5.8 (± 0.03)
2	3350 (± 31.5)	92.4 (± 0.85)	5.7 (± 0.48)
4	3290 (± 33.4)	88.7 (± 0.41)	5.7 (± 0.02)
6	3240 (± 26.3)	85.3 (± 0.55)	5.6 (± 0.21)
8	3120 (± 29.6)	47.0 (± 1.09)	1.9 (± 0.08)
10	3040 (± 43.6)	43.9 (± 0.57)	1.8 (± 0.04)
12	2890 (± 52.0)	37.8 (± 3.61)	1.6 (± 0.27)
D51N [wt. %]	E_t [MPa] @ 80 °C	σ_m [MPa] @ 80 °C	ϵ_m [%] @ 80 °C
0	2880 (± 18.0)	68 (± 0.24)	4.3 (± 0.05)
2	2850 (± 57.6)	64 (± 0.50)	4.3 (± 0.01)
4	2660 (± 28.8)	59 (± 0.08)	4.2 (± 0.04)
6	2590 (± 41.5)	56 (± 0.77)	3.9 (± 0.05)
8	2140 (± 41.7)	34 (± 0.99)	2.8 (± 0.06)
10	2000 (± 30.5)	27 (± 0.58)	2.5 (± 0.22)
12	1650 (± 41.0)	17 (± 0.84)	1.8 (± 0.32)



Figure 69: Tensile sample (a) before the test and sample (b) after the test showing the stress-whitening due to void formation during tensile tests.

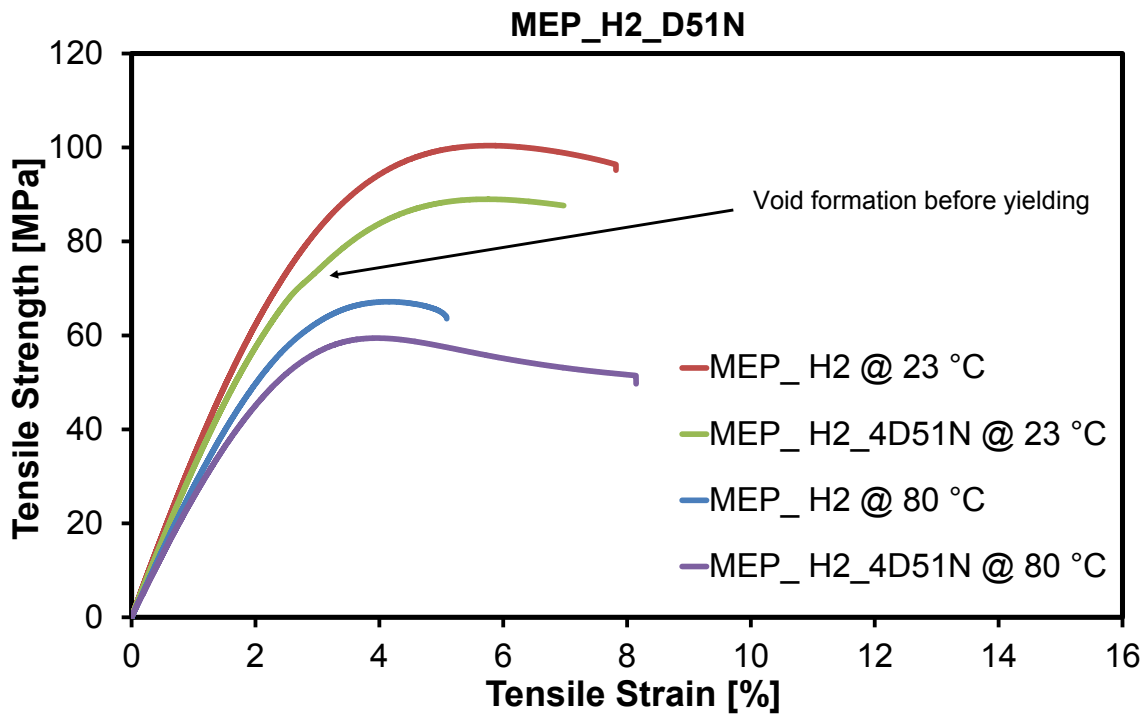


Figure 70: Graph showing tensile stress versus strain response of anhydride cured unmodified epoxy and anhydride cured epoxy system modified with D51N block copolymer measured at 23 °C and 80 °C.

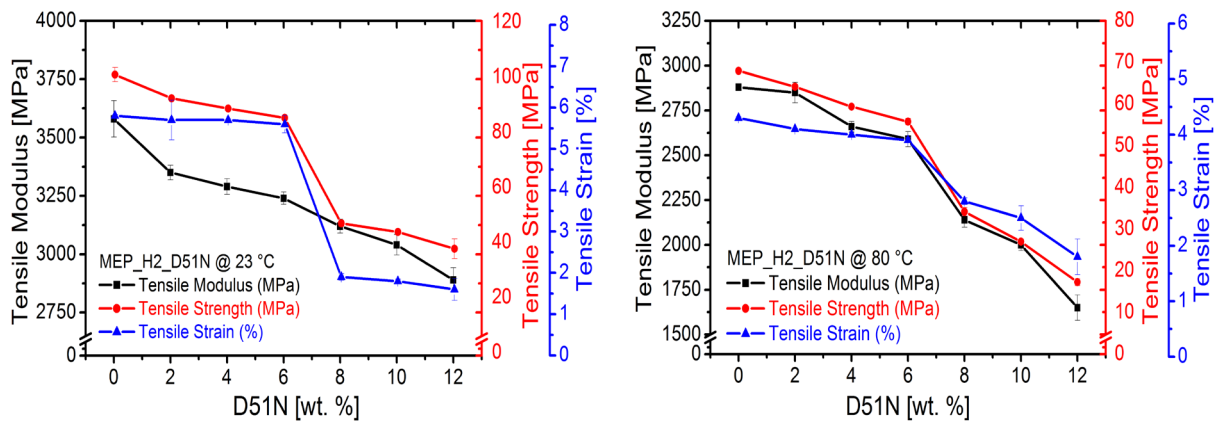


Figure 71: Graph showing tensile properties of anhydride cured unmodified epoxy system and anhydride cured epoxy system modified with the D51N block copolymer at 23 °C and 80 °C.

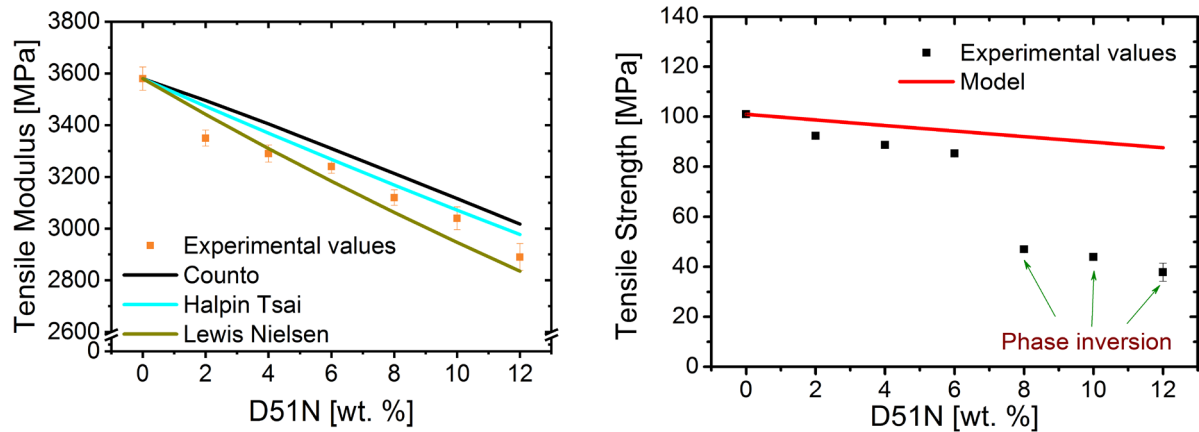


Figure 72: Tensile modulus vs D51N [wt. %] (Left) and tensile strength vs D51N [wt. %] (Right) MEP_H2_D51N systems 23 °C. Points were experimental data, lines were theoretical predictions.

Table 22: Tensile modulus and tensile strength of D51N modified composites as a function of D51N volume content. Comparison between experimental results and different theoretical predictions for MEP_H2_D51N systems at 23 °C.

D51N		Tensile Modulus [MPa]				Tensile Strength [MPa]	
wt. %	vol. %	Exp. [MPa]	Counto [MPa]	Halpin Tsai	Lewis Nielsen	Exp.	Model
0	0	3580	3580	3580	3580	101	101
2	2.23	3350	3496	3473	3442	92	99
4	4.45	3290	3405	3369	3310	89	97
6	6.66	3240	3310	3267	3183	85	94
8	8.87	3120	3213	3168	3062	47	92
10	11.05	3040	3116	3072	2946	44	90
12	13.24	2890	3018	2977	2836	38	88

The details of all the models used to evaluate the elastic modulus were discussed in section §3.11.1. The parameters incorporated into the model were $E_m=3580$ MPa, $E_{D51N}= 245$ MPa and BCP's were considered to be in spherical shape so shape factor was taken as 2 for Halpin Tsai model and $V_{max} = 0.632$ and the no-slip condition was considered for Lewis-Nielsen model. The predictions of the Counto, Halpin Tsai, and Lewis Nielsen models were compared with the experimental data in Table 22 and the agreement was fairly good. Halpin-Tsai model gives the best prediction out of all models used to predict the modulus of the system if the values at 2 wt. % and 4 wt. % were not considered. Counto model underestimates the modulus and overestimation was observed in case of Lewis Nielsen model, however, the

difference between theoretical and experimental values in no case higher than 5 %. For all the formulations the data was above the Lewis – Nielsen predictions which confirm that slip or debonding does not occur except at 2 wt. % and 4 wt. % data points, these deviations in value may be due to compliance error during the tests. Similarly, for tensile strength model which was discussed in §3.11.2 gives a fair prediction for tensile strength values with a deviation less than 10.6 % till 6 wt. % of the D51N composition, later the sudden decrease was observed in the tensile strength as the formation of co-continuous phase and phase inversion phenomenon was not considered in this model hence large deviations were observed in the tensile strength values after 6 wt. %. However, this effect was not observed in the case of elastic modulus.

6.4.5 Fracture properties

The fracture toughness, K_{IC} , and fracture energy, G_{IC} , values of the anhydride cured unmodified epoxy system and D51N modified epoxy systems were tabulated below. The fracture toughness and fracture energy of the unmodified epoxy was measured as $0.64 \text{ MPa}\cdot\text{m}^{1/2}$, 0.10 kJ/m^2 , and $0.70 \text{ MPa}\cdot\text{m}^{1/2}$, 0.15 kJ/m^2 at $23 \text{ }^\circ\text{C}$ and $80 \text{ }^\circ\text{C}$ respectively as shown in Figure 73. By the addition of block copolymers, these properties were increased gradually to $1.72 \text{ MPa}\cdot\text{m}^{1/2}$ and 0.93 kJ/m^2 for 10 wt. % of BCP wt. %. Later, with the addition of 12 wt. % of block copolymers, the K_{IC} and G_{IC} were decreased to $0.87 \text{ MPa}\cdot\text{m}^{1/2}$ and 0.22 kJ/m^2 due to the complete phase inversion at $23 \text{ }^\circ\text{C}$.

Table 23: Fracture toughness, K_{IC} and fracture energy, G_{IC} , values of the anhydride cured unmodified epoxy system and D51N modified epoxy systems in mode-I loading at $23 \text{ }^\circ\text{C}$ and $80 \text{ }^\circ\text{C}$.

D51N [wt. %]	K_{IC} [$\text{MPa}\cdot\text{m}^{1/2}$] @ $23 \text{ }^\circ\text{C}$	G_{IC} [kJ/m^2] @ $23 \text{ }^\circ\text{C}$
0	0.64 (± 0.13)	0.10 (± 0.14)
2	0.7 (± 0.07)	0.25 (± 0.03)
4	1.25 (± 0.09)	0.42 (± 0.06)
6	1.48 (± 0.05)	0.60 (± 0.03)
8	1.59 (± 0.14)	0.71 (± 0.11)
10	1.72 (± 0.26)	0.86 (± 0.28)
12	0.87 (± 0.14)	0.22 (± 0.15)

D51N [wt. %]	K_{IC} [MPa·m ^{1/2}] @ 80 °C	G_{IC} [kJ/m ²] @ 80 °C
0	0.70 (±0.15)	0.15 (±0.01)
2	1.81 (±0.17)	1.01 (±0.19)
4	2.04 (±0.08)	1.37 (±0.11)
6	1.97 (±0.08)	1.32 (±0.11)
8	1.87 (±0.17)	1.45 (±0.15)
10	1.63 (±0.07)	1.17 (±0.11)
12	0.93 (±0.18)	0.46 (±0.18)

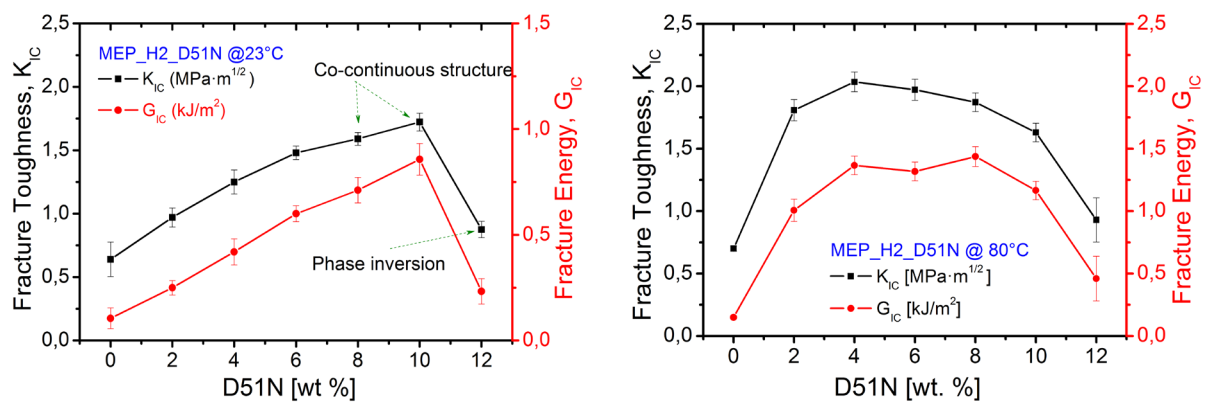


Figure 73: Graph showing fracture toughness, K_{IC} and fracture energy, G_{IC} , values of the anhydride cured unmodified epoxy system and D51N modified epoxy systems at 23 °C and 80 °C.

6.4.6 Fractography studies

A comprehensive fractography studies were performed on the fractured surfaces by using scanning electron microscope (SEM) to find reasons for the improvement of fracture toughness and bonding between the epoxy matrix and filler material. Several mechanisms were identified that were responsible for the increase in fracture toughness and they will be discussed in the following sections accordingly. The direction of the crack propagation for each image was from left to right. The fractured surface of the anhydride cured unmodified epoxy seems to be smooth without any traces of plastic deformation. This indicates a lack of plastic deformation during the fracture process. Only small-scale river lines were observed at the crack tip, which was caused by the presence of some local mixed-mode I/III stresses [191].

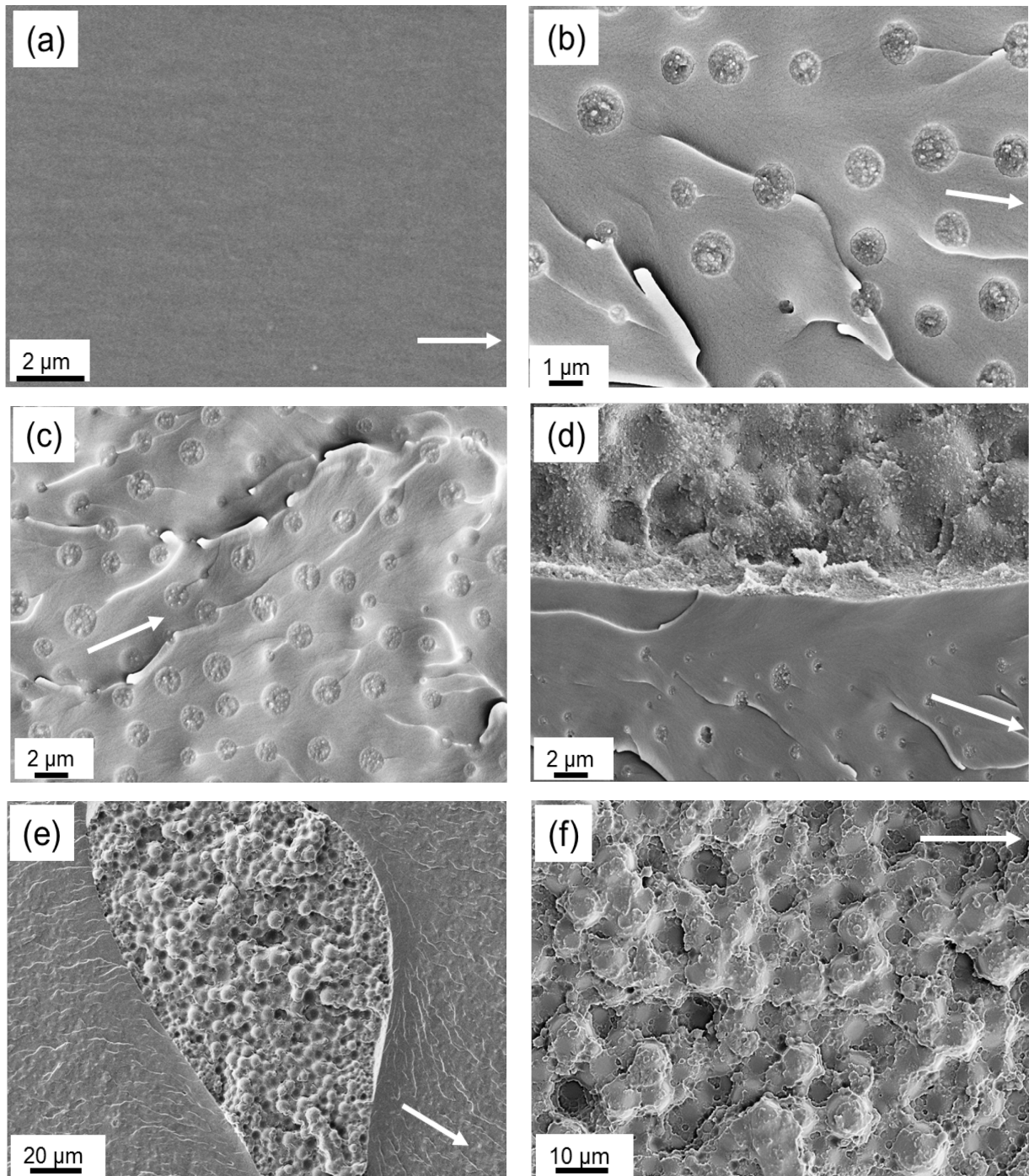


Figure 74: FEG-SEM micrographs of the fracture surface of the (a) 0 wt. %, (b) 4 wt. %, (c) 6 wt. %, (d) 8 wt. %, (e) 10 wt. %, (f) 12 wt. % D51N modified anhydride cured epoxy, taken in the vicinity of the tip of the pre-crack at 23 °C. The white arrow indicates the direction of crack propagation.

The fracture surface of diblock D51N modified epoxies was exhibiting very rough and multiplanar fracture surface with evenly dispersed micron size cavities. In D51N modified epoxies as the filler content was increased, the size of the cavities also found to be increased. Figure 74, shows micrographs of different wt. % of D51N modified with anhydride curing agent. From the Figure 74 (d), the radius of the cavities found to be in the range of \sim (400 nm – 1200 nm).

Cavitation of the D51N BCP particles and subsequent plastic void growth for epoxies, process absorbs energy, hence increasing the toughness. For 2 wt. % to 6 wt. % cavities with spherical inclusions on the fracture surface were observed as the main mechanism for the resulting fracture toughness besides crack pinning which has fractional influence for the improvement of fracture toughness. Co-continuous phase was observed in the modified epoxies containing more than 6 wt. % D51N up to 10 wt. %. Figure 75, shows the co-continuous phase containing 10 wt. % D51N, on which both the MAM-rich domains and the epoxy-rich domains can be clearly seen. For both 8 wt. % and 10 wt. % have almost same morphology with epoxy and MAM rich domains. The significant toughness enhancement provided by the co-continuous morphology comes from the interconnected epoxy-rich and MAM-rich domains which form a hard and soft composite-like structure. When the crack propagates through this structure the brittle epoxy phase fractures and the MAM phase was observed to stretch across the fracture surfaces. The MAM can be expected to possess a low yield stress and relatively high ductility. Hence as the crack opens, the MAM will deform and absorb energy, thus increasing the measured toughness. And at 12 wt. % the epoxy-D51N mixture was fully phase inverted which leads to a drastic decrease in fracture properties and a mechanism for phase inversion was still not understood.

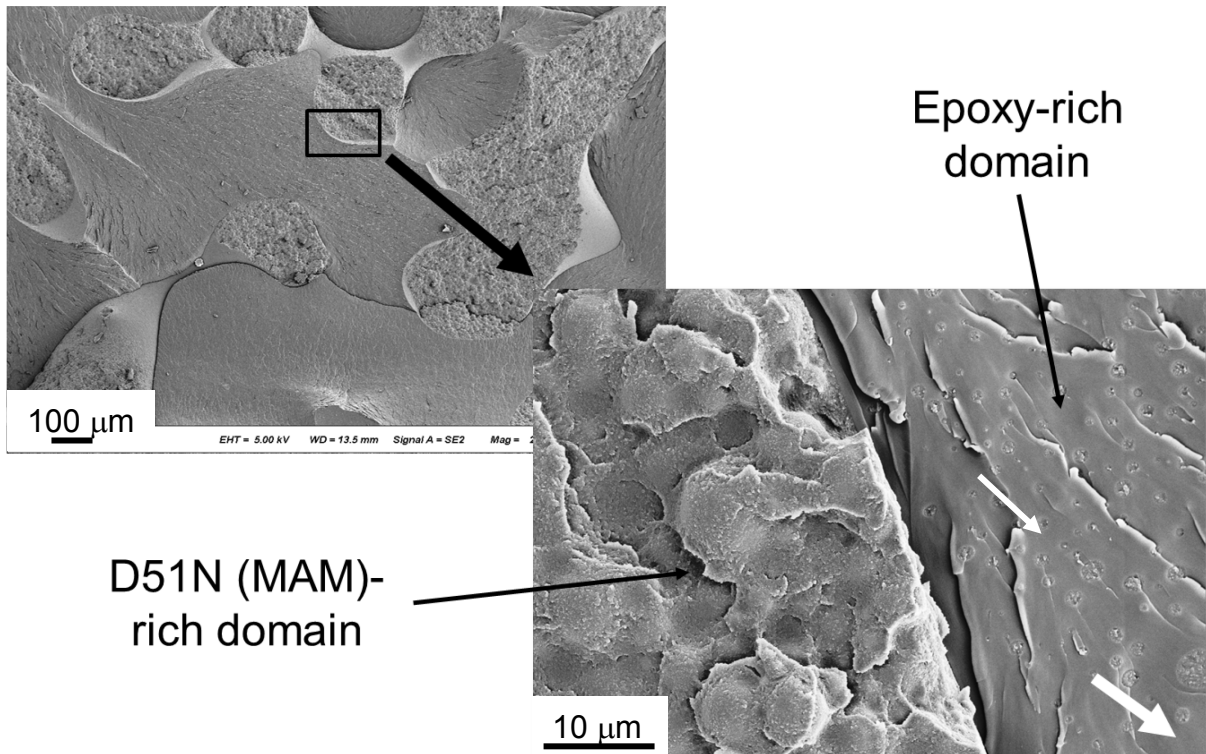


Figure 75: FEG-SEM micrograph of the anhydride cured 10 wt. % D51N modified epoxy system. Figure showing epoxy rich domain with micron-sized dispersed BCP's and D51N BCP rich domain at 23 °C. White arrow was showing the crack propagation direction.

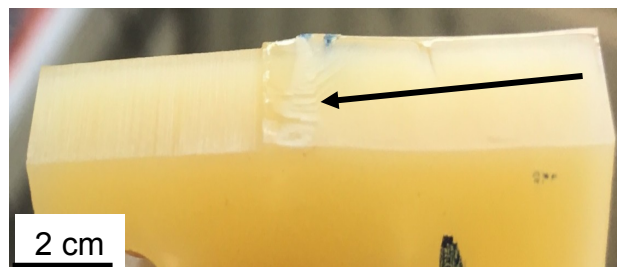


Figure 76: Fractured compact tension specimen of 6 wt. % D51N modified anhydride system at 80 °C. Arrow was showing stress whitening region around a crack-tip.

The high temperature tested composites show a typical fracture surface divided into two regions; the stress whitened and the fast-crack growth region. In the stress whitened region or plastic zone, ahead of the crack tip, the crack propagates slowly. It was characterized by a very rough fracture surface with numerous cavities and significant plastic deformation [186]. The cavities in this region were larger than those in the fast crack section and massive shear bands connecting the cavitated particles were also observed. The fast-crack growth region, located beyond the plastic zone, was characterized by rapid fracture propagation, smoother surface and some cavities of approximately same size as the undeformed rubber particles. Similar behavior was

reported in a CTBN rubber-modified epoxy resin and was explained due to the rubber particles induce more localized plastic deformations around the crack tip increasing the size of the plastic zone leading to a somewhat rougher fracture surface [187]. Yee also suggested that the triaxial tension at the crack tip must be relieved before the crack propagates, so the deviatoric stress can reach a critical value for yielding to occur [188]. The plastic zone absorbs the major fracture energy and once that the critical force was reached the total fracture takes place.

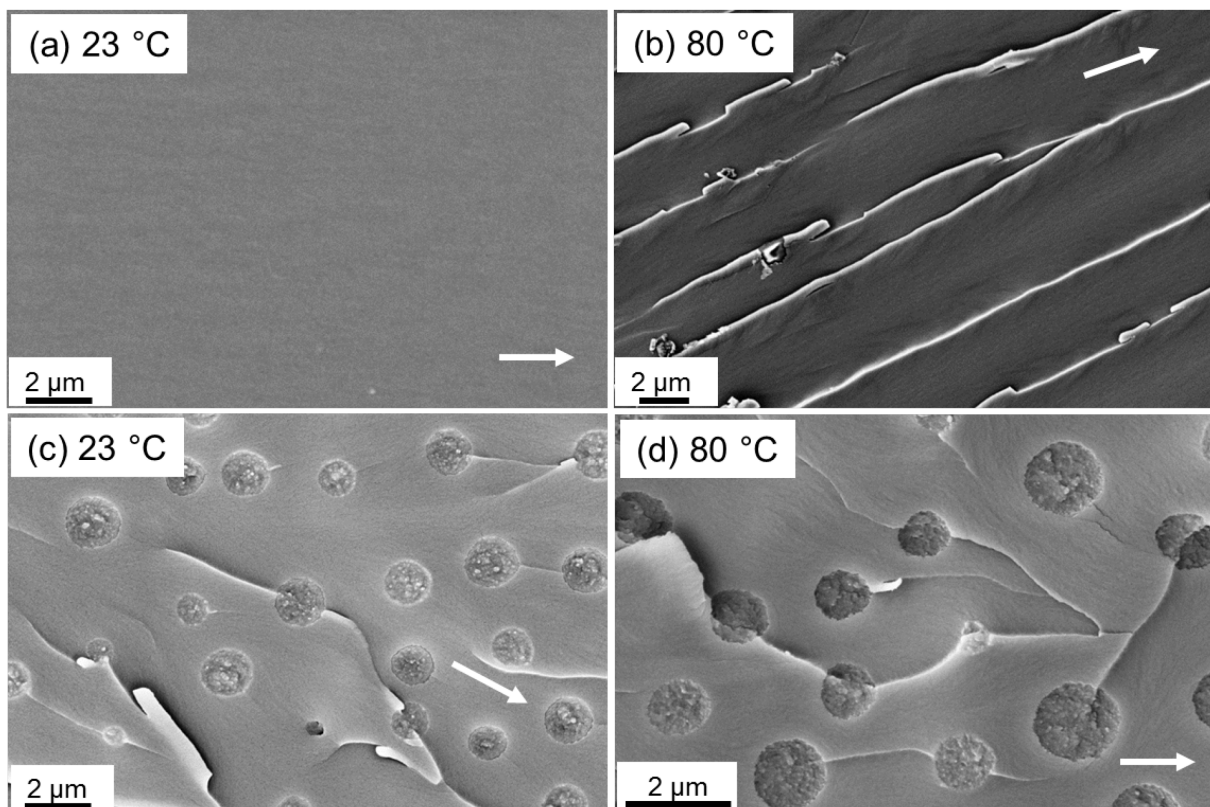


Figure 77: FEG-SEM micrograph of the anhydride cured (a) unmodified tailored epoxy system at 23 °C (b) unmodified tailored epoxy at 80 °C (c) 6 wt. % D51N modified epoxy system at 23 °C and (d) wt. % D51N modified epoxy system at 80 °C. White arrows were showing the crack propagation direction.

Based on the above-mentioned observations, Huang and Kinloch developed a model, proposing that the greater fracture resistance in rubber modified epoxies results from the great energy dissipating processes that take place in the vicinity of the crack tip. The three main energy-dissipating toughening mechanisms were: Shear banding, Cavitation and Rubber Bridging which were discussed in detailed in § 3.11.3

6.4.7 Modeling of Fracture Energy

The main toughening mechanisms for D51N BCP modified epoxy polymers were identified as plastic void growth initiated by the cavitation of the D51N particles and localized shear yielding as discussed in section §6.4.6. The individual contributions for each toughening mechanism can be predicted and compared with the experimental results as detailed in § 3.11.3. The used parameter in the modeling as tabulated in Table 24. The contribution in fracture energy from shear yielding was calculated by equation (3.15) and plastic void growth by equation (3.21), here the contribution from rubber bridging was not considered since rubber bridging was not found in fractography investigation.

Table 24: Parameters and values for the modeling studies to predict the fracture energy for MEP_H2_D51N systems at 23 °C.

Name	Variable	Value
Radius of the core-shell particles	r_p (μm)	Table 25
Void radius	r_{fv}	Table 25
$V_{fv} - V_{fp}$	V_{fv}, V_{fp}	Table 25
Poisson's ratio of the unmodified epoxy	ν	0.35
Plane-strain compressive yield true stress	σ_{yc} (MPa)	114
Plane-strain compressive fracture true strain	γ_f	0.98
Uniaxial tensile yield true stress	σ_{yt} (MPa)	101
Pressure-dependent yield stress parameter	μ_m	0.2
Fracture energy	G_{IC} (J/m ²)	105
Critical stress intensity factor	K_{IC} (MPa.m ^{1/2})	0.64
von Mises stress concentration factor	K_{vm}	$K_{vm} = 3.9337V_f + 2.1126$

Up to 6 wt. % the radius of D51N particles obtained from AFM pictures linearly increases with the increasing vol. %. Only three data points were selected to predict the G_c since up-to 6 wt. % the morphology of nanocomposites consist of spherically shaped particles and above 6 wt. % co-continuous structure formation starts and the sudden rise was observed in fracture toughness and fracture energy values from the experimental results.

Table 25: Mean radius, corresponding volume %, void radius and ($V_{fv} - V_{fp}$) values of anhydride based D51N BCP modified epoxy systems.

D51 N (wt. %)	D51 N (vol. %)	Radius (μm)	Void radius (μm)	$V_{fv} - V_{fp}$
2	2.2	0.16	0.316	0.151
4	4.5	0.25	0.495	0.301
6	6.7	0.36	0.713	0.451

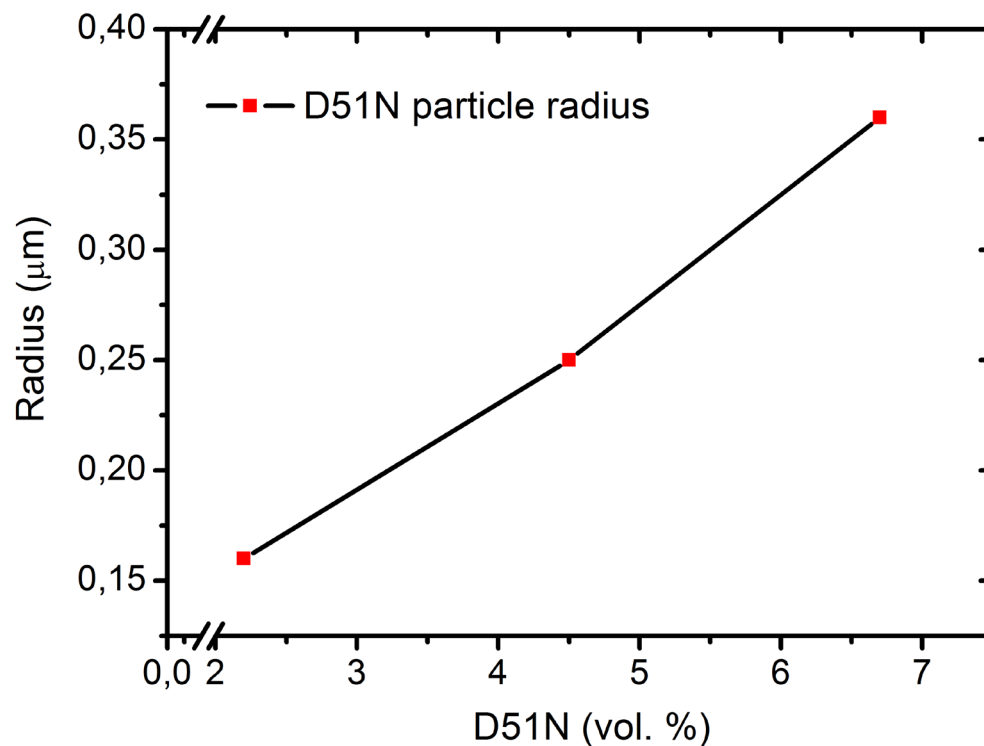


Figure 78: Radius of D51N BCP's in D51N modified epoxy systems at different vol. %.

The model which was used to quantify the G_c does not account for co-continuous and phase inverted morphologies. The calculated and measured values of fracture energy were tabulated in Table 26. It was difficult to accurately determine the volume fraction of particles that undergo cavitation experimentally. Finite element studies by Guild et al. [192] suggest that all rubbery particles should cavitate, and analysis of the fracture surfaces confirms this. Moreover, it was not assumed that all the cavities would undergo the maximum extent of plastic void growth, i.e. until void radius becomes equal to $(1 + \gamma_{fu})r_p$, due to a local reduction in stress near a void. An upper bound of 100 % and lower bound of 14.3 % [192] [193] of particles which cavitate and

undergo full plastic void growth would be expected. However, for the MEP_H2_D51N system, it is assumed that 100 % of the particles will cavitate.

Table 26 Predicted and measured values of fracture energy for D51N BCP modified MEP_H2 systems at 23 °C.

MEP_H2_D51N		ΔG_v	ΔG_s	G_{IC} predicted	G_{IC} experimental
[D51N] wt. %	[D51N] v_f	[J/m ²]	[J/m ²]	[J/m ²]	[J/m ²]
0	0	0	0	105	105
2	0.022	112	64	281	250
4	0.044	240	97	442	419
6	0.066	387	125	617	600

For D51N BCP modified epoxies, a fair agreement was found between experimentally measured and predicted values of fracture energy G_c .

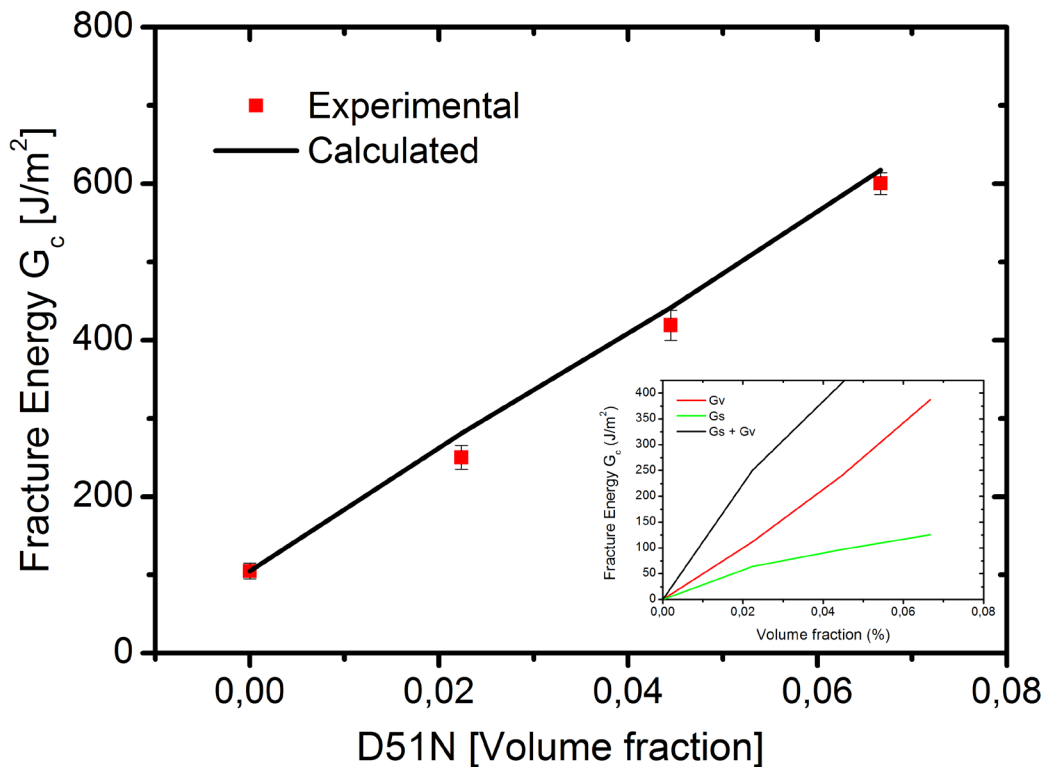


Figure 79: Fracture energy vs volume fraction for the D51N modified MEP_H2 system at 23 °C. Data points were experimental data, the line represents theoretical prediction. The contributions of G_s and G_v were shown in the inset.

6.5 Amine cured tailored epoxy modified with CSR particles

The epoxy was modified with CSR nanoparticles which were commercially called as Kane Ace MX170 supplied by Kaneka Belgium NV. The material supplied was in the form of a masterbatch which was a 25 wt. % concentrate of core-shell rubber (CSR) toughening agent in unmodified liquid epoxy resin based on Bisphenol-A. The amine-based modified epoxy system i.e. MEP_H1 was used as the epoxy hardener system and it was systematically modified with MX170 CSR nanoparticles for 2 wt. %, 4 wt. %, 6 wt. %, 8 wt. %, 10 wt. % and 12 wt. % respectively and the appropriate curing cycle was used for all the formulations.

6.5.1 Microstructure

The unmodified epoxy was found to be a homogeneous single phase material as expected, see Figure 80. All the epoxy amine hardener systems modified with MX170 were transparent before and after the curing process.

This suggests that, after the curing process, no macrophase separation occurred and nanostructure was formed in all MX170 modified epoxies since particle exceeding $1/15$ of the wavelength of visible light scatter light and reduces the transparency of the materials [182]. This also suggests that MX170 core-shell rubber nanoparticles were compatible with amine-based hardener systems.

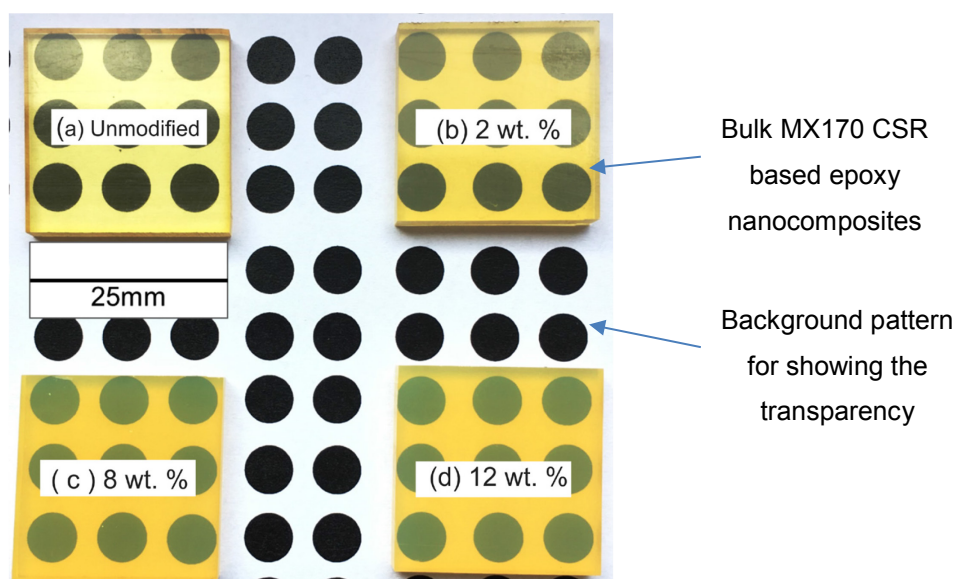


Figure 80: Pictures of the unmodified and MX170 modified amine cured bulk epoxy samples. (a) Unmodified epoxy; (b) 2 wt. % MX170 modified epoxy; (c) 8 wt. % MX170 modified epoxy; (d) 12 wt. % MX170 modified epoxy.

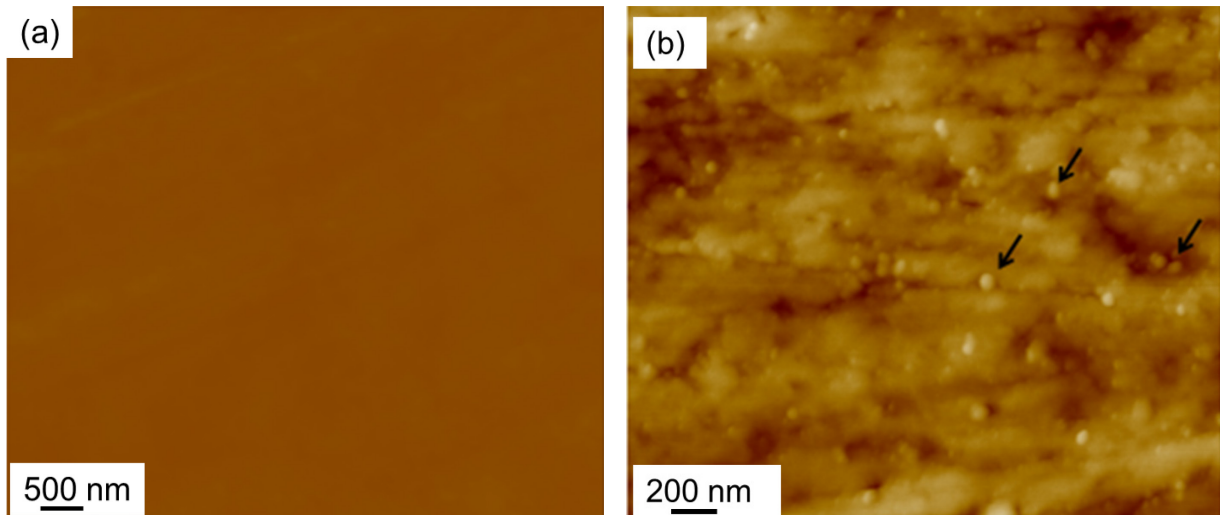


Figure 81 : (a) AFM height image of polished bulk unmodified epoxy. (b) AFM height image of polished bulk 4 wt. % MX170 modified epoxy-amine system. Black arrows were showing the CSR particles.

The morphologies of the unmodified and MEP-MX170 particles modified epoxies were observed using AFM. The morphology of the unmodified epoxy was homogeneous and featureless and the CSR particles were a bit softer than the epoxy and hence, show up as light-colored circles. For the epoxy systems examined, the CSR particles were well dispersed for all formulations up to 12 wt. %. Some of the CSR particles show a light colored ring around the soft cores, indicating the PMMA shell. The average core radii of the CSR particles were about 50 ± 5 nm. This agrees well with the literature provided by the supplier [166].

6.5.2 Rheology

The viscosity change of the different epoxy systems as a function of temperature was shown in Figure 82. This was because the particles present in the system tends to offer a resistance to the resin flow owing to increase in the viscosity. The viscosity of pure epoxy was 0.163 Pa.s at 50 °C and the addition of 12 wt. % of CSR particles has raised the viscosity to 0.75 Pa.s at the same temperature of 50 °C. The results obtained from the rheological tests were used to produce the graphs for showing the change in the viscosity with respect to temperature.

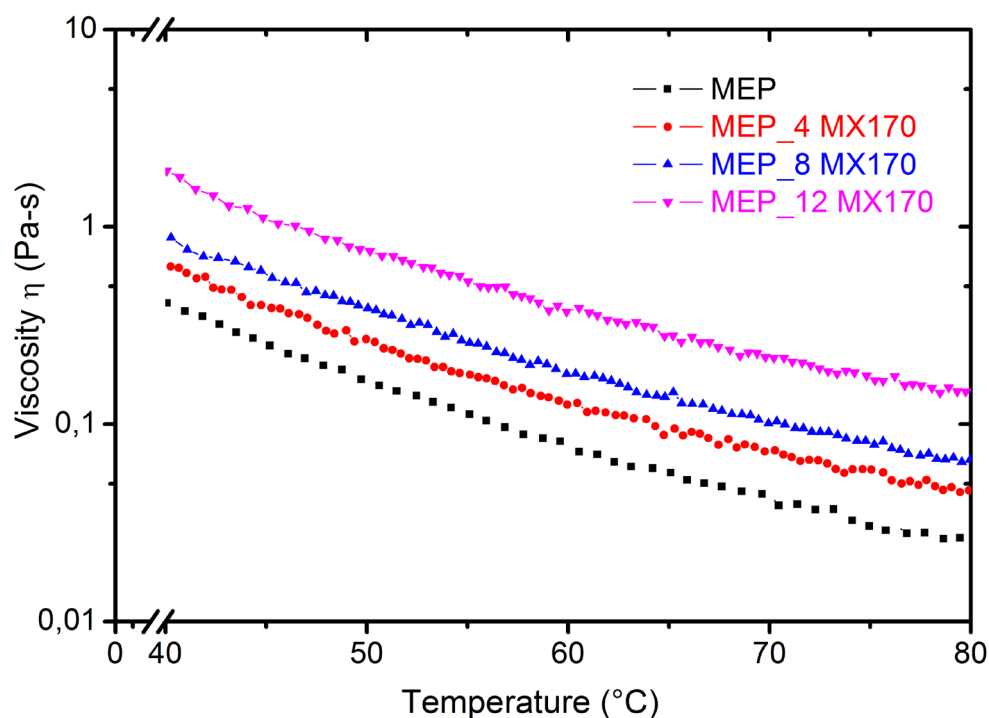


Figure 82: Graph showing variation in viscosity with respect to temperature for different tailored epoxy systems modified with MX170 CSR particles.

6.5.3 Glass transition temperature and viscoelastic properties

The glass transition temperatures of amine-cured unmodified and CSR particles modified epoxy systems were measured with the help DSC and DMTA techniques. The results were tabulated as shown in the Table 27. It's observed that for the unmodified epoxy system, the glass transition temperature was 134 °C and with the addition of CSR particles, there was an increase of T_g to around 136 °C at 2 wt. % and 4 wt. % concentrations. If all the systems were considered, it can be concluded that with the addition of CSR particles either the T_g increased or remains same, which explains that addition of CSR to the amine-based system does not have a detrimental effect on the glass transition temperature and the minor increase was due to the contribution of bisphenol-A from MX170 masterbatch.

Table 27: Glass transition temperature, T_g of amine-cured unmodified epoxy system and amine cured epoxy system modified with CSR particles.

MX170 [wt %]	T_g [°C]	
	DSC	DMTA [tan δ]
0	134	137
2	136	n/a
4	136	146
6	134	n/a
8	140	146
10	138	n/a
12	143	146

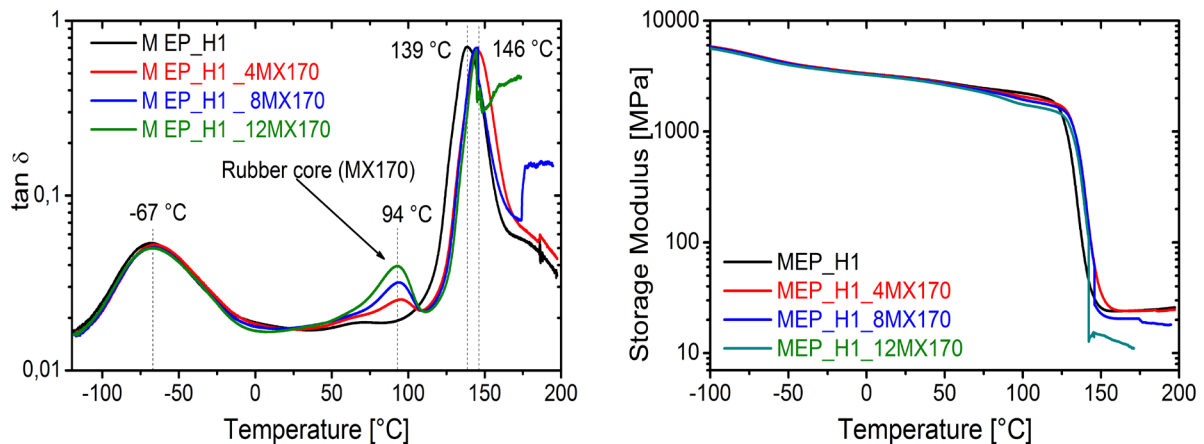


Figure 83: Graph showing storage modulus E' and damping $\tan \delta$, with respect to temperature, for the amine cured unmodified and CSR particles modified the epoxy system.

The graph of the temperature versus storage modulus E' and $\tan \delta$ was shown in Figure 83. It was observed that the storage modulus E' for unmodified epoxy at the temperature 170 °C was approximately 24.13 MPa and for the CSR particles modified epoxy with 12 wt. % of the particle content in the same temperature range was 11.77 MPa. This was about 43 % decrement when compared to the neat epoxy system which implies that the crosslink density was decreased. The microphase separation was observed for all compositions modified with MX170 CSR nanoparticles which were clearly evident from the small shoulders at 94 °C. The peak's height does not change considerably with the incorporation of CSR particles which explains that damping factor remains almost same for all wt. % of MX170, however right shift in the peak was observed which indicates the rise in glass

transition temperature which was due to the addition of bisphenol- A resin from the MX170 masterbatch. At around 95 °C, a peak was observed for all the CSR particles modified epoxy systems which represent the glass transition temperature of the rubbery core present in the CSR particle. It also indicates that the type of rubber used as a core for CSR was stiff in nature as its T_g lies in the range of (90 °C – 100 °C). Due to trade secret reasons, the core material of the CSR was not revealed by the supplier.

6.5.4 Tensile properties

The tensile properties such as tensile strength σ_m , strain ϵ_m , and elastic modulus E_t were measured at 23 °C and 80 °C were tabulated as shown in Table 28. For the unmodified epoxy system, the modulus was 3230 MPa and tensile strength was 95.0 MPa. Later, with the addition of CSR to the epoxy, the modulus and tensile strength were decreased with the increase in particle but this decrease was not same as of D51N BCP's which clearly indicates that rubber core of MX170 CSR was more stiff as compared to conventional CSR's moreover this was supported by the MX170 TDS which claims to maintain the flexural modulus even at higher loadings [166]. For the addition of 2 wt. % of the particle content, the values were observed to be 3190 MPa and 92.1 MPa. Then, they were decreased till 12 wt. %. For 12 wt. %, the modulus and strength were 3020 MPa and 84 MPa. This trend was due to the presence of the rubber particles which were having relatively lower modulus when compared to the unmodified epoxy system.

Table 28: Tensile properties E_t , σ_m and ϵ_m of the amine-cured unmodified epoxy system and amine cured epoxy system modified with CSR particles measured at 23 °C and 80 °C.

MX170 [wt.%]	E_t [MPa] @ 23 °C	σ_m [MPa] @ 23 °C	ϵ_m [%] @ 23 °C
0	3230 (\pm 18.7)	95.0 (\pm 0.4)	7.0 (\pm 0.1)
2	3190 (\pm 12.0)	92.1 (\pm 0.3)	6.8 (\pm 0.1)
4	3130 (\pm 14.4)	90.3 (\pm 0.8)	6.8 (\pm 0.3)
6	3110 (\pm 27.8)	86.0 (\pm 0.5)	6.8 (\pm 0.1)
8	3090 (\pm 40.5)	86.0 (\pm 0.5)	6.8 (\pm 0.1)
10	3050 (\pm 57.0)	85.0 (\pm 1.9)	6.6 (\pm 0.3)
12	3020 (\pm 34.6)	84.0 (\pm 0.5)	6.5 (\pm 0.3)

MX170 [wt. %]	E_t [MPa] @ 80 °C	σ_m [MPa] @ 80 °C	ϵ_m [%] @ 80 °C
0	2510 (± 28.0)	62.0 (± 0.28)	4.5 (± 0.20)
2	2400 (± 23.7)	57.2 (± 0.13)	4.7 (± 0.01)
4	2390 (± 50.6)	57.2 (± 0.20)	4.7 (± 0.09)
6	2360 (± 15.4)	56.5 (± 0.31)	4.6 (± 0.01)
8	2310 (± 10.1)	54.5 (± 0.56)	4.6 (± 0.04)
10	2240 (± 45.0)	53.4 (± 0.55)	4.6 (± 0.02)
12	2170 (± 13.8)	51.7 (± 0.10)	4.6 (± 0.03)

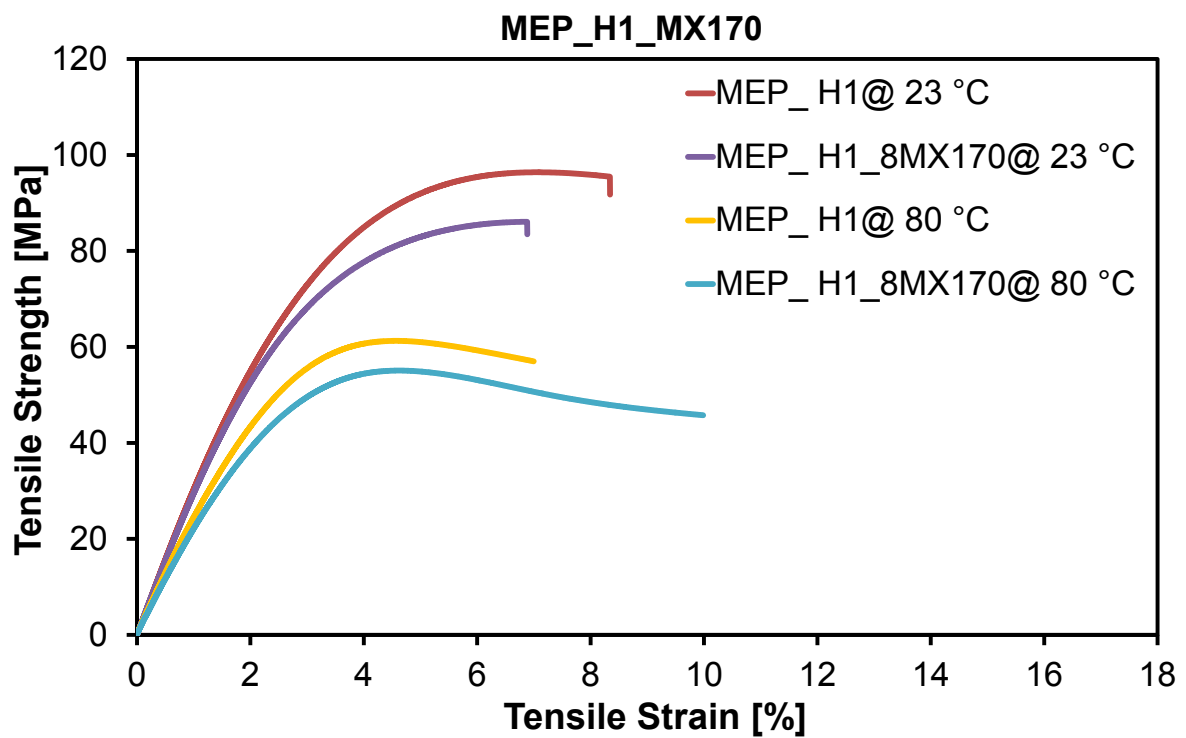


Figure 84: Graph showing tensile stress versus strain response of amine-cured unmodified epoxy and amine cured epoxy system modified with 8 wt. % of CSR particles measured at 23 °C and 80 °C.

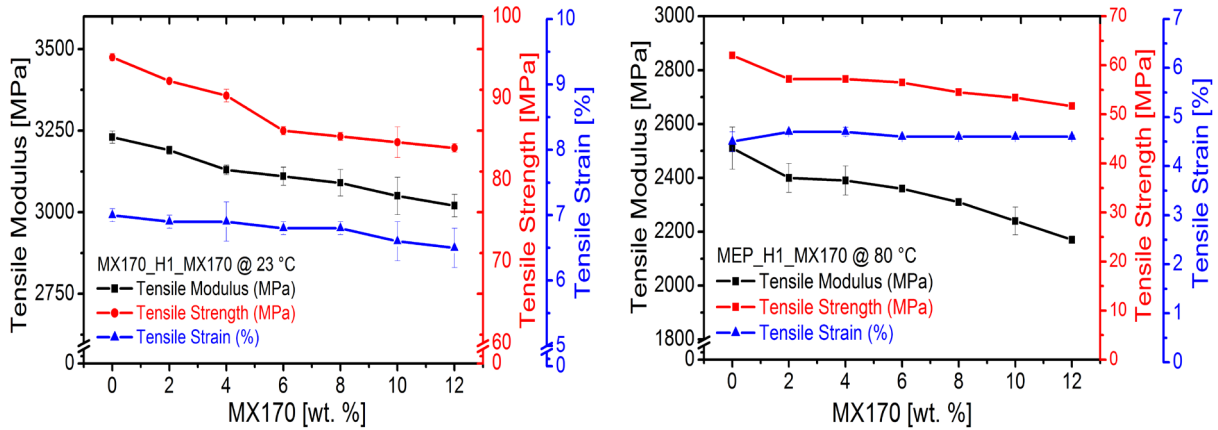


Figure 85: Graph showing tensile properties of amine cured unmodified epoxy system and amine cured epoxy system modified with CSR particles at 23 °C and at 80 °C.

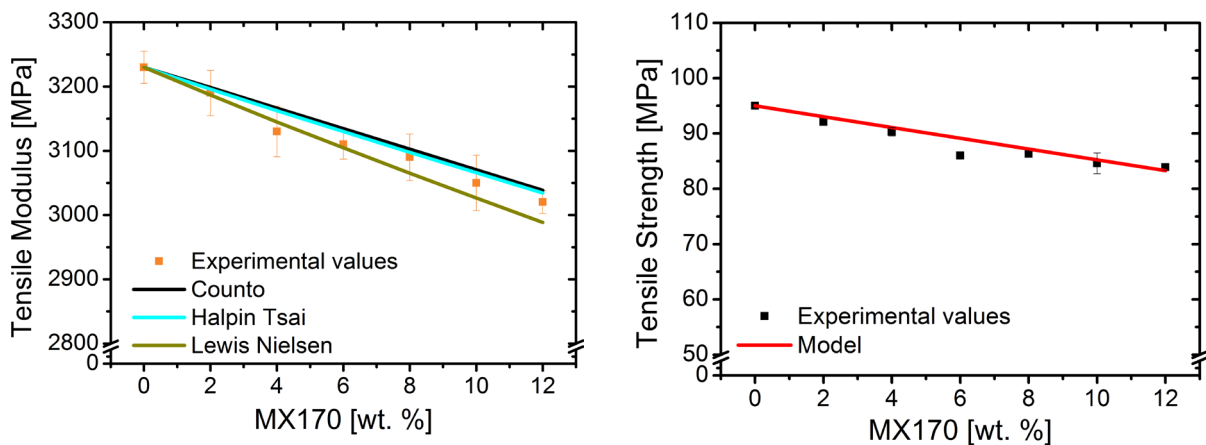


Figure 86 Tensile modulus vs MX170 [wt. %] (Left) and tensile strength vs MX170 [wt. %] (Right) for MEP_H1_MX170 systems at 23 °C. Points were experimental data, lines were theoretical predictions

The details of all the models used to evaluate the elastic modulus were already discussed in section §3.11.1. The parameters incorporated into the model were matrix modulus $E_m=3230$ MPa, and for MX170 CSR particles the values were unknown since supplier didn't reveal the properties due to company trade secret. Reverse calculation approach has been applied to calculate the modulus of CSR core. Using equation (3.4) and (3.5) in §3.11.1 the upper and lower limits of E_{core} and later the average of those two values have been taken and considered as modulus of rubber core (~ 2000 MPa). The CSR particles were considered to be in spherical shape and shape factor value of 2 was taken for Halpin Tsai model and $V_{max} = 0.632$ and the no-slip condition was considered for Lewis-Nielsen model. The predictions of the Counto, Halpin Tsai, and Lewis Nielsen models were compared with the experimental data in Table 29 and the agreement was fairly good. The difference

between theoretical and experimental values in no case was higher than 2 %. Counto model gives the upper bound and Lewis – Nielsen gives the lower bound. For all the formulations the data was above the Lewis – Nielsen predictions which confirm that slip or debonding does not occur except for 4 wt. % formulation. Similarly, for tensile strength model which was discussed in §3.11.2 gives a fair prediction for tensile strength values with a deviation less than 4 %.

Table 29: Tensile modulus and tensile strength of MX170 modified composites as a function of MX170 volume content. Comparison between experimental results and different theoretical predictions for MEP_H1_MX170 systems at 23 °C.

MX170		Tensile Modulus [MPa]				Tensile Strength [MPa]	
wt. %	vol. %	Exp. [MPa]	Counto [MPa]	Halpin Tsai	Lewis Nielsen	Exp.	Model
0	0	3230	3230	3230	3230	95	95
2	2.42	3190	3199	3196	3187	92	93
4	4.83	3130	3166	3162	3145	90	91
6	7.18	3110	3135	3130	3105	86	89
8	9.52	3090	3102	3098	3065	86	87
10	11.86	3050	3070	3066	3026	85	85
12	14.18	3020	3039	3034	2989	84	83

6.5.5 Fracture properties

The fracture toughness, K_{IC} , and fracture energy, G_{IC} , values of the amine cured unmodified epoxy system and CSR particles modified epoxy systems were tabulated below. The fracture toughness and fracture energy of the unmodified epoxy were observed to be $0.73 \text{ MPa}\cdot\text{m}^{1/2}$ and 0.14 kJ/m^2 . By the addition of CSR particles, these properties were increased linearly to $1.43 \text{ MPa}\cdot\text{m}^{1/2}$ and 0.57 kJ/m^2 for 12 wt. % of the CSR content at 23 °C and similarly fracture toughness and fracture energy increased to $1.79 \text{ MPa}\cdot\text{m}^{1/2}$ and 1.30 kJ/m^2 for 12 wt. % of CSR particles from $1.03 \text{ MPa}\cdot\text{m}^{1/2}$ and 0.37 kJ/m^2 at 80 °C.

Table 30: Fracture toughness, K_{IC} and fracture energy, G_{IC} , values of the amine cured unmodified epoxy system and CSR particles modified epoxy systems in mode-I loading at 23 °C and 80 °C.

MX170 [wt. %]	K_{IC} [MPa.m ^{1/2}] @23 °C	G_{IC} [kJ/m ²] @23 °C
0	0.73 (±0.08)	0.14 (±0.03)
2	0.84 (±0.08)	0.19 (±0.04)
4	1.05 (±0.05)	0.30 (±0.02)
6	1.19 (±0.06)	0.41 (±0.04)
8	1.29 (±0.10)	0.48 (±0.08)
10	1.40 (±0.05)	0.55 (±0.04)
12	1.43 (±0.07)	0.57 (±0.05)
MX170 [wt. %]	K_{IC} [MPa.m ^{1/2}] @80 °C	G_{IC} [kJ/m ²] @80 °C
0	1.03 (±0.10)	0.37 (±0.09)
2	1.52 (± 0.14)	0.84 (±0.10)
4	1.55 (±0.04)	0.88 (±0.04)
6	1.60 (±0.02)	0.95 (±0.02)
8	1.65 (±0.04)	1.03 (±0.04)
10	1.72 (±0.03)	1.16 (±0.03)
12	1.79 (±0.04)	1.30 (±0.05)

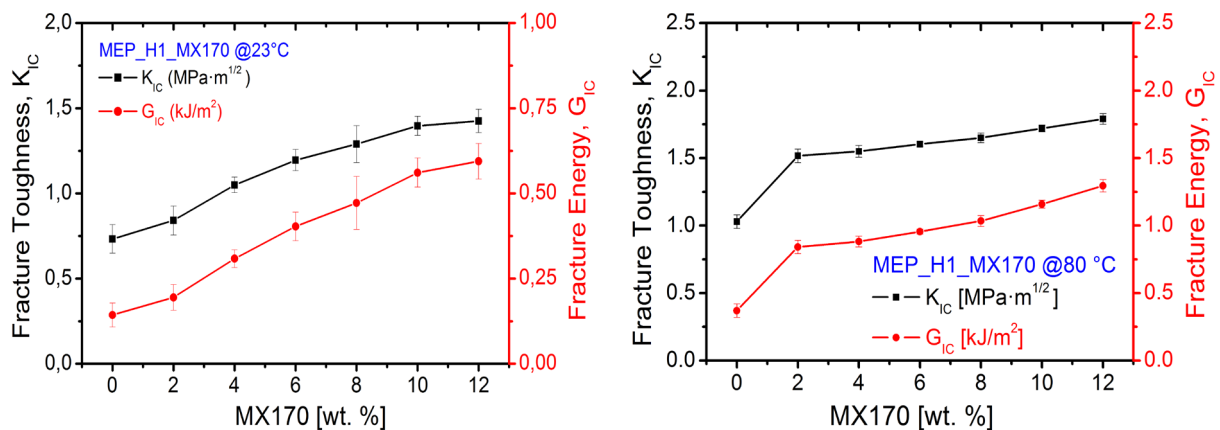


Figure 87: Graph showing fracture toughness, K_{IC} and fracture energy, G_{IC} , values of the amine cured unmodified epoxy system and CSR particles modified epoxy systems at 23 °C and 80 °C.

6.5.6 Fractography studies

A comprehensive fractography studies were performed on the fractured surfaces by using scanning electron microscope (SEM) to find reasons for the improvement of fracture toughness and bonding between the epoxy matrix and filler material. Several mechanisms were identified that were responsible for the increase in fracture toughness. The fractured surface of the amine curing unmodified epoxy seems to be smooth without any traces of plastic deformation. This was usually seen in all types of unmodified brittle epoxies due to the absence of any filler materials that promote plastic deformation. With the addition of CSR particles, the roughness of the surface was increased which indicates that the plastic deformation of the matrix occurred. At higher magnifications, the fractured surface of the CT specimen appeared to have cavitation of rubber particles and voids were formed due to this cavitation. The average diameter of the rubber particles was measured to be in the range of 100 nm and for few particles, it was in the range of 150 nm. A little increase in the diameter was observed for the voids formed by the cavitation of particles which says that there was a plastic void growth taken place around the particles during the deformation process. From the micrographs, it also has to be noted that the dispersion of the particles was uniform and there were hardly the agglomerates observed. So, the major toughening mechanisms were observed to be cavitation of rubber particles by void formation rubber particles and shear yielding of the matrix.

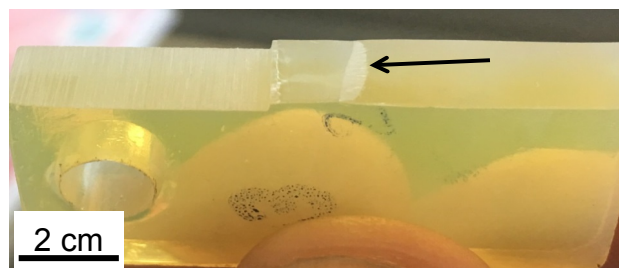


Figure 88: Fractured compact tension specimen of 10 wt. % of MX170 modified epoxy/ amine system at 80 °C. Arrow pointing towards stress whitened region.

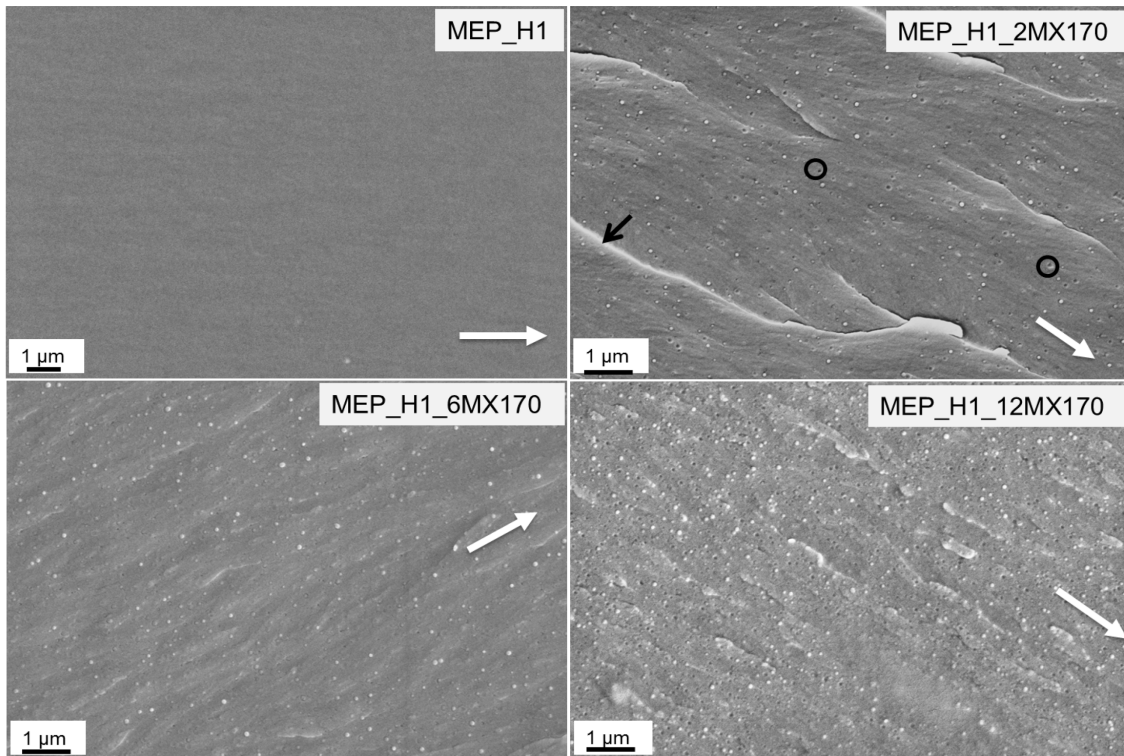


Figure 89: FEG-SEM micrograph of the amine cured unmodified epoxy, 2 wt. %, 6 wt. % and 12 wt. % CSR particles modified the epoxy system at 23 °C. Circles and black arrows indicate cavitation of particles and matrix tearing. White arrows were indicating the direction of crack propagation.

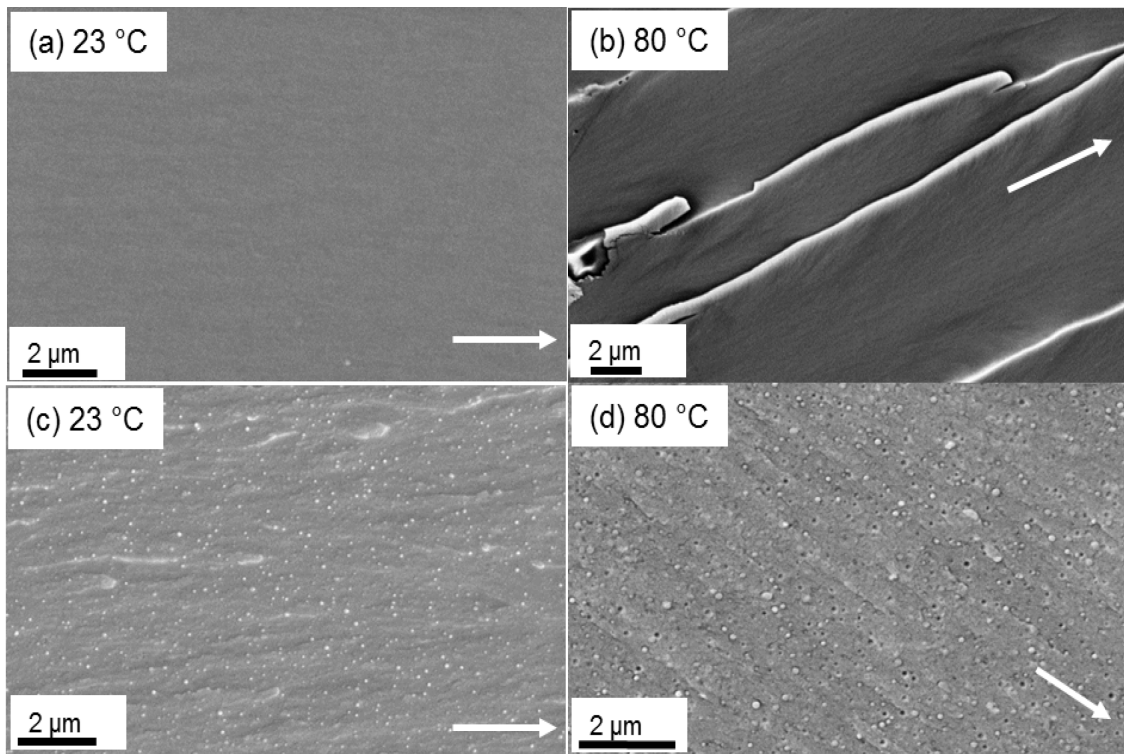


Figure 90: FEG-SEM micrograph of the amine cured (a) unmodified epoxy at 23 °C (b) unmodified epoxy at 80 °C (c) 8 wt. % CSR particles modified epoxy system at 23 °C and (d) 8 wt. % CSR particles modified epoxy system at 80 °C. White arrows were indicating the direction of crack propagation.

The high temperature tested composites show a typical fracture surface divided into two regions; the stress whitened (Figure 88) and the fast-crack growth region. In the stress whitened region or plastic zone, ahead of the crack tip, the crack propagates slowly. It was characterized by a very rough fracture surface with numerous cavities and significant plastic deformation [16]. The cavities in this region were larger than those in the fast crack section and massive shear bands connecting the cavitated particles were also observed. The fast-crack growth region, located beyond the plastic zone, was characterized by rapid fracture propagation, smoother surface and some cavities of approximately same size as the undeformed rubber particles. Similar behavior was reported in a CTBN rubber-modified epoxy resin and was explained due to the rubber particles induce more localized plastic deformations around the crack tip increasing the size of the plastic zone leading to a somewhat rougher fracture surface [187]. Yee also suggested that the triaxial tension at the crack tip must be relieved before the crack propagates, so the deviatoric stress can reach a critical value for yielding to occur [188]. The plastic zone absorbs the major fracture energy and once that the critical force was reached the total fracture takes place.

6.5.7 Modeling of Fracture Energy

The main toughening mechanisms for MX170 CSR particles modified epoxy polymers were identified as localized shear yielding and plastic void growth initiated by the cavitation of the CSR particles and as discussed in section §6.5.6. The individual contributions for each toughening mechanism can be predicted and compared with the experimental results as detailed in § 3.11.3. The used parameter in the modeling as tabulated in Table 31. The contribution in fracture energy from shear yielding was calculated by equation (3.15) and plastic void growth by equation (3.21), here the contribution from rubber bridging was not considered since rubber bridging was not found in fractography investigation.

Table 31: Parameters and values for the modeling studies to predict the fracture energy for MEP_H1_MX170 systems.

Name	Variable	Value
Radius of the core-shell particles	r_p (nm)	50
Void radius	r_{fv}	Table 32
$V_{fv} - V_{fp}$	V_{fv}, V_{fp}	Table 32
Poisson's ratio of the unmodified epoxy	ν	0.35
Plane-strain compressive yield true stress	σ_{yc} (MPa)	108
Plane-strain compressive fracture true strain	γ_f	0.98
Uniaxial tensile yield true stress	σ_{yt} (MPa)	95
Pressure-dependent yield stress parameter	μ_m	0.2
Fracture energy	G_{cu} (J/m ²)	143
Critical stress intensity factor	K_{cu} (MPa.m ^{1/2})	0.73
von Mises stress concentration factor	K_{vm}	$K_{vm} = 3.9337V_f + 2.1126$

The calculated and measured values of fracture energy were tabulated in Table 33. It was difficult to accurately determine the volume fraction of particles that undergo cavitation experimentally. Finite element studies by Guild et al. [192] suggest that all rubbery particles should cavitate, and analysis of the fracture surfaces confirms this. Moreover, it was not assumed that all the cavities would undergo the maximum extent of plastic void growth, i.e. until void radius becomes equal to $(1 + \gamma_{fu})r_p$, due to a local reduction in stress near a void. An upper bound of 100 % and lower bound

of 14.3 % [192] [193] of particles which cavitate and undergo full plastic void growth would be expected. However, in the current work, the CSR particles used were stiff as compared to conventional polysiloxane based CSR particles and this effect was evident from the mechanical properties of the MEP_H1_MX170 system as discussed in §6.5.4 and from fractography examination it can be concluded that only few CSR particles were cavitated. Therefore for the current work, only 10 % of CSR particles were to be assumed to undergone cavitation. For MX170 CSR particles modified epoxies, a good agreement was found between experimentally measured and predicted values of fracture energy G_{IC} .

Table 32 Mean radius (CSR particles), void radius and ($V_{fv} - V_{fp}$) for amine based MX170 modified tailored epoxy systems.

MX170 (wt. %)	MX170 (vol. fraction)	Radius (nm)	Void radius (nm)	$V_{fv} - V_{fp}$
2	0,021	50	99	0.139
4	0,041	50	99	0.278
6	0,062	50	99	0.417
8	0,082	50	99	0.556
10	0,103	50	99	0.695
12	0,123	50	99	0.833

Table 33 Predicted and measured values of fracture energy for MX170 CSR modified MEP_H1 system at 23 °C.

MEP_H1_MX170		$(10\%)\Delta G_v$	ΔG_s	G_{IC} predicted	G_{IC} experimental
[MX170] wt. %	[MX170] v_f	[J/m ²]	[J/m ²]	[J/m ²]	[J/m ²]
0	0,000	0	0	143	143
2	0,021	21	84	249	188
4	0,041	46	131	320	301
6	0,062	74	170	388	414
8	0,082	106	207	456	479
10	0,103	141	243	527	549
12	0,123	180	277	600	570

The same trend was reported by Giannakopoulos [194] where the author used core-shell rubber particles of two different diameters.

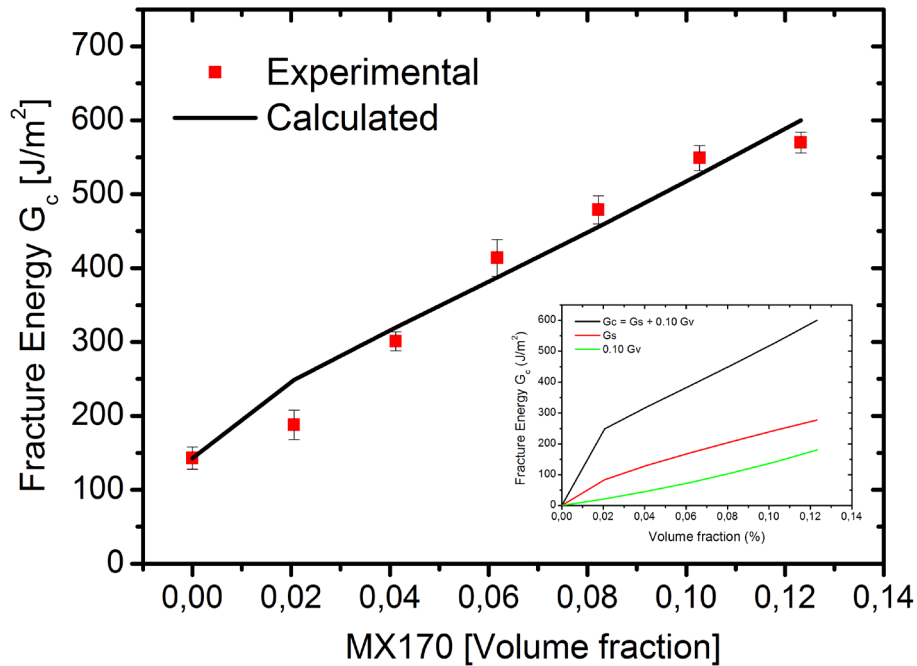


Figure 91: Fracture energy vs volume fraction for the MX170 CSR modified MEP_H1 system at 23 °C. Data points were experimental data, the line represents theoretical prediction. The contributions of G_s and G_v were shown in the inset.

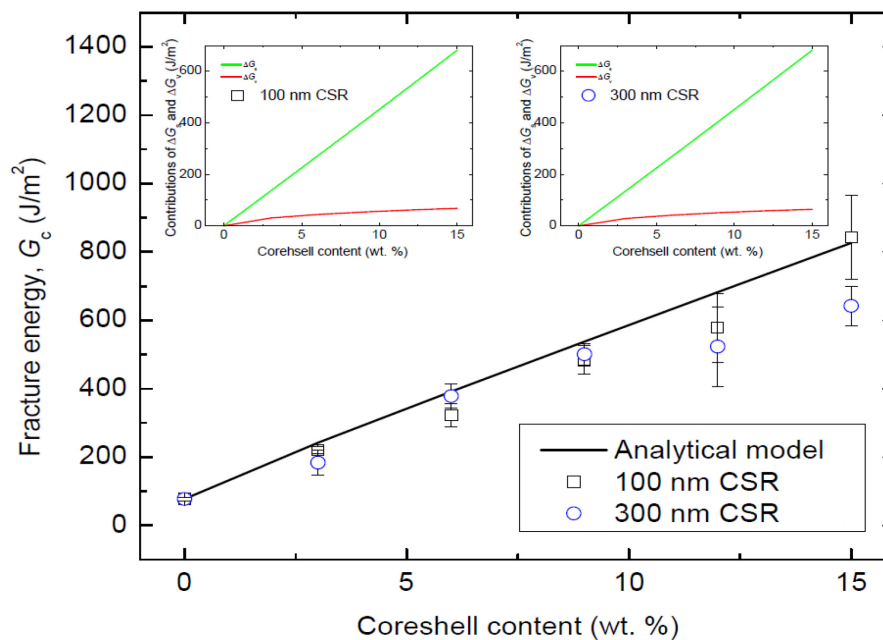


Figure 92: Fracture energy for anhydride cured bisphenol-A based epoxy modified with CSR particles of two different radii as mentioned in the graph [194]. The contributions of G_s and G_v were shown in insets.

6.6 Anhydride cured tailored epoxy modified with CSR particles

The epoxy was modified with CSR nanoparticles which were commercially called as Kane Ace MX170 supplied by Kaneka Belgium NV. The material supplied was in the form of a masterbatch which was a 25 wt. % concentrate of core-shell rubber (CSR) toughening agent in unmodified liquid epoxy resin based on Bisphenol-A. The anhydride based modified epoxy system i.e. MEP_H2 was used as the epoxy hardener system and it was systematically modified with MX170 CSR nanoparticles for 2 wt. %, 4 wt. %, 6 wt. %, 8 wt. %, 10 wt. % and 12 wt. % respectively and the appropriate curing cycle was used for all the formulations.

6.6.1 Microstructure studies

The unmodified epoxy was found to be a homogeneous single phase material as expected, see Figure 93. All the epoxy-anhydride hardener systems modified with MX170 were transparent before curing and opaque after the gelation process.

This suggests that no macrophase separation occurred which gave rise to opacity in all MX170 modified epoxies since particle exceeding $1/15$ of the wavelength of visible light (approx. 40nm) scatter light and reduce the transparency of the materials [182].

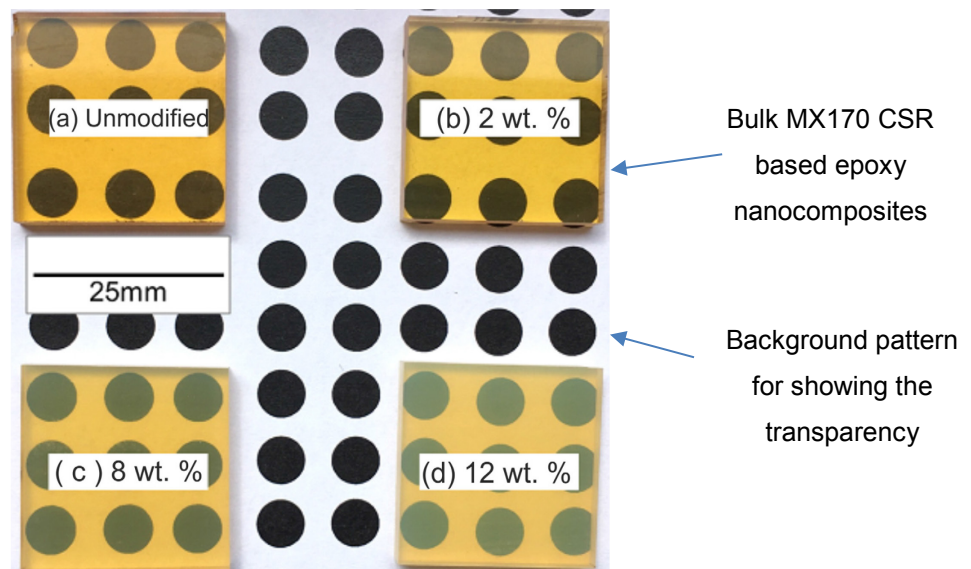


Figure 93: Pictures of the unmodified and MX170 modified anhydride cured bulk epoxy samples. (a) Unmodified epoxy; (b) 2 wt. % MX170 modified epoxy; (c) 8 wt. % MX170 modified epoxy; (d) 12 wt. % MX170 modified epoxy.

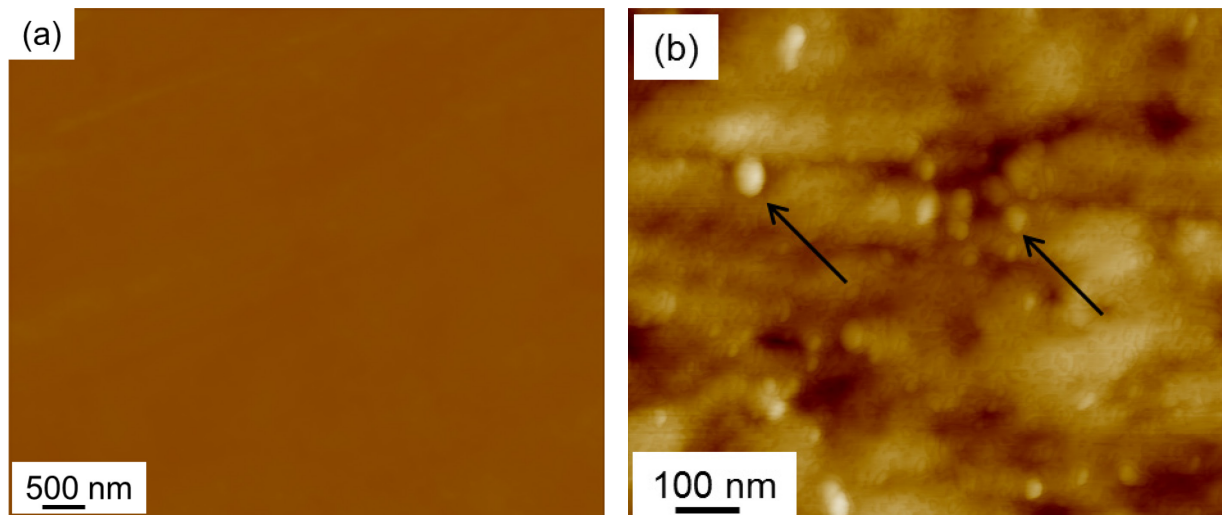


Figure 94:(a) AFM height image of polished bulk unmodified epoxy. (b) AFM height image of polished bulk 6 wt. % MX170 modified epoxy anhydride system. Black arrows showing the CSR particles.

The morphologies of the unmodified and MEP-MX170 particles modified epoxies were observed using AFM. The morphology of the unmodified epoxy was homogeneous and featureless and the CSR particles were a bit softer than the epoxy and hence, show up as light-colored circles. For the epoxy systems examined, the CSR particles were well dispersed for all formulations up to 12 wt. %. Some of the CSR particles show a light colored ring around the soft cores, indicating the PMMA shell. The average core radii of the CSR particles were about 50 ± 1 nm. This agrees well with the literature provided by the supplier [166].

6.6.2 Rheology

The viscosity change of the different epoxy systems as a function of temperature was shown in Figure 95. This was because the particles present in the system tends to offer a resistance to the resin flow owing to increase in the viscosity. The viscosity of pure epoxy was 0.030 Pa.s at 40 °C and the addition of 12 wt. % of CSR particles raised the viscosity to 0.470 Pa.s at the same temperature of 40 °C. The results obtained from the rheological tests were used to produce the graphs for showing the change in the viscosity with respect to temperature.

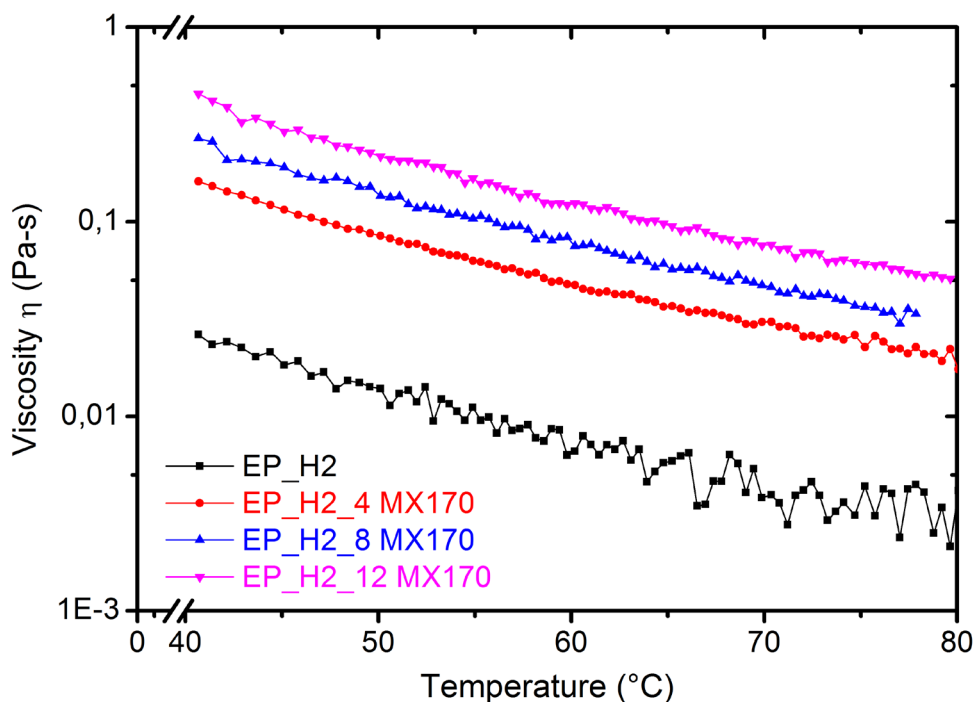


Figure 95: Graph showing variation in viscosity with respect to temperature for different anhydride based tailored epoxy systems modified with MX170 CSR particles.

6.6.3 Glass transition temperature and viscoelastic properties

The glass transition temperatures of anhydride cured unmodified and CSR particles modified epoxy systems were measured with the help DSC and DMTA techniques. The results were tabulated as shown in the Table 34. It's observed that for the unmodified epoxy system, the glass transition temperature T_g was 143 °C and with the addition of 2 wt. % and 4 wt. % CSR particles, it was increased to 144 °C but it was decreased to 144 °C for 6 wt. %. If all the systems were considered, it can be concluded that with the addition of CSR particles either the T_g increased or remains same, which explains that addition of CSR to the amine-based system do not have a detrimental effect on the glass transition temperature and the minor increase was due to the contribution of bisphenol-A from MX170 masterbatch.

Table 34: Glass transition temperature, T_g of anhydride cured unmodified epoxy system and anhydride cured epoxy system modified with CSR particles.

MX170 [wt. %]	T_g [°C]	
	DSC	DMTA [$\tan\delta$]
0	143	147
2	144	n/a
4	144	149
6	144	n/a
8	145	150
10	145	n/a
12	146	148

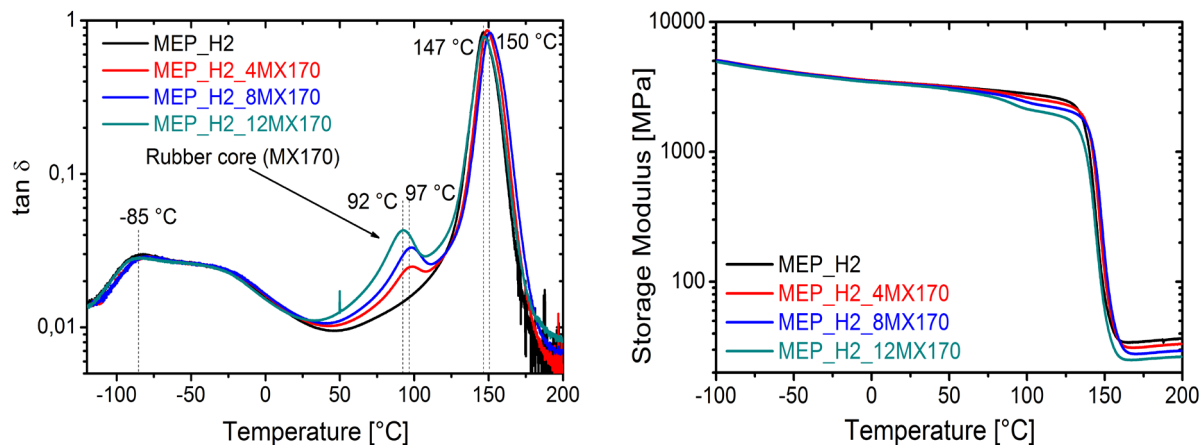


Figure 96: Graph showing damping $\tan \delta$ and storage modulus E' , with respect to temperature, for the anhydride cured unmodified and CSR particles modified the epoxy system.

The graph of the $\tan \delta$ vs. temperature was shown in Figure 96. The small shoulders observed between temperature 90 °C and 100 °C for all the modified systems representing the T_g of the rubber core used in MX170 master batch and for all the formations the $\tan \delta$ value almost remains the same. It was observed that the storage modulus E' for unmodified epoxy at the temperature 180 °C was approximately 35.09 MPa and for the CSR particles modified epoxy with 12 wt. % of the particle content in the same temperature range was 25.59 MPa. This was about 27 % decrement when compared to the neat epoxy system implies that the crosslink density was decreased.

6.6.4 Tensile properties

The tensile properties such as tensile strength σ_m , strain ϵ_m , and elastic modulus E_t were measured at room temperature and were tabulated as shown in the table. For the unmodified epoxy system, the modulus was 3580 MPa and tensile strength was 101.0 MPa. Later, with the addition of 2 wt. % CSR particles, the tensile modulus, and strength were decreased to 3470 MPa and 95.6 MPa. From the addition of 4 wt. % and till 12 wt. %, both the values were linearly decreased to 3360 MPa and 86.3 MPa. This was because the rubber particles act as softer material and therefore having relatively lower modulus and strength when compared to the unmodified epoxy system which was generally brittle in nature. The results obtained from the tensile testing were tabulated as shown below.

Table 35: Tensile properties E_t , σ_m , and ϵ_m of anhydride cured unmodified epoxy system and anhydride cured epoxy system modified with CSR particles measured at 23 °C and at 80 °C.

MX170 [wt. %]	E_t [MPa] @ 23 °C	σ_m [MPa] @ 23 °C	ϵ_m [%] @ 23 °C
0	3580 (\pm 78.0)	101.0 (\pm 2.5)	5.8 (\pm 0.0)
2	3540 (\pm 36.1)	96.4 (\pm 0.6)	5.8 (\pm 0.0)
4	3470 (\pm 54.5)	95 (\pm 0.6)	5.6 (\pm 0.0)
6	3420 (\pm 30.0)	93.3 (\pm 0.7)	5.6 (\pm 0.0)
8	3410 (\pm 46.7)	90.8 (\pm 0.6)	5.6 (\pm 0.1)
10	3360 (\pm 18.4)	87.4 (\pm 0.6)	5.6 (\pm 0.1)
12	3320 (\pm 28.8)	86.3 (\pm 0.7)	5.5 (\pm 0.3)
MX170 [wt. %]	E_t [MPa] @ 80 °C	σ_m [MPa] @ 80 °C	ϵ_m [%] @ 80 °C
0	2880 (\pm 18.0)	68 (\pm 0.61)	4.3 (\pm 0.02)
2	2850 (\pm 17.6)	65 (\pm 0.33)	4.3 (\pm 0.08)
4	2800 (\pm 11.2)	63 (\pm 0.53)	4.3 (\pm 0.12)
6	2770 (\pm 34.3)	61 (\pm 0.33)	4.3 (\pm 0.03)
8	2690 (\pm 40.4)	59 (\pm 0.34)	4.2 (\pm 0.03)
10	2650 (\pm 30.1)	58 (\pm 0.20)	4.2 (\pm 0.05)
12	2610 (\pm 34.3)	55 (\pm 0.16)	4.2 (\pm 0.01)

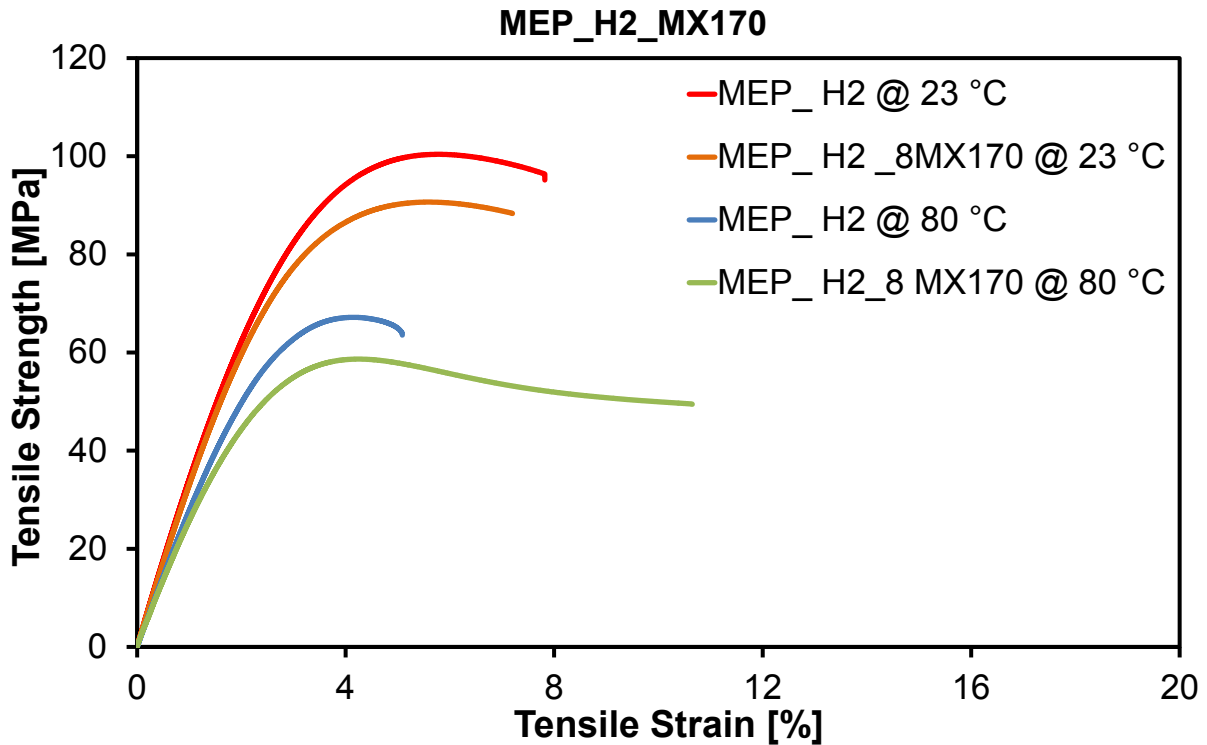


Figure 97: Graph showing tensile stress versus strain response of anhydride cured unmodified epoxy and amine cured epoxy system modified with 8 wt. % of CSR particles at 23 °C and 80 °C.

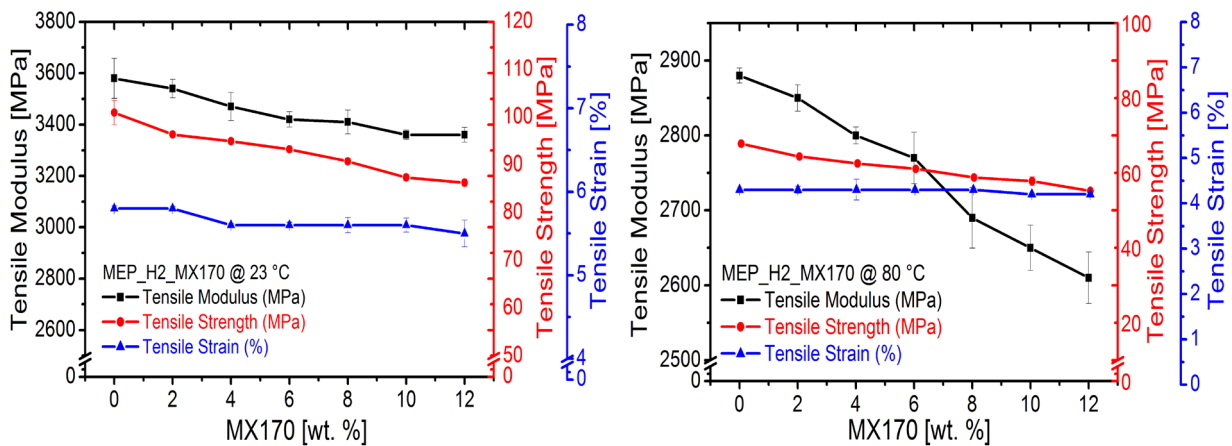


Figure 98: Graph showing tensile properties of anhydride cured unmodified epoxy system and anhydride cured epoxy system modified with the CSR particles at 23 °C and at 80 °C.

The details of all the models used to evaluate the elastic modulus were already discussed in section §3.11.1. The parameters incorporated into the model were $E_m=2950$ MPa, $E_{D51N}= 245$ MPa and BCP's were considered to be in spherical shape so shape factor was taken as 2 for Halpin Tsai model and $V_{max}= 0.632$ and the no-slip condition was considered for Lewis-Nielsen model. The predictions of the

Counto, Halpin Tsai, and Lewis Nielsen models were compared with the experimental data in Table 36 and the agreement was fairly good.

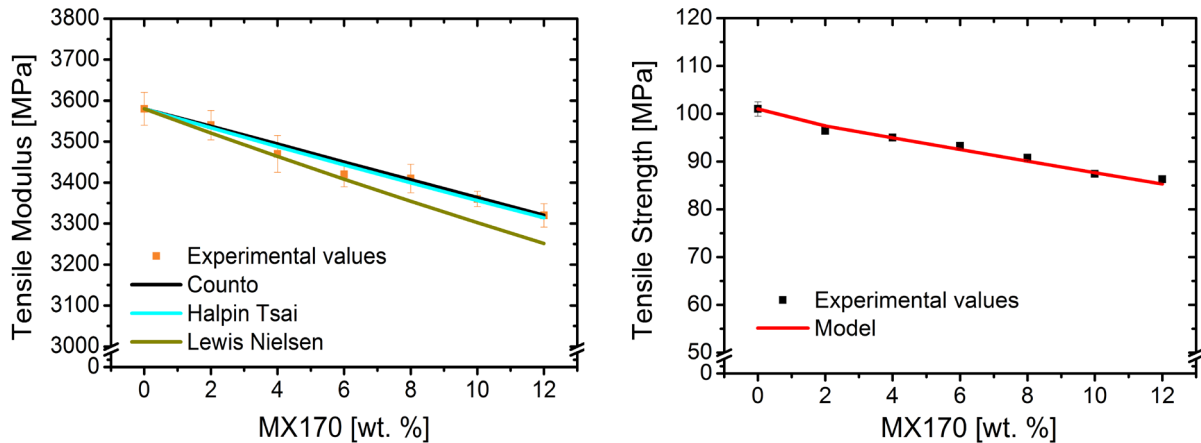


Figure 99: Tensile modulus vs MX170 [wt. %] (Left) and tensile strength vs MX170 [wt. %] (Right) for MEP_H2_MX170 systems at 23 °C. Points were experimental data, lines were theoretical predictions.

Table 36: Tensile modulus and tensile strength of MX170 modified composites as a function of MX170 volume content. Comparison between experimental results and different theoretical predictions for MEP_H2_MX170 systems at 23 °C.

MX170		Tensile Modulus [MPa]				Tensile Strength [MPa]	
wt. %	vol. %	Exp. [MPa]	Counto [MPa]	Halpin Tsai	Lewis Nielsen	Exp.	Model
0	0	3580	3580	3580	3580	101	101
2	2.53	3540	3538	3533	3521	96.4	97
4	5.01	3470	3494	3488	3464	95	95
6	7.48	3420	3450	3443	3408	93.3	93
8	9.91	3410	3407	3399	3355	90.8	90
10	12.33	3360	3363	3356	3302	87.4	88
12	14.72	3320	3320	3314	3252	86.3	85

Up to 6 wt. % all the models underestimate the modulus of the composite, however the difference between theoretical and experimental values in no case higher than 5 %. After 6 wt. % the experimental data lie between Halpin – Tsai, and Lewis – Nielsen predictions, where Halpin – Tsai gives the upper bound and Lewis – Nielsen gives the lower bound. For all the formulations the data was above the Lewis – Nielsen predictions which confirm that slip or debonding does not occur. Similarly, for tensile

strength model which was discussed in §3.11.2 gives a fair prediction for tensile strength values with a deviation less than 5 %.

6.6.5 Fracture properties

The fracture toughness, K_{IC} , and fracture energy, G_{IC} , values of the anhydride cured unmodified epoxy system and D51N modified epoxy systems were tabulated below. The fracture toughness K_{IC} and fracture energy G_{IC} of the unmodified epoxy were observed to be $0.64 \text{ MPa.m}^{1/2}$ and 0.10 kJ/m^2 .

Table 37: Fracture toughness, K_{IC} and fracture energy, G_{IC} , values of the anhydride cured unmodified epoxy system and CSR particles modified epoxy systems in mode-I loading at $23 \text{ }^\circ\text{C}$ and at $80 \text{ }^\circ\text{C}$.

MX170 [wt. %]	K_{IC} [$\text{MPa.m}^{1/2}$] @23 °C	G_{IC} [kJ/m^2] @23 °C
0	0.64 (± 0.13)	0.10 (± 0.05)
2	0.84 (± 0.10)	0.18 (± 0.05)
4	1.00 (± 0.07)	0.25 (± 0.04)
6	1.03 (± 0.08)	0.28 (± 0.05)
8	1.20 (± 0.07)	0.37 (± 0.05)
10	1.21 (± 0.03)	0.39 (± 0.02)
12	1.30 (± 0.13)	0.45 (± 0.09)
MX170 [wt. %]	K_{IC} [$\text{MPa.m}^{1/2}$] @80 °C	G_{IC} [kJ/m^2] @80 °C
0	0.70 (± 0.02)	0.15 (± 0.01)
2	1.19 (± 0.15)	0.43 (± 0.11)
4	1.25 (± 0.04)	0.49 (± 0.02)
6	1.54 (± 0.07)	0.75 (± 0.06)
8	1.65 (± 0.09)	0.89 (± 0.10)
10	1.72 (± 0.04)	0.95 (± 0.04)
12	1.77 (± 0.02)	1.05 (± 0.02)

By the addition of CSR particles, these properties were increased gradually and reached to $1.30 \text{ MPa.m}^{1/2}$ and 0.45 kJ/m^2 . This was about 203 % and 450 % increment to the K_{IC} and G_{IC} values of the unmodified epoxy system.

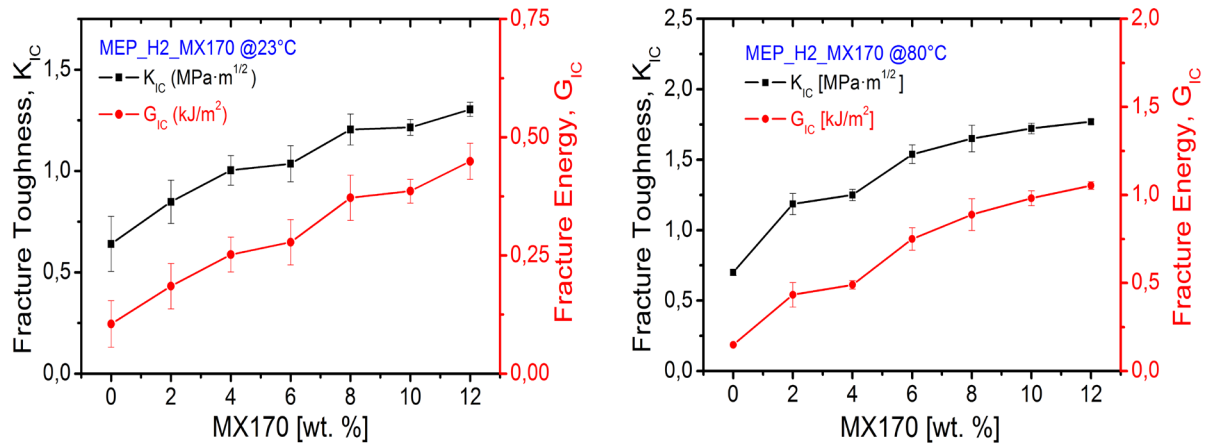


Figure 100: Graph showing fracture toughness, K_{IC} and fracture energy, G_{IC} , values of the anhydride cured unmodified epoxy system and CSR particles modified epoxy systems at 23 °C and at 80 °C.

6.6.6 Fractography studies

A comprehensive fractography studies were performed on the fractured surfaces by using scanning electron microscope (SEM) to find reasons for the improvement of fracture toughness and bonding between the epoxy matrix and filler material. Several mechanisms were identified that were responsible for the increase in fracture toughness and they will be discussed in the following sections accordingly. The direction of the crack propagation for each image was from left to right. The fractured surface of the anhydride cured unmodified epoxy seems to be smooth without any traces of plastic deformation. This was usually seen in all types of unmodified brittle epoxies due to the absence of any filler materials that promote plastic deformation and toughness. With the addition of CSR particles, the roughness of the surface has been increased and certain toughening mechanisms were witnessed for the increase in fracture toughness.

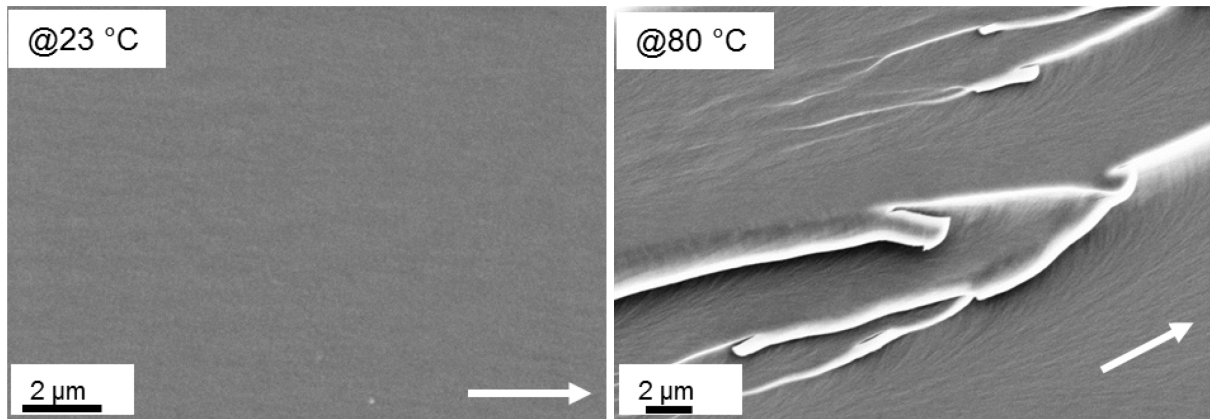


Figure 101: FEG-SEM micrograph showing the fracture surface of anhydride cured unmodified epoxy system taken in the vicinity of the tip of the pre-crack at 23 °C (left) and 80 °C (right). White arrows were indicating the crack propagation direction.

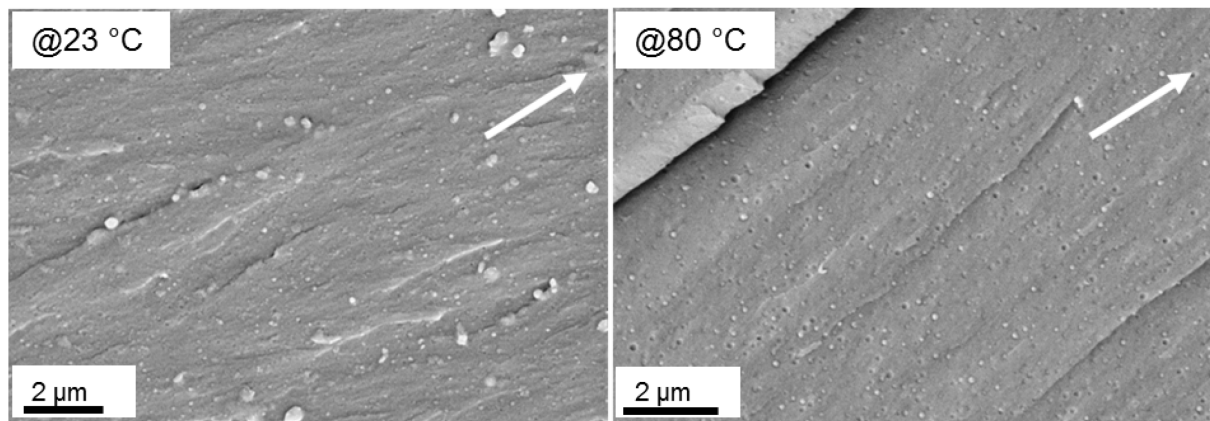


Figure 102: FEG-SEM micrograph of the anhydride cured 8 wt. % CSR particles modified the epoxy system at 23 °C (left) and 80 °C (right). White arrows were indicating the crack propagation direction.

Certain toughening mechanisms were observed on the fracture surfaces of the specimens. Matrix tearing, crack deflection and cavitation were taken into consideration as main mechanisms besides the riverlines were also observed which have negligible impact in increasing the fracture toughness. Moreover, the dispersion of the rubber particles was good and there were hardly any agglomerates even at higher concentrations of the particle content. The average diameter of the particles measured over a surface was in the range 100 nm ~ 250 nm. For the addition of 6 wt. % of the particles and higher, cavitation and debonding of the rubber particles were the main toughening mechanisms. Some of the cavitations were observed to be bigger in diameter than that of the rubber particle which attributes that considerable plastic deformation has taken place around the particle during the process of debonding from the matrix.

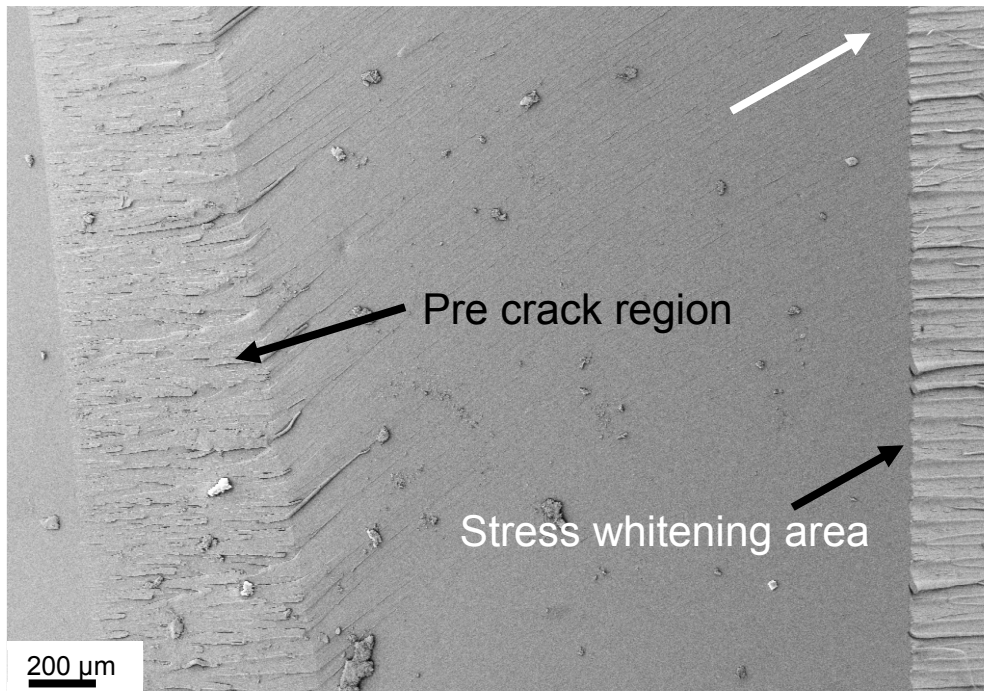


Figure 103: FEG-SEM micrograph of the anhydride cured 8 wt. % CSR particles modified the epoxy system at 80 °C. White arrow was showing the crack propagation direction.

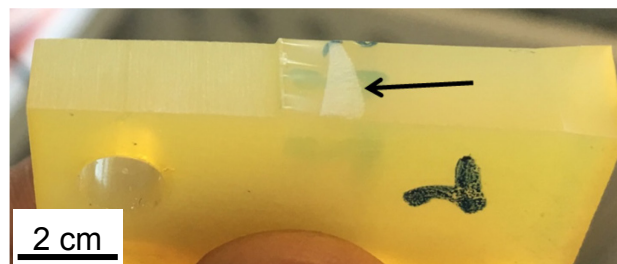


Figure 104: Fractured compact tension specimen of 10 wt. % of MX170 modified epoxy/ anhydride system at 80 °C. Black arrow was pointing towards stress whitened region.

6.6.7 Modeling of Fracture Energy

The main toughening mechanisms for MX170 CSR particles modified epoxy polymers were identified as localized shear yielding and plastic void growth initiated by the cavitation of the CSR particles and as discussed in section §6.6.6. The individual contributions for each toughening mechanism can be predicted and compared with the experimental results as detailed in § 3.11.3. The used parameter in the modeling as tabulated in Table 38. The contribution in fracture energy from shear yielding was calculated by equation (3.15) and plastic void growth by equation (3.21), here the contribution from rubber bridging was not considered since no rubber bridging was observed in fractography investigation.

Table 38: Parameters and values for the modeling studies to predict the fracture energy for MEP_H2_MX170 systems.

Name	Variable	Value
Radius of the core-shell particles	r_p (nm)	50
Void radius	r_{fv}	Table 39
$V_{fv} - V_{fp}$	V_v, V_p	Table 39
Poisson's ratio of the unmodified epoxy	ν	0.35
Plane-strain compressive yield true stress	σ_{yc} (MPa)	114
Plane-strain compressive fracture true strain	γ_f	0.98
Uniaxial tensile yield true stress	σ_{yt} (MPa)	101
Pressure-dependent yield stress parameter	μ_m	0.2
Fracture energy	G_{cu} (J/m ²)	105
Critical stress intensity factor	K_{cu}	0.64
von Mises stress concentration factor	K_{vm}	$K_{vm} = 3.9337 V_f + 2.1126$

The calculated and measured values of fracture energy were tabulated in Table 40. It was difficult to accurately determine the volume fraction of particles that undergo cavitation experimentally. Finite element studies by Guild et al. [192] suggest that all rubbery particles should cavitate, and analysis of the fracture surfaces confirms this. Moreover, it was not assumed that all the cavities would undergo the maximum extent of plastic void growth, i.e. until void radius becomes equal to $(1 + \gamma_{fu})r_p$, due to a local reduction in stress near a void. An upper bound of 100 % and lower bound

of 14.3 % [192] [193] of particles which cavitate and undergo full plastic void growth would be expected. However, in the current work, the CSR particles used were stiff as compared to conventional polysiloxane based CSR particles and this effect was evident from the mechanical properties of the MEP_H2_MX170 system as discussed in §6.6.3 and from fractography examination it can be concluded that only few CSR particles were cavitated. Therefore for the current work, only 5 % of CSR particles were assumed to undergone cavitation. For MX170 CSR particles modified epoxies, a good agreement was found between experimentally measured and predicted values of fracture energy G_{IC} .

Table 39: Mean radius (CSR particles), void radius and ($V_{fv} - V_{fp}$) for amine based MX170 modified tailored epoxy systems.

MX170 (wt. %)	MX170 (vol. fraction)	Radius (nm)	Void radius (nm)	$V_{fv} - V_{fp}$
2	0,025	50	99	0.171
4	0,050	50	99	0.339
6	0,075	50	99	0.506
8	0,099	50	99	0.670
10	0,123	50	99	0.834
12	0,147	50	99	0.996

Table 40: Predicted and measured values of fracture energy for MX170 CSR modified MEP_H2 system at 23 °C.

MEP_H2_MX170		$(5\%)\Delta G_v$	ΔG_s	G_{IC} predicted	G_{IC} experimental
[MX170] wt. %	[MX170] v_f	[J/m ²]	[J/m ²]	[J/m ²]	[J/m ²]
0	0,000	0	0	105	105
2	0,025	13	71	189	185
4	0,050	28	111	244	252
6	0,075	46	145	296	278
8	0,099	65	177	347	372
10	0,123	88	207	400	386
12	0,147	112	236	454	449

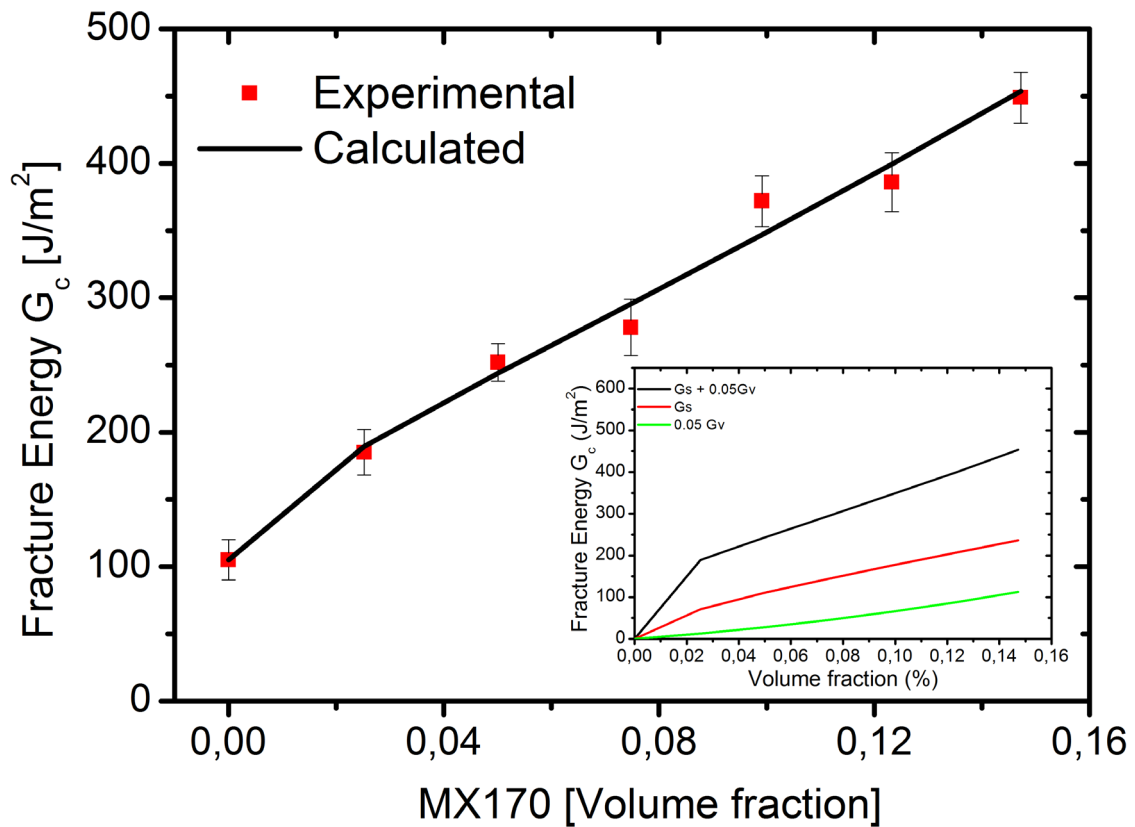


Figure 105: Fracture energy vs. volume fraction for the MX170 CSR modified MEP_H2 system at 23 °C. Data points were experimental data, the line represents theoretical prediction. The contributions of G_s and G_v were shown in the inset.

6.7 Amine cured epoxy hybrid composites modified with D51N BCP's and CSR particles

The epoxy was modified with a D51N diblock copolymer which was commercially available called as 'Nanostrength D51N' supplied by Arkema, France, and CSR nanoparticles which were commercially available called as 'Kane Ace MX170' supplied by Kaneka Belgium NV. The D51N particle contains two blocks out of which one was a softer poly (butyl acrylate) also called as PbuA and the other was harder poly (Methyl methacrylate) also called as PMMA. The MX170 material supplied was in the form of a masterbatch which was a 25 wt. % concentrate of core-shell rubber toughening agent in unmodified liquid epoxy resin based on Bisphenol-A. MEP_H1 was used as the standard epoxy system and amine-based hardener denoted as H1 was used for curing with appropriate curing cycle. The concentrations of 4 wt. %, 8 wt. % and 12 wt. % were considered for the manufacturing of final composites. In these, both D51N block copolymers and CSR particles contribute in equal percentages.

6.7.1 Rheology

The viscosity change of the different epoxy systems as a function of temperature was shown in Figure 106. The viscosity of pure epoxy was 0.163 Pa.s at 50 °C and the addition of (6 + 6) wt. % of D51N block copolymers and CSR particles raised the viscosity to 1.317 Pa.s at the same temperature of 50 °C. The results obtained from the rheological tests were used to produce the graphs for showing the change in the viscosity with respect to temperature.

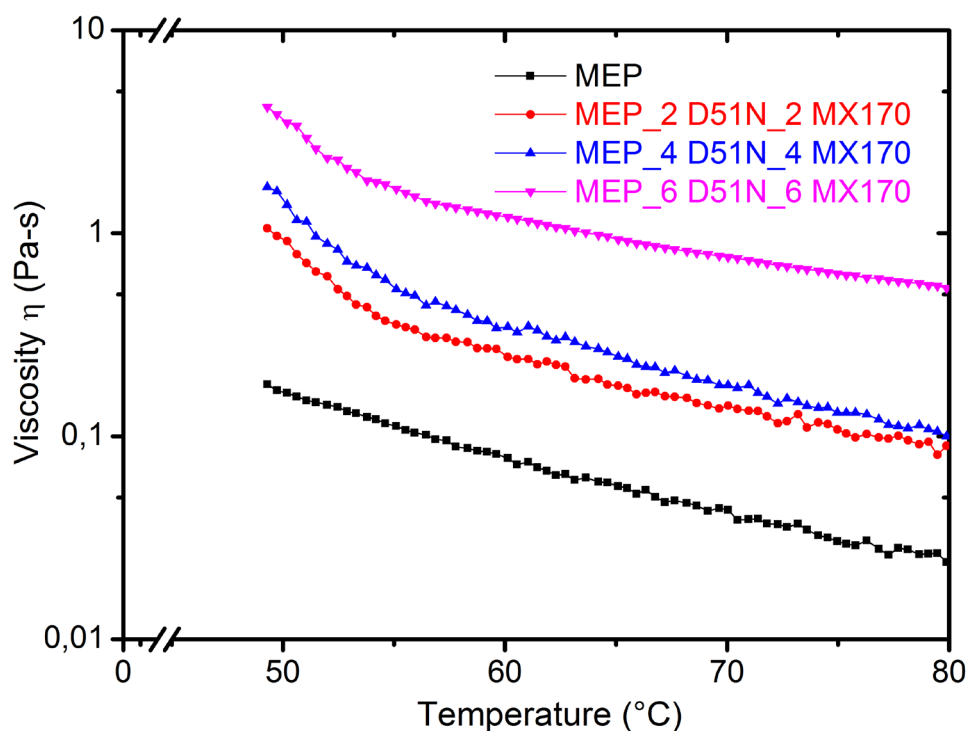


Figure 106: Graph showing variation in viscosity with respect to temperature for different tailored epoxy systems modified with D51N BCP's and MX170 CSR particles

6.7.2 Glass transition temperature and viscoelastic properties

The glass transition temperatures of amine-cured tailored and D51N block copolymer and CSR particles modified epoxy systems were measured with the help DSC and DMTA techniques. The results were tabulated as shown in the Table 41. It was observed that, for unmodified epoxy system, glass transition temperature was 134 °C and with the addition of D51N and CSR particles, T_g increased to 141 °C at 4 wt. % concentration. If all the systems were considered, it can be concluded that with the addition of CSR particles either the T_g increased or remains same, which explains that addition of CSR to the amine-based system do not have a detrimental effect on the glass transition temperature and the minor increase was due to the contribution of bisphenol-A from MX170 masterbatch.

Table 41: Glass transition temperature, T_g of amine-cured unmodified and D51N block copolymer, CSR particles modified epoxy systems obtained from DSC and DMTA.

D51N [wt. %] MX170 [wt. %]	T_g [°C] DSC	T_g [°C] DMTA [tan δ]
0	134	139
2 + 2 (4)	141	146
4 + 4 (8)	138	138
6 + 6 (12)	140	146

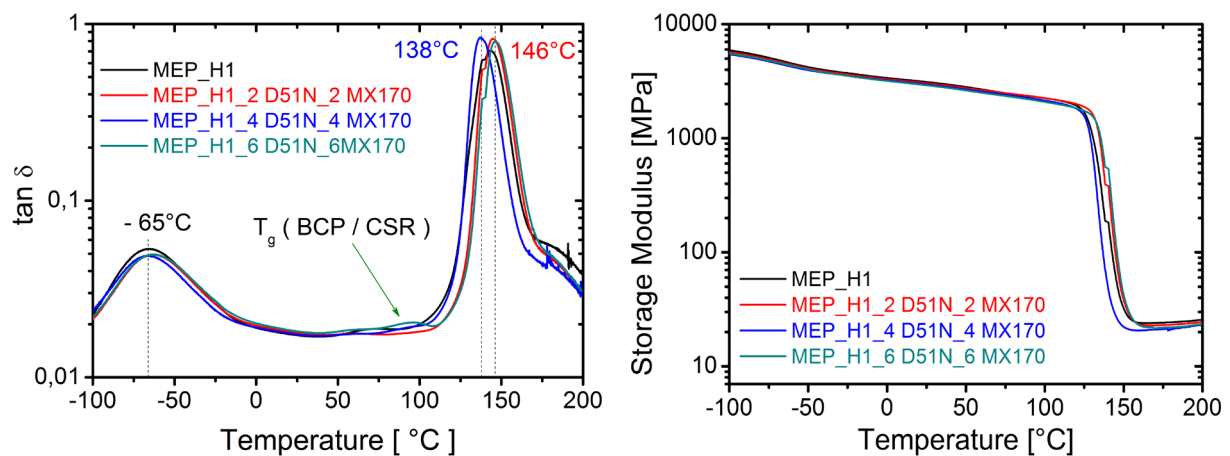


Figure 107: Graph showing storage modulus E' and damping $\tan \delta$, with respect to temperature, for the amine cured unmodified and D51N block copolymer, CSR particles modified epoxy systems.

From the DMTA graph, it was observed that the storage modulus E' for unmodified epoxy at the temperature 180 °C was approximately 24.61 MPa and for the D51N and CSR, particles modified epoxy with 12 wt. % of the particle content in the same temperature range was 21.97 MPa. This was about 11 % decrement when compared to the neat epoxy system which implies that the crosslink density was decreased with an increase in softer phase i.e. CSR and BCP's. At -65 °C, a peak was also observed in the graph for all the systems and was attributed to the β -transition peak. For hybrid nanocomposites, the stiff CSR particles suppress the microphase separation of block copolymers providing lower and broader peaks of the $\tan \delta$ curve as compared to the epoxy / CSR and epoxy / BCP modified epoxies for the same composition alone see Figure 108. This phenomenon was responsible for better tensile properties and lower fracture toughness and fracture energy as compared to the ones which were having a single phase of toughening agent for the same wt. %.

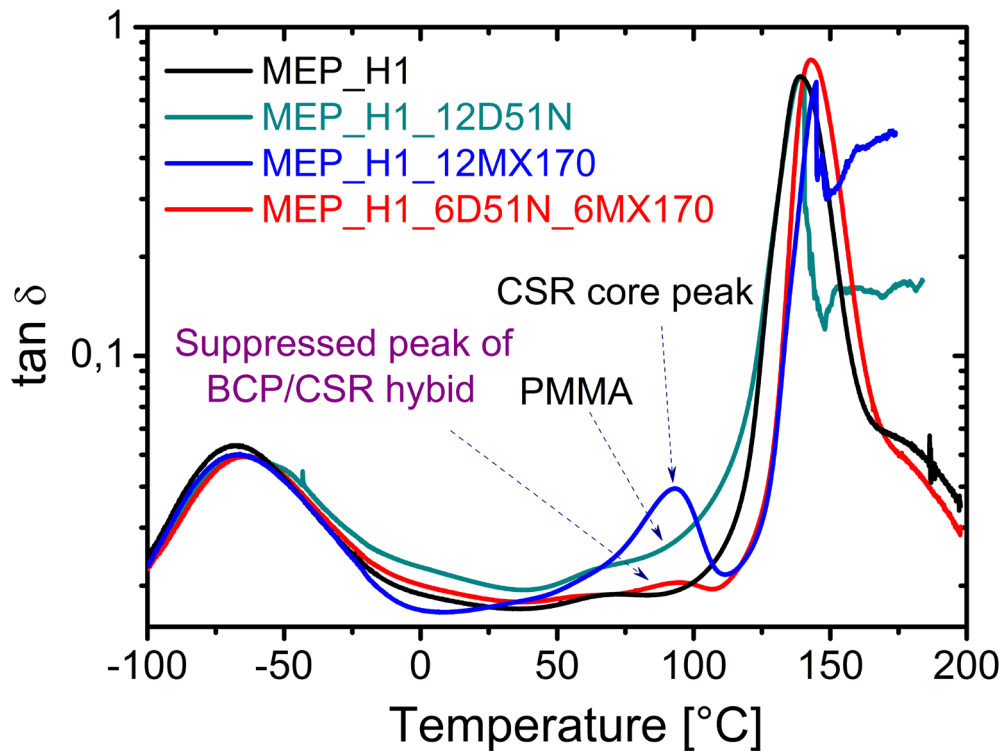


Figure 108: Graph showing $\tan \delta$ vs temperature curve for the amine cured unmodified and D51N BCP, MX170 CSR and hybrid particles modified systems.

6.7.3 Tensile properties

The tensile properties such as tensile strength σ_m , strain ϵ_m , and elastic modulus E_t were measured at room temperature and were tabulated as shown in Table 42. For the unmodified epoxy system, the modulus was 3230 MPa and tensile strength was 95.0 MPa. Later, with the addition of block copolymers and CSR particles to the epoxy, the modulus and tensile strength were decreased with the increase in particle content the tensile reduced to 2920 MPa and strength to 84.4 MPa at 23 °C and similar kind of trend was observed for all the systems at 80 °C where tensile modulus and tensile strength reduces to 2380 MPa and strength to 58 MPa from 2510 MPa and 62 MPa respectively.

Table 42: Tensile properties E_t , σ_m and ϵ_m of the MEP_H1 system and MEP_H1 system modified with the D51N block copolymer, CSR particles measured at 23 °C and at 80 °C.

D51N [wt. %]	MX170 [wt. %]	E_t [MPa] @ 23 °C	σ_m [MPa] @ 23 °C	ϵ_m [%] @ 23 °C
0	0	3230 (± 18.7)	95.0 (± 0.4)	7.0 (± 0.1)
2	2	3100 (± 58.2)	91.3 (± 1.5)	6.7 (± 0.3)
4	4	3050 (± 61.0)	89.0 (± 1.3)	6.4 (± 0.2)
6	6	2920 (± 7.21)	84.4 (± 0.6)	6.0 (± 0.4)
D51N [wt. %]	MX170 [wt. %]	E_t [MPa] @ 80 °C	σ_m [MPa] @ 80 °C	ϵ_m [%] @ 80 °C
0	0	2510 (± 58.5)	62 (± 0.3)	4,5 (± 0.02)
2	2	2510 (± 50.4)	61 (± 0.3)	4.6 (± 0.04)
4	4	2450 (± 50.4)	60 (± 0.5)	4.5 (± 0.05)
6	6	2380 (± 37.1)	58 (± 0.5)	4.5 (± 0.01)

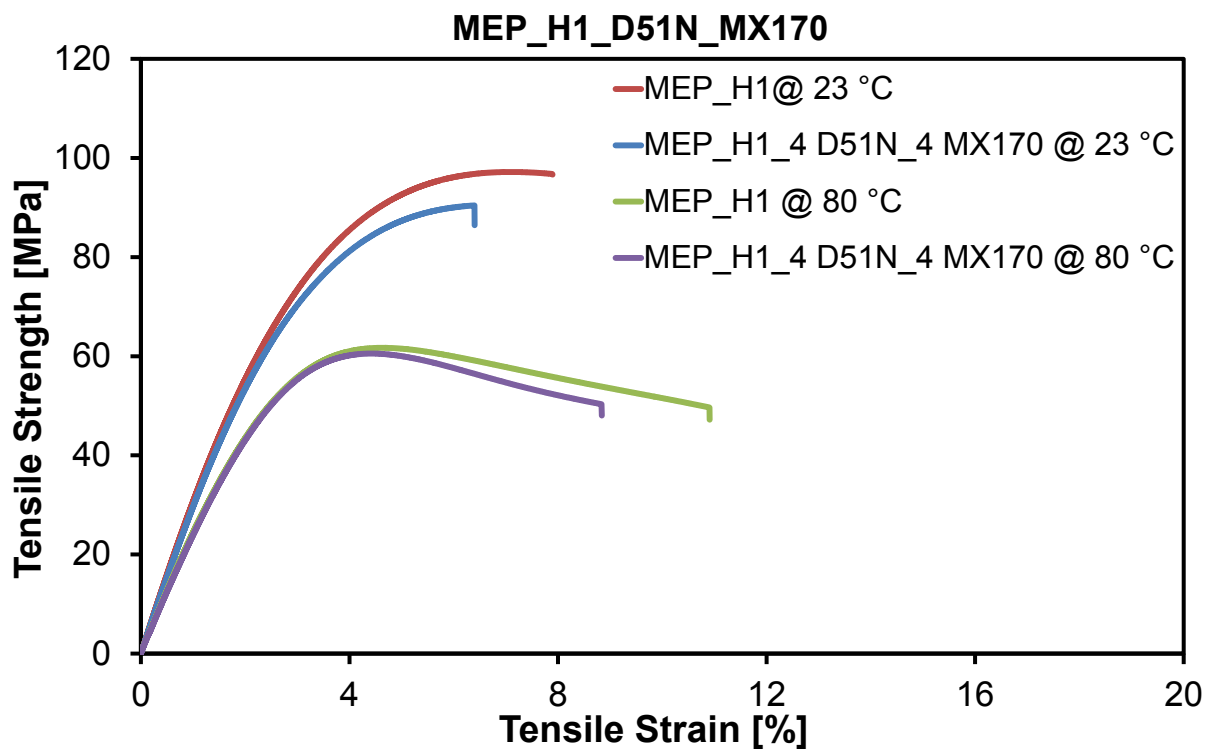


Figure 109: Graph showing tensile stress versus strain response of amine-cured unmodified epoxy and amine cured epoxy system modified with CSR and BCP particles at 23 °C and 80 °C.

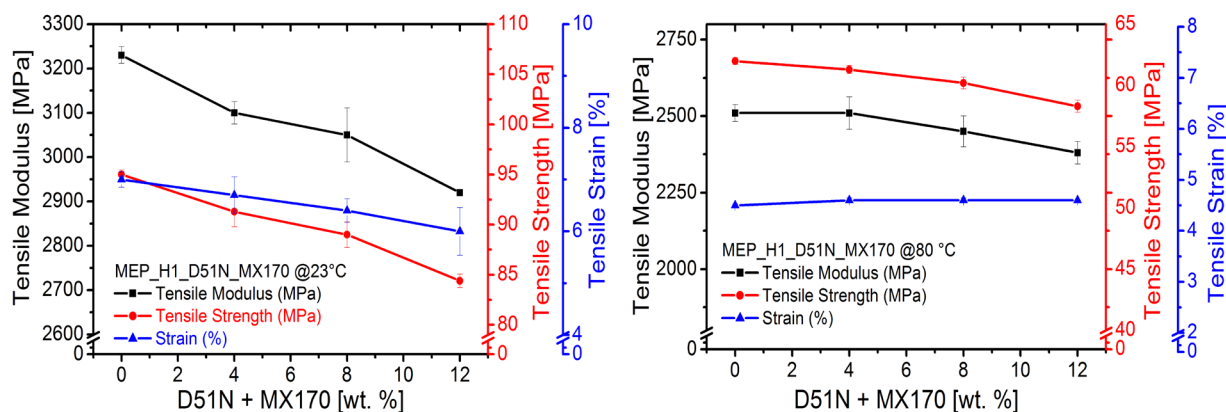


Figure 110: Graphs showing tensile stress versus strain response (left) and tensile properties (right) of the MEP_H1 system and MEP_H1 system modified with the D51N block copolymer, CSR particles at 23 °C and 80 °C.

6.7.4 Fracture properties

The fracture toughness, K_{IC} , and fracture energy, G_{IC} , values of the amine cured unmodified epoxy system and D51N, CSR particles modified epoxy systems were tabulated below.

Table 43: Fracture toughness, K_{IC} and fracture energy, G_{IC} , values of the amine cured unmodified epoxy system and D51N; CSR particles modified epoxy systems at 23 °C and at 80 °C.

D51N [wt. %]	MX170 [wt. %]	K_{IC} [MPa.m ^{1/2}] @23 °C	G_{IC} [kJ/m ²] @23 °C
0	0	0.73 (±0.08)	0.14 (±0.03)
2	2	1.01 (±0.01)	0.29 (±0.01)
4	4	1.15 (±0.03)	0.39 (±0.02)
6	6	1.31 (±0.05)	0.52 (±0.04)
D51N [wt. %]	MX170 [wt. %]	K_{IC} [MPa.m ^{1/2}] @80 °C	G_{IC} [kJ/m ²] @80 °C
0	0	0.80 (±0.10)	0.37 (±0.09)
2	2	1.39 (±0.02)	0.68 (±0.02)
4	4	1.47 (±0.06)	0.78 (±0.06)
6	6	1.53 (±0.07)	0.86 (±0.08)

By the addition of block copolymers and CSR particles, these properties were increased gradually to 1.01 MPa.m^{1/2} and 0.29 kJ/m² for 4 wt. % of the particles content at 23 °C. Later by the addition of 12 wt. %, the properties were increased significantly and reached till 1.31 MPa.m^{1/2} and 0.52 kJ/m². This was about 180 %

and 370 % increment in the toughness and energy values when compared to the unmodified epoxy system. It was also observed that the fracture toughness and energy values were increased linearly without any deterioration till higher concentrations.

Similarly at 80 °C by the addition of BCP's and CSR particles, the properties were increased gradually to 1.39 MPa.m^{1/2} and 0.68 kJ/m² for 4 wt. % of the particles content at 23 °C. Later by the addition of 12 wt. %, the properties were increased significantly and reached till 1.53 MPa.m^{1/2} and 0.86 kJ/m². This was about 180 % and 370 % increment in the toughness and energy values when compared to the unmodified epoxy system.

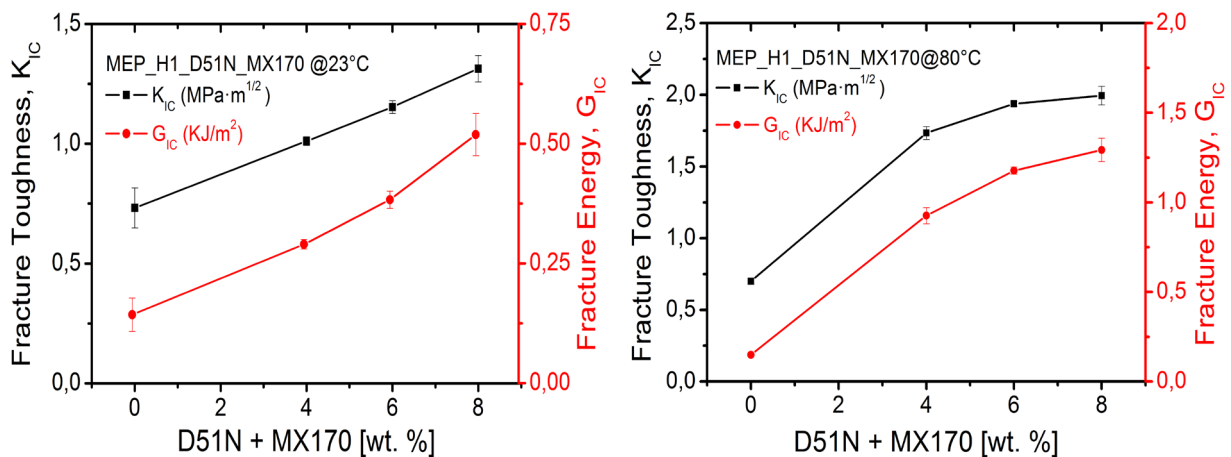


Figure 111: Graph showing fracture toughness, K_{IC} and fracture energy, G_{IC} , values of the amine cured unmodified epoxy system and D51N, CSR particles modified epoxy systems at 23 °C and at 80 °C.

6.7.5 Fractography studies

After the comprehensive fractography studies which were conducted on the fractured surfaces of the final cured composite specimens, certain toughening mechanisms were identified that were responsible for the increase in fracture toughness and they will be discussed in the following sections accordingly. The direction of the crack propagation for each image was from left to right. The fractured surface of the amine cured unmodified epoxy system seems to be smooth without any traces of plastic deformation. This was usually seen in all types of unmodified brittle epoxies due to the absence of any filler materials that promote plastic deformation and toughness. Shear yielding and rubber particles cavitation followed by void growth were observed to be a main toughening mechanism for the hybrid composites. Although the D51N particles can be hardly seen under the microscope, they were properly bonded to the

matrix material and have contributed enough to the increase of fracture toughness by considerable plastic deformation.

At 80 °C enhanced shear yielding and enhanced cavitation followed by void growth were the main toughening mechanisms. The fractured surface examined for 80 °C specimen shows enhanced void growth as compared to the 23 °C specimen. The enhanced void growth was responsible for the stress-whitening near the crack tip at 80 °C.

The high temperature tested composites show a typical fracture surface divided into two regions; the stress whitened and the fast-crack growth region. In the stress whitened region or plastic zone, ahead of the crack tip, the crack propagates slowly. It was characterized by a very rough fracture surface with numerous cavities and significant plastic deformation [186]. The cavities in this region were larger than those in the fast crack section and massive shear bands connecting the cavitated particles were also observed. The fast-crack growth region, located beyond the plastic zone, was characterized by rapid fracture propagation, smoother surface and some cavities of approximately same size as the undeformed rubber particles. Similar behavior was reported in a CTBN rubber-modified epoxy resin and was explained due to the rubber particles induce more localized plastic deformations around the crack tip increasing the size of the plastic zone leading to a somewhat rougher fracture surface [187]. Yee also suggested that the triaxial tension at the crack tip must be relieved before the crack propagates, so the deviatoric stress can reach a critical value for yielding to occur [188]. The plastic zone absorbs the major fracture energy and once that the critical force was reached the total fracture takes place.

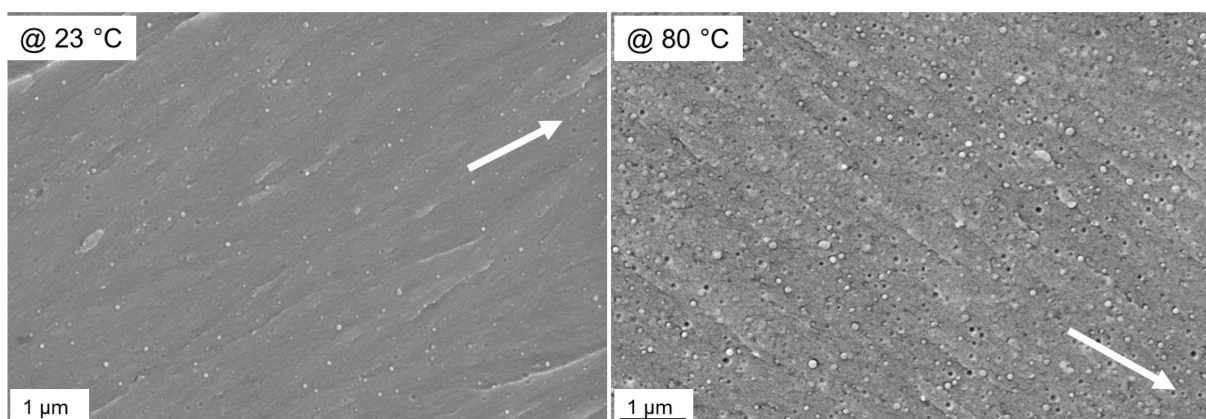


Figure 112: FEG-SEM micrograph of the amine cured (4 wt. % + 4 wt. %) of D51N and CSR particles respectively modified the epoxy system at 23 °C and 80 °C. The White arrow indicates the crack propagation direction.

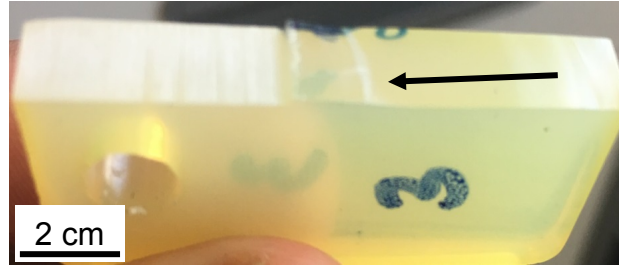


Figure 113: Fractured compact tension specimen of (6 + 6) wt. % of D51N and MX170 modified epoxy-amine system at 80 °C. Black arrow was pointing towards stress whitened region.

6.8 Anhydride cured epoxy hybrid composites modified with D51N BCP's and CSR particles

The epoxy was modified with D51N diblock copolymer which was commercially available called as 'Nanostrength D51N' supplied by Arkema, France, and CSR nanoparticles which were commercially available called as 'Kane Ace MX170' supplied by Kaneka Belgium NV. The D51N particle contains two blocks out of which one was a softer poly (butyl acrylate) also called as PbuA and the other was harder poly (Methyl methacrylate) also called as PMMA. The MX170 material supplied was in the form of a masterbatch which was a 25 wt. % concentrate of core-shell rubber toughening agent in unmodified liquid epoxy resin based on Bisphenol-A. The MEP_H2 was used as the epoxy system and anhydride-based hardener denoted as H2 was used for curing with appropriate curing cycle. The concentrations of 4 wt. %, 8 wt. % and 12 wt. % were considered for the manufacturing of final composites. In these, both D51N block copolymers and CSR particles contribute in equal percentages.

6.8.1 Rheology

The viscosity of the different epoxy systems as a function of temperature was shown in Figure 114. This was because the particles present in the system tends to offer a resistance to the resin flow owing to increase in the viscosity.

The viscosity of pure epoxy was 0.030 Pa.s at 40 °C and the addition of 12 wt. % of D51N block copolymers and CSR particles raised the viscosity to 0.370 Pa.s at the same temperature of 40 °C. The results obtained from the rheological tests were used to produce the graphs for showing the change in the viscosity with respect to temperature.

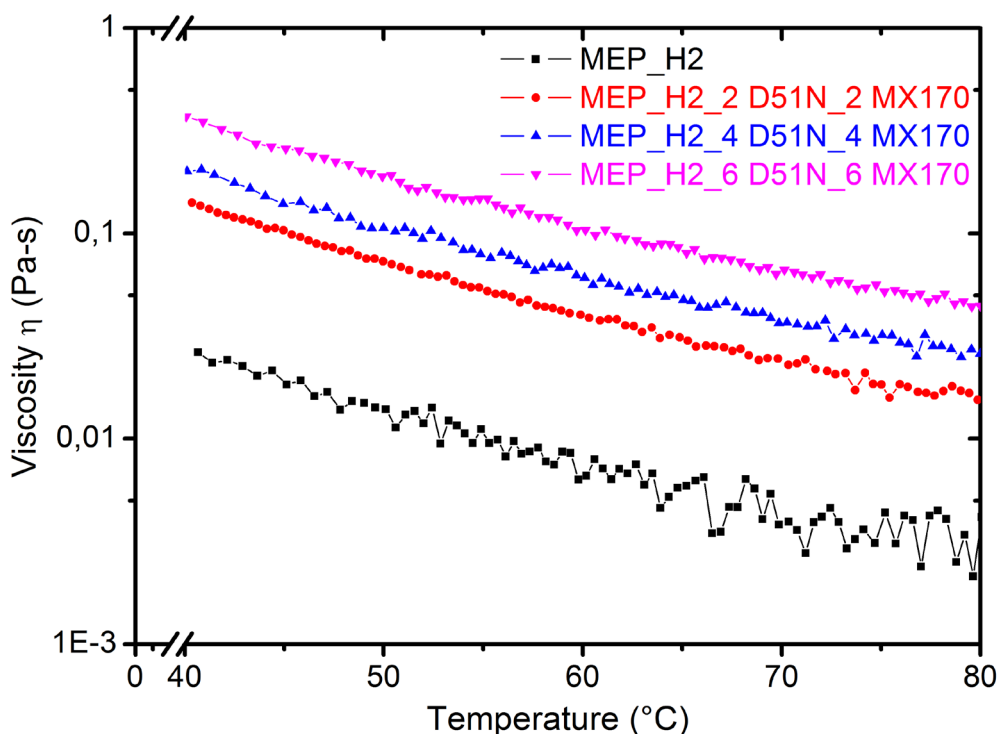


Figure 114: Graph showing variation of viscosity with respect to temperature for different anhydride based tailored epoxy systems modified with D51N BCP's and MX170 CSR particles.

6.8.2 Glass transition temperature and viscoelastic properties

The glass transition temperatures of anhydride cured unmodified and D51N block copolymer and CSR particles modified epoxy systems were measured with the help DSC and DMTA techniques. The results were tabulated as shown in Table 44. It was observed that for the unmodified epoxy system, the glass transition temperature was 144 °C and with the addition of D51N and CSR particles, no significant change was observed in the T_g values.

Table 44: Glass transition temperature, T_g of anhydride cured unmodified and D51N block copolymer, CSR particles modified epoxy systems.

D51N [wt. %] MX170 [wt. %]	T_g [°C] DSC	T_g [°C] DMTA [tan δ]
0	144	145
2 + 2 (4)	145	145
4 + 4 (8)	143	145
6 + 6 (12)	148	144

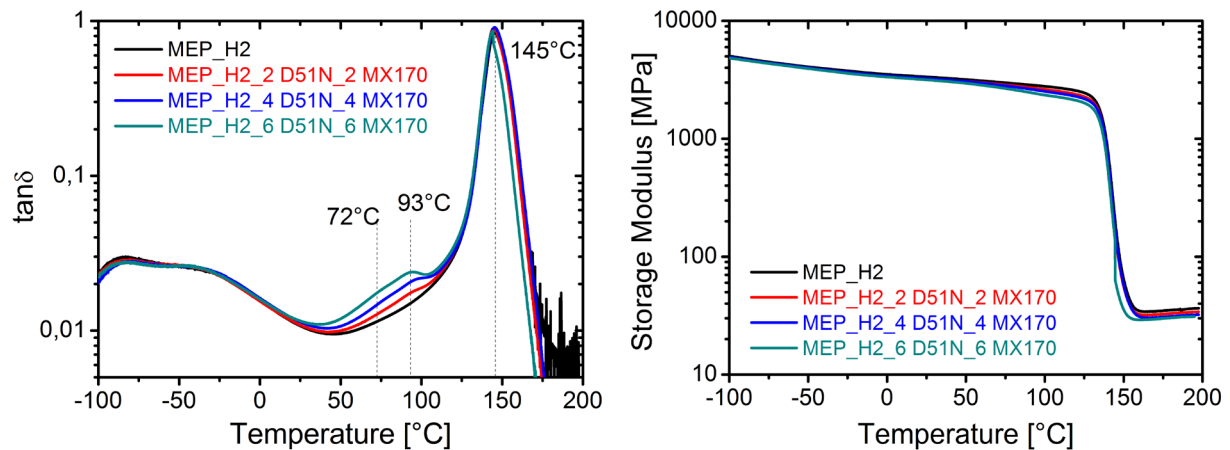


Figure 115: Graph showing storage modulus E' and damping $\tan \delta$, with respect to temperature, for the anhydride cured unmodified and D51N block copolymer, CSR particles modified the epoxy system.

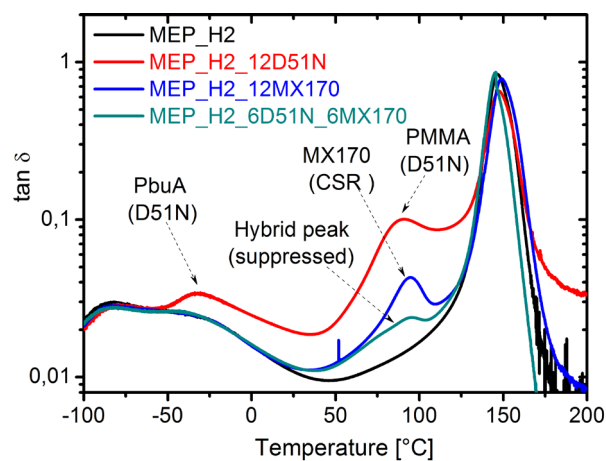


Figure 116: Graph showing $\tan \delta$ vs temperature curve for the anhydride cured unmodified and D51N BCP, MX170 CSR and hybrid particles modified systems.

For the DMTA graph, it was observed that the storage modulus E' for unmodified epoxy at the temperature 180 °C was approximately 35.09 MPa and for the D51N and CSR, particles modified epoxy with 12 wt. % of the particle content in the same temperature range was 30.25 MPa. This was about 14 % decrement when compared to the neat epoxy system which implies that the crosslink density was decreased and fracture toughness was increased. At around 93 °C, a peak was observed for all the concentrations which represent the glass transition temperature of the mixture of PMMA present in D51N and the rubber core present around the rubber particle. For hybrid nanocomposites, the stiff CSR particles suppress the macrophase separation of block copolymers (see Figure 116) providing lower and broader peaks of the $\tan \delta$ curve as compared to the epoxy / CSR and epoxy / BCP modified epoxies for the same composition alone. This phenomenon was providing better tensile properties

and lower fracture toughness and fracture energy as compared to the ones which were having a single phase of toughening agent for the same wt. %.

6.8.3 Tensile properties

The tensile properties such tensile strength σ_m , strain ϵ_m , and elastic modulus E_m were measured at 23 °C and 80 °C were tabulated as shown in Table 45. For the unmodified epoxy system, the modulus was 3580 MPa and tensile strength was 101 MPa. Later with the addition of block copolymers and CSR particles to the epoxy, the modulus and tensile strength were decreased with the increase in particle content which was true for 80 °C temperature testing as well where tensile modulus and tensile strength reduces to 2700 MPa and strength to 60 MPa from 2880 MPa and 68 MPa respectively.

Table 45: Tensile properties E_t , σ_m and ϵ_m of anhydride cured unmodified epoxy system and anhydride cured epoxy system modified with the D51N block copolymer, CSR particles measured at 23 °C and 80 °C.

D51N [wt. %]	MX170 [wt. %]	E_t [MPa] @ 23 °C	σ_m [MPa] @ 23 °C	ϵ_m [%] @ 23 °C
0	0	3580 (\pm 78.0)	101 (\pm 2.6)	5.8 (\pm 0.01)
2	2	3460 (\pm 14.2)	98.7 (\pm 0.3)	5.8 (\pm 0.01)
4	4	3440 (\pm 28.6)	95.1 (\pm 0.9)	5.6 (\pm 0.04)
6	6	3320 (\pm 62.3)	91.1 (\pm 0.9)	5.6 (\pm 0.01)
D51N [wt. %]	MX170 [wt. %]	E_t [MPa] @ 80 °C	σ_m [MPa] @ 80 °C	ϵ_m [%] @ 80 °C
0	0	2880 (\pm 18.0)	68.0 (\pm 2.6)	4.3 (\pm 0.05)
2	2	2850 (\pm 33.8)	67.0 (\pm 0.3)	4.4 (\pm 0.01)
4	4	2800 (\pm 11.5)	62.0 (\pm 0.9)	4.3 (\pm 0.03)
6	6	2700 (\pm 50.3)	60.0 (\pm 0.9)	4.2 (\pm 0.03)

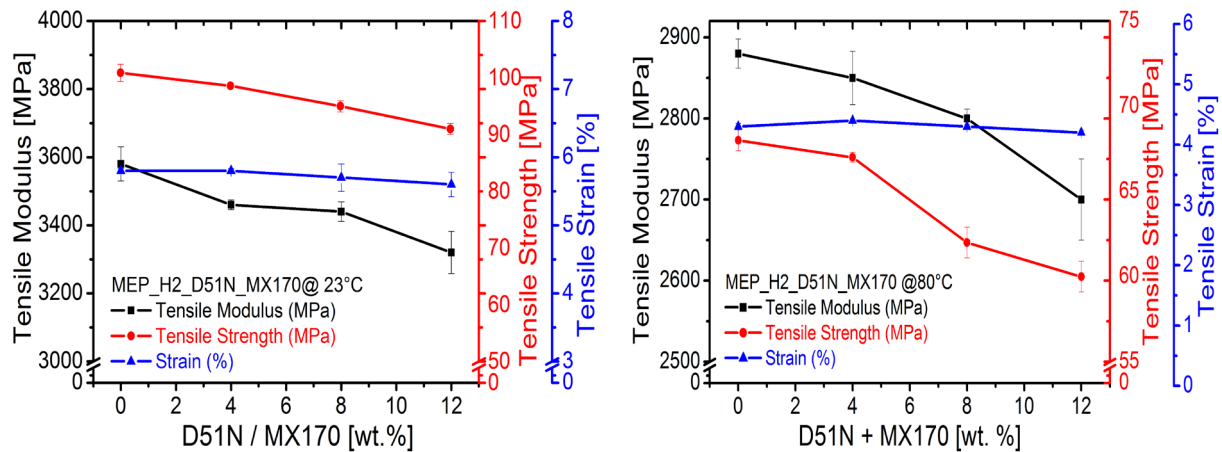


Figure 117: Graphs showing tensile properties (left) and tensile properties (right) of anhydride cured unmodified epoxy and anhydride cured epoxy system modified with the D51N block copolymer, CSR particles at 23 °C and at 80 °C.

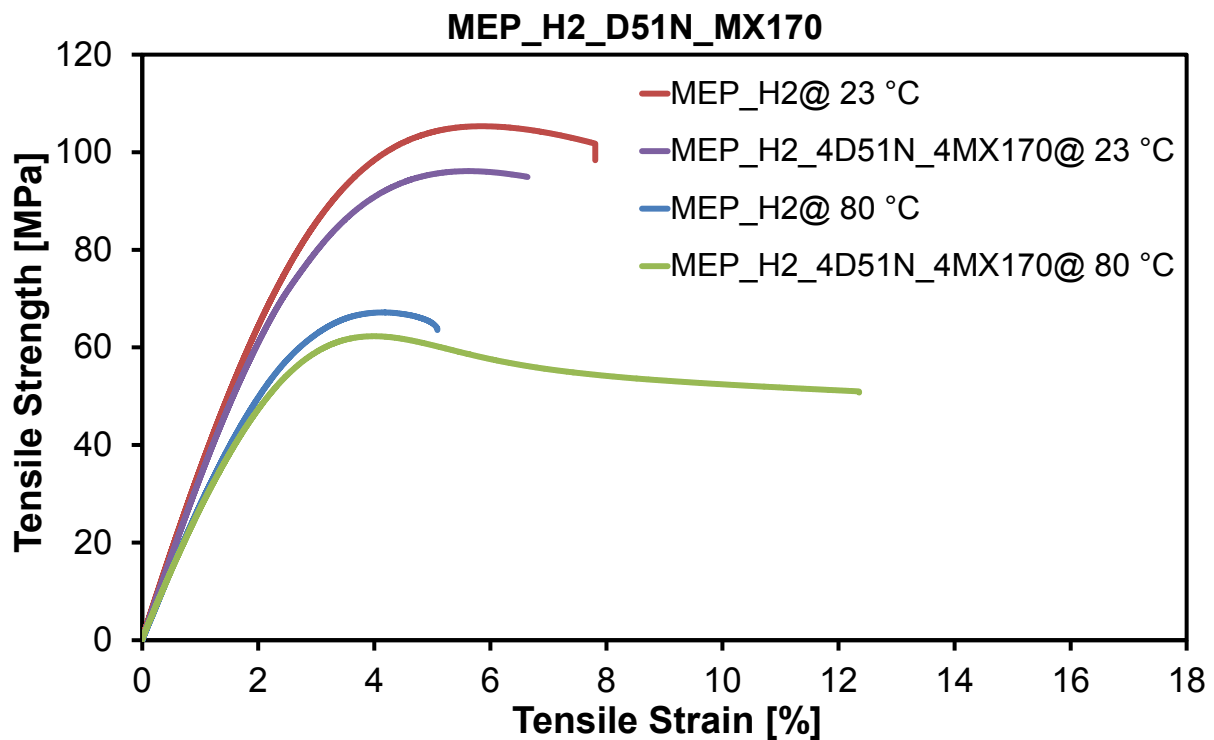


Figure 118: Graph showing tensile stress versus strain response of anhydride cured unmodified epoxy and anhydride cured epoxy system modified with CSR and BCP particles at 23 °C and at 80 °C.

6.8.4 Fracture properties

The fracture toughness, K_{IC} , and fracture energy, G_{IC} , values of the anhydride cured unmodified epoxy system and D51N, CSR particles modified epoxy systems were measured at 23 °C and 80 °C, tabulated in Table 46.

By the addition of block copolymers and CSR particles, the fracture toughness and fracture energy were increased to $1.27 \text{ MPa}\cdot\text{m}^{1/2}$ and 0.43 kJ/m^2 for 12 wt. % at 23

°C and to 1.99 MPa.m^{1/2} and 1.28 kJ/m² for 12 wt. % particles content at 80 °C. This was about 198 % and 430 % increment in the toughness and energy values when compared to the unmodified epoxy system at 23 °C. It was also observed that the fracture toughness and energy values were increased linearly without any deterioration till higher concentrations at both the testing temperatures.

Table 46: Fracture toughness, K_{IC} , and fracture energy, G_{IC} , values of the anhydride cured unmodified epoxy system and D51N, CSR particles modified epoxy systems in mode-I loading at 23 °C and at 80 °C.

D51N [wt. %]	MX170 [wt. %]	K_{IC} [MPa.m ^{1/2}] @ 23 °C	G_{IC} [kJ/m ²] @ 23 °C
0	0	0.64 (±0.14)	0.10 (±0.05)
2	2	0.87 (±0.03)	0.19 (±0.02)
4	4	1.10 (±0.03)	0.31 (±0.02)
6	6	1.27 (±0.05)	0.43 (±0.03)
D51N [wt. %]	MX170 [wt. %]	K_{IC} [MPa.m ^{1/2}] @ 80 °C	G_{IC} [kJ/m ²] @ 80 °C
0	0	0.70 (±0.02)	0.15 (±0.01)
2	2	1.73 (±0.11)	0.92 (±0.11)
4	4	1.94 (±0.04)	1.18 (±0.04)
6	6	1.99 (±0.10)	1.28 (±0.13)

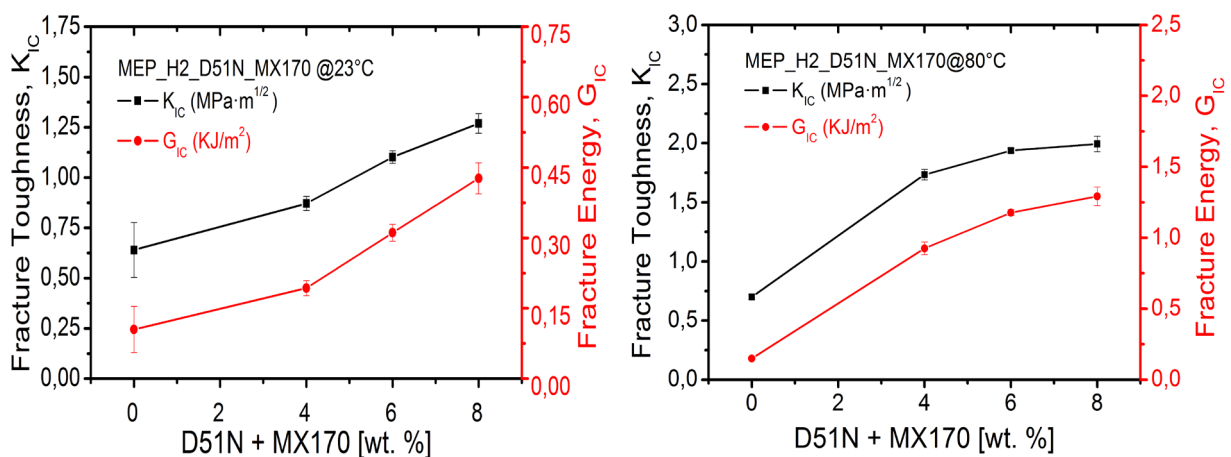


Figure 119: Graph showing fracture toughness, K_{IC} and fracture energy, G_{IC} , values of the anhydride cured unmodified epoxy system and D51N, CSR particles modified epoxy systems at 23 °C and at 80 °C.

6.8.5 Fractography studies

After the comprehensive fractography studies which were conducted on the fractured surfaces of the final cured composite specimens, certain toughening mechanisms identified which were responsible for the increase in fracture toughness and they will be discussed in the following sections accordingly. The SEM picture of the fractured surface of the anhydride cured unmodified epoxy system as shown in Figure 101, seems to be smooth without any traces of plastic deformation. This was usually seen in all types of unmodified brittle epoxies due to the absence of any filler materials that promote plastic deformation and toughness. Cavitation of the BCP particles and subsequent plastic void growth for epoxies, process absorbs energy, hence increasing the toughness. For 2 wt. % to 6 wt. % cavities with spherical inclusions on the fracture surface were observed as the main mechanism for the resulting fracture toughness besides crack pinning which has fractional influence for the improvement of fracture toughness. Cavitation and debonding, particle inclusions, matrix tearing, and crack deflection were also observed for the anhydride cured hybrid composites at 23 °C.

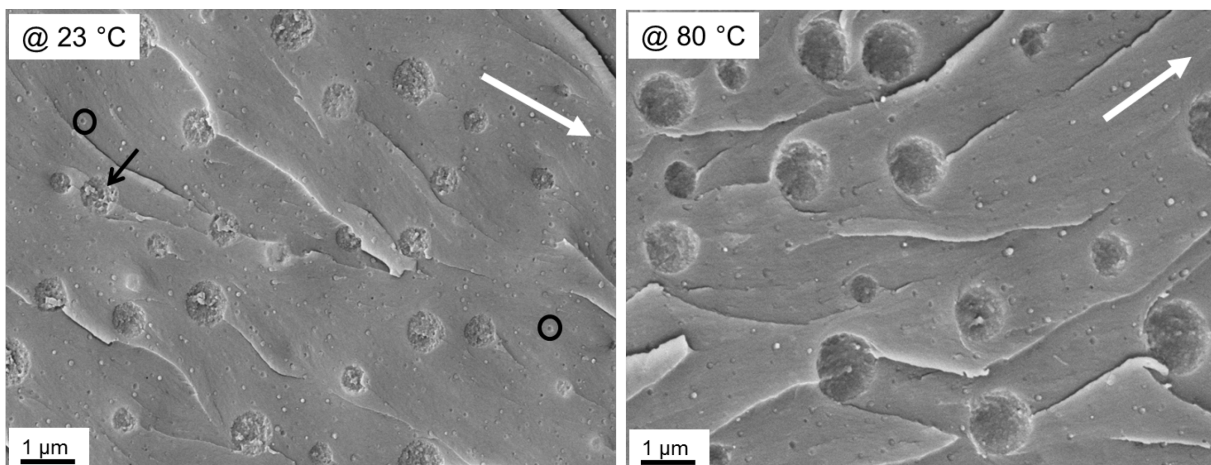


Figure 120: FEG-SEM micrograph of the anhydride cured (6wt. % + 6wt. %) of D51N, CSR particles modified the epoxy-anhydride system at 23 °C (left) and 80 °C (right). Circles indicate debonding of rubber particles and black arrows indicate particle inclusions and cavitation of block copolymer particles. White arrows were representing the crack propagation direction.

At 80 °C enhanced shear yielding and enhanced cavitation followed by void growth were the main toughening mechanisms which can be seen clearly in Figure 120 (right). The fractured surface examined for 80 °C specimen shows enhanced void growth as compared to the 23 °C specimen. The enhanced void growth was responsible for the stress-whitening near the crack tip at 80 °C.

The high temperature tested composites show a typical fracture surface divided into two regions; the stress whitened and the fast-crack growth region. In the stress whitened region or plastic zone, ahead of the crack tip, the crack propagates slowly. It was characterized by a very rough fracture surface with numerous cavities and significant plastic deformation [186]. The cavities in this region were larger than those in the fast crack section and massive shear bands connecting the cavitated particles were also observed. The fast-crack growth region, located beyond the plastic zone, was characterized by rapid fracture propagation, smoother surface and some cavities of approximately same size as the undeformed rubber particles. Similar behavior was reported in a CTBN rubber-modified epoxy resin and was explained due to the rubber particles induce more localized plastic deformations around the crack tip increasing the size of the plastic zone leading to a somewhat rougher fracture surface [187]. Yee also suggested that the triaxial tension at the crack tip must be relieved before the crack propagates, so the deviatoric stress can reach a critical value for yielding to occur [188]. The plastic zone absorbs the major fracture energy and once that the critical force was reached the total fracture takes place.

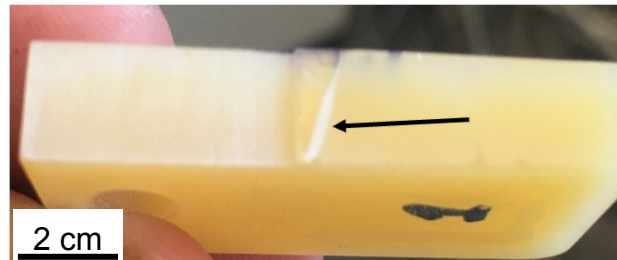


Figure 121 Fractured compact tension specimen of (6+6) wt. % of D51N andMX170 modified epoxy/ anhydride system at 80 °C. Black arrow was pointing towards stress whitened region

6.9 Amine cured epoxy hybrid composites modified with D51N BCP's and TiO₂ nanoparticles

TiO₂ nanoparticles were added to the D51N BCP modified epoxies to create hybrid toughened epoxies, consisting of soft and rigid phases. Many researchers have reported an increase in the fracture toughness of epoxies to next level than that obtained using a single toughening agent [13] [171] [195] [196]. In the previous study with block copolymers, by increasing the BCP content the tensile properties tend to decrease and to combat this, one of the possible way was to introduce the rigid fillers along with BCP, without disturbing other properties and also to further increase the fracture toughness with the help of hybrid toughening. The aim of this chapter was to examine whether we can compensate the decrease in modulus and strength by adding rigid nanofillers into the system or not.

The bisphenol-F based EP862 was used as the epoxy resin, D51N BCP as soft toughening phase, aeroxide TiO₂ P25 [167] was used as rigid fillers and amine hardener H1 was selected as curing agent for hybrid toughening

The mechanical, fracture and visco-elastic properties of these hybrid modified epoxies will be studied. The toughening mechanisms of the hybrid modified epoxies containing block copolymers and TiO₂ nanoparticles were identified.

6.9.1 Rheology

The viscosity change of the different epoxy systems as a function of temperature is shown in Figure 122.

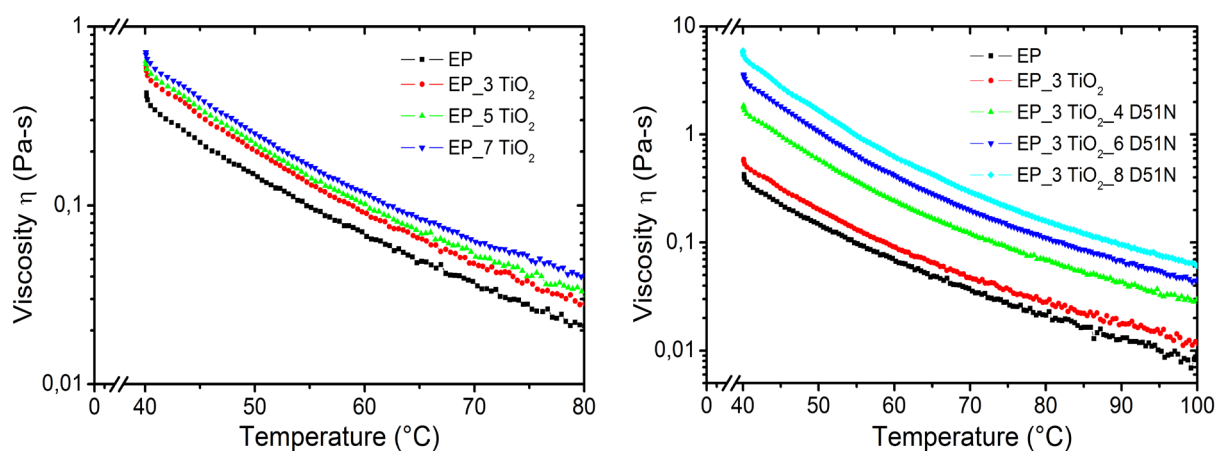


Figure 122: Graphs showing a change in viscosity as a function of temperature for TiO₂ (left) and hybrid TiO₂ & D51N (right) modified amine cured epoxy resins.

6.9.2 Glass transition temperature and viscoelastic properties

The T_g values obtained from DSC and DMTA measurements were summarized in Table 47. The addition of TiO_2 causes a gradual increase or remained same in the range of the epoxy T_g , from 136 °C of the neat epoxy, up to 140 °C of the epoxy-containing 7 wt. % TiO_2 . This increment may be explained by the adsorption of polymer onto the particle surface, which reduces the polymer net mobility and modifies the conformation of chain segments.

Table 47: Glass transition temperature, T_g , of the unmodified amine cured epoxy and the TiO_2 and Hybrid TiO_2 +D51N BCP modified amine cured epoxies.

Content of modifiers	T_g [°C] DSC	T_g [°C] DMTA
unmodified	136	132
3 wt. % TiO_2	139	138
5 wt. % TiO_2	139	n/a
7 wt. % TiO_2	140	n/a
4 wt. % D51N+ 3 wt. % TiO_2	137	138
6 wt. % D51N+ 3 wt. % TiO_2	137	138
8 wt. % D51N+ 3 wt. % TiO_2	137	138

Dynamic mechanical thermal analysis (DMTA) results show a shift of the peak in mechanical damping ($\tan \delta$) towards higher temperatures, e.g. from 136 °C (epoxy) to ~ 138 °C in the case of EP/ TiO_2 (7 wt. %), Figure 123. The damping of the epoxy resin records no important change in the glassy stage (-120 °C to 50 °C) due to the addition of nanofillers. It indicates that storage modulus increases almost in the same proportion, along with this temperature range irrespective of a shift in the β -transition to the right side in case of particle filled resins. Small shoulders were observed next to the main α relaxation of the epoxies on the $\tan \delta$ curves of the D51N modified epoxies, and a similar shoulder was not observed in the $\tan \delta$ curve of the unmodified epoxy. These shoulders represent the micro-phase separation of the PMMA block occurred in the D51N+ TiO_2 modified epoxy during the polymerization process because the α relaxation of PMMA has been reported to be in the same temperature range (~ 100 °C) as the small shoulders.

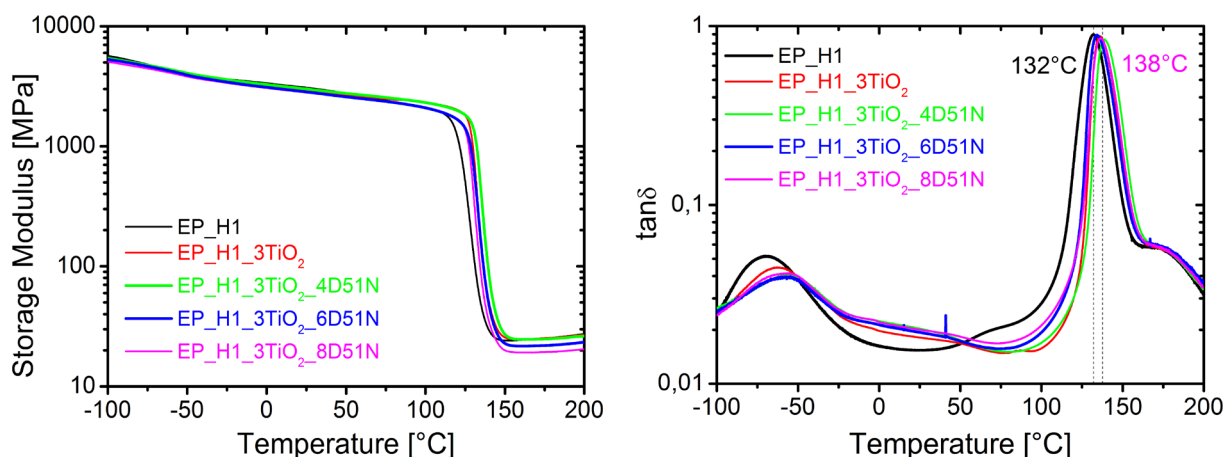


Figure 123: Graphs showing storage modulus E' , and damping $\tan \delta$, with respect to temperature, for the unmodified amine cured epoxy and amine cured epoxies modified with TiO_2 and Hybrid D51N+ TiO_2 composites.

The nanoparticles induce a higher stiffness on the epoxy resin, and by the other hand, they induce new mechanisms of energy dissipation, as filler/filler and filler/matrix friction, which was suggested as the main reason for damping in composites systems [143]. In the temperature zone (50 °C to 140 °C), damping of the neat epoxy was higher than the damping of nanocomposites. In this stage, the macromolecules start to move. The particles hinder the movement of the polymer chains resulting in lower energy dissipation. And it was vice versa in the rubbery state (140 °C to 200 °C), due to the reinforcement effect of nanoparticles on the matrix.

6.9.3 Tensile properties

Figure 125 shows the tensile properties of the TiO_2 and hybrid D51N+ TiO_2 modified amine cured epoxies. The tensile modulus of the epoxy matrix was increased linearly by the addition of TiO_2 . It was important to see an increment on the modulus even at low particle content. The elastic modulus of the pure epoxy resin was found to be 2950 MPa, while the modified epoxy containing 7 wt. % TiO_2 reaches a modulus 8 % higher, up to 3210 MPa. Strength and strain increased up to the addition of 7 wt. % TiO_2 . Even in the hybrid epoxies containing varying % of D51N with constant 3 wt. % TiO_2 , modulus, and strength tend to decrease with the increase of D51N BCP particle concentration.

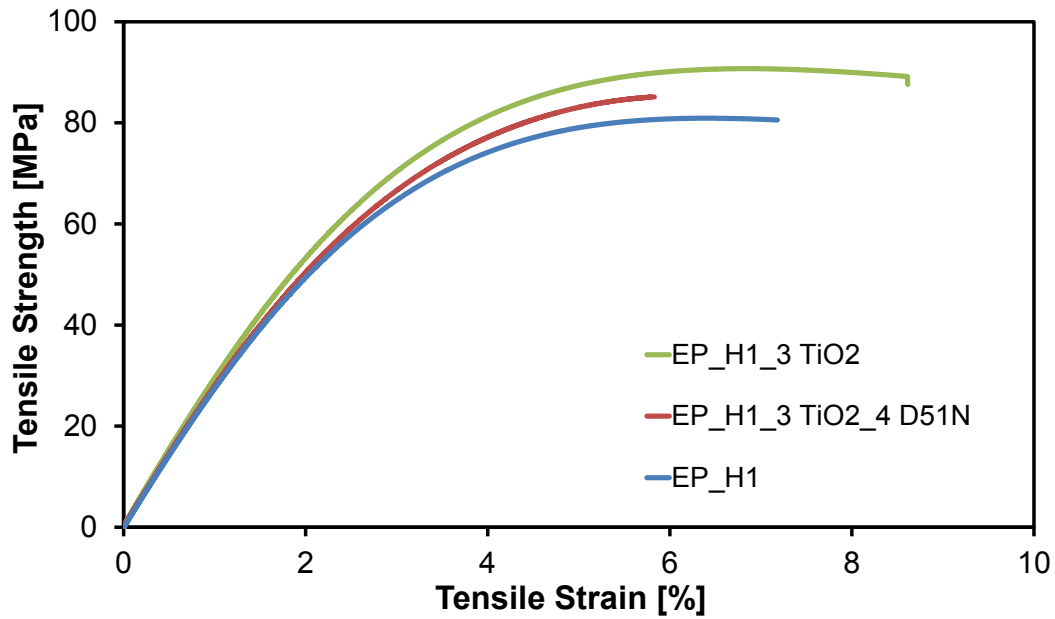


Figure 124: Graph showing representative tensile stress versus strain response of amine-cured unmodified reference epoxy, 3 wt. % TiO_2 modified EP_H1 system and (3 wt. % TiO_2 + 4 wt. % of D51N) modified EP_H1 system at 23 °C.

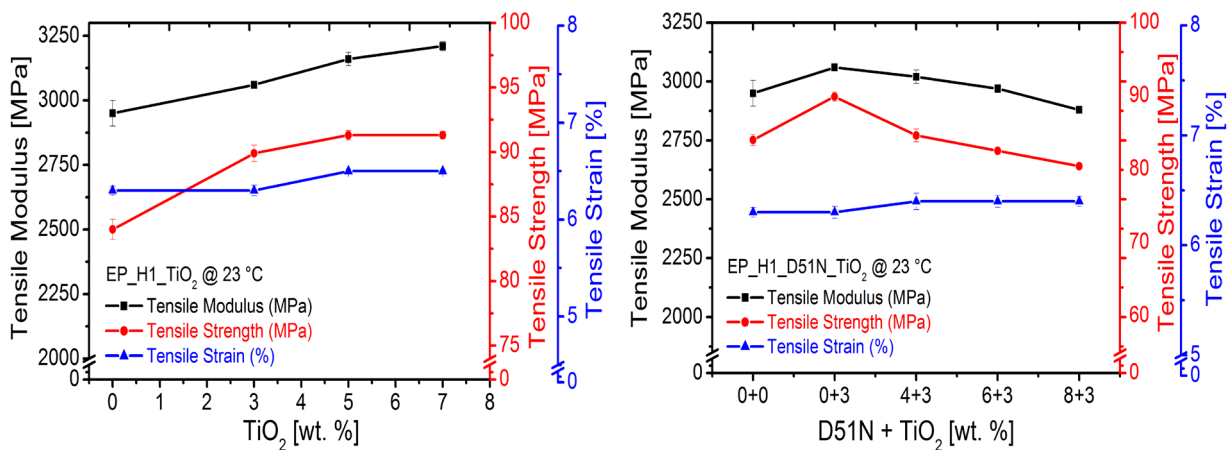


Figure 125: Tensile properties of TiO_2 (left) and D51N+ TiO_2 (right) modified amine cured epoxies at 23 °C.

The increment in strength and modulus was attributed to the fact that the TiO_2 has a much higher strength and modulus than the epoxy matrix and also to the good bonding between filler and epoxy, which permits the right stress distribution into both composite phases. The reduction of strength at high filler content was due to the presence of agglomerates which were found in the investigation of the fracture surface. The agglomerates tend to reduce the strength by increasing the stress concentration in the matrix, which led to the failure of the composite when stress was applied.

6.9.4 Fracture properties

Fracture toughness of nano-modified epoxy resins increases with particle content, Figure 126. The addition of 3 wt. % TiO_2 results in an approximately 153 % enhanced K_{IC} up to $0.89 \text{ MPa}\cdot\text{m}^{1/2}$. While the nanocomposite with 7 wt. % TiO_2 shows a $K_{IC} = 1.10 \text{ MPa}\cdot\text{m}^{1/2}$, almost two-fold higher than for unmodified epoxy ($K_{IC} = 0.57 \text{ MPa}\cdot\text{m}^{1/2}$). The TiO_2 nanoparticle induces a superior toughness at low concentrations in the epoxy matrices. The hybrid epoxy resins containing 3 wt. % TiO_2 and 4 wt. % D51N records fracture toughness around 143 % higher than the analog nanocomposites. Hence, the epoxy-containing 3 wt. % TiO_2 and 8 wt. % D51N reach fracture toughness up to $1.72 \text{ MPa}\cdot\text{m}^{1/2}$ that means three times higher than unmodified epoxy fracture toughness.

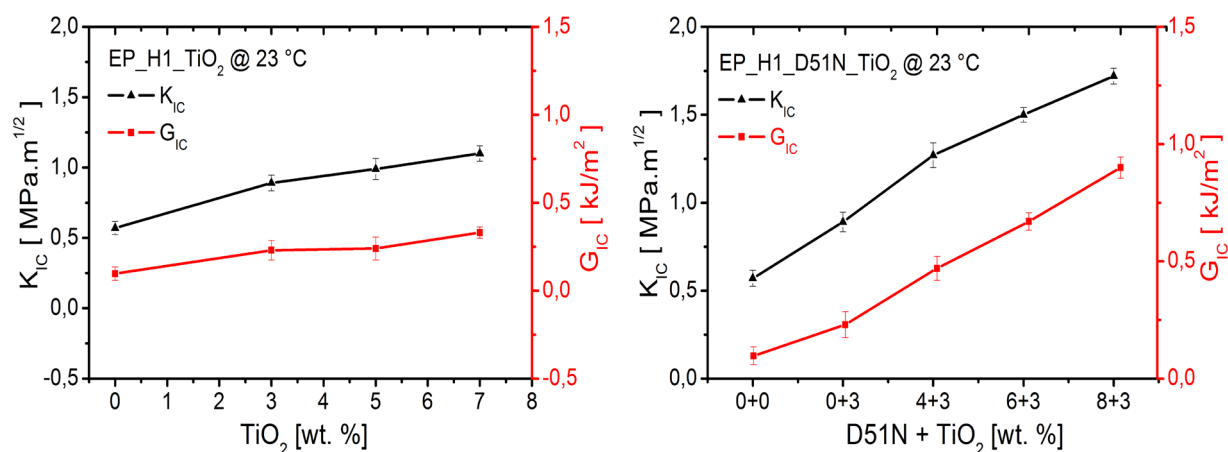


Figure 126: Graphs showing fracture toughness and fracture energy of TiO_2 & D51N+ TiO_2 modified amine cured epoxies at 23 °C.

The fracture energy of the studied epoxies varies with same tendency but a higher proportion than the fracture toughness, Figure 126. The fracture energy of the neat epoxy ($G_{IC} = 0.1 \text{ kJ}/\text{m}^2$) was enhanced up to $0.33 \text{ kJ}/\text{m}^2$ due to the addition of 7 wt. % TiO_2 , that means an increment around 300 % compared to unmodified epoxy. Hybrid compounds containing 3 wt. % TiO_2 and 8 wt. % D51N may register fracture energies more than 4 fold higher than the fracture energies of the nanocomposites.

6.9.5 Fractography studies

Visual analysis of the fracture surface of TiO_2 modified epoxy resin with the help of SEM can give an insight on the cause and location of failure as well as the dispersion state of the particles within the epoxy matrix. The fracture surface of the neat epoxy resin was brittle and with a smooth surface. Figure 127 (left) shows a close-up of the

crack surface in a nanocomposite containing 7 wt. % of TiO₂ nanoparticles, some nano, and micro reinforcing mechanisms can be observed with more detail. Some of these mechanisms include particle pullout, particle crack pinning [6] [154] [197] indicated by the small tails behind the particles, these ridges were caused by the reconcile of the crack front after passing the obstacle created by the particles, and crack deflection due to the nanometer scale agglomerates. Particle pull-out and plastic void growth around individual nanoparticles were not expected to be major reinforcing mechanisms due to the good quality of the particle-matrix bonding in these composites.

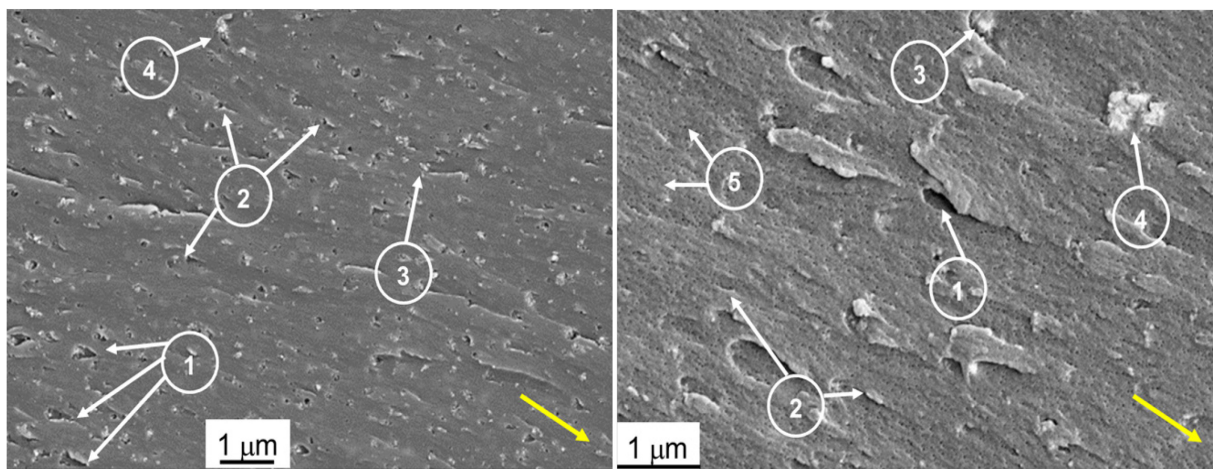


Figure 127: FEG-SEM micrograph of the fracture surface showing with homogeneous dispersion of epoxy modified with 7 wt. % TiO₂ (top), 4 wt. % D51N+ 3 wt. % TiO₂ taken near the tip of the crack. Some of the mechanisms involved were (1) particle pull out, (2) Crack pinning, (3) Crack deflection, (4) Agglomerates, (5) Cavities/debonding. Yellow arrows were showing crack propagation direction.

TiO₂-nanoparticles occur to be well bonded to the matrix, and they induce a crack pinning effect. The fracture surfaces and fracture toughness of the hybrid D51N/titanium dioxide nanoparticle modified epoxies were almost the same as the epoxies modified with D51N alone. It can be concluded that the addition of the titanium dioxide nanoparticles has little effect on the toughening mechanisms it was due to the lower volume % of TiO₂ particles. The presence of agglomerates was more obvious in the D51N/TiO₂ hybrid composites, and again these agglomerates were the cause of crack deflection and matrix plastic deformation. The toughening mechanisms in hybrid modified epoxies were dominated by D51N, they were cavitation of the D51N, Figure 127 (right), spherical micelles and the enhanced plastic deformation of the epoxy matrix due to the localized plasticization of the epoxy/PMMA interface.

6.10 Effect of morphology on different mechanical properties

The normalized fracture energies of the BCP modified epoxies for the different epoxy systems were shown in Figure 128, D51N BCP modified epoxies and MX170 CSR modified MEP_H1 and MEP_H2 systems. The fracture energies increased with D51N BCP content, but at different rates for different hardener systems.

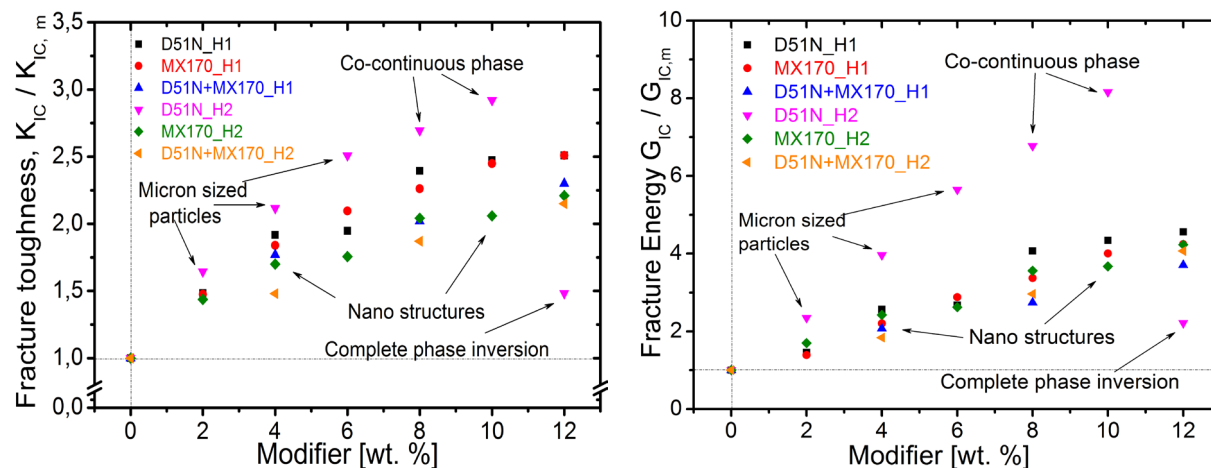


Figure 128: Comparison of normalized fracture toughness vs. modifier wt. % (left) and fracture energy vs. modifier wt. % (right) for the different toughened systems.

The fracture energies of the BCP modified epoxies were strongly dependent on the morphology. The change to a co-continuous phase structure results in the largest increase in fracture performance, as seen for the MEP_H2_D51N system. This was because the interconnected nature of the BCP and epoxy phases in such co-continuous structures gives a good balance between strength and deformation. The low strength and high ductility of the BCP phase were stabilized by the stronger, more brittle epoxy phase. This was contrasted by complete phase inversion, where the fracture performance decreases dramatically with increasing BCP content, such as that observed for the 12 wt. % MEP_H2_D51N, as shown in Figure 128. Here, the low strength of the D51N BCP phase dominates the failure process and leads to failure at a much lower stress and hence, low toughness.

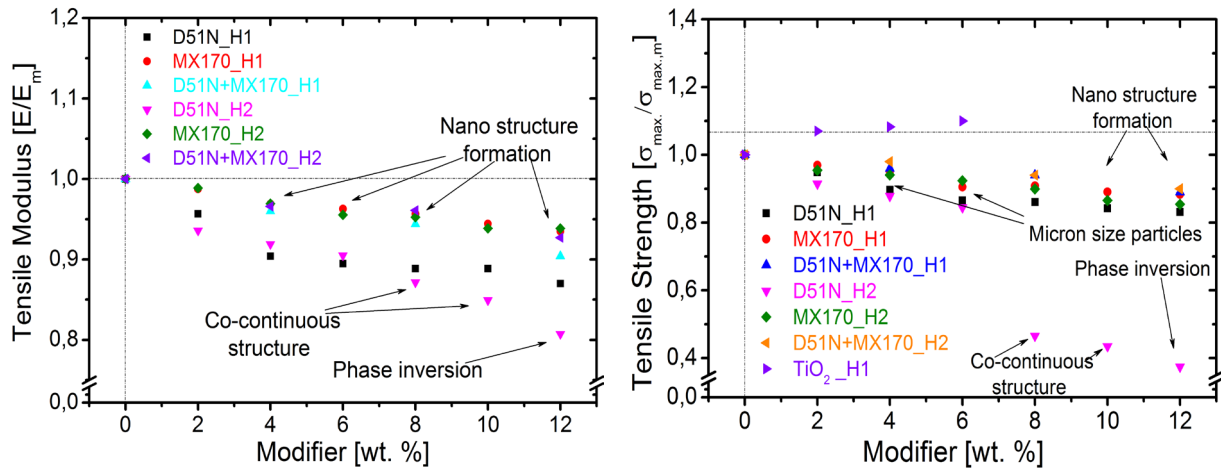


Figure 129: Comparison of normalized tensile modulus vs. modifier wt. % (left) and normalized tensile strength vs. modifier wt. % (right) for all different toughened systems.

The morphology, mechanical and fracture performance of BCP and CSR particles modified epoxies were reviewed and discussed. It was found that while the BCP phase separates into well dispersed spherical particles for anhydride hardner based epoxy systems. The BCP modified epoxies show well dispersed spherical particles, co-continuous microstructures, partial and complete phase inverted structures within the epoxy/anhydride system. The addition of CSR particles was also found to affect the morphology, through changing the interactions between particles, phase separation behavior and reactivity. The result of the change in microstructures gives lower fracture toughness value with increased strength and modulus values due to stiff CSR particles. The addition of TiO_2 nanoparticles can compensate the decrease in modulus and strength caused by BCP's in reference epoxy-amine systems while no synergistic effects were found, due to the lower volume percentage of TiO_2 being used for the composites manufactured.

6.11 Toughening mechanisms for all the systems

Table 48: Toughening mechanisms observed for different systems at 23 °C.

Epoxy system	Toughening agent	Morphology	Toughening Mechanism
Amine cured modified system	D51N (BCP)	Evenly dispersed block copolymer (nano-structuration)	Shear yielding and cavitation of nano-scale spherical micelles followed by void growth
	MX170 (CSR)	Evenly dispersed CSR particles of 100nm-150nm diameter	Shear yielding initiated by rubber particles, debonding and cavitation of the rubber particles followed by void growth.
	D51N + MX170 (BCP + CSR)	Evenly dispersed block copolymer and CSR particles of 100nm diameter	Combination of above two mechanisms
Amine cured reference system	D51N + TiO ₂ (BCP)	Evenly dispersed block copolymer and TiO ₂ nanoparticles	<ol style="list-style-type: none"> 1. Shear yielding and cavitation of nano-scale spherical micelles followed by void growth 2. Debonding, crack deflection and crack pinning of TiO₂ nanoparticles

Epoxy system	Toughening agent	Morphology	Toughening Mechanism
Anhydride cured modified system		Dispersed micron-sized block copolymer particles	Shear yielding and cavitation of particles followed by void growth.
	D51N (BCP)	Co-continuous microstructure	Shear yielding and cavitation of particles in epoxy rich zone followed by void growth.
		Complete phase inverted microstructure	Difficult to understand from SEM fractography hence no understanding.
	MX170 (CSR)	Evenly dispersed CSR particles of 100nm-150nm diameter	Shear yielding initiated by rubber particles, debonding and cavitation of the rubber particles followed by void growth.
	D51N + MX170 (BCP + CSR)	Evenly dispersed micron-sized block copolymer and CSR particles of 100nm diameter	Shear yielding and cavitation of particles followed by void growth initiated by both type of particles.

6.12 Map of reinforcing effect

The enhancement in mechanical and fracture mechanical properties by the block copolymers and core-shell rubber particles can be represented in a fracture energy ($G_c/G_{IC,m}$) vs tensile strength ($\sigma_{max.}/\sigma_{max.,m}$) chart. All measured values were shown with respect to the reference value of the respective system i.e. amine and anhydride. Figure 130 and Figure 131 shows a comparison of different systems for amine-based systems at 23 °C and at 80 °C respectively.

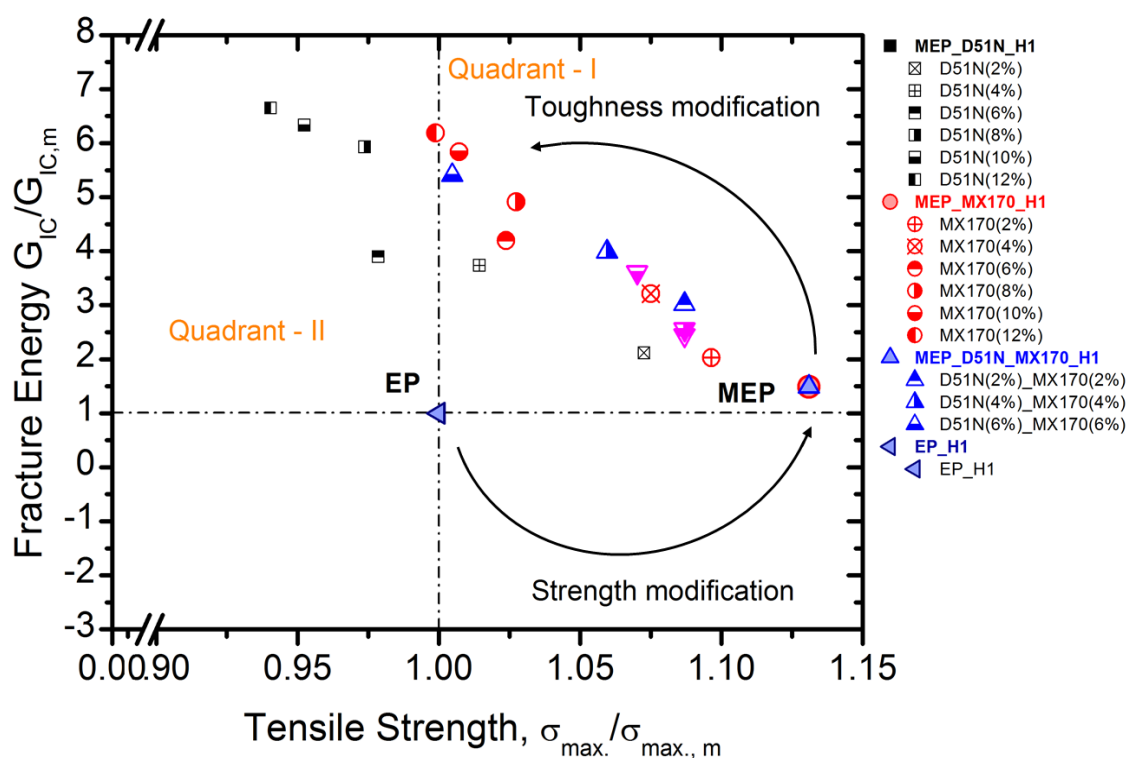


Figure 130: Graph showing the relation between normalized fracture energy and normalized tensile strength for modified amine-based systems at 23 °C.

Similarly, Figure 132 and Figure 133 shows a comparison of different systems for anhydride based systems at 23 °C and at 80 °C respectively. The large data set enables users to select a particular system according to the properties required for a certain application.

By analyzing all the normalized graphs it can be concluded that most of the data points fall in quadrant I or in quadrant II, which reveals that all the modified systems have superior tensile strength and fracture energy as compared to the reference system which was shown as EP (in quadrant I) and higher fracture energy and ~ 10

% less tensile strength for systems containing higher wt. % of D51N and MX170 (quadrant II) at both the temperatures i.e. at 23 °C and at 80 °C.

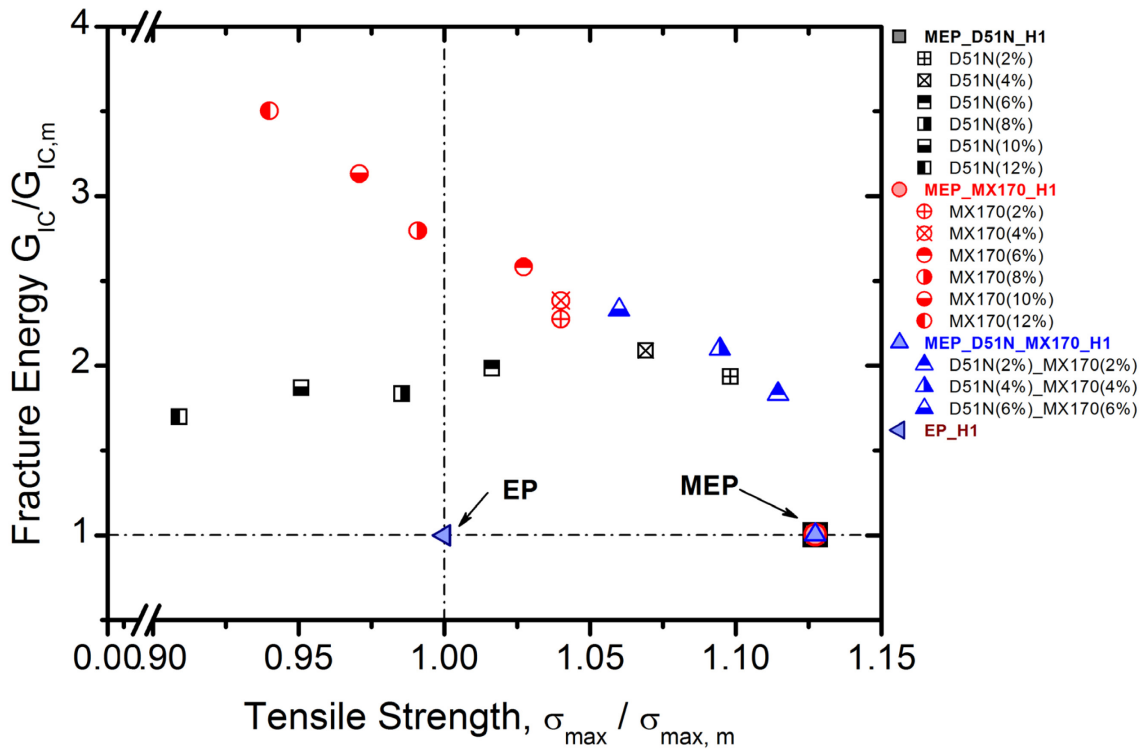


Figure 131: Graph showing the relation between normalized fracture energy and normalized tensile strength for modified amine-based systems at 80 °C.

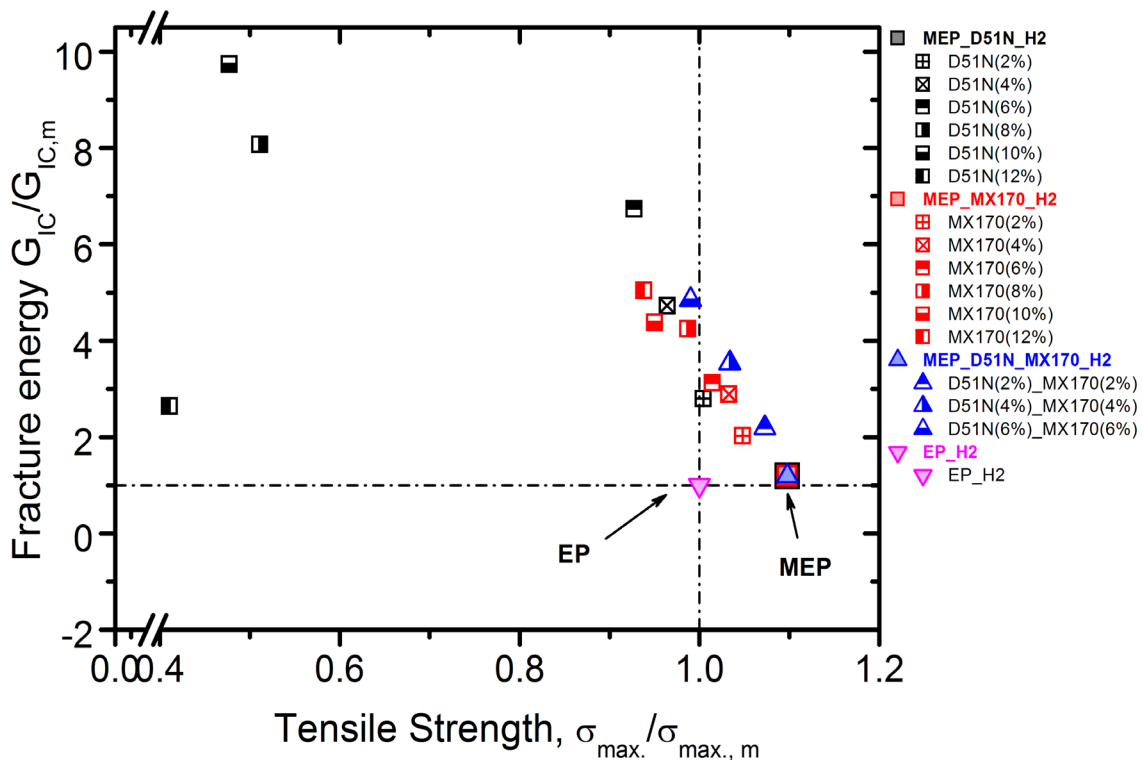


Figure 132: Graph showing the relation between normalized fracture energy and normalized tensile strength for modified anhydride-based systems at 23 °C.

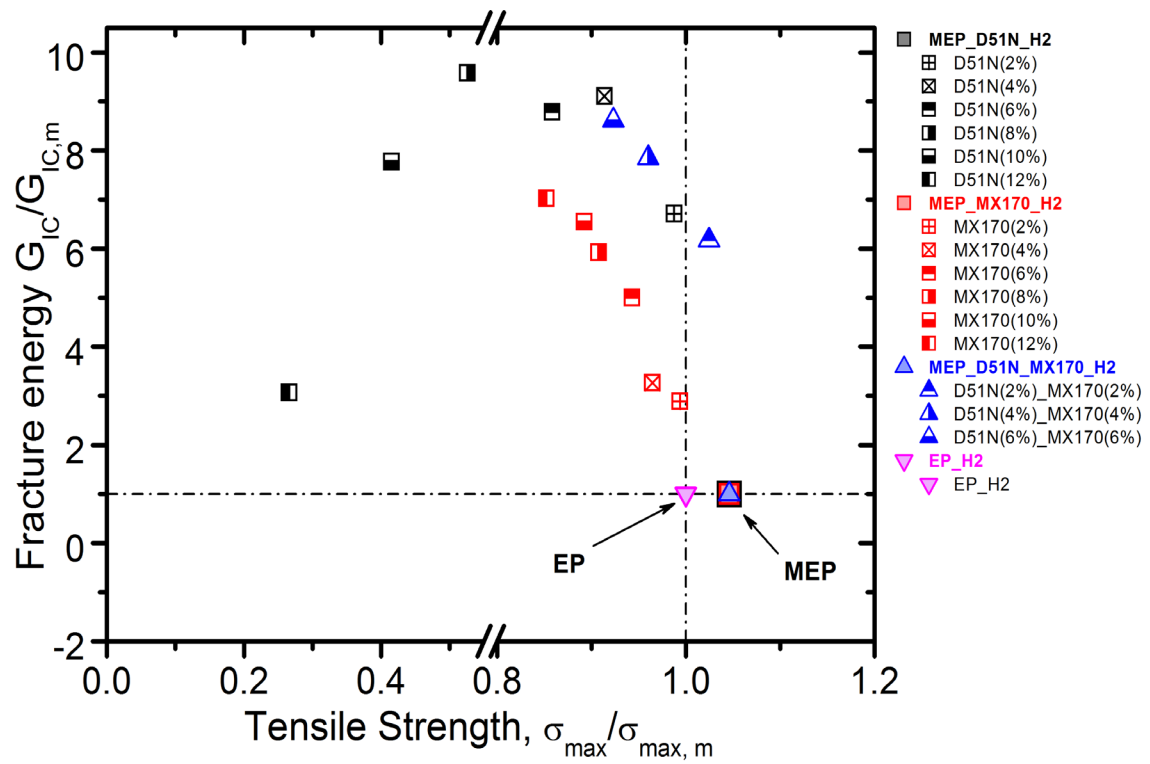


Figure 133: Graph showing the relation between normalized fracture energy and normalized tensile strength for modified anhydride-based systems at 80 °C.

7. Conclusion and outlook

In the present work, various multifunctional epoxy systems were employed to increase the tensile properties of reference epoxy systems. The multifunctional epoxy systems include fluorene diepoxy, epoxy based on meta-amino phenol and epoxy based on naphthalene diepoxy. Two specially designed toughening agents (a) BCP's and (b) CSR particles were used to enhance the fracture toughness of the modified systems up to the desired level. Results showed that modified systems exhibit superior tensile properties and thermal properties as compared to the reference systems when the effect of moisture, temperature, and strain rate was considered. Even after the addition of soft toughening phases (BCP's and CSR), the modified systems exhibit superior tensile properties, fracture properties and thermal properties at certain wt. % of CSR and BCP's as compared to the reference epoxy/hardener systems.

- Firstly the reference epoxy system was modified with different available multifunctional epoxy resins with amine hardener and anhydride hardener respectively. The best systems were selected based on the tensile strength, tensile strain at maximum strength and T_g values. Results revealed that both modified systems (MEP_H1 and MEP_H2) have superior tensile properties as compared to the reference systems (EP_H1 and EP_H2) at 23 °C and at 80 °C.

Systems (MEP_H1 and MEP_H2) were selected for toughness modification. The specially designed block copolymer (D51N) and core-shell rubber nanoparticles (MX170) were selected for toughening purpose. For MEP_H1 and MEP_H2 systems modified with MX170, D51N, and hybrids respectively, the following results were obtained.

- The effect of filler material for the given matrix system mainly depends on these parameters: properties of the matrix material used, type of the hardener or curing agent, appropriate dispersion technique employed for mixing of the filler in the matrix in case if the filler material was nanoparticles, proper

distribution of the filler particles in the matrix, and the compatibility between the matrix, hardener and filler materials used.

- For amine cured epoxy system modified with block copolymers, the viscosity was increased with increase in the particle content. The BCP's have no detrimental effect on glass transition temperature of composites. The tensile test showed that the tensile strength and modulus were decreased upon an increase in the filler concentration, because of the soft block content PbuA present in D51N. At the same time, the fracture toughness K_{IC} was increased by a factor of 2.5 and fracture energy G_{IC} was increased by a factor of 4.5. The toughening mechanisms responsible for this increment were identified as shear yielding, nano cavitation of spherical micelles followed by the void growth.
- For anhydride cured epoxy system modified with block copolymers, the viscosity was increased with increase in the particle content. The BCP's have no detrimental effect on glass transition temperature of composites. The tensile test showed that the tensile strength and modulus were gradually decreased upon an increase in the filler concentration because of the complete phase inversion and weak bonding between the matrix and filler at higher concentrations. But at the same time, the fracture toughness K_{IC} was increased by an average factor of 2.9 and fracture energy G_{IC} was increased by an average factor of 8 till the addition of 10 wt. % of particle content but there was a sharp decline in the both properties due to the complete phase inversion. The main toughening mechanisms observed were shear yielding, cavitation followed by void growth, crack pinning.
- The amine cured epoxy modified with MX170 core-shell rubber particles was also discussed. From the viscosity graph, it was observed that the viscosity was increased with increase in the particle content. The glass transition temperature either remains the same or increased due to the addition of bisphenol-A based masterbatch of MX170 CSR particles. Tensile tests showed that the tensile strength and modulus were decreased due to the presence of rubber particles which were having lower modulus when compared to the unmodified epoxy system, but this decreasing rate was less when compared with block copolymer particles. But at the same time, the fracture toughness K_{IC} was increased significantly by an average factor of 2.5

and fracture energy G_{IC} was increased by an average factor of 4.2. The principle toughening mechanisms observed were cavitation of rubber particles, shear yielding of the matrix.

- For anhydride cured epoxy system modified with CSR particles, the viscosity was increased with increase in the particle content. The glass transition temperature either remains the same or increased due to the addition of bisphenol-A based masterbatch of MX170 CSR particles. The tensile tests results indicate that the tensile strength and modulus were decreased upon an increase in the filler concentration because of the presence of rubber particles having low modulus and strength than unmodified epoxy. But at the same time, the fracture toughness K_{IC} was increased by an average factor of 2.2 and fracture energy G_{IC} was increased by an average factor of 4.2. The toughening mechanisms responsible for this increment were identified as shear yielding of matrix and cavitation of rubber particles followed by void growth.
- The amine-based and anhydride based hybrid composites consist of equal wt. % of D51N BCP's and MX170 CSR particles exhibit better tensile strength and modulus as compared to the single toughening agent (BCP or CSR) of the same wt. %.
- For TiO_2 / D51N modified reference amine based system, elastic modulus and tensile strength will be recovered with the addition of stiff TiO_2 particles.
- For most of the toughened systems except hybrid systems of BCP / CSR and TiO_2 modified systems analytical modeling was done for properties like elastic modulus, tensile strength, and fracture energy.
- For tensile modulus the Halpin-Tsai, Counto and Lewis Nielsen Models were used for most of the systems Counto and Halpin Tsai acts as the upper limit and for most of the systems Lewis-Nielsen model acts as lower limit; however most of the predicted values were in ± 5 % range except few values, where the phase inversion occurs.
- For tensile strength, a simple semi-empirical equation was used to predict the strength of composites. For most of the systems, the strength was predicted with an error of ± 5 %, except for phase inverted systems.
- Fracture energy was predicted by using the modified Huang-Kinloch fracture energy model, which assumes that the total fracture energy of the modified systems consists of fracture energy of an unmodified epoxy sample, energy

contribution from shear band yielding, energy contribution from void growth mechanism and energy contribution from rubber bridging mechanism. For the D51N modified anhydride based system the total fracture energy contribution considered from shear band yielding and cavitation followed by void growth and the predicted results were in good agreement with the experimental values. Similarly, for CSR particles modified systems, the main contribution comes from shear band yielding and relatively low contribution from debonding and void growth which was 10 % for amine-based systems and 5 % for anhydride based systems.

Outlook

Through the course of the present research focused on enhancing the strength, toughness and other mechanical properties of epoxy resin with the addition of different multi-functional epoxy systems, block copolymers and core-shell rubber nanoparticles potential areas for future research have been identified. There were some recommendations for future work based on the results of the present study.

1. In the present study, only one curing cycle was used for amine and anhydride hardener systems respectively, it would be recommended to use different post-curing temperature and post-curing time to evaluate its influence on overall mechanical properties.
2. Higher volume % of ceramic-based nanoparticles can be used to quantify the synergy between soft phase and hard phase in case of epoxy based hybrid nanocomposites.
3. In the present study, only Mode I fracture tests were performed for the unmodified, BCP, CSR modified composites and for hybrid composites. In future, Mode II and mixed mode fracture tests can be performed to investigate the fracture properties. The results of these tests will complement the results of the Mode I fracture tests and serves as input in the composite design process for parts manufacturing.
4. The use of interpenetrating networks approach to increase the strength of the modified systems by selecting appropriate networks will be recommended as an alternating approach for increasing the strength of the thermoset systems.
5. The transfer of strength and toughness to the continuous fiber-reinforced composite material can be examined for the best formulations. Qualitative work will further explain the importance of fiber-matrix adhesion and stress transfer across the fiber-matrix interface and this can be used to explain the toughening mechanisms that were observed.

8. Literature

- [1] E. M. Petrie, *Epoxy Adhesive Formulations*, 1st ed., New York: McGraw-Hill, 2006.
- [2] J. Glazer, "Monolayer Studies of Some Ethoxylin Resin Adhesives and Related Compounds," *POLYMER SCIENCE*, vol. XIII, pp. 355-369, 1954.
- [3] A. J. Kinloch., *Adhesion and Adhesives: Science and Technology.*, London: Chapman & Hall, 1987.
- [4] "<http://www.schaeferrolls.com/de>," SchäferRolls GmbH & Co. KG, 1 9 2017. [Online]. Available: <http://www.schaeferrolls.com/de/compositebezeuge.htm>.
- [5] Y. L. Liang and R. A. Pearson, "The toughening mechanism in hybrid epoxy-silica-rubber nanocomposites.," *Polymer*, vol. 51, pp. 4880-4890, 2010..
- [6] B. Wetzel, P. Rosso, F. Hauptert and K. Friedrich, "Epoxy nanocomposites – fracture and toughening mechanisms," *Engineering Fracture Mechanics*, vol. 73, pp. 2375-2398, 2006.
- [7] L. Weiping, V. Suong and P. Martin, "Morphology and Performance of Epoxy Nanocomposites Modified With Organoclay and Rubber," *Polymer Engineering Science*, vol. 44, pp. 1178-1186, 2004.
- [8] M. R. Ayatollahi, S. Shadlou and M. M. Shokrieh, "Mixed mode brittle fracture in epoxy/multi-walled carbon nanotube nanocomposites," *Engineering Fracture Mechanics*, vol. 78, pp. 2620-2632, 2011.
- [9] G. Giannakopoulos, K. Masania and A. C. Taylor, "Toughening of epoxy using core-shell particles," *Journal of Materials Science*, vol. 46, no. 2, pp. 327-338, August 2010.
- [10] D. Kim, K. Cho, J. Kim and C. Park, "Effects of particle size and rubber content on fracture toughness in rubber-modified epoxies," *Polymer Engineering & Science*, vol. 36, no. 6, pp. 755-768, 1996.
- [11] L. N. Bacigalupo and R. A. Pearson, "On the use of triblock copolymers to toughen epoxy resins," in *33rd Annual Meeting of the Adhesion Society*, Daytona Beach, FL, 2009.
- [12] R. Barsotti, "Nanostrength block copolymers for epoxy toughening," in

- Thermoset Resin Formulators Association*, Chicago, IL, 2008.
- [13] J. Chen and A. C. Taylor, "Epoxy modified with triblock copolymers: morphology, mechanical properties and fracture mechanisms," *Materials Science*, vol. 47, no. 11, pp. 4546-4560, 2012.
- [14] J. A. Gannon, "History and Development of Epoxy Resins.," in *The History of High Performance Polymers at the American Chemical Society Meeting*, New York, 1986.
- [15] P. K. Mallick, *Fiber-Reinforced Composites: Materials, Manufacturing, and Design*, 3rd ed., Boca Raton: CRC Press, 2008.
- [16] I. Hamerton, *Recent Developments in Epoxy Resins*, England: Rapra Technology Ltd, 1996.
- [17] J. P. Pascault and R. J. J. Williams, *Epoxy Polymers- New Materials and Innovations*, Weinheim: Wiley-VCH Verlag GmbH & Co. KGaA, 2010.
- [18] G. Lelli, A. Terenzi, C. Vedova, L. Torre and J. Kenny, "Modelling of the Chemo–Rheological Behaviour of Thermosetting Polymer Nanocomposites," in *COMSOL Users Conference*, Milan, 2006.
- [19] L. Henry and K. Neville, *Handbook of Epoxy Resins*, McGraw Hill Book, 1967.
- [20] P. J. Flory, *Principles of Polymer Chemistry*, Ithaca, Newyork: Cornell University Press, 1953.
- [21] G. Wisanrakkit and J. K. Gillham, *Journal of Applied Polymer Science*, vol. 41, pp. 2885-2929, 1990.
- [22] J. Lange, R. Ekelof and G. A. George, "Charge-recombination luminescence as a monitor of network formation during cure of epoxy resin," *Polymer*, vol. 40, pp. 149-155, 1998.
- [23] J. K. Gillham, "Formation and Properties of Thermosetting and High Tg Polymeric Materials," *Polymer Engineering and Science*, vol. 26, no. 20, pp. 1429-1433, 1986.
- [24] U. P. Breuer, *Civil Aircraft Composite Technology WS 15/16*, Kaiserslautern: IVW GmbH, Department of Mechanical and Process Engineering, TU Kaiserslautern, 2015.
- [25] S. Mostovoy and Ripling, "Fracture toughness of an epoxy system," *Journal of applied polymer science*, vol. 10, pp. 1351-1371, 1966.

- [26] J. P. Bell, "Mechanical properties of a glassy epoxide polymer. Effect of molecular weight between crosslinks," *Journal of Applied Polymer Science*, vol. 14, pp. 1901-1906, 1970.
- [27] S. L. Kim, M. D. Skibo, J. A. Manson, R. W. Hertzberg and J. Janiszewski, "Tensile, impact and fatigue behavior of an amine-cured epoxy resin," *Polymer Engineering and Science*, vol. 18, no. 14, p. 1093–1100, 1978.
- [28] G. R. Palmese and R. L. McCullough, "Effect of Epoxy-Amine stoichiometry on cured resin material properties," *Journal of Applied Polymer Science.*, vol. 46, pp. 1863-1873, 1992.
- [29] V. Bellenger, W. Dhaoui, J. Verdu, J. Boye and C. Lacabanne, "Internal antiplasticization in diglycidyl ether of bisphenol A diamino diphenyl methane non-stoichiometric epoxy networks," *Polymer Engineering and Science*, vol. 30, no. 6, pp. 321-325, 1990.
- [30] E. R. Mafi, M. Ebrahimi and M. R. Moghbeli, "Effect of Matrix Crosslink Density, Varied by Stoichiometry and Resin Molecular Weight, on Fracture Behavior of Epoxy Resins," *Journal of Polymer Engineering*, vol. 29, no. 5, 2009.
- [31] J. Boye, J. J. Martinez and C. Lacabanne, "Thermally stimulated creep spectroscopy for the study of DGEBA-DDM networks," *Journal of thermal analysis*, vol. 37, no. 8, p. 1775–1783, 1991.
- [32] S. Palmer, D. Dixon and S. B. Jaques, "The development of shear and compression elastic moduli in curing epoxy adhesives measured using non-contact ultrasonic transducers.," *Journal of Physics D : Applied Physics*, vol. 36, pp. 753-759, 2003.
- [33] H. Dodiuk and S. H. Goodman, "Introduction," in *Handbook of Thermoset Plastics*, Elsevier, 2014, p. 8.
- [34] G. Odian, *Principles of Polymerization*, 3rd edition, Newyork: McGraw-Hill, 1991.
- [35] V. Bellenger, J. Verdu and E. Morel, "Effect of structure on glass transition temperature of amine crosslinked epoxies," *J. Polym. Sci. B Polym. Phys. (Journal of Polymer Science Part B: Polymer Physics)*, vol. 25, no. 6, pp. 1219-1234, 1987.
- [36] V. A. Bershtein, V. M. Yegorov and Y. A. Yemel, "Relations between the main

- relaxation transitions in polymers and the length of segments and the character and degree of cooperation in molecular motion in the vicinity of T_g ," *Polymer Science U.S.S.R.*, vol. 27, no. 11, pp. 2757-2764, 1985.
- [37] W. A. Lee and J. H. Sewell, "Influence of Cohesive Forces on the Glass Transition Temperature of Polymers," *Journal of Applied Polymer Science*, vol. 12, pp. 1397-1409, 1968.
- [38] K. Balani, V. Verma, A. Agarwal and R. Narayan, "Physical, thermal and mechanical properties of polymers," in *Biosurfaces*, Hoboken, NJ, USA, John Wiley & Sons, 2014, pp. 337-340.
- [39] J. G. Williams, in *Fracture mechanics of polymers*, England, Ellis Horwood Limited, 1987, pp. 17-18.
- [40] A. F. Yee, J. Du and M. D. Thouless, "Toughening of epoxies in Polymer Blends," in *Polymer Blends Volume 2: Performance*, vol. 2, New York, John Wiley & Sons, 2000, pp. 225-267.
- [41] J. L. Halary, F. Laupretre and L. Monnerie, in *Polymer Materials: Macroscopic Properties and Molecular Interpretations*, John Wiley & Sons, Inc., 2011.
- [42] S. Yamini and R. J. Young, "The mechanical properties of epoxy resins," *Journal of Material Science*, vol. 15, no. 7, pp. 1814-1822, 1980.
- [43] W. D. Cook, A. E. Mayr and G. H. Edward, "Yielding behaviour in model epoxy thermosets — II. Temperature dependence," *Polymer*, vol. 39, no. 16, pp. 3725-3733, 1998.
- [44] A. E. Mayr, W. D. Cook and G. H. Edward, "Yielding behaviour in model epoxy thermosets — I. Effect of strain rate and composition," *Polymer*, vol. 39, no. 16, pp. 3719-3724, 1998.
- [45] B. Crist, "Yield processes in glassy polymers," in *The Physics of Glassy Polymers*, London, Harward RN and Young RJ, Editors. Chapman & Hall, 1997, pp. 155-212.
- [46] I. M. Ward, "Review: The yield behaviour of polymers," *Journal of Materials Science*, vol. 6, no. 11, pp. 1397-1417, 1971.
- [47] J. P. Pascault, H. Sautereau, J. Verdu and R. J. J. Williams, *Thermosetting Polymers*, New York: Mercel Dekker, 2002.
- [48] B. Crist, " The Physics of Glassy Polymers," in *Yield processes in glassy*

- polymers*, London, Chapman & Hall, 1997, pp. 155-212.
- [49] D. Hull, *Fractography: observing, measuring and interpreting fracture structure topography*, Cambridge: Cambridge University Press, 1999.
- [50] D. Hull, *Fractography: observing, measuring and interpreting fracture structure topography.*, Cambridge: Cambridge University Press, 1999.
- [51] A. J. Kinloch, S. J. Shaw, D. A. Tod and D. L. Hunston, "Deformation and fracture behaviour of a rubber-toughened epoxy: 1. Microstructure and fracture studies," *Polymer*, vol. 24, no. 10, pp. 1341-1354, 1983.
- [52] D. Ratna, "Toughened Thermoset Resins," in *Handbook of Thermosets*, iSmithers - A Smithers Group Company, 2009, pp. 187-188.
- [53] Y. Chen and R. A. Pearson, "Epoxy toughened with self-assembling block copolymers," in *36th Annual Meeting of the Adhesion Society*, Daytona Beach, USA, 2013, 2013.
- [54] M. Murali, D. Ratna, A. B. Samui and B. C. Chakraborty, "Synthesis, characterization, and evaluation of carboxyl-terminated poly (ethylene glycol) adipate modified epoxy networks," *Journal of Applied Polymer Science*, vol. 103, no. 3, pp. 1723-1730, 2006.
- [55] R. G. Jones, E. S. Wilks, W. V. Metanomski, J. Kahovec, M. Hess, R. Stepto and T. Kitayama, *Compendium of Polymer Terminology and Nomenclature*, vol. 79, Cambridge: Royal Society of Chemistry, 2009, pp. 1801-1829.
- [56] Z. G. Shaker, R. M. Browne, H. A. Stretz, P. E. Cassidy and M. T. Blanda, "Epoxy-toughened, unsaturated polyester interpenetrating networks," *Journal of Applied Polymer Science*, vol. 84, no. 12, pp. 2283-2286, 2002.
- [57] A. B. Cherian, L. A. Varghese and E. T. Thachil, "Epoxy-modified, unsaturated polyester hybrid networks," *European Polymer Journal*, vol. 43, no. 4, pp. 1460-1469, 2007.
- [58] K. Dinakaram and M. Alagar, "Preparation and characterization of epoxy-cyanate ester interpenetrating network matrices/organoclay nanocomposites," *Polymers for Advanced Technologies*, vol. 14, no. 8, pp. 574-585, 2003.
- [59] M. Lin, C. Liu and C. Lee, "Toughened interpenetrating polymer network materials based on unsaturated polyester and epoxy," *Journal of Applied Polymer Science*, vol. 72, no. 4, pp. 585-592, 1999.

- [60] J. W. Aylsworth, "Plastic Composition". USA Patent US1111284 A, 04 November 1914.
- [61] N. Platzer, "Polymer-plastics technology and engineering," *Journal of Polymer Science: Polymer Letters Edition*, vol. 26, no. 12, p. 538–539, 1988.
- [62] K. S. Kishore, "Analysis of deformation behaviour and fracture features in glass-epoxy composites toughened by rubber and carbon additions," *Journal of Material Science Letters*, pp. 86-88, 1992.
- [63] T. T. Wang and H. M. Zupko, "Phase separation behavior of rubber-modified epoxies," *Journal of Applied Polymer Science*, vol. 26, p. 2391–2401, 1981.
- [64] C. Riew, *Rubber, Chemistry and Technology*, vol. 58, p. 622, 1985.
- [65] A. Cunliffe, M. Huglin, P. Pearce and D. Rechards, "An anionically prepared flexible adhesive: 3. Physical testing," *Polymer*, vol. 16, p. 622, 1975.
- [66] A. H. Rezaifard, K. A. Hodd, D. A. Tod and J. M. Barton, "Toughening epoxy resins with poly (methyl methacrylate)- grafter - natural rubber, and its use in adhesive formulations," *International Journal of Adhesion and Adhesives*, vol. 14, no. 2, pp. 153-159, April 1994.
- [67] Q. Ji, M. Todd and M. Edwards, "Evaluation of various elastomers as modifiers to reduce stress in liquid epoxy encapsulants and flip chip underfills.," Loctite corporation, Technical Paper, 2002.
- [68] D. Ratna, "Toughened Epoxy Resins," in *Handbook of Thermosets*, iSmithers - A Smithers Group Company, 2009, pp. 237-279.
- [69] R. A. Pearson and A. F. Yee, "Toughening mechanisms in thrmoplastic modified epoxies. 1. modificatin using poly(phenylene oxide)," *polymer*, vol. 34, pp. 3658-3670, 1993.
- [70] C. B. Bucknall and A. H. Gilbert, "Toughening tetrafunctional epoxy resins using polyetherimide," *Polymer*, vol. 30, no. 2, pp. 213-217, 1989.
- [71] Y. Luo, M. Zhang, G. Dang, Y. Li, X. An, C. Chen and X. Yi, "Toughening of epoxy resin by poly(ether ether ketone) with pendant fluorocarbon groups," *Journal of Applied Polymer*, vol. 122, no. 3, p. 1758–1765, 2011.
- [72] C. B. Bucknall, C. M. Gomez and I. Quintard, "Phase separation from solutions of poly (ether sulphone) in epoxy resins," *Polymer*, vol. 35, no. 353, 1994.
- [73] A. J. Kinloch, M. L. Yuen and S. D. Jenkins, "Thermoplastic-toughened epoxy

- polymers," *Journal of Material Science*, vol. 29, no. 14, pp. 3781-3790, 1994.
- [74] X. Yi, "Development of multifunctional composites for aerospace application," in *Multifunctionality of polymer composites : Challenges and new solutions*, Elsevier, 2015, p. 373.
- [75] R. Liu, J. Wang, J. Li and X. Jian, "An investigation of epoxy/thermoplastic blends based on addition of a novel copoly(aryl ether nitrile) containing phthalazinone and biphenyl moieties," *Polymer International*, vol. 64, no. 12, p. 1786–1793, 2015.
- [76] S. R. Raghava, "Role of matrix-particle interface adhesion on fracture toughness of dual phase epoxy-polyethersulfone blend," *Journal of Polymer Science, Polymer Physics*, vol. 25, no. 5, pp. 1017-1031, 1987.
- [77] V. Di Liello, E. Martuscelli, P. Musto, G. Ragosta and G. Scarinzi, "Toughening of highly crosslinked epoxy resins by reactive blending with bisphenol A polycarbonate- Yield and fracture behaviour," *Journal of Polymer Science, Polymer Physics*, vol. 32, pp. 409-419, 1994.
- [78] Ian W. Hamley, *The physics of block copolymers*, Oxford University Press, 1999.
- [79] A. D. Jenkins, P. Kratochvil, R. Stepto and U. W. Suter, "Glossary of basic terms in polymer science (IUPAC Recommendations 1996).," *Pure and Applied chemistry*, vol. 68, no. 12, pp. 2287-2311, 1996.
- [80] J. Liu, Z. J. Thompson, H. J. Sue, F. S. Bates, M. A. Hillmyer, M. Dettlof, G. Jacob, N. Verghese and H. Pham, "Toughening of Epoxies with Block Copolymer Micelles of Wormlike Morphology," *Macromolecules*, vol. 43, pp. 7238-7243, June 2010.
- [81] M. A. Hillmyer, P. M. Lipic, D. A. Hajduk, K. Almdal and F. S. Bates, "Self-assembly and polymerization of epoxy resin-amphiphilic block copolymer nanocomposites.," *Journal of American Chemical Society*, vol. 119, pp. 2749-2750, 1997.
- [82] L. Ruiz-Pérez, G. J. Royston, J. P. A. Fairclough and A. J. Ryan, "Toughening by nanostructures," *Polymer*, vol. 49, pp. 4475-4488, 2008.
- [83] S. Owen, P. Y. D. Chan and M. Shoichet, "Polymeric micelle stability," *Nano Today*, vol. 7, pp. 53-65, 2012.

- [84] K. Kataoka, T. Matsumoto, M. Yokoyama, T. Okano, Y. Sakurai, S. Fukushima, K. Okamoto and G. S. Kwon, "Doxorubicin-loaded poly (ethylene glycol)-poly (beta-benzyl-L-aspartate) copolymer micelles: their pharmaceutical characteristics and biological significance.," *Journal of Controlled release: official journal of the Controlled Release Society.*, vol. 64, pp. 143-153, January 2000.
- [85] S. Ritzenthaler, F. Court, E. Girard-Reydet, I. Leibler and P. Pascault J., "ABC Triblock Copolymers/Epoxy diamine Blends. 2. Parameters controlling the morphologies and properties," *Macromolecules*, vol. 36, no. 1, pp. 118-226, January 2003.
- [86] R. Barsotti, T. Fine, R. Inoubli, P. Gerard, S. Schmidt, N. Macy, S. Magnet and C. Navarro, "Nanostrength Block Copolymers for Epoxy Toughening," in *Thermoset Resin Formulators Association*, Chicago, USA, 2008.
- [87] R. Pearson, L. Bacigalupo, Y. Liang, B. Marouf and R. Oldak, "Plastic zone size - fracture toughness correlations in rubber-modified epoxies," in *Proceedings of the 31st Annual Meeting of the Adhesion Society*, Austin, TX, 2008.
- [88] Y. Thio, J. Wu and F. Bates, "The role of inclusion size in toughening of epoxy resins by spherical micelles," *Journal of Polymer Science Part B: Polymer Physics*, vol. 47, no. 11, pp. 1125-1129, 2009.
- [89] B. Wetzel, "Mechanische Eigenschaften von Nanoverbundwerkstoffen aus Epoxydharz und keramischen Nanopartikeln. PhD, IVW Schriftenreihe Band 69 (2006). ISBN: 3-934930-65-4," Technische Universität Kaiserslautern, Kaiserslautern, 2006.
- [90] B. Bittmann, F. Hauptert and A. K. Schlarb, "Preparation of TiO₂ epoxy nanocomposites by ultrasonic dispersion and resulting properties.," *Applied Polymer Science*, vol. 124, no. 3, pp. 1906-1911, 2012.
- [91] P. Carballeira and F. Hauptert, "Toughening Effects of Titanium Dioxide Nanoparticles on TiO₂ /Epoxy Resin Nanocomposites," *Society of Plastics Engineers*, vol. 31, pp. 1241-1246, 2009.
- [92] A. J. Kinloch and A. C. Taylor, "The mechanical properties and fracture behaviour of epoxy-inorganic micro- and nano-composites," *Journal of Material Science*, vol. 41, no. 11, pp. 3271-3297, 2006.
- [93] K. Masania, "Toughening mechanisms of silica nanoparticle-modified epoxy

- polymers. PhD Thesis," Department of Mechanical Engineering, Imperial College, London, 2010.
- [94] H. R. Azimi, R. Pearson and R. Hertzberg, "Role of crack tip shielding mechanisms in fatigue of hybrid epoxy composites containing rubber and solid glass spheres.," *Journal of Applied Polymer Science.*, vol. 58, no. 2, pp. 449-463, 1995.
- [95] J. Spanoudakis and R. and Young, "Crack propagation in a glass particle-filled epoxy resin Part 1 Effect of particle volume fraction and size.," *Journal of Materials Science*, vol. 19, pp. 473-486, 1984.
- [96] J. Spanoudakis and R. Young, "Crack propagation in a glass particle-filled epoxy resin Part 2 Effect of particle-matrix adhesion.," *Journal of Materials Science*, vol. 19, pp. 487-496, 1984.
- [97] S. Sprenger, "Epoxy resin composites with surface-modified silicon dioxide nanoparticles: A review," *Journal of Applied Polymer Science*, vol. 130 (3), pp. 1421-1428, 2013.
- [98] D. Maxwell, R. J. Young and A. J. Kinloch, "Hybrid particulate-filled epoxy-polymers," *Journal of Materials Science Letters*, vol. 3, no. 1, pp. 9-12, 1984.
- [99] D. P. Carmelo, "Toughness in block copolymer modified epoxies," 2014.
- [100] A. C. Garg and Y. W. Mai, "Failure Mechanisms in toughened epoxy resins - A review," *Composites Science and Technology*, vol. 31, no. 3, pp. 179-223, 1988.
- [101] R. K. Bregg, *Frontal Polymer Research*, illustrated ed., R. K. Bregg, Ed., Nova Publishers, 2006, 2006, pp. 1-255.
- [102] S. Newman and S. Strella, "Stress-strain behaviour of rubber-reinforced glassy polymers," *Applied Polymer*, vol. 9, no. 6, pp. 2297-2310, June 1965.
- [103] R. P. Petrich, "Impact reinforcement of poly(vinyl chloride)," *Polymer Engineering & Science*, vol. 13, no. 4, pp. 248-254, July 1973.
- [104] F. F. Lange, "The interaction of a crack front with a second phase dispersions," *Philosophical Magazine*, vol. 22, no. 179, p. 0983-0992, 1970.
- [105] A. G. Evans, "The strength of a brittle material containing second phase dispersions.," *Philosophical Magazine*, vol. 26, p. 1327, 1972.
- [106] D. J. Green, P. S. Nicholson and J. D. Embury, "Fracture of a brittle particulate

- composite," *Journal of Materials Science*, vol. 14, no. 6, p. 1413–1420, 1979.
- [107] M. Konstantakopoulou, A. Deligianni and G. Kotsikos, "Failure of dissimilar material bonded joints," in *Nanomaterials in Joining*, Walter de Gruyter GmbH & Co. KG, 2016, pp. 103-122.
- [108] H. J. Sue, E. I. Garcia-Meitin and D. M. Pickelman, "Fracture Behaviour of Rubber-Modified High-Performance Epoxies," in *Polymer Toughening*, C. Arends, Ed., CRC Press, 1996, pp. 131-174.
- [109] K. T. Faber and A. G. Evans, "Crack deflection processes - I Experimental," *Theory Acta Metall*, vol. 31, no. 4, pp. 565-576, April 1983.
- [110] K. T. Faber and A. G. Evans, "Crack deflection process - II Experimental," *Theory Acta Metall*, vol. 31, no. 4, pp. 577-584, April 1983.
- [111] R. A. Pearson and A. F. Yee, "Toughening mechanisms in elastomer-modified epoxies," *Journal of Materials Science*, vol. 24, no. 7, pp. 2571-2580, July 1989.
- [112] P. A. O'Connell and G. B. McKenna, "Yield and Crazing in Polymers," *Encyclopedia of Polymer Science and Technology*, pp. 657-681, July 2004.
- [113] H. J. Sue, "Study of Rubber-Modified Brittle Epoxy Systems. Part II: Toughening Mechanisms under Mode-I Fracture," *Polymer Engineering and Science.*, vol. 31, no. 4, 1991.
- [114] K. Sritama and A. K. Banthia, "Recent trends in developing reactive liquid oligomers for toughening of epoxy resin," in *Frontal Polymer Research*, New York, Nova Science Publishers, 2006, pp. 2-59.
- [115] C. B. Bucknall and T. Yoshii, "Relationship between structure and mechanical properties in rubber-toughened epoxy resins," *British Polymer Journal*, vol. 10, no. 1, 1978.
- [116] S. C. Kunz, J. A. Sayre and R. A. Assink, "Morphology and toughness characterization of epoxy resins modified with amine and carboxyl," *Polymer*, vol. 23, no. 13, 1982.
- [117] A. J. Kinloch and D. L. Hunston, "Effect of volume fraction of dispersed rubbery phase on the toughness of rubber toughened epoxy polymers," *Journal of Material Science Letters*, vol. 6, pp. 131-139, 1987.
- [118] A. J. Kinloch, M. B. Kodokian and M. B. Jamarani, "Impact properties of epoxy polymers," *Journal of Material Science*, vol. 22, pp. 4111-4120, 1987.

- [119] Y. Huang and A. J. Kinloch, "The Use of Time-Temperature Superpositioning in Studying the Fracture Properties of Rubber-Toughened Epoxy Polymers," *The Journal of Adhesion*, vol. 41, no. 1-4, pp. 5-22, 1993.
- [120] D. L. Hunston, A. J. Kinloch, S. J. Shaw and S. S. Wang, "Characterization of the Fracture Behavior of Adhesive Joints," in *Mittal (Ed.) 1984 – Adhesive Joints*, Boston, MA, Springer US, 1984.
- [121] A. R. Siebert, "Morphology and Dynamic Mechanical Behavior of Rubber-Toughened Epoxy Resins," in *Rubber-Modified Thermoset Resins*, vol. 208, Washington, D.C, American Chemical Society, 1984, pp. 179-191.
- [122] A. Lowe, O. Kwon and Y. Mai, "Fatigue and fracture behaviour of novel rubber modified epoxy resins," *Polymer*, vol. 37, no. 4, pp. 565-572, 1996.
- [123] L. C. Chan, J. K. Gillham, A. J. Kinloch and S. J. Shaw, "Rubber-Modified Epoxies," in *Rubber-Modified Thermoset Resins*, Washington, D.C, American Chemical Society, 1984, p. 261–279.
- [124] J. N. Sultan, R. C. Laible and F. J. McGarry, "Scanning electron micrographs of rubber modified epikote," *Applied Polymer Symposium*, vol. 6, p. 127, 1971.
- [125] J. N. Sultan and F. J. McGarry, "Effect of rubber particle size on deformation mechanisms in glassy epoxy," *Polymer Engineering and Science*, vol. 13, no. 1, pp. 29-34, January 1973.
- [126] S. Kunz-Douglass, P. W. R. Beaumont and M. F. Ashby, "A model for the toughness of epoxy-rubber particulate composites," *Journal of Materials Science*, vol. 15, no. 5, pp. 1109-1123, May 1980.
- [127] R. A. Pearson and A. F. Yee, "Influence of particle size and particle size distribution on toughening mechanisms in rubber-modified epoxies," *Journal of Materials Science*, vol. 26, no. 14, pp. 3828-3844, March 1991.
- [128] C. B. Bucknall and T. Yoshii, *The British Polymer Journal*, vol. 10, no. 3, p. 53, 1978.
- [129] Y. B. Zeng, L. Z. Zhang, W. Z. Peng and Q. Yu, "Microstructure, mechanical properties, and fracture behaviour of liquid rubber toughened thermosets," *Journal of Applied Polymer Science*, vol. 42, no. 1905, pp. 1905-1910, April 1991.
- [130] L. C. Chan, J. K. Gillham, A. J. Kinloch and S. J. Shaw, "Rubber-modified

- epoxies (Morphology, Transitions, and Mechanical Properties)," *Advance in Chemistry*, vol. 208, pp. 261-279, December 1984.
- [131] S. Wu, "Impact fracture mechanisms in polymer blends: Rubber-toughened nylon," *Journal of Polymer Science: Polymer Physics Edition*, vol. 21, no. 5, pp. 699-716, May 1983.
- [132] G. Levita, "Matrix Ductility and Toughening of Epoxy Resins," in *Rubber-Toughened Plastics; Advances in Chemistry*, vol. 222, C. K. Riew, Ed., 1989, pp. 93-118.
- [133] Y. Huang, A. J. Kinloch, R. Bertsch and A. R. Siebert, "Particle matrix interfacial bonding-effect on the fracture properties of rubber-modified epoxy polymers," *Advances in Chemistry Series*, vol. 233, pp. 189-210, 1993.
- [134] J. P. Chen and Y. D. Lee, "A real-time study of the phase-separation process during polymerization of rubber-modified epoxy," *Polymer*, vol. 36, no. 1, pp. 55-65, January 1995.
- [135] F. McGarry and A. M. Willner, "Toughening of an epoxy resin by an elastomeric second phase," 1968.
- [136] A. J. Kinloch, C. A. Finch and S. J. Hashemi, *Polymer Communication*, vol. 28, pp. 322-325, 1987.
- [137] S. Y. Fu and B. Lauke, "Characterization of tensile behaviour of hybrid short glass fibre calcite particle ABS composites," *Composites Part A*, vol. 29A, pp. 575-83, 1998.
- [138] U. J. Counto, "The effect of the elastic modulus of the aggregate on the elastic modulus, creep and creep recovery of concrete," *Magzine of Concrete Research*, vol. 16, pp. 129-138, 1964.
- [139] J. C. Halpin, "Stiffness and expansion estimates for oriented short fiber composites," *Journal of Composite Materials*, vol. 3, no. 4, p. 732, 1969.
- [140] J. C. Halpin and S. Tsai, "Effects of environmental factors on composite materials," AFML - TR 67-423, 1969.
- [141] J. C. Halpin and J. C. Kardos, "The Halpin-Tsai equations: A review," *Polymer Engineering & Science*, vol. 16, no. 5, pp. 344-352, 1969.
- [142] S. McGee and R. McGullough, "Combining rules for predicting the thermoelastic properties of particulate filled polymers, polymers, polyblends,

- and foams," *Polymer Composites*, vol. 2, no. 4, pp. 149-161, 1981.
- [143] E. L. Nielsen and R. F. Landel, Mechanical properties of polymers and composites, New York: Marcel Dekker, Inc., 1994.
- [144] S. Y. Fu, X. Feng, B. Lauke and Y. W. Mai, "Effects of particle size, particle/matrix interface adhesion and particle loading on mechanical properties of particulate - polymer composites," *Composites Part B: Engineering*, vol. 39, no. 6, p. 933–961, 2008.
- [145] F. Danusso and G. Tieghi, "Strength versus composition of rigid matrix particulate composites.," *Polymer*, vol. 27, pp. 1385-1390, 1986.
- [146] G. Levita, A. Marchetti and A. Lazzeri, "Fracture of ultrafine calcium carbonate/polypropylene composites.," *Polymer Composites* , vol. 10, pp. 39-43, 1989.
- [147] T. H. Hsieh, A. J. Kinloch, K. Masania, A. C. Taylor and S. Sprenger, "The toughness of epoxy polymers and fibre composites modified with rubber microparticles and silica nanoparticles," *Journal of Materials Science*, vol. 45, no. 5, pp. 1193-1210, 2010.
- [148] Y. Huang and A. J. Kinloch, "Modelling of the toughening mechanisms in rubber rubber modified polymers part I finite element analysis studies," *Journal of Material Science*, vol. 24, pp. 2753-2762, 1992.
- [149] Y. Huang and A. J. Kinloch, "Modelling of the toughening mechanisms in rubber modified epoxy polymers part ii a quantitative description of the microstructure fracture property relationships," *Journal of Materials Science*, vol. 27, no. 10, pp. 2763-2769, 1992.
- [150] H. M. Chong and A. C. Taylor, "The microstructure and fracture performance of styrene–butadiene–methacrylate block copolymer-modified epoxy polymers," *Materials Science*, vol. 48, no. 19, pp. 6762-6777, 2013.
- [151] J. Chen, "Toughening Epoxy Polymers and Carbon Fibre Composites with Core - Shell particles, Block Copolymers and Silica Nanoparticles," Imperial College , London, 2013.
- [152] H. M. Chong, "Toughening mechanisms of block copolymer and graphene nanoplatelet modified epoxy polymers," Imperial College , London, 2015.
- [153] J. N. Sultan and F. McGarry, "Effect of rubber particle size on deformation

- mechanisms in glassy epoxy," *Polymer Engineering & Science*, vol. 13, no. 1, pp. 29-34, 1973.
- [154] A. J. Kinloch and R. J. Young, *Fracture Behaviour of Polymers*, New York: Elsevier Applied Science, 1983.
- [155] T. H. Hsieh, A. J. Kinloch, K. Masania, A. C. Taylor and S. Sprenger, "The mechanisms and mechanics of the toughening of epoxy polymers modified with silica nanoparticles," *Polymer*, vol. 51, no. 26, pp. 6284-6294, 2010.
- [156] J. Chen, A. J. Kinloch, S. Sprenger and A. C. Taylor, "The mechanical properties and toughening mechanisms of an epoxy polymer modified with polysiloxanebased core shell particles," *Polymer*, vol. 54, no. 16, pp. 4276-4289, 2013.
- [157] S. C. Kunz and P. W. R. Beaumont, "Low-temperature behaviour of epoxy-rubber particulate composites," *Journal of Material Science*, vol. 16, no. 11, pp. 3141-3152, 1981.
- [158] Hexoin Inc., "Product specifications for the EPON862 and Technical Data Sheet.," 2005.
- [159] D. J. Durig, "Comparisons of epoxy technology for protective coatings and linings in wastewater facilities," in *The Industrial Protective Coatings Conference and exhibit*, Houston, TX, USA, 1999.
- [160] Huntsman Corp., "Technical Data Sheet for developmental resin LME10169," Huntsman Advance Materials GmbH, Basel, 2015.
- [161] Huntsman Corp., "Technical data sheet for Araldite MY 0610 Trifunctional resin," Huntsman Advance Materials GmbH, Basel, 2015.
- [162] Huntsman Corp., "Technical Data Sheet for Araldite MY 0816," Huntsman Advance Materials GmbH, Basel, 2015.
- [163] Huntsman Corp., "Advance Material Raising performance with building blocks," 10 2012. [Online]. Available: http://www.huntsman.com/advanced_materials/Media%20Library/global/files/EUR_HL_Components_Raising%20performance%20with%20Building%20blocks.pdf.
- [164] Arkema, "Technical Data Sheet - Nanostrength ® Epoxy Application," Paris, France, 2013.

- [165] S. Maiez-Tribut, J. P. Pascault, E. R. Soule, J. Borrajo and R. J. J. Williams, "Nanostructured Epoxies Based on the Self-Assembly of Block Copolymers: A New Miscible Block That Can Be Tailored to Different Epoxy Formulations," *Macromolecules*, pp. 1268-1273, 2007.
- [166] Kaneka Belgium NV, "Technical Data Sheet- Kane Ace Trade Mark MX-170," Brussels, Belgium, 2015.
- [167] Evonik Resource Efficiency GmbH, "Product information AEROXIDE® TiO₂ P 25," 2016.
- [168] H. P. Boehm, "Die Chemie der Oberfläche fester Stoffe," *Polymer*, vol. 227, pp. 17-27, 1968.
- [169] H. C. Hamaker, "The London-Van der Waals attraction between spherical particles.," *Physica*, vol. 4, no. 10, pp. 1058-1072., 1937.
- [170] T. A. Instruments, "ARES-G2 Rheometer," 2014.
- [171] G. Gkikas, N. M. Barkoula and A. S. Paipetis, "Effect of dispersion conditions on the thermo-mechanical and toughness properties of multi walled carbon nanotubes-reinforced epoxy," *Composites*, vol. 43, p. 2697–2705, 2012.
- [172] DIN-EN-ISO-527-1 : General principles for the determination of tensile properties, Berlin: DIN Deutsches Institut für Normung e.V., 1996.
- [173] D. Moore, The application of fracture mechanics to polymers, adhesives and composites, Oxford: Elsevier, 2004.
- [174] K. Xiao, L. Ye and Y. S. Kwok, " Effects of pre-cracking methods on fracture behaviour of an Araldite-F epoxy and its rubber-modified systems," *Journal of Material Science*, vol. 33, no. 11, pp. 2831-2836, 1998.
- [175] ISO 13586:2000(E): Plastics — Determination of fracture toughness (GIC and KIC) — Linear elastic fracture mechanics (LEFM) approach, Switzerland: ISO (the International Organization for Standardization).
- [176] K. P. Menard, Dynamic Mechanical Analysis: A Practical Introduction, CRC Press, 2008.
- [177] "Atomic Force Microscopy - A Guide to Understanding and Using the AFM.," Galloway Group - Texas State University Manuals. <http://www.txstate.edu>.
- [178] A. Smith, "Atomic force microscopy," vol. 26, 1999.
- [179] J. Wylde and J. Spelt, "Measurement of Adhesive Joint Fracture Properties as a

- Function of Environmental Degradation," *International Journal of Adhesion and Adhesives*, vol. 18, pp. 237-246, 1998.
- [180] M. Wahab, A. Crocombe, A. Beevers and K. Ebtehaj, "Coupled Stress Diffusion Analysis for Durability Study in Adhesively Bonded Joints," *International Journal of Adhesion and Adhesives*, vol. 22, pp. 61-73, 2002.
- [181] S. Rosen, *Fundamental Principles of Polymeric Materials*, New York: John Wiley and Sons, 1993.
- [182] H. C. Van de Hulst, "Light Scattering by Small Particles," *Mineola: Dover Publications Inc.*, 1982.
- [183] S. Ritzenthaler, E. Girard-Reydet and J. P. Pascault, "Influence of epoxy hardener on miscibility of blends of poly(methyl methacrylate) and epoxy networks," *Polymer*, vol. 41, no. 16, pp. 6375-6386, 2000.
- [184] S. Ritzenthaler, F. Court, L. David, E. Girard-Reydet, L. Leibler and J. P. Pascault, "ABC Triblock Copolymers/Epoxy - Diamine Blends. 1. Keys To Achieve Nanostructured Thermosets," *Macromolecules*, vol. 35, pp. 6245 - 6254, 2002.
- [185] R. Bagheri and R. A. Pearson, "Role of plastic cavitation in rubber toughened epoxies," *Polymer*, vol. 37, pp. 5597-600, 1996.
- [186] A. J. Kinloch, D. L. Maxwell and R. J. Young, "The fracture of hybrid-particulate composites," *Journal of Materials Science*, vol. 20, no. 11, pp. 4169-4184, 1985.
- [187] D. Verchere, H. Sautereau and J. Pascault, "Rubber modified epoxy. Influence of CTBN," *Journal of Applied Material Science.*, vol. 41, pp. 467-76, 1990.
- [188] A. Yee and R. Pearson, "Toughening mechanisms in elastomer modified epoxies.," *Journal of Material Science*, vol. 21, p. 2462, 1986.
- [189] F. J. Guild, A. J. Kinloch and A. C. Taylor, "The debonding of nanoparticles in toughening adhesives.," in *37th Annual Meeting of the Adhesion Society, 23-26 February 2014*, San Diego, USA, 2014.
- [190] T. H. Hsieh, A. J. Kinloch, K. Masania, J. Sohn Lee, A. C. Taylor and S. Sprenger, "The toughness of epoxy polymers and fibre composites modified with rubber microparticles and silica nanoparticles," *Journal of Materials Science*, vol. 46, no. 11, p. 4092, 2011.

- [191] D. Hull, *Fractography: observing, measuring and interpreting fracture structure topography*, Cambridge University Press, 1999.
- [192] F. J. Guild, A. J. Kinloch and A. C. Taylor, "The debonding of nanoparticles in toughening adhesives.," in *37th Annual Meeting of the Adhesion Society*, San Diego, USA, 2014.
- [193] T. H. Hsieh, A. J. Kinloch, K. Masania, J. Sohn Lee, A. C. Taylor and S. Sprenger, "The toughness of epoxy polymers and fibre composites modified with rubber microparticles and silica nanoparticles," *Journal of Materials Science*, vol. 46, no. 11, p. 4092, 2011.
- [194] I. Giannakopoulos, "Manufacture and properties of hybrid particle-modified fibre composites by RIFT, MSc Thesis," Department of Mechanical Engineering and Department of Aeronautics, Imperial College , London, 2008.
- [195] M. Salinas-Ruiz, A. Skordos and I. Partridge, "Rubber toughened epoxy loaded with carbon nanotubes: structure – property relationships," *Material science*, vol. 45, no. 10, pp. 2633-2639, 2010.
- [196] S. Guang, M. Q. Zhang, Z. M. Rong, B. Wetzel and K. Friedrich, "Sliding wear behavior of epoxy containing nano- Al_2O_3 particles with different pretreatments," *Wear*, vol. 256, pp. 1072-1081, 2004.
- [197] A. J. Kinloch, D. Maxwell and R. J. Young, "Micromechanisms of crack propagation in hybrid-particulate composites," *Journal of Materials Science Letters*, vol. 4, no. 10, pp. 1276-1279, 1985.

9. Appendix

9.1 Surface roughness measurement of fractured surfaces

Table 49: Amine cured epoxy composites modified with D51N BCP and MX170 CSR particles.

D51N (wt. %)	Ra (μm)	MX170 (wt. %)	Ra (μm)
0	0.150	0	0.150
2	0.183	2	0.190
4	0.201	4	0.210
6	0.223	6	0.225
8	0.230	8	0.230
10	0.235	10	0.312
12	0.241	12	0.335

Table 50: Anhydride cured epoxy composites modified with D51N BCP's and CSR nanoparticles.

D51N (wt. %)	Ra (μm)	MX170 (wt. %)	Ra (μm)
0	0.136	0	0.136
2	0.296	2	0.176
4	0.431	4	0.186
6	0.544	6	0.220
8	1.557	8	0.245
10	5.176	10	0.275
12	1.875	12	0.310

Table 51: Amine cured epoxy hybrid composites modified with D51N block copolymers and MX170 core-shell rubber particles

D51N (wt. %)	MX170 (wt. %)	Ra (μm)
0	0	0.150
2	2	0.200
4	4	0.264
6	6	0.288

Table 52: Anhydride cured epoxy hybrid composites modified with D51N block copolymers and MX170 core-shell rubber particles

D51N (wt. %)	MX170 (wt. %)	Ra (μm)
0	0	0.136
2	2	0.300
4	4	0.354
6	6	0.365

9.2 Compressive test results data

Table 53: Compressive stress data for amine based systems (modified with MX170 and D51N) and anhydride based systems (modified with MX170 and D51N).

Samples	E_c [MPa]	σ_{yc} [MPa]	σ_{fc} [MPa]	ϵ_f [%]
MEP_H1	2020	124 – 125	273 – 274	49
MEP_H1_2MX170	2280	125 – 126	298 – 299	52
MEP_H1_4MX170	2170	123 – 124	270 – 271	48
MEP_H1_6MX170	2150	121 – 122	240 – 241	48
MEP_H1_8MX170	2240	121 – 122	277 – 278	52
MEP_H1_10MX170	2250	122 – 123	295 – 296	50
MEP_H1_12MX170	2220	121 – 122	305 – 306	50
Samples	E_c [MPa]	σ_{yc} [MPa]	σ_{fc} [MPa]	ϵ_f [%]
MEP_H1	2020	124 – 125	273 – 274	49
MEP_H1_2D51N	2170	124 – 125	263 – 264	51
MEP_H1_4 D51N	2080	118 – 119	294 – 295	52
MEP_H1_6 D51N	2120	122 – 123	288 – 289	50
MEP_H1_8 D51N	2080	117 – 118	313 – 314	54
MEP_H1_10 D51N	1950	118 – 119	324 – 325	54
MEP_H1_12D51N	1890	113 – 114	298 – 299	58
Samples	E_c [MPa]	σ_{yc} [MPa]	σ_{fc} [MPa]	ϵ_f [%]
MEP_H2	2440	131 – 133	306 – 308	53
MEP_H2_2MX170	2430	126 – 127	305 – 306	52
MEP_H2_4MX170	2440	122 – 123	254 – 255	51
MEP_H2_6MX170	2530	124 – 125	260 – 261	50
MEP_H2_8MX170	2540	125 – 126	260 – 261	49
MEP_H2_10MX170	2450	124 – 125	283 – 284	54
MEP_H2_12MX170	2480	122 – 123	256 – 257	48
Samples	E_c [MPa]	σ_{yc} [MPa]	σ_{fc} [MPa]	ϵ_f [%]
MEP_H2	2440	131 – 133	306 – 308	53
MEP_H2_2 D51N	2470	126-127	264-265	50
MEP_H2_4 D51N	2450	120-121	309-310	53
MEP_H2_6 D51N	2280	120-121	319-320	55
MEP_H2_8 D51N	2300	116-116	226-227	50
MEP_H2_10 D51N	2230	111-112	191-192	44
MEP_H2_12 D51N	2060	105 - 106	130 - 131	32

9.3 Viscosity values at different temperatures

Table 54: Viscosity values at different temperatures for anhydride based system modified with D51N, MX170 and hybrids.

System	Viscosity (mPa.s)			
	40 °C	50 °C	60 °C	70 °C
MEP_H2	0.0267	0.0136	0.0066	0.0039
MEP_H2_4 D51N	0.3385	0.1623	0.0939	0.0553
MEP_H2_8 D51N	0.7810	0.4026	0.2014	0.1205
MEP_H2_12 D51N	0.9023	0.4632	0.2474	0.1528
MEP_H2_4 MX170	0.1610	0.0790	0.0441	0.0288
MEP_H2_8 MX170	0.2948	0.1509	0.0851	0.0514
MEP_H2_12 MX170	0.4701	0.2755	0.1277	0.0687
MEP_H2_4 HBD	0.1458	0.0731	0.0401	0.0235
MEP_H2_8 HBD	0.2002	0.1063	0.0606	0.0365
MEP_H2_12 HBD	0.3702	0.1893	0.1035	0.0665

Table 55: Viscosity values at different temperatures for amine based system modified with D51N, MX170 and hybrids.

System	Viscosity (mPa.s)			
	40 °C	50 °C	60 °C	70 °C
MEP_H1	0.423	0.1634	0.0780	0.0433
MEP_H1_4 D51N	1.517	0.5484	0.2437	0.1304
MEP_H1_8 D51N	2.5129	0.8345	0.4246	0.1992
MEP_H1_12 D51N	10.071	3.5695	1.4184	0.6211
MEP_H1_4 MX170	0.7031	0.2700	0.1257	0.0727
MEP_H1_8 MX170	0.8827	0.3870	0.1799	0.1008
MEP_H1_12 MX170	1.9291	0.7534	0.3713	0.2177
MEP_H1_4 HBD	0.7691	0.3351	0.1611	0.0987
MEP_H1_8 HBD	0.9419	0.3960	0.1979	0.1095
MEP_H1_12 HBD	2.4267	1.3163	0.7892	0.5473

9.4 Mixing ratios for different formulations

Table 56: Mixing ratios for LME10169 modified EP_H1 systems.

LME10169 (wt. %)	EP862 (gm)	LME10169 (gm)	H1 (gm)	Total wt. (gm)
0	315.2	0	84.8	400
5	299.44	15.76	83.4	399
7	293.13	22.06	82.84	398
10	283.68	31.52	82	397

Table 57: Mixing ratios for MY0816 modified EP_H1 systems.

MY0816 (wt. %)	EP862 (gm)	MY0816 (gm)	H1 (gm)	Total wt. (gm)
0	315.2	0	84.8	400
5	299.44	15.76	85.53	401
7	293.13	22.064	85.82	401
10	283.68	31.52	86.26	401

Table 58: Mixing ratios for MY0610 modified EP_H1 systems.

MY0610 (wt. %)	EP862 (gm)	MY0610 (gm)	H1 (gm)	Total wt. (gm)
0	315.2	0	84.8	400
5	299.44	15.76	87.63	403
7	293.13	22.06	88.77	404
10	283.68	31.52	90.47	406

Table 59: Mixing ratios for LME10169 modified EP_H2 systems.

LME10169 (wt. %)	EP862 (gm)	LME10169 (gm)	H2 (gm)	DY070 (gm)	Total wt. (gm)
EP_H2	238	0	238	4.06	480
EP_A	221.32	16.68	238	4.06	480
EP_B	221.32	16.68	214.2	4.06	456.26
EP_C	221.32	16.68	261.8	4.06	503.76

Table 60: Mixing ratios for MY0816 modified EP_H2 systems.

MY0816 (wt. %)	EP862 (gm)	MY0816 (gm)	H2 (gm)	DY070 (gm)	Total wt. (gm)
EP_H2	238	0	238	4.06	480
EP_D	221.32	16.68	238	4.06	480
EP_E	221.32	16.68	214.2	4.06	456.26
EP_F	221.32	16.68	261.8	4.06	503.76

Table 61: Mixing ratios for MY0610 modified EP_H2 systems.

MY0610 (wt. %)	EP862 (gm)	MY0610 (gm)	H2 (gm)	DY070 (gm)	Total wt. (gm)
EP_H2	238	0	238	4.06	480
EP_I	221.32	16.68	238	4.06	480
EP_J	221.32	16.68	214.2	4.06	456.26
EP_K	221.32	16.68	261.8	4.06	503.76

Table 62: Mixing ratios for MEP_H1_D51N system.

D51N (wt. %)	EP862 (gm)	LME10169 (gm)	H1 (gm)	D51N (gm)	Total wt. (gm)
0	293.14	22.06	82.84	0	398.04
2	344.74	25.95	97.43	9.60	477.72
4	337.70	25.41	97.68	19.20	479.99
6	310.00	23.31	89.67	27.00	449.98
8	323.63	24.36	93.67	38.40	480.06
10	316.60	23.83	91.57	48.00	480.00
12	309.57	23.30	89.54	57.60	480.01

Table 63: Mixing ratios for MEP_H1_MX170 system.

MX170 (wt. %)	EP862 (gm)	LME10169 (gm)	H1 (gm)	MX170 (gm)	Total wt. (gm)
0	293.14	22.06	82.84	0	398.04
2	323.20	24.32	90.80	9.0	477.32
4	337.70	25.41	94.28	19.20	476.59
6	330.80	24.89	91.77	28.60	476.06
8	323.87	24.38	89.23	38.06	475.54
10	316.95	23.86	86.71	47.52	475.04
12	310.02	23.34	84.18	56.98	474.52

Table 64: Mixing ratios for MEP_H2_D51N system.

D51N (wt. %)	EP862 (gm)	MY0610 (gm)	H2 (gm)	D51N (gm)	DY070 (gm)	Total wt. (gm)
0	221.32	16.65	261.76	0	4.06	503.79
2	214.83	16.17	254.09	10.01	4.21	499.31
4	210.69	15.82	248.61	19.96	4.21	499.29
6	205.56	15.47	243.14	29.92	4.21	498.30
8	200.95	15.12	237.69	39.84	4.21	497.81
10	196.35	14.78	232.24	49.75	4.21	497.33
12	191.73	14.43	226.79	59.66	4.21	496.82

Table 65: Mixing ratios for MEP_H2_MX170 system.

MX170 (wt. %)	EP862 (gm)	MY0610 (gm)	H2 (gm)	MX170 (gm)	DY070 (gm)	Total wt.
0	221.32	16.65	261.76	0	4.06	503.79
2	214.82	16.17	254.09	10.02	4.21	499.31
4	210.19	15.82	248.62	19.97	4.21	498.81
6	205.57	15.48	243.14	29.93	4.21	498.33
8	200.95	15.13	237.69	39.84	4.21	497.82
10	196.35	14.78	232.24	49.75	4.21	497.33
12	191.75	14.43	226.79	59.67	4.21	496.85

Table 66: Mixing ratios for MEP_H1_D51N_MX170 system.

D51N (wt. %)	MX170 (wt. %)	EP862 (gm)	LME10169 (gm)	H1 (gm)	D51N (gm)	MX170 (gm)	Total wt. (gm)
0	0	293.14	22.06	82.84	0	0	398.04
2	2	359.1	27.02	102.36	5	5	498.48
4	4	351.77	26.46	99.94	10	10	498.17
6	6	344.52	25.92	97.60	15	14.9	497.94

Table 67: Mixing ratios for MEP_H2_D51N_MX170 system.

D51N (wt. %)	MX170 (wt. %)	EP862 (gm)	MY0610 (gm)	H2 (gm)	D51N (gm)	MX170 (gm)	DY070 (gm)	Total wt. (gm)
0	0	221.32	16.65	261.76	0	0	4.06	503.79
2	2	227.55	17.14	269.16	5.3	5.3	4.21	528.66
4	4	226.66	16.75	263.36	10.58	10.58	4.21	532.14
6	6	217.76	16.4	257.54	15.85	15.85	4.21	527.61

Table 68: Mixing ratios for EP_H1_TiO₂ system.

TiO ₂ (wt. %)	Epoxy (gm)	Hardener (gm)	TiO ₂ (gm)	Total (gm)
0	374.30	100.70	0	475
3	363.08	97.66	14.25	475
5	355.59	95.65	23.75	475
7	348.10	93.64	33.25	475

Table 69: Mixing ratios for EP_H1_D51N_TiO₂ system

TiO ₂ (wt. %)	D51N (wt. %)	Epoxy (gm)	H1 (gm)	TiO ₂ (gm)	BCP (gm)	Total (gm)
0	0	374.30	100.70	0	0	475
3	4	348.10	93.64	14.25	19	475
3	6	340.62	91.62	14.25	28.5	475
3	8	333.13	89.61	14.25	38	475

9.5 Boiling water test results

Specimen size: 2.5 cm x 2.5 cm, Temperature: 100 °C, Time: 2 hours

Plate No	Specimen composition	Initial weight (gm)	Final weight (gm)	weight gain	% gain
1	EP_H1	3,3869	3,3926	0,00168	0,04969
2	MEP_H1	3,5368	3,5422	0,00153	0,04317
3	MEP_H1_2MX170	3,3841	3,3892	0,00151	0,04453
4	MEP_H1_4MX170	3,3838	3,3902	0,00189	0,05589
5	MEP_H1_6MX170	3,4636	3,4697	0,00176	0,05085
6	MEP_H1_8MX170	3,3989	3,4043	0,00159	0,04674
7	MEP_H1_10MX170	3,5301	3,5361	0,00170	0,04815
8	MEP_H1_12MX170	3,3917	3,3974	0,00168	0,04955
9	MEP_H1_2D51N	3,3482	3,354	0,00173	0,05174
10	MEP_H1_4D51N	3,4886	3,4948	0,00178	0,05094
11	MEP_H1_6D51N	3,4468	3,4528	0,00174	0,05050
12	MEP_H1_8D51N	3,462	3,4686	0,00191	0,05507
13	MEP_H1_10D51N	3,5581	3,5648	0,00188	0,05292
14	MEP_H1_12D51N	3,4451	3,4524	0,00212	0,06151
15	MEP_H1_2D51N_2MX170	3,5162	3,5221	0,00168	0,04772
16	MEP_H1_4D51N_4MX170	3,616	3,6226	0,00183	0,05048
17	MEP_H1_6D51N_6MX170	3,6273	3,6339	0,00182	0,05016
Plate No	Specimen composition	Initial weight (gm)	Final weight (gm)	weight gain	% gain
18	EP_H2	3,564	3,5689	0,00137	0,03858
19	MEP_H2	3,654	3,6593	0,00145	0,03970
20	MEP_H2_2MX170	3,4647	3,4699	0,00150	0,04332

21	MEP_H2_4MX170	3,5638	3,5691	0,00149	0,04173
22	MEP_H2_6MX170	3,677	3,6823	0,00144	0,03920
23	MEP_H2_8MX170	3,5356	3,5414	0,00164	0,04640
24	MEP_H2_10MX170	3,4242	3,4297	0,00161	0,04691
25	MEP_H2_12MX170	3,4487	3,4547	0,00174	0,05045
26	MEP_H2_2D51N	3,4356	3,441	0,00157	0,04575
27	MEP_H2_4D51N	3,6267	3,6323	0,00154	0,04258
28	MEP_H2_6D51N	3,6536	3,6603	0,00183	0,05019
29	MEP_H2_8D51N	3,5009	3,5082	0,00209	0,05956
30	MEP_H2_10D51N	3,5594	3,5676	0,00230	0,06472
31	MEP_H2_12D51N	3,4027	3,4115	0,00259	0,07600
32	MEP_H2_2D51N_2MX170	3,6163	3,6216	0,00147	0,04053
33	MEP_H2_4D51N_4MX170	3,5865	3,5923	0,00162	0,04509
34	MEP_H2_6D51N_6MX170	3,5664	3,572	0,00157	0,04403

10. List of publications

- [1] A. Bajpai, A. K. Alapati and B. Wetzel, "Toughening and mechanical properties of epoxy modified with block co-polymers and MWCNT's," *Procedia Structural Integrity*, vol. 2, pp. 104-111, 2016.
- [2] A. Bajpai and B. Wetzel, "The mechanical properties and toughening mechanisms of tailored epoxy based hybrid nanocomposites.," in *14th International Conference on Fracture, ICF14, June 18-23, 2017*, Rhodes, Greece, 2017.
- [3] A. Bajpai and B. Wetzel, "Tailored epoxy system modified with block co-polymer, core shell rubber and hybrid," in *Polymer Processing Society, Europe Africa Conference, June 26-29, 2017*, Dresden, Germany, 2017.
- [4] A. Bajpai, "Modification of epoxy systems for mechanical performance improvement," in *Institut für Verbundwerkstoffe GmbH, Internes Kolloquium, March 06, 2017*, Kaiserslautern, Germany, 2017.
- [5] A. Bajpai and B. Wetzel, "Toughening and mechanical properties of epoxy modified with block co-polymers and titanium dioxide nanoparticles," in *17th European Conference on Composite Materials, ECCM17, June 26-30, 2016*, Munich, Germany, 2016.
- [6] A. Bajpai, A. K. Alapati and B. Wetzel, "Toughening and mechanical properties of epoxy modified with block co-polymers and MWCNT's," in *21st European Conference on Fracture, ECF 21, June 20-24, 2017*, Catania, Italy, 2016.

11. List of student support works

1. Toughening and mechanical properties of epoxy modified with different block polymers and CNT's, Institut für Verbundwerkstoffe GmbH, Masterarbeit, 2016.
2. Toughening and mechanical properties of tailored epoxy with block copolymers and core shell rubber nanoparticles, Institut für Verbundwerkstoffe GmbH, Masterarbeit, 2017.

12. Curriculum Vitae

Personal Data

Name Ankur Bajpai
Address Kanpur, India



Education

2001 Matriculation, Kanpur India.
2003 Intermediate, Kanpur India.
2004 – 2008 Bachelor's in Mechanical Engineering, University Institute of Engineering and Technology, C.S.J.M. University, Kanpur, India.
2010 – 2012 Master's in Technology, Industrial Tribology and Maintenance Engineering Center and ILK, TU Dresden (Sept'11-May'12). Indian Institute of Technology Delhi, New Delhi, India.

Working Experience

2013 – Today Research Associate at the Institut für Verbundwerkstoffe GmbH
Doctoral student in the "Tailored Thermosets" group of material science department.
2011-2012 DAAD exchange student in Institute of Lightweight Engineering and Polymer Technology, TU Dresden under DAAD sandwich program between TU9 – 7 IIT's Universities.